



**ISSN: 2067-3809**

**ACTA TECHNICA  
CORVINIENSIS  
- Bulletin  
of Engineering**

**Tome XI [2018]  
Fascicule 2  
[April - June]**

**Editura Politehnica  
2018**



Edited by:

UNIVERSITY POLITEHNICA TIMISOARA



with kindly supported by:

THE GENERAL ASSOCIATION OF ROMANIAN ENGINEERS (AGIR)  
– branch of HUNEDOARA



Editor / Technical preparation / Cover design:

Assoc. Prof. Eng. KISS Imre, PhD.  
UNIVERSITY POLITEHNICA TIMISOARA,  
FACULTY OF ENGINEERING HUNEDOARA

Commenced publication year:  
2008

## ASSOCIATE EDITORS and REGIONAL COLLABORATORS


### MANAGER & CHAIRMAN


**ROMANIA**  **Imre KISS**, University Politehnica TIMIȘOARA, Faculty of Engineering HUNEDOARA, Department of Engineering & Management, General Association of Romanian Engineers (AGIR) – branch HUNEDOARA


### EDITORS from:

**ROMANIA**  **Vasile ALEXA**, University Politehnica TIMIȘOARA – HUNEDOARA  
**Sorin Aurel RAȚIU**, University Politehnica TIMIȘOARA – HUNEDOARA  
**Vasile George CIOATĂ**, University Politehnica TIMIȘOARA – HUNEDOARA  
**Simona DZIȚAC**, University of Oradea – ORADEA  
**Valentin VLĂDUȚ**, Institute of Research-Development for Machines & Installations – BUCUREȘTI  
**Dan Ludovic LEMLE**, University Politehnica TIMIȘOARA – HUNEDOARA  
**Dragoș UȚU**, University Politehnica TIMIȘOARA – TIMIȘOARA  
**Emanoil LINUL**, University Politehnica TIMIȘOARA – TIMIȘOARA  
**Virgil STOICA**, University Politehnica TIMIȘOARA – TIMIȘOARA  
**Cristian POP**, University Politehnica TIMIȘOARA – TIMIȘOARA  
**Sorin Ștefan BIRIȘ**, University Politehnica BUCUREȘTI – BUCUREȘTI  
**Mihai G. MATACHE**, Institute of Research-Development for Machines & Installations – BUCUREȘTI  
**Adrian DĂNILĂ**, “Transilvania” University of BRASOV – BRASOV  
**Dan GLĂVAN**, University “Aurel Vlaicu” ARAD – ARAD  
**Valentina POMAZAN**, University “Ovidius” CONSTANȚA – CONSTANȚA  
**Bogdan LUNGU**, “Horia Hulubei” National Institute of Physics & Nuclear Engineering – MĂGURELE

### REGIONAL EDITORS from:

**SLOVAKIA**  **Juraj ŠPALEK**, University of ŽILINA – ŽILINA  
**Peter KOŠTÁL**, Slovak University of Technology in BRATISLAVA – TRNAVA  
**Otakav BOKŮVKA**, University of ŽILINA – ŽILINA  
**Tibor KRENICKÝ**, Technical University of KOŠICE – PREŠOV  
**Beata HRICOVÁ**, Technical University of KOŠICE – KOŠICE  
**Peter KRIŽAN**, Slovak University of Technology in BRATISLAVA – BRATISLAVA

**HUNGARY**  **Tamás HARTVÁNYI**, Széchenyi István University in GYŐR – GYŐR  
**Arpád FERENCZ**, Pallasz Athéné University – KECSKEMÉT  
**József SÁROSI**, University of SZEGED – SZEGED  
**Attila BARCZI**, Szent István University – GÖDÖLLŐ  
**György KOVÁCS**, University of MISKOLC – MISKOLC  
**Zsolt Csaba JOHANYÁK**, Pallasz Athéné University – KECSKEMÉT  
**Gergely DEZSÓ**, College of NYÍREGYHÁZA – NYÍREGYHÁZA  
**Krisztián LAMÁR**, Óbuda University BUDAPEST – BUDAPEST  
**Loránt KOVÁCS**, Pallasz Athéné University – KECSKEMÉT  
**Valeria NAGY**, University of SZEGED – SZEGED  
**Sándor BESZÉDES**, University of SZEGED – SZEGED

**SERBIA**  **Zoran ANIŠIĆ**, University of NOVI SAD – NOVI SAD  
**Milan RACKOV**, University of NOVI SAD – NOVI SAD  
**Igor FÜRSTNER**, SUBOTICA Tech – SUBOTICA  
**Eleonora DESNICA**, University of NOVI SAD – ZRENJANIN  
**Blaža STOJANOVIĆ**, University of KRAGUJEVAC – KRAGUJEVAC  
**Aleksander MILTENOVIC**, University of NIŠ – NIŠ  
**Milan BANIC**, University of NIŠ – NIŠ  
**Slobodan STEFANOVIĆ**, Graduate School of Applied Professional Studies – VRANJE  
**Sinisa BIKIĆ**, University of NOVI SAD – NOVI SAD  
**Masa BUKUROV**, University of NOVI SAD – NOVI SAD  
**László GOGOLÁK**, SUBOTICA Tech – SUBOTICA  
**Ana LANGOVIC MILICEVIC**, University of KRAGUJEVAC – VRNJAČKA BANJA  
**Imre NEMEDI**, SUBOTICA Tech – SUBOTICA  
**Živko PAVLOVIĆ**, University of NOVI SAD – NOVI SAD

	<b>BULGARIA</b> Krasimir Ivanov TUJAROV, “Angel Kanchev” University of ROUSSE – ROUSSE Ognyan ALIPIEV, “Angel Kanchev” University of ROUSSE – ROUSSE Ivanka ZHELEVA, “Angel Kanchev” University of ROUSSE – ROUSSE Atanas ATANASOV, “Angel Kanchev” University of ROUSSE – ROUSSE
	<b>CROATIA</b> Gordana BARIC, University of ZAGREB – ZAGREB Goran DUKIC, University of ZAGREB – ZAGREB
	<b>BOSNIA &amp; HERZEGOVINA</b> Tihomir LATINOVIC, University in BANJA LUKA – BANJA LUKA Sabahudin JASAREVIC, University of ZENICA – ZENICA Šefket GOLETIĆ, University of ZENICA – ZENICA
	<b>POLAND</b> Jarosław ZUBRZYCKI, LUBLIN University of Technology – LUBLIN Maciej BIELECKI, Technical University of LODZ – LODZ Bożena GAJDZIK, The Silesian University of Technology – KATOWICE
	<b>TURKEY</b> Önder KABAŞ, Akdeniz University – KONYAALTI/Antalya
	<b>CHINA</b> Yiwen JIANG, Military Economic Academy – WUHAN

The Editor and editorial board members do not receive any remuneration. These positions are voluntary. The members of the Editorial Board may serve as scientific reviewers.

We are very pleased to inform that our journal **ACTA TECHNICA CORVINIENSIS – Bulletin of Engineering** is going to complete its ten years of publication successfully. In a very short period it has acquired global presence and scholars from all over the world have taken it with great enthusiasm. We are extremely grateful and heartily acknowledge the kind of support and encouragement from you.

**ACTA TECHNICA CORVINIENSIS – Bulletin of Engineering** seeking qualified researchers as members of the editorial team. Like our other journals, **ACTA TECHNICA CORVINIENSIS – Bulletin of Engineering** will serve as a great resource for researchers and students across the globe. We ask you to support this initiative by joining our editorial team. If you are interested in serving as a member of the editorial team, kindly send us your resume to [redactie@fih.upt.ro](mailto:redactie@fih.upt.ro).




ISSN: 2067-3809

copyright © University POLITEHNICA Timisoara,  
Faculty of Engineering Hunedoara,  
5, Revolutiei, 331128, Hunedoara, ROMANIA  
<http://acta.fih.upt.ro>

# INTERNATIONAL SCIENTIFIC COMMITTEE MEMBERS and SCIENTIFIC REVIEWERS


## MANAGER & CHAIRMAN


**ROMANIA**  **Imre KISS**, University Politehnica TIMIȘOARA, Faculty of Engineering HUNEDOARA, Department of Engineering & Management, General Association of Romanian Engineers (AGIR) – branch HUNEDOARA

## INTERNATIONAL SCIENTIFIC COMMITTEE MEMBERS & SCIENTIFIC REVIEWERS from:

**ROMANIA**  **Viorel–Aurel ȘERBAN**, University Politehnica TIMIȘOARA – TIMIȘOARA  
**Teodor HEPUȚ**, University Politehnica TIMIȘOARA – HUNEDOARA  
**Caius PĂNOIU**, University Politehnica TIMIȘOARA – HUNEDOARA  
**Mircea BEJAN**, Tehnical University of CLUJ-NAPOCA – CLUJ-NAPOCA  
**Liviu MIHON**, University Politehnica TIMIȘOARA – TIMIȘOARA  
**Ilare BORDEAȘU**, University Politehnica TIMIȘOARA – TIMIȘOARA  
**Corneliu CRĂCIUNESCU**, University Politehnica TIMIȘOARA – TIMIȘOARA  
**Liviu MARȘAVIA**, University Politehnica TIMIȘOARA – TIMIȘOARA  
**Nicolae HERIȘANU**, University Politehnica TIMIȘOARA – TIMIȘOARA  
**Dumitru TUCU**, University Politehnica TIMIȘOARA – TIMIȘOARA  
**Valer DOLGA**, University Politehnica TIMIȘOARA – TIMIȘOARA  
**Ioan VIDA-SIMITI**, Technical University of CLUJ-NAPOCA – CLUJ-NAPOCA  
**Csaba GYENGE**, Technical University of CLUJ-NAPOCA – CLUJ-NAPOCA  
**Sava IANICI**, “Eftimie Murgu” University of REȘIȚA – REȘIȚA  
**Ioan SZÁVA**, “Transilvania” University of BRASOV – BRASOV  
**Liviu NISTOR**, Technical University of CLUJ-NAPOCA – CLUJ-NAPOCA  
**Sorin VLASE**, “Transilvania” University of BRASOV – BRASOV  
**Horatiu TEODORESCU DRĂGHICESCU**, “Transilvania” University of BRASOV – BRASOV  
**Maria Luminița SCUTARU**, “Transilvania” University of BRASOV – BRASOV

**SLOVAKIA**  **Iulian RIPOȘAN**, University Politehnica BUCUREȘTI – BUCUREȘTI  
**Ioan DZITAC**, Agora University of ORADEA – ORADEA  
**Daniel STAN**, University Politehnica TIMIȘOARA – TIMIȘOARA  
**Adrian STUPARU**, University Politehnica TIMIȘOARA – TIMIȘOARA  
**Corina GRUESCU**, University Politehnica TIMIȘOARA – TIMIȘOARA  
**Carmen ALIC**, University Politehnica TIMIȘOARA – HUNEDOARA  
**Ștefan NIZNIK**, Technical University of KOŠICE – KOŠICE  
**Karol VELIŠEK**, Slovak University of Technology BRATISLAVA – TRNAVA  
**Juraj ŠPALEK**, University of ŽILINA – ŽILINA  
**Ervin LUMNITZER**, Technical University of KOŠICE – KOŠICE  
**Miroslav BADIDA**, Technical University of KOŠICE – KOŠICE  
**Milan DADO**, University of ŽILINA – ŽILINA  
**Ladislav GULAN**, Slovak University of Technology – BRATISLAVA  
**Ľubomir ŠOOŠ**, Slovak University of Technology in BRATISLAVA – BRATISLAVA  
**Miroslav VEREŠ**, Slovak University of Technology in BRATISLAVA – BRATISLAVA  
**Milan SAGA**, University of ŽILINA – ŽILINA  
**Imrich KISS**, Institute of Economic & Environmental Security – KOŠICE  
**Michal CEHLÁR**, Technical University KOSICE – KOSICE  
**Pavel NEČAS**, Armed Forces Academy of General Milan Rastislav Stefanik – LIPTOVSKÝ MIKULÁŠ  
**Vladimir MODRAK**, Technical University of KOSICE – PRESOV  
**Michal HAVRILA**, Technical University of KOSICE – PRESOV

**CROATIA**  **Drazan KOZAK**, Josip Juraj Strossmayer University of OSIJEK – SLAVONKI BROD  
**Predrag COSIC**, University of ZAGREB – ZAGREB  
**Milan KLJAJIN**, Josip Juraj Strossmayer University of OSIJEK – SLAVONKI BROD  
**Miroslav CAR**, University of ZAGREB – ZAGREB  
**Antun STOIĆ**, Josip Juraj Strossmayer University of OSIJEK – SLAVONKI BROD  
**Ivo ALFIREVIĆ**, University of ZAGREB – ZAGREB

**GREECE**  **Nicolaos VAXEVANIDIS**, University of THESSALY – VOLOS

HUNGARY



Imre DEKÁNY, University of SZEGED – SZEGED  
Béla ILLÉS, University of MISKOLC – MISKOLC  
Imre RUDAS, Óbuda University of BUDAPEST – BUDAPEST  
Tamás KISS, University of SZEGED – SZEGED  
Cecilia HODÚR, University of SZEGED – SZEGED  
Arpád FERENCZ, Pallasz Athéné University – KECSKEMÉT  
Imre TIMÁR, University of Pannonia – VESZPRÉM  
Kristóf KOVÁCS, University of Pannonia – VESZPRÉM  
Károly JÁRMAI, University of MISKOLC – MISKOLC  
Gyula MESTER, University of SZEGED – SZEGED  
Ádám DÖBRÖCZÖNI, University of MISKOLC – MISKOLC  
György SZEIDL, University of MISKOLC – MISKOLC  
István PÁCZELT, University of Miskolc – MISKOLC – BUDAPEST  
István JÓRI, BUDAPEST University of Technology & Economics – BUDAPEST  
Miklós TISZA, University of MISKOLC – MISKOLC  
Attila BARCZI, Szent István University – GÖDÖLLŐ  
István BIRÓ, University of SZEGED – SZEGED  
Gyula VARGA, University of MISKOLC – MISKOLC  
József GÁL, University of SZEGED – SZEGED  
Ferenc FARKAS, University of SZEGED – SZEGED  
Géza HUSI, University of DEBRECEN – DEBRECEN  
Ferenc SZIGETI, College of NYÍREGYHÁZA – NYÍREGYHÁZA  
Zoltán KOVÁCS, College of NYÍREGYHÁZA – NYÍREGYHÁZA

BULGARIA



Kliment Blagoev HADJOV, University of Chemical Technology and Metallurgy – SOFIA  
Nikolay MIHAILOV, “Anghel Kanchev” University of ROUSSE – ROUSSE  
Krassimir GEORGIEV, Institute of Mechanics, Bulgarian Academy of Sciences – SOFIA  
Stefan STEFANOV, University of Food Technologies – PLOVDIV

SERBIA



Sinisa KUZMANOVIC, University of NOVI SAD – NOVI SAD  
Zoran ANIŠIĆ, University of NOVI SAD – NOVI SAD  
Mirjana VOJINOVIĆ MILORADOV, University of NOVI SAD – NOVI SAD  
Miroslav PLANČAK, University of NOVI SAD – NOVI SAD  
Milosav GEORGIJEVIC, University of NOVI SAD – NOVI SAD  
Vojislav MILTENOVIC, University of NIŠ – NIŠ  
Aleksandar RODIĆ, “Mihajlo Pupin” Institute – BELGRADE  
Milan PAVLOVIC, University of NOVI SAD – ZRENJANIN  
Radomir SLAVKOVIĆ, University of KRAGUJEVAC, Technical Faculty – CACAK  
Zvonimir JUGOVIĆ, University of KRAGUJEVAC, Technical Faculty – CACAK  
Branimir JUGOVIĆ, Institute of Technical Science of Serbian Academy of Science & Arts – BELGRAD  
Miomir JOVANOVIĆ, University of NIŠ – NIŠ  
Vidosav MAJSTOROVIC, University of BELGRADE – BELGRAD  
Predrag DAŠIĆ, Production Engineering and Computer Science – TRSTENIK  
Lidija MANČIĆ, Institute of Technical Sciences of Serbian Academy of Sciences & Arts – BELGRAD  
Vlastimir NIKOLIĆ, University of NIŠ – NIŠ  
Nenad PAVLOVIĆ, University of NIŠ – NIŠ

ITALY



Alessandro GASPARETTO, University of UDINE – UDINE  
Alessandro RUGGIERO, University of SALERNO – SALERNO  
Adolfo SENATORE, University of SALERNO – SALERNO  
Enrico LORENZINI, University of BOLOGNA – BOLOGNA

BOSNIA &  
HERZEGOVINA



Tihomir LATINOVIC, University of BANJA LUKA – BANJA LUKA  
Safet BRDAREVIĆ, University of ZENICA – ZENICA  
Ranko ANTUNOVIC, University of EAST SARAJEVO – East SARAJEVO  
Isak KARABEGOVIĆ, University of BIHAĆ – BIHAĆ

MACEDONIA



Valentina GECEVSKA, University “St. Cyril and Methodius” SKOPJE – SKOPJE  
Zoran PANDILOV, University “St. Cyril and Methodius” SKOPJE – SKOPJE  
Robert MINOVSKI, University “St. Cyril and Methodius” SKOPJE – SKOPJE

PORTUGAL



João Paulo DAVIM, University of AVEIRO – AVEIRO  
Paulo BÁRTOLO, Polytechnique Institute – LEIRIA  
José MENDES MACHADO, University of MINHO – GUIMARÃES

SLOVENIA



Janez GRUM, University of LJUBLJANA – LJUBLJANA  
Štefan BOJNEC, University of Primorska – KOPER

- POLAND**  
 Leszek DOBRZANSKI, Silesian University of Technology – GLIWICE  
Stanisław LEGUTKO, Polytechnic University – POZNAN  
Andrzej WYCISLIK, Silesian University of Technology – KATOWICE  
Antoni ŚWIĆ, University of Technology – LUBLIN  
Marian Marek JANCZAREK, University of Technology – LUBLIN  
Michał WIECZOROWSKI, POZNAN University of Technology – POZNAN  
Jarosław ZUBRZYCKI, LUBLIN University of Technology – LUBLIN  
Aleksander SŁADKOWSKI, Silesian University of Technology – KATOWICE  
Tadeusz SAWIK, Akademia Górniczo–Hutnicza University of Science & Technology – CRACOW  
Branko KATALINIC, VIENNA University of Technology – VIENNA
- AUSTRIA**  

- FRANCE**  
 Bernard GRUZZA, Universite Blaise Pascal – CLERMONT-FERRAND  
Abdelhamid BOUCHAIR, Universite Blaise Pascal – CLERMONT-FERRAND  
Khalil EL KHAMLICH DRISSI, Universite Blaise Pascal – CLERMONT-FERRAND  
Mohamed GUEDDA, Université de Picardie Jules Verne – AMIENS  
Ahmed RACHID, Université de Picardie Jules Verne – AMIENS  
Yves DELMAS, University of REIMS – REIMS  
Jean GRENIER GODARD, L'école Supérieure des Technologies et des Affaires – BELFORT  
Jean–Jacques WAGNER, Université de Franche-Comte – BELFORT
- ARGENTINA**  
 Gregorio PERICHINSKY, University of BUENOS AIRES – BUENOS AIRES  
Atilio GALLITELLI, Institute of Technology – BUENOS AIRES  
Carlos F. MOSQUERA, University of BUENOS AIRES – BUENOS AIRES  
Elizabeth Myriam JIMENEZ REY, University of BUENOS AIRES – BUENOS AIRES  
Arturo Carlos SERVETTO, University of BUENOS AIRES – BUENOS AIRES
- SPAIN**  
 Patricio FRANCO, Universidad Politecnica de CARTAGENA – CARTAGENA  
Luis Norberto LOPEZ De LACALLE, University of Basque Country – BILBAO  
Aitzol Lamikiz MENTXAKA, University of Basque Country – BILBAO  
Carolina Senabre BLANES, Universidad Miguel Hernández – ELCHE
- CUBA**  
 Norge I. COELLO MACHADO, Universidad Central “Marta Abreu” LAS VILLAS – SANTA CLARA  
José Roberto Marty DELGADO, Universidad Central “Marta Abreu” LAS VILLAS – SANTA CLARA
- INDIA**  
 Sugata SANYAL, Tata Consultancy Services – MUMBAI  
Siby ABRAHAM, University of MUMBAI – MUMBAI  
Anjan KUMAR KUNDU, University of CALCUTTA – KOLKATA
- TURKEY**  
 Ali Naci CELIK, Abant Izzet Baysal University – BOLU  
Önder KABAŞ, Akdeniz University –KONYAAALI/Antalya
- CZECH REPUBLIC**  
 Ivo SCHINDLER, Technical University of OSTRAVA – OSTRAVA  
Jan VIMMR, University of West Bohemia – PILSEN  
Vladimir ZEMAN, University of West Bohemia – PILSEN
- ISRAEL**  
 Abraham TAL, University TEL-AVIV, Space & Remote Sensing Division – TEL-AVIV  
Amnon EINAV, University TEL-AVIV, Space & Remote Sensing Division – TEL-AVIV
- LITHUANIA**  
 Egidijus ŠARAUSKIS, Aleksandras Stulginskis University – KAUNAS  
Zita KRIAUCIŪNIENĖ, Experimental Station of Aleksandras Stulginskis University – KAUNAS
- FINLAND**  
 Antti Samuli KORHONEN, University of Technology – HELSINKI  
Pentti KARJALAINEN, University of OULU – OULU
- NORWAY**  
 Trygve THOMESSEN, Norwegian University of Science and Technology – TRONDHEIM  
Gábor SZIEBIG, Narvik University College – NARVIK  
Terje Kristofer LIEN, Norwegian University of Science and Technology – TRONDHEIM  
Bjoern SOLVANG, Narvik University College – NARVIK
- UKRAINE**  
 Sergiy G. DZHURA, Donetsk National Technical University – DONETSK  
Alexander N. MIKHAILOV, DONETSK National Technical University – DONETSK  
Heorhiy SULYM, Ivan Franko National University of LVIV – LVIV  
Yevhen CHAPLYA, Ukrainian National Academy of Sciences – LVIV
- SWEEDEN**  
 Ingvar L. SVENSSON, JÖNKÖPING University – JÖNKÖPING

BRAZIL



Alexandro Mendes ABRÃO, Universidade Federal de MINAS GERAIS – BELO HORIZONTE  
Márcio Bacci da SILVA, Universidade Federal de UBERLÂNDIA – UBERLÂNDIA  
Sergio Tonini BUTTON, Universidade Estadual de CAMPINAS – CAMPINAS  
Leonardo Roberto da SILVA, Centro Federal de Educação Tecnológica – BELO HORIZONTE  
Juan Campos RUBIO, Universidade Federal de MINAS GERAIS – BELO HORIZONTE

USA



David HUI, University of NEW ORLEANS – NEW ORLEANS

CHINA



Wenjing LI, Military Economic Academy – WUHAN  
Zhonghou GUO, Military Economic Academy – WUHAN

The Scientific Committee members and Reviewers do not receive any remuneration. These positions are voluntary. We are extremely grateful and heartily acknowledge the kind of support and encouragement from all contributors and all collaborators!

**ACTA TECHNICA CORVINIENSIS – Bulletin of Engineering** is dedicated to publishing material of the highest engineering interest, and to this end we have assembled a distinguished Editorial Board and Scientific Committee of academics, professors and researchers.

**ACTA TECHNICA CORVINIENSIS – Bulletin of Engineering** publishes invited review papers covering the full spectrum of engineering. The reviews, both experimental and theoretical, provide general background information as well as a critical assessment on topics in a state of flux. We are primarily interested in those contributions which bring new insights, and papers will be selected on the basis of the importance of the new knowledge they provide.

**ACTA TECHNICA CORVINIENSIS – Bulletin of Engineering** encourages the submission of comments on papers published particularly in our journal. The journal publishes articles focused on topics of current interest within the scope of the journal and coordinated by invited guest editors. Interested authors are invited to contact one of the Editors for further details.

**ACTA TECHNICA CORVINIENSIS – Bulletin of Engineering** accept for publication unpublished manuscripts on the understanding that the same manuscript is not under simultaneous consideration of other journals. Publication of a part of the data as the abstract of conference proceedings is exempted.

Manuscripts submitted (original articles, technical notes, brief communications and case studies) will be subject to peer review by the members of the Editorial Board or by qualified outside reviewers. Only papers of high scientific quality will be accepted for publication. Manuscripts are accepted for review only when they report unpublished work that is not being considered for publication elsewhere. The evaluated paper may be recommended for:

- ✓ **Acceptance without any changes** – in that case the authors will be asked to send the paper electronically in the required .doc format according to authors' instructions;
- ✓ **Acceptance with minor changes** – if the authors follow the conditions imposed by referees the paper will be sent in the required .doc format;

✓ **Acceptance with major changes** – if the authors follow completely the conditions imposed by referees the paper will be sent in the required .doc format;

✓ **Rejection** – in that case the reasons for rejection will be transmitted to authors along with some suggestions for future improvements (if that will be considered necessary).

The manuscript accepted for publication will be published in the next issue of **ACTA TECHNICA CORVINIENSIS – Bulletin of Engineering** after the acceptance date.

All rights are reserved by **ACTA TECHNICA CORVINIENSIS – Bulletin of Engineering**. The publication, reproduction or dissemination of the published paper is permitted only by written consent of one of the Managing Editors.

All the authors and the corresponding author in particular take the responsibility to ensure that the text of the article does not contain portions copied from any other published material which amounts to plagiarism. We also request the authors to familiarize themselves with the good publication ethics principles before finalizing their manuscripts.



ISSN: 2067-3809

copyright © University POLITEHNICA Timisoara,  
Faculty of Engineering Hunedoara,  
5, Revolutiei, 331128, Hunedoara, ROMANIA  
<http://acta.fih.upt.ro>



## TABLE of CONTENTS

1.	Isak KARABEGOVIĆ – BOSNIA & HERZEGOVINA THE ROLE OF INDUSTRIAL AND SERVICE ROBOTS IN THE 4 <sup>th</sup> INDUSTRIAL REVOLUTION – “INDUSTRY 4.0”	11
2.	Milan RADOŠEVIĆ, Sebastijan BALOŠ, Dragan RUŽIĆ – SERBIA METALLOGRAPHIC TESTS AND STRENGTH OF THE MATERIAL OF CHAINS SNOW	17
3.	Igor SHESHO, Done TASHEVSKI, Filip MOJSOVSKI – MACEDONIA METHODOLOGY FOR TECHNO-ECONOMIC OPTIMIZATION OF SOLAR ASSISTED HEATING SYSTEMS	21
4.	Srbislav ALEKSANDROVIĆ, Slavisa ĐAČIĆ, Milentije STEFANOVIĆ, Milan ĐORĐEVIĆ, Vukic LAZIC, Dusan ARSIC – SERBIA/MONTENEGRO INFLUENCE OF PROCESS PARAMETERS ON THE FRICTION COEFFICIENT IN ONE AND MULTI PHASE STEEL STRIP DRAWING IRONING TEST	29
5.	Milan ŠLJIVIĆ, Milija KRAIŠNIK, Jovica ILIĆ, Jelica ANIĆ – BOSNIA & HERZEGOVINA DEVELOPMENT OF SMALL BATCHES OF FUNCTIONAL PARTS USING INTEGRATION OF 3D PRINTING AND VACUUM CASTING TECHNOLOGY	35
6.	Ile MIRCHESKI, Tashko RIZOV – MACEDONIA NONDESTRUCTIVE DISASSEMBLY PROCESS OF TECHNICAL DEVICE SUPPORTED WITH AUGMENTED REALITY AND RFID TECHNOLOGY	39
7.	Jasna GLIŠOVIĆ, Jovanka LUKIĆ, Blaža STOJANOVIĆ, Nadica STOJANOVIĆ – SERBIA AIRBORNE WEAR PARTICLES FROM AUTOMOTIVE BRAKE SYSTEMS IN URBAN AND RURAL AREAS	45
8.	Ahmed Abdel Hamid A. ABDALLAH – EGYPT MODERN TECHNOLOGY AND ECONOMICAL DEVELOPMENTS IN DESALINATION ON EMPHASIS OF NUCLEAR METHODOLOGY	49
9.	Habib BENBOUHENNI – ALGERIA FIVE-LEVEL DTC BASED ON ANN OF IM USING 13-LEVEL HYSTERESIS CONTROL TO REDUCE TORQUE RIPPLE COMPARING WITH CONVENTIONAL CONTROL	55
10.	Malik Muhammad ZAID, Muhammad NAUMAN, Mudasser RAHIM, Muhammad Usama MALIK – PAKISTAN DSP BASED ENERGY MONITORING WITH ONLINE DAQ SYSTEM	59
11.	Gagandeep KAUR, Sunaina SAINI – INDIA DISTRIBUTED GENERATION PLACEMENT IN DISTRIBUTION NETWORK USING SELECTIVE PARTICLE SWARM OPTIMIZATION	65
12.	Igor MIKLÓŠIK, Peter KELLO, Juraj SPALEK – SLOVAKIA FIRE DETECTION IN TuSim BY FibroLaser	71
13.	I.O. OLADELE, O.T. BETIKU, A.M. OKORO, O. EGHONGHON – NIGERIA MICROSTRUCTURE AND MECHANICAL PROPERTIES OF 304L AND MILD STEEL PLATES DISSIMILAR METAL WELD JOINT	77
14.	Saša VASILJEVIĆ, Nataša ALEKSIĆ, Dragan RAJKOVIĆ, Rade ĐUKIĆ, Milovan ŠARENAC, Nevena BANKOVIĆ – SERBIA THE BENEFITS OF APPLICATION OF CAD/CAE TECHNOLOGY IN THE DEVELOPMENT OF VEHICLES IN THE AUTOMOTIVE INDUSTRY	83

15.	S. ABDULKAREEM, E.J. EDACHE, I.I. OLOWOSULE, M.Y. KOLAWOLE, I.I. AHMED, T.K. AJIBOYE – NIGERIA EFFECT OF DATE SEED PARTICULATES ON MECHANICAL PROPERTIES OF ALUMINIUM ALLOY	89
16.	Ahmet SHALA, Ramë LIKAJ – KOSOVO DYNAMIC MODELING OF 3 DoF ROBOT MANIPULATOR	95
17.	Zorica DJORDJEVIĆ, Saša JOVANOVIĆ, Milan STANOJEVIĆ, Mirko BLAGOJEVIĆ, Sandra VELIČKOVIĆ – SERBIA OPTIMIZATION OF FIBER ORIENTATION ANGLE OF A HYBRID AI / COMPOSITE CARDAN SHAFT	99
18.	B. O. AKINNULI, S. P. AYODEJI, O.O. OJO – NIGERIA RECLAMATION OF BASE OIL FROM OIL WELLS DRILL CUTTINGS AND ITS DISPOSAL ECOLOGICAL HAZARD CONTROL	103
19.	Viktor József VOJNICH, Endre PÖLÖS, András PALKOVICS, Ferenc BAGLYAS – HUNGARY EXAMINATION OF WEED VEGETATION OF A VINEYARD ON SANDY SOIL	109
20.	Zoran PANDILOV, Betim SHABANI, Dejan SHISHKOVSKI, Gligorche VRTANOSKI – MACEDONIA/KOSOVO REVERSE ENGINEERING – AN EFFECTIVE TOOL FOR DESIGN AND DEVELOPMENT OF MECHANICAL PARTS	113
21.	Radko Petrov MIHAJLOW, Lazar Georgiev PANAIOTOV, Svilen Hristov STOIANOV, Desislava Palcheva MIHAJLOVA – BULGARIA SIMULATION MODELING AND PROCESSING THE DATA RECEIVED IN MEASURING WASTE BIOMASS	119
22.	Monday Itopa MOMOH, Mohammed Sani ADAMS – NIGERIA CORROSION BEHAVIOR OF GALVANNEALED STEEL SUBSTRATE IN SALINE ENVIRONMENT	123
23.	Milica JOVIĆ, Mirjana LAKOVIĆ – SERBIA CARBON FOOTPRINT METHOD – A CASE STUDY FOR THERMAL POWER PLANTS IN REPUBLIC OF SERBIA	127
24.	Dimitar LOLOV, Svetlana V. LILKOVA- MARKOVA – BULGARIA DYNAMIC STABILITY OF DOUBLE-WALLED CARBON NANOTUBES	131
25.	Adewole Ayobami ADERINLEWO, Abdul Kareem Adisa AGBOOLA, Olayemi Johnson ADEOSUN, Emmanuel Sunday Akin AJISEGIRI, Alex Folami ADISA – NIGERIA INVESTIGATION OF SEPARATION OF PALM KERNEL AND SHELL ON AN INCLINED PLANE SEPARATOR	135
***	MANUSCRIPT PREPARATION – GENERAL GUIDELINES	139

The ACTA TECHNICA CORVINIENSIS – Bulletin of Engineering, Tome XI [2018], Fascicule 2 [April – June], includes scientific papers presented in the sections of:

- » The 13th International Conference on Accomplishments in Mechanical and Industrial Engineering – DEMI 2017, organized by University of Banja Luka, Faculty of Mechanical Engineering, in Banja Luka, BOSNIA & HERZEGOVINA, 26 - 27 May 2017. The current identification number of the papers are the #1–7, #17 and #23, according to the present contents list.
- » The 7th International Conference Industrial Engineering and Environmental Protection 2017 – IIZS 2017, organized by University of Novi Sad, Technical Faculty "Mihajlo Pupin", in Zrenjanin, SERBIA, 12 – 13 October 2017. The current identification number of the paper is the #14, according to the present contents list.

Also, the ACTA TECHNICA CORVINIENSIS – Bulletin of Engineering, Tome XI [2018], Fascicule 2 [April – June] includes

original papers submitted to the Editorial Board, directly by authors or by the regional collaborators of the Journal.



ISSN: 2067-3809

copyright © University POLITEHNICA Timisoara,  
Faculty of Engineering Hunedoara,  
5, Revolutiei, 331128, Hunedoara, ROMANIA  
<http://acta.fih.upt.ro>

# THE ROLE OF INDUSTRIAL AND SERVICE ROBOTS IN THE 4<sup>th</sup> INDUSTRIAL REVOLUTION – “INDUSTRY 4.0”

<sup>1</sup> University of Bihać, Technical Faculty Bihać, BOSNIA & HERZEGOVINA

**Abstract:** As it is well known, the fourth industrial revolution, entitled "INDUSTRY 4.0" appeared for the first time at the Hannover Fair in 2011. It comes from the high-tech strategy of the German federal government that promotes automation and computerization of industry. Ever since 2012, the working group of the German government presented recommendations for the introduction of "Industry 4.0" in the production processes. The strategy consists of adjustment of industrial production to complete smart automation, which means the introduction of self-automation method, self-configuration method, self-diagnosing and removal of problem, knowledge and intelligent decision making. The central figures of "Industry 4.0" are industrial robots, as well as service robots. Their application in all production processes, with the support of information technology, will lead to "intelligent automation" and "intelligent factories". In the nearby future (expected by 2025), machines, devices, robots and humans need to be mutually connected, so that they can work side by side and communicate with each other via the internet platform (IOT). The paper states the role of robots in the fourth industrial revolution, as well as predictions of the development and implementation of robots in the industrial processes. Smart automation or smart factories will create a society in which the wealth, created through the strengthening of global competitiveness, would serve to meet social issues in the society.

**Keywords:** industrial robot, service robot, intelligent automation, industry 4.0, smart factory, robotic revolution

## INTRODUCTION

In the past 20 years the development of digital technologies, new methods and new technologies in the world as well as their implementation in production, urged the companies worldwide to constantly monitor these developments and conduct modernization and automation of their production processes in order to stay competitive. The fourth technological revolution "Industry 4.0" (the term originated in Germany, and can in many ways be labeled as "smart factories", "smart industry" or "advanced manufacturing") refers to the implementation in production technologies, supported by a variety of digital technologies (e.g. 3D printing, Cloud computing, ICT, advanced robotics) and new materials. One of the reasons that above mentioned technologies are already partially available is constant decrease in costs, and it is expected that they will be fully represented in the production processes in the near future. The other reason why companies need to follow the development and implementation of these technologies is because customers quickly obtain information through ICT and expand their requirements, so that products they demand become more complex and complicated for a production process [1, 2, 3, 4, 5, 6, 7]. The application of these technologies, or the digitized production, provides a wide range of changes in the production process, greater flexibility in production process, and easier automation of production processes by using adjustable or collaborative robots, so that different products can be produced during the same production process. In this way, manufacturers will be able to produce very small series (one product if needed) because this technology provides a possibility of fast configuration of

machines and production process, as well as their adaptation to customer requirements. In other words, we have the ability to produce rapidly without the installation of new production line. The application of digital design and virtual modeling of the production process reduces the time needed for the production process from design of a product to the distribution to the customer. In addition, we have high improvement of the finished product quality and reduced level of production errors. With the implementation in the technology production process (such as ICT technology, sensor technology and robotic technology) we have the ability to record the production process of each element (instead of sampling and control) and detecting errors that occur during the process. When detecting errors, the machines can be adjusted in real time. The development of ICT technologies, sensor technologies and their application in robotic technology leads to the development of new industrial robots that can work together with the workers. For this reason, the companies are trying to introduce "intelligent automation" or use "smart machines" in the production processes that will be the product of the fourth industrial revolution "Industry 4.0". If we take into account the fact that large companies in the developed countries incorporate the application of "intelligent automation" in their business strategies, we come to the conclusion that in 10 to 20 years we will reach "smart factories", which will easily be able to satisfy all the needs demanded by the customers. Industrial robots are being developed in the sense of cooperation between robots and workers, simplification of use, industrial robots with multiple hands, robot integration with the existing systems, modular robots, compact and lightweight

robots, and their implementation in a production processes that is supported by the ICT technologies, and followed by the objective towards "smart factories". Intelligent robots will completely replace the workers in the production process, and at the same time the workers will work on more effective creative tasks [3, 16, 18].

### THE ROLE OF DIGITAL TECHNOLOGY IN THE FOURTH INDUSTRIAL REVOLUTION "INDUSTRY 4.0"

As we already mentioned, the fourth industrial revolution is the result of digital technologies, and the participation of various digital technologies initiates the transformation of industrial production. In the next period, everything will depend on a number of new and innovative technological achievements. The application of information and communication technology (ICT), enable us to acquire information based on which we can carry out the integration of all systems in all phases of creating new products, both within the production process and outside of the production process (referring to the logistics and supply). Figure 1 outlines the key digital technologies (ICT) that enable digital transformation of the industrial production processes [1,3,15].

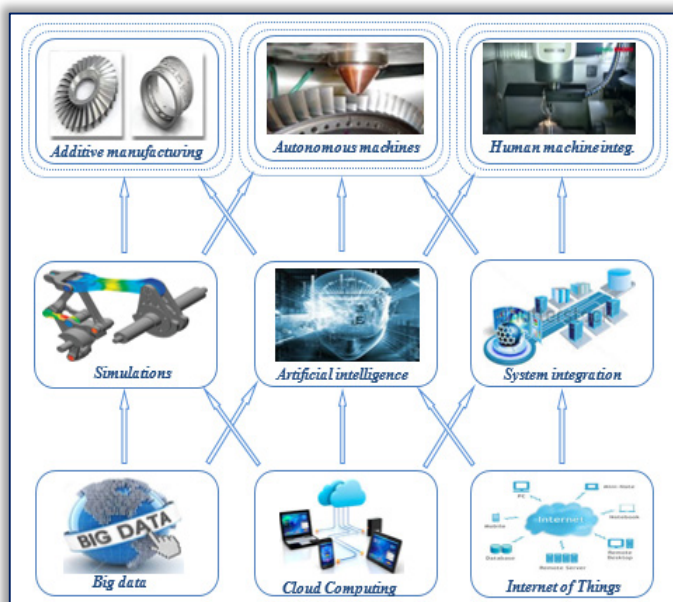


Figure 1. The transformation of production processes with digital technologies

The analysis of Figure 1 provides us with the conclusion that following technologies will lead us towards digital transformation of the industrial processes: Big Data, Cloud Computing, Internet, Simulations, Artificial Intelligence, and System integration, all representing support technologies on top of the Figure 1, such as Additive Manufacturing, Autonomous Machines and Human-Machine Integration. There are two reasons why digital technology will transform the production processes in the industry: the first is that their representation in the production processes is increasing every day, and the second is that the combination of various ICT technologies converges with other technologies. The main effect that influences the productivity in the production process is technologies depicted at the bottom of Figure that

enable the work of technologies on the top of Figure 1. In order to use the above mentioned technologies and in order to achieve all that was not possible until now (for example, to control each piece during the production, follow the distribution, changing parameters during production, etc.), we have to implement all digital technologies shown in Figure 1. The best example of future technology is shown in Figure 2. It gives the scheme of fourth industrial revolution and the role of robots in the "Industry 4.0" [3,8,17,19,20].

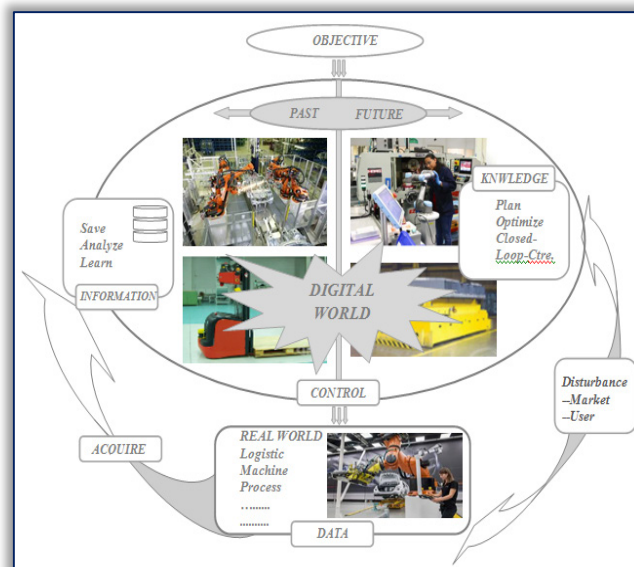


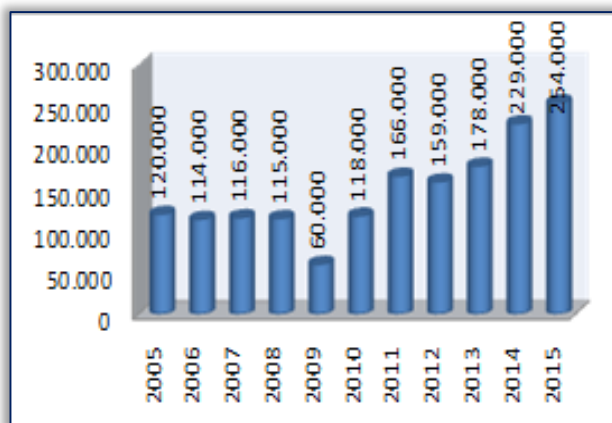
Figure 2. The basis of the fourth industrial revolution "Industry 4.0" are industrial robots and service robots

As Figure 2 shows, the current method of production is ever-changing and is being replaced by new productions methods, i.e. the transformation and production processes with the participation of digital technology in all processes of production, distribution and monitoring products throughout their life. It is impossible to automate the production processes with the "smart automation" without the participation of the industrial and service robots. Robotic technology and robots are one of the foundations of the fourth industrial revolution. The reason for this is that there has been the development of robotic technology owing to digital technologies, and above all, information technology and sensor technology, which led to the development and application of new types of industrial and service robots that make independent decisions and can work together with workers, but also take into account that they are not hurt during operation. In the period to come, i.e. future, it will not be possible to imagine any production process without the participation of the robots because they will be very flexible in order to perform any activity. In this way, robots significantly increase productivity, which is the objective of the companies engaged in the production. They produce faster, stronger and more consistent than workers with a combination of new sensors and actuators, and extensive data analysis. By using digital technology, such as Cloud Computing and Internet of Things, we get the ability to produce by independent production machines, that increase

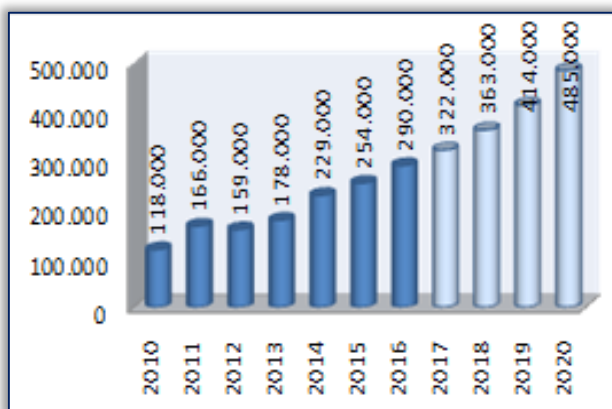
productivity, they are automatically maintained, and maintain communication during the production process.

### THE DEVELOPMENT OF ROBOTIC TECHNOLOGY WITH THE SUPPORT OF ICT TECHNOLOGY

Automation of production processes began in the 60s of the last century with the introduction of industrial robots in the production process in the automotive industry. The automation of production systems by introducing industrial robots is an ongoing process, and nowadays is performed differently because of the development of information technologies that affected its application in the automation because today they are performing multiple tasks, with the possibility of reprogramming. One of the disadvantages of the first-generation industrial and service robots is that they have to be programmed for every operation. The second disadvantage is that industrial robots were separated with barriers from the workers, so as not to hurt them during operation in the production process. Digital technology, sensor technology and new materials support the development of robotic technologies and their convergence enabled the development of second-generation industrial robots.



a)



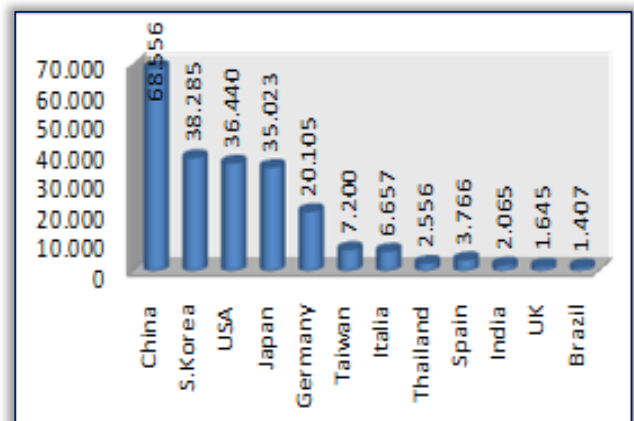
b)

Figure 3. The representation of industrial robots worldwide in the period 2005–2015 and the prediction of representation until 2020: a) Annual representation of robots; b) Prediction of representation

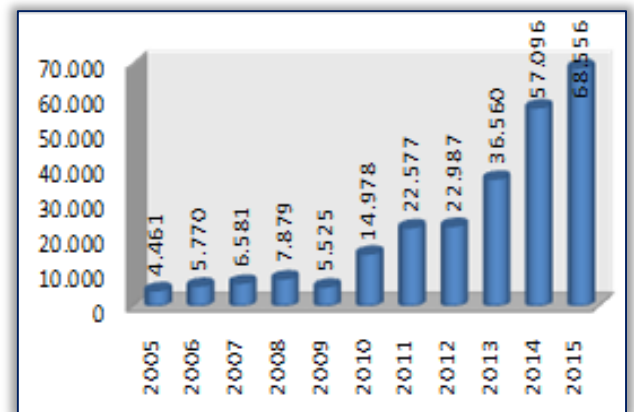
In order to understand the speed of convergence of digital and other technologies with robot technologies and their implementation in manufacturing processes in the industry,

we have to conduct the analysis of the representation of industrial and service robots in the world in the last ten years. Statistical data were taken from the IFR (International Federation of Robotics) and shown in diagram in Figure 1 [9, 10, 11, 12, 13, 14].

Based on Figure 3a), we can conclude that the representation of industrial robots in production processes worldwide is increasing every year, so that in last ten years the representation of robot units increased from 120.000 robot units in 2005 to 254.000 robot units in 2015. This statement provides us with the assumption that the development of information technology and robotic technology and their implementation in production processes is increased by the automation and modernization of production processes, thus increasing the productivity.



a)



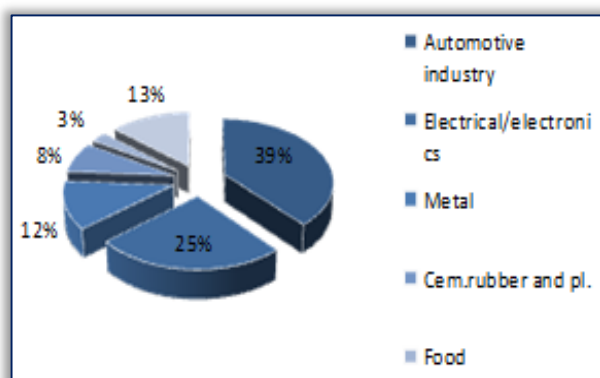
b)

Figure 4. The representation of industrial robots in top twelve countries in the world in the period 2005–2015 and the representation of industrial robots in China in the period 2005–2015: a) Representation of robots in top countries; b) Representation of robots in China

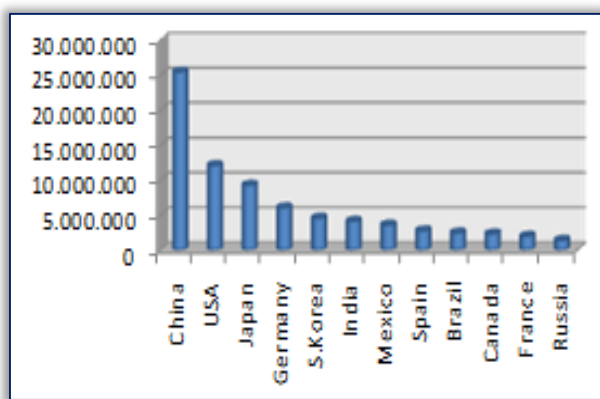
The predictions of representation of industrial robots in the coming period are given in Figure 3b). We can see that the increase of the representation is going to continue, and it will reach around 485.000 robot units in 2020. We need to conduct the analysis of the representation of industrial robots in top twelve countries in the world in 2015, as shown in Figure 4.

Among twelve countries in the world that have the highest representation of industrial robots in production processes in

2015 are the following: China, North Korea, USA, Japan, Germany, Taiwan, Italy, Spain, India, UK and Brazil. As we can see based on Figure 4a), the first place is held by China with 68.556 industrial robot units, followed by the countries in which the automotive industry is highly developed, such as North Korea, USA, Japan and Germany. If we look at the representation of industrial robots in production processes in China in the last ten years, Figure 4b), we see that it holds the first place in the last years, the reason being the strategy developed by China named "Made in China 2025", which aims to make China the leading technology country in the world. In order to determine the effect of such representation of industrial robots, we need to examine the percentage of the representation of industrial robots in the world in 2015 in different industries and vehicle production, which is shown in Figure 5 [6,13,14].



a)



b)

Figure 5. The percentage of representation of industrial robots in different industries worldwide in 2015, as well as vehicle production in top twelve countries in the world in 2015:

a) Representation of robots; b) Vehicle production

The first place by representation of industrial robots Figure 5a) is held by automotive industry with 39%, the second place is held by electrical/electronics industry with 25% and in the third place is metal industry with 12%.

Based on the image 3b), we conclude that China has installed most industrial robots in production processes in the automotive industry because they are the first in the world in vehicle production. In 2015 China produced close to 25 million vehicle units, followed by countries that are among top five countries in the representation of industrial robots in 2015: USA, Japan, Germany and North Korea.

In addition to development and increase of application of industrial robots in production processes, the development and increase of application of service robots in the production process is also growing. As an example, we take service robots for logistics in the production process, as shown in Figure 6 [3, 4, 17, 20].

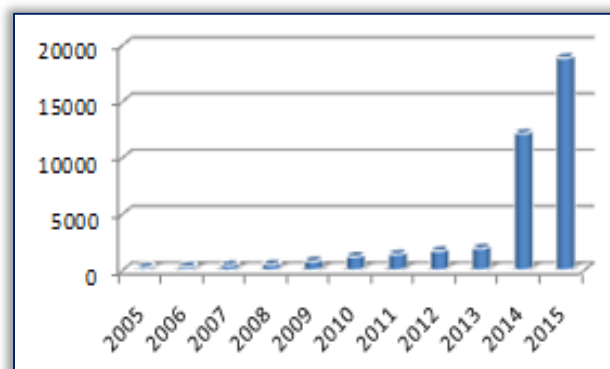


Figure 6. The representation of service robots for logistics worldwide for the period 2005-2015

The development of digital technology and the development of other technologies are contributing to the development of robotic technology, so that each year the representation of service robots for logistics in the production process is being developed and increased, as evidenced in Figure 6. It can be seen that in 2015 about 18.000 service robot units of different constructions and for different purposes are represented in the production processes. The convergence of digital technologies with other technology created the second generation of industrial robots, which will rapidly lead to the third generation of industrial robots that will be smaller than the current, less expensive, more autonomous, flexible and fully rendered, with simplified programming so that they can be programmed by workers.

The third generation of industrial robots is intelligent and autonomous robots and their improvement will be as follows: identifying specific objects, manipulation, knowledge, increase in computing performance, numerical remote controlling, working with miniature and complex products that require adjustment in the installation, reliability and precision that exceeds human capabilities.

For these reasons, industrial and service robots are presently at the center of automation of production processes, and in the future it will be impossible to create "intelligent automation" and "intelligent factory" without the participation of a new generation of robots, as shown in Figure 7.

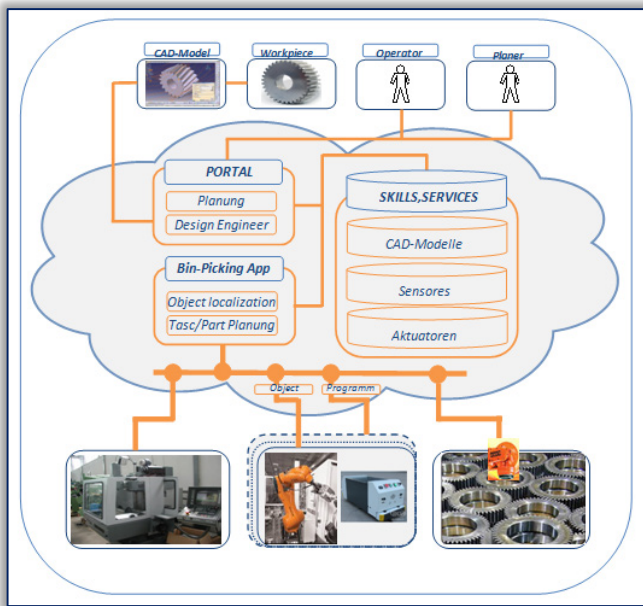


Figure 7. Intelligent production process of gear realized with digital and robotic technology

Digital technology and other technologies, which include robotic technology, are the foundation of every intelligent production, as is the case of production of gear shown in Figure 7. The advanced information technology enabled the design, simulation of actual plant at all stages of production (virtual reality), assembly, quality control, planning, management, diagnosis and optimization of production all from one place. This method leads to the highly productive production process, low cost and high quality of production.

## CONCLUSIONS

The development of digital, sensor, and robotic technology with other technologies and new materials is introducing the intelligent industrial development leading to the "intelligent factories". This is the period of the fourth industrial revolution based on intelligent production processes that use network technology and equipment for monitoring technology in order to have the means to adjust the production. Production system has the ability to reason, predict, simulate, self-configuration of optimal production system, independent learning and maintenance (using saved files and updates), automatic error diagnosis, problem-solving and maintenance. The new production system will have the ability to communicate with the machine and be complementary at different levels. All the above is impossible to achieve without the application of industrial and service robots in the production process. It is well-known that robotic technology is developing rapidly, and the industrial robots of the second generation are already installed in production processes, where they work alongside with the workers, whereas in the past they had to be separated by compartments so that they wouldn't hurt workers. In addition, service robots for logistics are being installed in the production processes, that are completely intelligent and communication related to the production machines. Intelligent automation allows greater flexibility in the

production, so that different products can be produced in the same production facility. Digital design and virtual modeling of production process enable us to reduce the time between the design of a product and its delivery to the market. In this way we acquire great improvements in product quality and a significant reduction of production errors. The fourth industrial revolution which includes digital and other technologies will lead us towards the "intelligent production" in the next 10 years.

## Note:

This paper is based on the paper presented at 13th International Conference on Accomplishments in Mechanical and Industrial Engineering – DEMI 2017, organized by University of Banja Luka, Faculty of Mechanical Engineering, in Banja Luka, BOSNIA & HERZEGOVINA, 26 - 27 May 2017.

## References

- [1] Verl A., (2016), Robotick & Industrie 4.0,ISW, Stuttgart, Germany.
- [2] Sulavik C., Portnoy M., Waller T., (2014), How a new generation of robots is transforming manufacturing, Manufacturing Institute USA, September 2014. Gaithersburg, USA pp.1-13.
- [3] Bunse B.; Kagermann H.; Wahister W.; (2015), Industrija 4.0. Smart Manufacturing for the Future, Germany Trade & Invest,Berlin,Germany.
- [4] Smart industry-a strategy for new industrialisatuon for Sweden, (2015), Government Offices of Sweden,Stockholm,Sweden.
- [5] Pires N., (2015), New development on Industrijal Robotics, Lisabon,Portugal, <https://www.robotics.dem.uc.pt>
- [6] Karabegović I., (2016), Role of Industrial Robots in the Development of Automotive Industry in China, International Journal of Engineering Works, Vol.3., Iss.12.,Kambohwel Publisher Enterprises, Multan, Pakistan, ISSN: 2349-6495, pp:92-97
- [7] Sulavik C., Portnoy M., Waller T., (2014), How a new generation of robots is transforming manufacturing, Manufacturing Institute USA, September 2014. Gaithersburg, USA pp.1-13.
- [8] Doleček V., Karabegović I.; (2008), Robots in the industry", Technical Faculty of Bihac, Bihac, Bosnia and Herzegovina.
- [9] World Robotics 2015, (2015),United Nations, New York and Geneva.
- [10] World Robotics 2013, (2013), United Nations, New York and Geneva,
- [11] World Robotics 2012, (2012), United Nations, New York and Geneva.
- [12] World Robotics 2008, (2008),United Nations, New York and Geneva.
- [13] Verband Deutscher Verkehrsunternehmen VDV:"Jahresbericht 2014/2015, Koln, Deutschland
- [14] Karabegović I.; Husak E.; (2016), China as a leading country in the world in automation of automotive industry manufacturing processes, IV International Congress Motor Vehicles & Motors 2016, "MVM-2016", 06-08. October 2016. Kragujevac, Serbia.
- [15] Jeschke S., (2015), Roboter in der Automobilindustrie, Fachkonferenz, 27 Oktober 2015, Augsburg, Germany.

- [16] Richard Kozul-Wright, (2015), Robots and industrialization in developing countries, UNCTAD/PRESS/PB/2016/6 (No. 50), United Nations Conference on Trade And Development UNCATD, Geneva, Switzerland, pp.1-4. [www.unctad.org](http://www.unctad.org)
- [17] Robotics 2020 Strategic Research Agenda for Robotics in Europe, Produced by euRobotics aisbl, Draft 0v42 11/10/2013, pp.25-43. <http://www.eurobotics-project.eu>
- [18] Guang-Zhong Yang, (2016), The Next Robotic Industrial Revolution, Manufacturing Robotics, Robotics and Autonomous Systems (RAS). UK-RAS Manufacturing Review 2015-2016 ISSN 2398-4422, pp.2-17. [www.ukras.org](http://www.ukras.org)
- [19] Good Jobs in the Age of Automation, BSR-The Business of a Better World, 2015, New York, USA, pp.1-28.
- [20] Fris D., Editorial, (2016), Universal Robots, Editorial\_WR\_Industrial\_Robots\_2016. [www.ifr.org/news/ifr-press.../world-robotics-report-2016-832/](http://www.ifr.org/news/ifr-press.../world-robotics-report-2016-832/)



ISSN: 2067-3809

copyright © University POLITEHNICA Timisoara,  
Faculty of Engineering Hunedoara,  
5, Revolutiei, 331128, Hunedoara, ROMANIA  
<http://acta.fih.upt.ro>



<sup>1</sup>Milan RADOŠEVIĆ, <sup>2</sup>Sebastijan BALOŠ, <sup>3</sup>Dragan RUŽIĆ

# METALLOGRAPHIC TESTS AND STRENGTH OF THE MATERIAL OF CHAINS SNOW

<sup>1-3</sup>University of Novi Sad, Faculty of Technology, Novi Sad, SERBIA

**Abstract:** Driver safety in winter conditions depends not only on the technical correctness of the transport vehicles, but also on winter equipment used. Snow chains, in addition to technically correct vehicles and tires, are one of the most important factors for driving safely on snowy roads. This paper presents an analysis of the quality of materials and anti-corrosion protection of snow chains that are frequently used in Bosnia and Herzegovina, Croatia and Serbia. For the purpose of analysis several tests were performed on tensioning the chains (at room temperature and at a temperature of -200C), hardness of the chains (Vickers method) as well as the test of the thickness of galvanized layer (metallographic method). All tests were performed in accordance with the relevant standards such as EN ISO 6507-1:2005; EN ISO 6892-1:2009; EN ISO 1461:200.

**Keywords:** metallographic test, straining, hardness, snow chains, safety and security in traffic

## INTRODUCTION

Safety and health of all road users represents a topic that has a very important role on the global level. In addition there is the fact that every day a variety of organizations around the world adopt new regulations when it comes to traffic safety, bring new acts and laws and so on. Agencies such as the AAA Foundation for Traffic Safety (founded in 1947), the World Road Association-PIARC (established in 1909), the Fédération Internationale de l'Automobile - FIA (founded 1904), and many others contribute to the rapid and successful development of the base for the adoption of legal directives in terms of traffic safety. The report of the Commission for Global Road Safety presents individual cases of successful countries such as Norway, Japan, Sweden, Australia, etc., in terms of the road safety. An example of good practice is certainly Vietnam, whose policies on the road safety in 2008 successfully reduced traffic accidents with the consequences of injuries by 12.2%, while the death consequences were reduced for 24.3% [1-5].

This work is divided into two parts. The first part will be related to the theoretical overview on the impact of snow in traffic accidents and factors affecting accidents during this period. The second part refers to the analysis of tire chains that are most common on the market of Bosnia and Herzegovina, the Republic of Serbia and the Republic of Croatia. The question proposed by the authors of this research was whether products, offered on the market, provide sufficient quality that allows traffic safety during their utilization. For the purposes of the chains' analysis the authors tested a straining (at room temperature and at a temperature of -20°C), hardness of the chains (Vickers-method), and the galvanized layer thickness by metallographic method.

## THEORETICAL BACKGROUND

As the focus of the paper is directed on winter conditions, in the continuation of the research we will focus on the elements that are involved in that annual period. Since in

winter period there are a significant number of accidents because of poor road conditions, it is important to note that in addition to the drivers, on more factor influence the number of accidents. Those are other road users - pedestrians. In their study Knoblauch, Pietrucha, & Nitzburg [6] conducted a survey in which it was included 7123 pedestrians. It was found that during the winter pedestrians are moving significantly slower than in other weather conditions, and particularly pedestrians whose age exceeds 65 years. Their speed of movement in winter conditions is amounted to 0.9 m/s in ratio to other weather condition, when the average speed was 1.2 m/s, while the younger population speed was 1.5m/s, and during the winter 1.2m/s.

Another factor affecting the traffic accidents are certainly the weather conditions. Hildebrand (2003) explored the visibility of signs in conditions of frost and snow. A very interesting study of other factors of snow on segments such as designing horizontal curves, the maximum rates of super elevation, etc., was issued by the Institute of Transportation Engineers [7].

Literary review does not provide a significant number of works dealing with the topic of the influence of using snow chains on car accidents, as well as the theme of the quality of tire chains that are on the market. Also, in the review of the available information by the European Commission - the EU's road safety policy, we cannot find a specific directive that deals with the topic of quality of snow chains. Only in the Commission directive 94/78/EC it is noted that „the manufacturer shall certify that the vehicle is so designed that at least one type of snow chain can be used on at least one of the types of wheel and tire approved for the drive wheels of that type of vehicle“ [8].

Olszewski et al. [9] presented a numerical analysis of the stress distribution in the car when the tires are snow chains, and they did not deal with the quality of chains. The authors have defined the snow chains as „an optional equipment of the vehicle consisting of two sections covering the rim of the tire,

connected by a series of chains or plates overlapping crosswise the tread”.

Another definition of snow chains is given by the European Commission where the snow chains are as defined ‘snow traction device’. „Snow traction device means a snow chain or other equivalent device providing traction in snow, which shall be able to be mounted onto the vehicle's tire/wheel combination and which is not a snow tire, winter tire, all-season tire or any other tire by itself” (Commission regulation (EU) No 1009/2010) [10]. Their primary function is to increase the traction of the vehicle in contact with the snowy or icy road.

Topolnik et al. [11] in his study analyzed the likelihood of passing vehicles by applying the appropriate equations and graphs, but this paper also does not include weather conditions and any additional equipment like snow chains. Tominc & Šebjan [12] showed that environmental and external factors have a significant impact on fatal injuries in road traffic accidents. According to them „traffic density and bed road conditions (wet and slippery road) lead to more cautious driving – individuals involved in an accident, where heavy traffic or wet and slippery road is the cause of accident, are approximately only half as likely to suffer from severe injuries as compared to those accidents where normal traffic density and dry road have been observed”.

As previously mentioned, the authors of this research decided to explore the level of the quality of snow chains that are provided by producers, which are presented on the market.

#### METALLOGRAPHIC TESTS AND STRENGTH ANALYSIS

For the purpose of testing the hardness we used the device for testing by Vickers hardness test "VEB HPO-250" in accordance with EN ISO 6507-1:2005. Measuring the thickness of galvanized layer was carried out with the light microscope "Leitz Orthoplan ", while for the purposes of the straining testing at room temperature and on the temperature of -20°C, the authors used a mechanical testing machine "WPM ZDM 9/91" of the maximum force of 50 kN, in working range of 25 kN, in accordance with standard EN ISO 6892-1:2009.

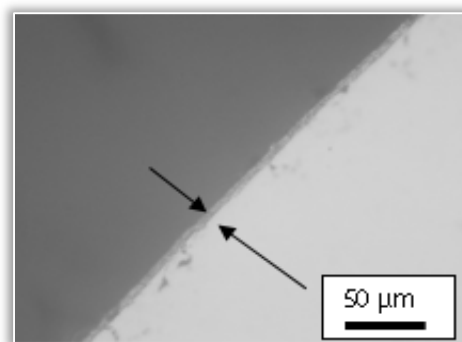
Measuring in the ambient of room temperature was carried out under controlled conditions at a temperature determined by the standard  $23^{\circ}\text{C} \pm 5^{\circ}\text{C}$ , while for the purpose of measuring a temperature from  $-20^{\circ}\text{C}$  the liquid nitrogen is used. Measurements were performed for each chain, with the thickness of 9mm, 12mm, and 16mm. In order to obtain a more precise measurement, for each complementary chain there are carried out 10 measurements, and for the final information the mean value of the rupture was taken.

To protect the discretion of the manufacturer, whose chains were used in the analysis, snow chains in the analysis will be labeled with "RS" – a manufacturer of snow chains is the company in the Asian region. Table 1 provides an overview of the surveyed value of breaking force in the [N], and measured hardness of the snow chains.

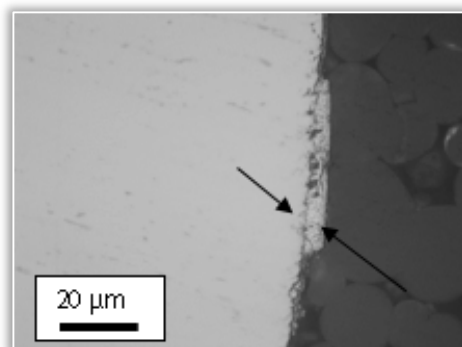
Table 1. Mean value of the breaking force and hardness of the snow chains, for n=10 measurements for each chain (source: the author)

Chain type	Thickness (mm)	Breaking force at ( $23^{\circ}\text{C} \pm 5^{\circ}\text{C}$ )		Breaking force at ( $-20^{\circ}\text{C}$ )		Hardness - HV30	
		No. of measurements	Mean value (N)	No. of measurements	Mean value (N)	No. of measurements	Mean value
A	9	10	3498	10	4773	10	217
	12		6245		6932		466
	16		15042		11935		415

Figures 1a and 1b show the surface galvanized layer. The thickness of this layer ranges from 0.002 to 0.02 mm (2 to 20  $\mu\text{m}$ ). Figure 1b presents variations of the thickness of galvanized layer.



a)



b)

Figure 1. Galvanized (zinc-coating) layer of the chains (thickness 9 mm)

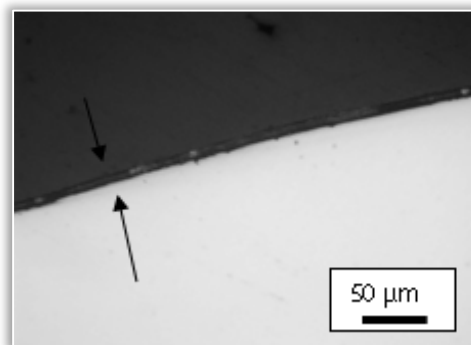


Figure 2. Galvanized (zinc-coating) layer of the chains (thickness 12 mm)

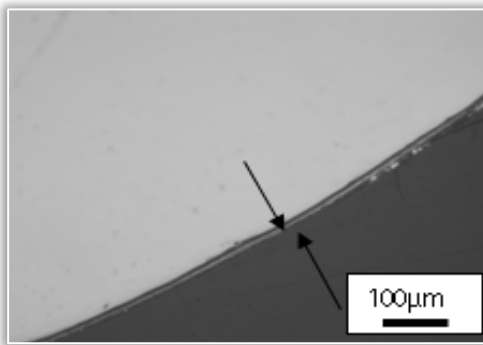
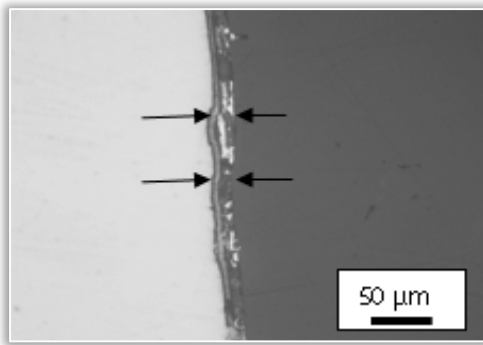


Figure 3a and 3b. Galvanized (zinc-coating) layer of the chains (thickness 16 mm)

Measured values of the galvanized (zinc-coating) layer of the chains of the thickness of 9mm (figure 1) ranges from 0,002 to 0,02 mm (2 do 20  $\mu\text{m}$ ), in case of the thickness of 12mm (figure 3) ranges from 0,006 to 0,009 mm (6 do 9  $\mu\text{m}$ ), and in case of chains with the thickness of 16mm (figure 4) it ranges from 0,012 to 0,025 mm (12 do 25  $\mu\text{m}$ ), which is significantly less than the value proposed by Standard EN ISO 1461:2009. This standard proposes the thickness of the layer (for chains from  $> 3\text{mm}$  to  $\leq 6\text{mm}$ ) of 55  $\mu\text{m}$  do 70  $\mu\text{m}$ . Also, on several samples there were evident variations in the thickness of the galvanized layer (figure 1b and 3a). These variations (unevenness) in the thickness of the galvanized (zinc-coating) layer are probably related to the poor quality of the process of zinc coating or low quality of the preparation of material before zinc coating process.

### CONCLUSIONS

The analysis of the tightening of the chains at the room temperature and at a temperature of  $-20^{\circ}\text{C}$  pointed that there is an inconsistency in the thickness of the individual chains. For the chains of 9mm thickness it can be concluded that the chains at room temperature having an average value of tensile strength of 3498 N and at temperatures below 4773 N, which is a good ration and preferred values for the operating conditions. Chains with the thickness of 12 mm at room temperature having an average value of tensile strength of 6245 N and at temperatures below 6932 N which is a good, but not so great ratio of differences of the values for the operating conditions.

Also, these chains have twice higher hardness compared to chains of 9mm thickness. 16mm chains at room temperature having an average value of the tensile strength of 15042 N at the lower temperatures 11935 N which represents a very

unfavorable ratio and values of operating conditions. In other words, chains of 16 mm thickness have a significantly lower exploitation value, and lower hardness in relation to the chains of 12mm thickness. The study found significantly lower values than those recommended by the standard EN ISO 1461:2009, which recommended zinc-coating thickness for elements of a thickness from  $> 3\text{mm}$  to  $6\text{mm} \leq$  of 55  $\mu\text{m}$  do 70  $\mu\text{m}$ . Also, some samples were found to have unevenness in the thickness of the coated layer.

During the analysis of new snow chain it has been noted that on some chains there is the presence of corrosion, which the maximum measured thickness is 0.2 mm (200  $\mu\text{m}$ ). The presence of corrosion is probably the result of poor thickness of galvanized layer which is not in accordance with the standards SRPS EN ISO 1461:2005, identical to EN ISO 1461:2009 and which is prescribed by the Institute for Standardization of Serbia. Also, there have been observed unevenness in the thickness of the zinc coating layer which indicates a low-grade galvanizing or poor preparation of the material before the process of galvanization. The corrosion would certainly have a more aggressive development on the chains and the quality of galvanized layer in real conditions (the influence of water – snow, salt on the roads).

Based on the above mentioned, it is concluded that the quality of snow chains which are the most common on the market is quite questionable. As a continuation of the research authors will provide a comparative analysis with other snow chains that are present on the market of Bosnia and Herzegovina, Serbia and other countries in the region.

### Note

This paper is based on the paper presented at 13th International Conference on Accomplishments in Mechanical and Industrial Engineering – DEMI 2017, organized by University of Banja Luka, Faculty of Mechanical Engineering, in Banja Luka, BOSNIA & HERZEGOVINA, 26 - 27 May 2017.

### References

- [1] Fastenmeier, W., Gstalter, H. (2007) Driving task analysis as a tool in traffic safety research and practice. *Safety Science*, vol. 45, no. 9, pp. 952-979.
- [2] Ewing, R., & Dumbaugh, E. (2009). The Built Environment and Traffic Safety A Review of Empirical Evidence. *Journal of Planning Literature*, vol. 23, no. 4, pp. 347-367.
- [3] Bojić, Ž., Radošević, M., Čosić, I., Morača, S., Avramović, N., Antić, A. (2017). The analysis of the impact on the safety of traffic participants and causing the accidents of working machines – tractors. *Tehnički vijesnik – Technical Gazzete*, vol. 24, no. 5 (accepted paper)
- [4] Make Roads Safe, A Decade of Action for Road Safety. London, Commission for Global Road Safety, 2011 [http://www.makeroadssafehellas.com/images/stories/publications/decade\\_of\\_action\\_report\\_lr.pdf](http://www.makeroadssafehellas.com/images/stories/publications/decade_of_action_report_lr.pdf)
- [5] Elvik, R., Vaa, T., Erke, A., Sorensen, M. (2009). The handbook of road safety measures. Emerald Group Publishing, 2009.
- [6] Knoblauch, R., Pietrucha, M., & Nitzburg, M. (1996). Field studies of pedestrian walking speed and start-up time. *Transportation Research Record: Journal of the Transportation Research Board*, vol. 1538, pp. 27-38.

- [7] Institute of transportation engineering. (2016). Traffic engineering handbook. 7<sup>th</sup> edition, Wiley
- [8] Commission directive 94/78/EC (1994). Official journal of the European Communities, No. L 354, pp. 10-15
- [9] Olszewski, Z., Waluś, K., Krawiec P., Warguła L. (2015) Numerical Analysis of Stress Distribution in a Car Tire Equipped with Snow Chains, Machine Dynamics Research, vol. 39, no. 1, pp. 135-142
- [10] Commission regulation (EU) No 1009/2010, Official Journal of the European Union, Vol. L292, pp. 21-29
- [11] Topolnik, D., Zebec, Z., Horvat, R. (2000). Overtaking as indicator of road traffic condition. Traffic safety. vol. 12, pp. 213-216
- [12] Tominc, P., & Šebjan, U. (2015). The Impact of Selected Individual and External Factors on the Occurrence of Severe Injuries: Case Study of Slovenia. PROMET-Traffic & Transportation, vol. 27, no. 4, pp. 325-334.



ISSN: 2067-3809

copyright © University POLITEHNICA Timisoara,  
Faculty of Engineering Hunedoara,  
5, Revolutiei, 331128, Hunedoara, ROMANIA  
<http://acta.fih.upt.ro>

<sup>1</sup>Igor SHESHO, <sup>2</sup>Done TASHEVSKI, <sup>3</sup>Filip MOJSOVSKI

# METHODOLOGY FOR TECHNO–ECONOMIC OPTIMIZATION OF SOLAR ASSISTED HEATING SYSTEMS

<sup>1-3</sup> Faculty of Mechanical Engineering, Skopje, MACEDONIA

**Abstract:** This paper has objective, to estimate the thermal performance of solar assisted heating systems in regard of solar fraction and perform life cycle cost analysis to assess the feasibility of their implementation in residential sector. In general it is known that the resource for solar thermal systems i.e. the solar irradiation is free, but the equipment to collect it and convert in to useful form (heat or electricity) has a cost. Solar thermal systems are characterized by high investment and low operational cost. It is presented methodology for obtaining the right size of a solar thermal assisted heating system that gives the lowest combination of solar and auxiliary energy costs. Thermal performance of the solar thermal systems are estimated using numerical methods and software since the solar processes are transient in nature been driven by time dependent forcing functions and loads. The system components are defined with mathematical relationships that describe how components function. They are based on first principles (energy balances, mass balances, rate equations and equilibrium relationships) at one extreme or empirical curve fits to operating data from specific machines. As a result of the analysis specific indicators are derived in order to facilitate the techno-economic analysis and design of solar assisted heating systems.

**Keywords:** solar assisted heating systems, thermal performance, specific indicators

## INTRODUCTION

Reduction of fossil fuel consumption and harmful emissions to the environment could be reduced by implementing the solar energy in heating and cooling of the buildings. It is well known that in the European Union more than 25% of the total energy consumption is due to buildings with heating and cooling representing a major percentage. In the EU–32 countries the final energy consumption in 2003 for heating and cooling the buildings represented about 3600 TWh with 93% for heating and only 7% for cooling [1]. But a tremendous increase in the market for air–conditioning can be observed worldwide especially in developing countries such as Macedonia.

On Figure 1 are presented the sales rates for room air–conditioners (RAC units) in different regions of the world (blue representing worldwide sales and green one European ones). In 2002 were sold 44 million units worldwide and more than 94 million units in 2012 (source by Japan Air–conditioning & Refrigeration News 2013). In order to limit the negative impact on the energy consumption and on the electricity network management, new environmentally sound concepts are of particular importance.

Energy consumption in Europe is expected to face an increase within the next 30 years. This is due the climate and comfort requirements, architecture and technical equipment of larger, commercial buildings require more and more cooling. Space cooling is moving quickly from luxury into necessity and represents a fast growing market. The rise in cooling demands is due to more reasons such as: greater comfort expectations, the perception that cooling contributes to higher productivity and the increase of internal loads of electronic equipment.

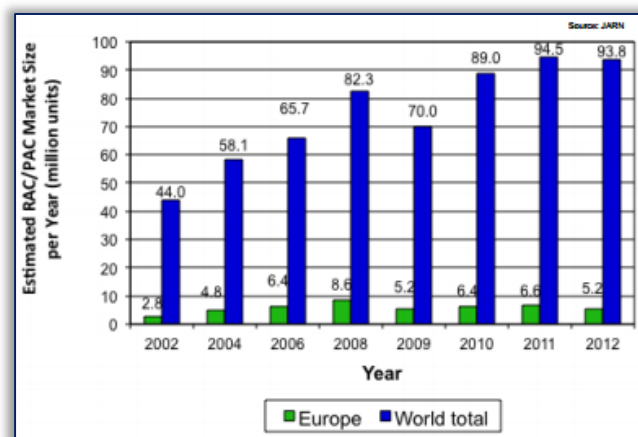


Figure 1. Evolution of air–conditioning market worldwide  
By 2020 all new and refurbished buildings should be near zero energy. So the cooling demand will have to decrease. But this means as well that a massive use of renewable energy sources will have to be done.

Building air–conditioning is today based mainly on electrically driven mechanical vapour compression technologies. In [2], R. Ciconkov performed survey on refrigerating and air–conditioning systems regarding the use of CFS fluids in Macedonia Although for new developed predominately large capacity scale developments it is reported about high efficiencies in the compression cycle, for the standard air–conditioning in existing buildings can be assumed that on an average less than 3 kWh ‘cold’ are produced with the electricity input of 1 kWh<sub>el</sub>. Subsequently this implies that 1 kWh primary energy is used for the provision of 1 kWh useful cooling energy. Until now mostly the electrical peak loads were occurring during the winter period, but now are shifting to the summer months and

challenging capacity limits and therefore increasing the need of solar cooling technology even in Europe. In [3] is examined TEWT concept for estimating of the global warming from refrigerating and air-conditioning systems.

Solar technologies can supply the energy for all of the building's needs—heating, cooling, hot water, light and electricity—without the harmful effects of greenhouse gas emissions created by fossil fuels thus solar applications can be used almost anywhere in the world and are appropriate for all building types.

Solar thermal systems for hot water production are already mandatory in new buildings according to solar ordinances for example in Spain [4], Portugal, Italy, Greece and other European countries [5].

It is very logical to apply solar energy for cooling purposes since in many applications, such as air-conditioning cooling loads and solar gains are more or less in phase on daily time basis. Thermally driven cooling was applied within last decades in niche-markets preferably in the large capacity scale range, using waste heat or heat from combined heat and power production. A survey made on the basis of IEA Task 38 and Task 48 work has shown the estimated number of installation worldwide nearly of 600 systems in 2010 and nearly 1000 systems in 2012.

In 2013, Solar Air-Conditioning is more than ever representing a huge potential of development for solar energy but this promising technology is facing one main issue, a general lack of economic competitiveness – as it is still the case for many renewable energies unless incentives are in place.

#### **SIMULATION SOFTWARES FOR SOLAR THERMAL SYSTEMS**

In order to assess the performance of the solar air-conditioning system under weather conditions for Macedonia, simulation model is developed for solar assisted air-conditioning system applied in residential building.

Simulation in solar cooling and air-conditioning is possible at different levels. A classification may be made by sorting the tools into:

- materials level – analyzing the effect of e.g. different sorption materials on the sorption process;
- component level: detailed analysis of a system component, e.g., chillers, cooling towers, etc.
- process quality level: theoretical analysis of various processes.
- detailed system simulation for optimizing control strategies

Few simulation programs for planning support and sizing of solar assisted air-conditioning systems exist. Also some more programs used internally may exist; additionally, more commercial simulation platforms like Matlab/Simulink, Modelica, etc. can be used, but do not provide of a sufficient number of components for modeling a complete solar air-conditioning system yet.

In this paper is used TRNSYS simulation software and the TESS library for the system component numerical models.

TRNSYS is a commercial time step simulation tool worldwide available. High flexibility in the choice and arrangement of the system components, the desired system can be constructed by selecting and connecting the individual components and by defining the system control. Own written, types'(component models) may be added. Once the time step of the simulation is chosen, it is constant during the simulation run. A major advantage of the program is the availability of a building model, which can be edited in a special building editor and allows the calculation of building loads.

#### **SOLAR SYSTEM COMPONENT DEFINITION**

Up to now, existing SHC prototypes were mostly designed on an empirical basis. For small-size systems, simple layouts are generally preferred, in order to improve the reliability and reduce the capital cost of the plant. For example, fixed-volume pumps are selected, and a gas-fired heater is used as the only auxiliary device. For large-size plants, more expensive but also more efficient components can be taken into consideration, such as variable-speed pumps and auxiliary electric chillers. In any case, the main choices to be taken when designing the layout of a SHC system concern:

- the type of solar collectors;
- the thermal-driven chiller (for example, absorption or adsorption machine);
- the auxiliary system for cooling and heating have been developed.

Usually, SHC systems are based on absorption chillers, since the commercial availability of adsorption chillers is very scarce. In addition, adsorption chillers are only available for small cooling capacities, and their cost is significantly higher than for absorption chillers. Thus, most of the SHC prototypes installed all over the world are equipped with an absorption chiller. Single-effect absorption chillers are usually adopted, since double-effect devices must be supplied with an hot stream at temperature higher than 150°C, that would involve the use of concentrating solar collectors [6]. Such configuration – high temperature solar collectors and double-effect chillers – is obviously interesting from an energetic point of view, but is presently too expensive to be considered in pre-commercial applications.

Thus, the most common configuration is based on the coupling of evacuated-tube solar collectors with single-effect absorption chillers. In particular, LiBr-H<sub>2</sub>O models are commonly preferred, since H<sub>2</sub>O-NH<sub>3</sub> chillers require higher temperatures for the inlet hot stream, and in addition handling ammonia can be somewhat dangerous. For such arrangement, three different system layouts were investigated in this paper, whose characteristics and working principles are briefly summarized in the following:

The model i.e. analyzed system, generally consists of four main subsystems:

- First subsystem is composed of solar collectors with complete hydraulic fittings and control – differential controllers, plate heat exchangers ie this system is

represented the source of thermal energy for heating or thermal energy for driving the cooling the absorption machine

- Second is the subsystem for hot and cold storage which includes the storage tanks for hot / cold water that actually represents the connection between the heating system in the building ie absorption cooling machine and the source of heat.
- The heating system introduced with heating / cooling devices, hydraulic components, heat exchangers, cooling absorption machine and eventually existing conventional sources of heat and / or cooling energy.
- The fourth subsystem is the consumer of thermal energy ie the building. This system is represented by the thermal characteristics of the object, i.e its orientation in space.

In the analyses are considers vacuum tube and flat plate collectors product of Camel Solar, type: CS Full Plate 2.0–4 and Vacuum CS 10. The thermal performances of the solar collectors are given in their solar key mark certificate.

At the simulated building internal heat gains are consider by the lighting power density 5 W/m<sup>2</sup> and home appliances with specific power of 2 W/m<sup>2</sup>. The absorption chiller condenser is connected to the wet cooling tower product of Baltimore AirCoil type PF2–0406AA–31–3. Numerical modeling of the cooling tower is provided by the TRNSYS Type510 model from Tess library, a closed circuit cooling tower which cools the liquid stream by evaporating water from the outside of coils containing the working fluid. The working fluid is completely isolated from the air and water in this type of system.

The cooling system in the building is represented with ventilation air distribution system. The heat exchange between the chilled water from the absorption chiller and the ventilation air is provided with heat exchanger water–air modeled Type 508a which is a cooling coil modeled using a bypass approach in which the user specifies a fraction of the air stream that bypasses the coil. The remainder of the air stream is assumed to exit the coil at the average temperature of the fluid in the coil and at saturated conditions. The two air streams are remixed after the coil. Chilled water flow from the absorption chiller to the cooling coil is set to 2900 kg/h and the air flow rate to the building is 4000 kg/h. The auxiliary heater power is modeled 12 kW and the outlet temperature is 80°C, which is the absorption machine driving temperature.

### SYSTEM COMPONENT MODELS DEFINITION AND VALIDATION

Validation is performed for the basic solar thermal system components: solar collector, storage tank and differential controller. The experimental system consist of: flat plate solar collector with area of 2 m<sup>2</sup>, connected with the internal heat exchanger of the storage tank. Control is provided by differential controller which is set to turn the circulation pump on, when the temperature difference between the collector outlet temperature and the tank temperature is greater than five. There is no consumption of hot water from

the storage tank i.e. the only heat transfer is with the surroundings. The circulating pump is set to maintain fluid (water) flow rate set to 7.5 lit/min.

Measurements are made on at an hour interval for the fluid inlet T1 and outlet T2 temperatures from the solar collector, tank fluid temperature T3 and the solar radiation is measured with the pyrometer S as presented on Figure 3. The experimental setup of the analyzed solar thermal system is located in Skopje, R. Macedonia, northern latitude of 42° and 21.43° east longitude. Temperature measurements are performed with temperature data logger thermocouple probes type K.

Solar collector type is evacuated tubular direct flow, product of Camel Solar type Vacuum CS 15 Solar KeyMark certified. During the measurements was placed under tilt of 45°, south orientated i.e. azimuth angle of 0°. The collector thermal performance test results according EN 12975 are presented in Table 1.

Table 1. Reference building physical and thermal performance data

Surface	Orientation	Area, m <sup>2</sup>	Building I Building II Building III		
			U value, W/m <sup>2</sup> K		
Out.wall 1	North	42	0.58	0.33	0.18
Windows 1	North	3	1.40	1.40	1.40
Out.wall 2	East	25.5	0.58	0.33	0.18
Windows 2	East	4.5	1.40	1.40	1.40
Out.wall 3	West	25.5	0.58	0.33	0.18
Windows 3	West	4.5	1.40	1.40	1.40
Out.wall 4	South	42	0.58	0.33	0.18
Windows 4	South	3	1.40	1.40	1.40
Floor	-	150	0.33	0.33	0.24
Roof	-	150	0.54	0.42	0.35
Window type	Double glazed TRNSYS library (w4-lib data)				
Windows solar heat gain coefficient;g-value	0.589				
Out.wall construction	2 x Plaster 2cm, brick 25cm	Insulation 5 cm	Insulation 10 cm	Insulation 20 cm	
Floor	Granite tile 6cm, cement mortar 5cm, concrete slab 20cm	Insulation 10 cm	Insulation 10 cm	Insulation 15 cm	
Roof	Concrete slab 20cm, hydro isolation, cement mortar 5cm	Insulation 15 cm	Insulation 20 cm	Insulation 25 cm	
Outside convective heat transfer coefficient	$\alpha_{out} = 25 \text{ W/m}^2\text{K}$				
Inside convective heat transfer coefficient	$\alpha_{in} = 7,7 \text{ W/m}^2\text{K}$				

In the TRNSYS model solar collector is model with the Type 538 from the Tess library with commercial solar collector performances used from Solar Key Mark certificate for producer CamelSolar. The storage tank is modeled with the Type 60d including the internal heat exchanger for which are supplied technical data from the producer “Sun System”. Type 2b–2 is used to simulate the differential controller set with upper dead band of 5 and lower dead band 2, the high limit cut–off temperature set to 100°C. Between the solar collector and storage tank is connected pipe Type 31 modeled with internal diameter 0.0025 m, length of 10 m and loss coefficient of 0.3 W/m<sup>2</sup>K to account for the heat losses.

The pipe network modeled with Type 31 is used to increase the thermal capacity of the system and thus increase the simulation stability. Circulating pump is represented with the component Type 3d with mass flow rate 450 kg/h i.e. 7.5 l/min same as in the experimental setup 2.

Measurements are performed starting from date 18.09.2013 until 28.03.2014 and in parallel are measured two systems with same capacity storage tank of 150l but different type of collector's i.e. flat plate and vacuum tube solar collectors. Validation process use data for the vacuum tube collector and the results are presented only for one day period (18.09.2013) with collection time interval ranging between 20min and 45min interval, from 10:40 up to 16:05 h.

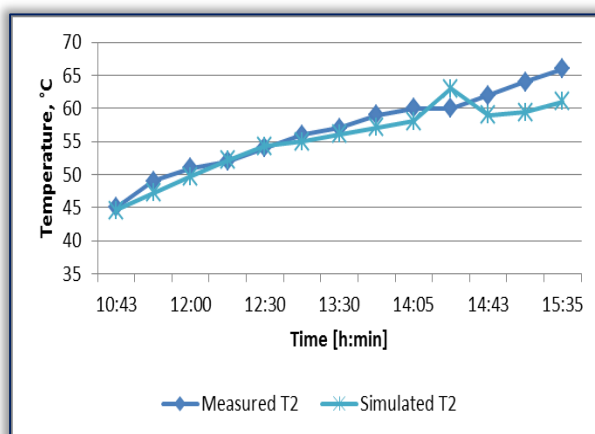
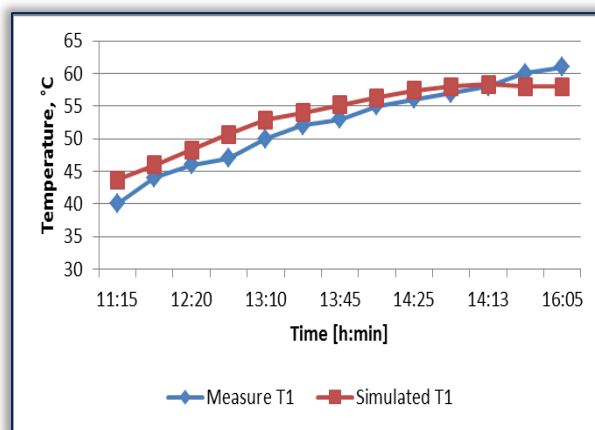
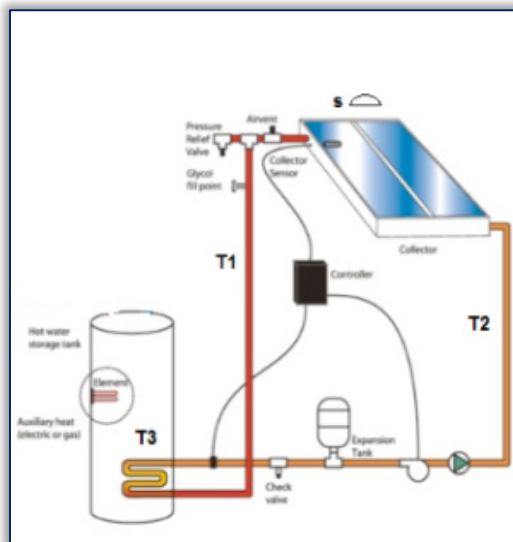


Figure 3. Measured and simulated results for the collector inlet and outlet temperature

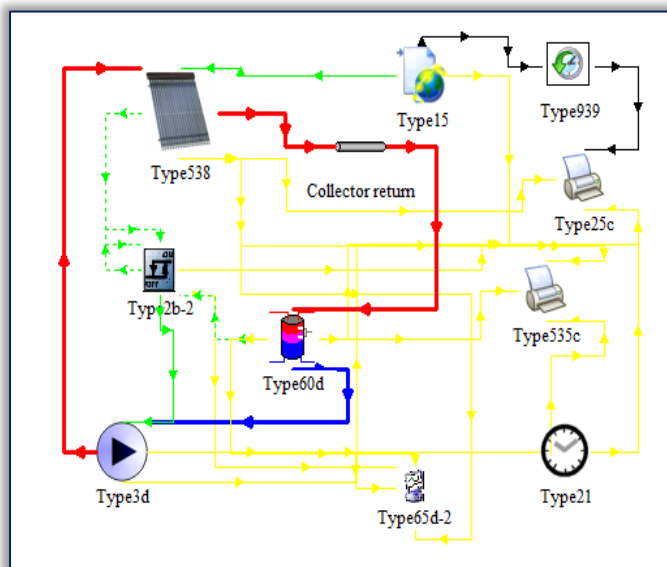


Figure 2. Solar system experimental and simulation scheme

According above presented data i.e. diagrams can be concluded that there is acceptable match between the measured and simulated results Figure 3, and Figure 4. The discrepancies between the measured and simulated results are expected since the solar radiation has different values i.e. simulated values are taken from the Meteororm database for the selected location while the measure are obtained directly for the specific location as given on Figure 6.

Another influencing factor is the uncertainty of the measurements error and last but not the least it should not be neglected the transition nature of the solar thermal systems.

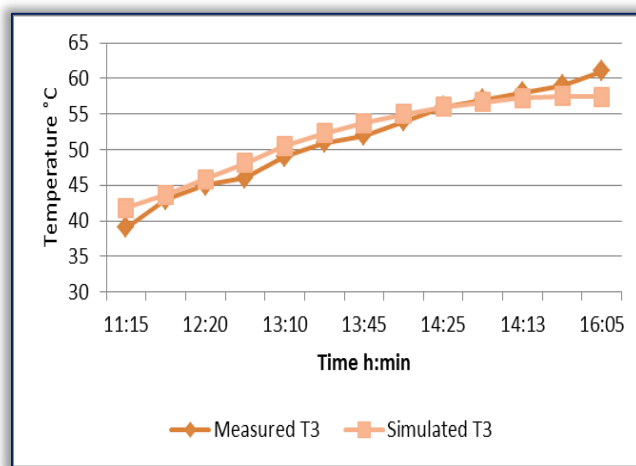


Figure 4. Measured and simulated temperatures inside storage tank

The resulting simulations reveal the individual thermal behaviour of the solar collector, storage tank, differential controller and circulating pump as well as their assembled thermal behaviour. These results coincidence with the respective experimental data, thus this fact validates these models for future application in the heating/cooling system. Validation for the absorption chiller is performed for the TRNSYS component Type 177.

This component type offers four numerical modes of absorption chiller. In this simulation is used mode "a" i.e. Type



177a which is standard mode using user supplied characteristic parameters. Since in this paper are considered only solar air-conditioning for residential buildings. In the simulation is modelled the absorption chiller  $H_2O/LiBr$  produced by Sonnenklima type Suninverse 10. Simulation of the absorption chiller is done with the component Type 177a, whereas input parameters are used the values for Suninverse provided in Table 3. As output for the absorption chiller cooling power is obtained 10,1 kW, which corresponds with the factory value. Validation exists for the Type 177 mode “d” performed by Albers and Ziegler [7], using the measurement results from Kühn [8]. According to this, final conclusion is that this numerical model of absorption chiller provides reliable results, thus it is suitable to be used as model for further simulations.

### ASSESSMENT OF THE SOLAR AIR-CONDITIONING SYSTEM

Because of the interactions of components, optimal system performance occurs under conditions different from those for optimal behaviour of each component. For example, optimal collection efficiency would not necessarily be coupled with least auxiliary energy.

Many different hydraulic schemes are designed which makes difficult to compare the installations performances [9]. Methods used to determine solar heating and/or cooling energy requirements for both active and passive/hybrid systems are described by Feldman and Merriam, Hunn, Nowag and other. For thermally driven systems the scheme on Figure 5 is used to identify main components and energy flows of the system. On Figure 5 is presented small scale system for family houses, small multi dwellings, using a small size packaged ab/adsorption solar system. This configuration is an adaptation of the solar combi-system including the cooling function is also called SSC + Solar Combi.

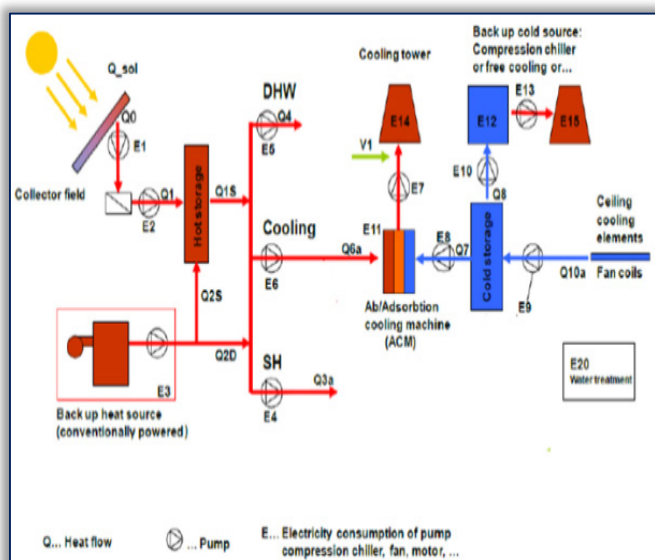


Figure 5. Components and energy flows for solar air-conditioning system

There are four generally accepted measures of solar system performance:

- Collector efficiency applies to the performance of the solar energy collection subsystem. It is the energy collected, divided by the radiation incident upon the collectors. Influence of the collector position on the collector thermal efficiency is done in [10].
- System efficiency, or solar heating performance factor is the solar heat delivered to the load divided by the total radiation incident upon the collector.
- Solar fraction is the fraction of the total heat requirement that is met by solar energy.
- Electrical coefficient of performance is the solar heat delivered to the load, divided by the electrical energy used to operate the system.

Each solar system operates at characteristic efficiency level resulting from the interaction of the subsystems, environmental conditions and system configurations. The net savings per square meter of solar collector indicate the relative performance of each of these systems.

The five categories of system-level design parameters that limit solar system performance.

- Solar resource assessment. This category represents the solar reference weather data values used by the solar design community
- Collection subsystem. This category represents the solar collection sub-system, including devices used to capture incoming solar radiation
- Storage subsystem. This category deals with all aspects of the system effects caused by storage components.
- Controls. This category refers to equipment and methods for controlling solar components within the solar system

This category deals with the types and magnitude of the heat requirements in the buildings

### MODEL OF REFERENCE BUILDING

Building as energy consumer has a major impact on the overall efficiency of the solar system i.e. can be simply said that the building itself is one of the leading parameter in sizing the system. Since the analyses are made for climatic conditions in Macedonia also the thermal performance of buildings must be in accordance with the Regulations on energy efficiency in Macedonia. Furthermore the analysis is taken into account the impact of the specific consumption of heating / cooling energy of the building  $kWh/m^2 a$  to the response and the performance of the solar collector system.

Main governing indicators according to which is based the system comparison are: thermal efficiency of solar collectors, solar fraction and power consumption for the auxiliary devices.

In Table 1 are listed three “types” of the building i.e. physically is the same building only the insulation thickness on the external walls, roof and floor are varied in order to obtain different values for specific annual heat. The main idea for this analysis is to assess the influence of the thermal performance of buildings on the economic viability of the use of solar thermal systems in air-conditioning.

Constant value of 0.3 1/h is defined for the infiltration of outdoor air, while for the summer when cooling is required in the building is envisaged/ modeled mechanical ventilation defined with air mass flow and temperature entered through the models of fan and heat exchanger air–water which is directly connected with the cooling absorption machine.

Regarding the thermal comfort, in the heating mode the inside temperature is defined to be 20°C from 05:00 – 22:00 and for the rest is defined setback temperature of 16°C, for the cooling mode is defined constant inside temperature of 26°C. Building I has 90 kWh/m<sup>2</sup>a, Building II with 70 kWh/m<sup>2</sup>a and Building III has 57 kWh/m<sup>2</sup>a. Comparing the energy consumption Building III has 42% lower than Building I and 19% than Building II.

The performance of future conventional space–conditioning systems affects the economic potential of active solar systems. The performance and cost of today's conventional heating, cooling and domestic hot water system can be readily determined, but conventional heating and cooling technology is constantly improving

In the analysis for the heating considered two reference: Buildings Type II and III (as given in Table 1), with specific heat energy consumption of 70 kWh/m<sup>2</sup>a and 57 kWh/m<sup>2</sup>a respectively. In the analysis for the cooling is considered only Building type III which has specific cooling energy of 12 kWh/m<sup>2</sup>a. The time step used in the simulations is 7.5 min and the heating and loads are integrated on hourly basis. On Figure 6, are presented the results from the simulation of solar assisted heating with flat plate collectors varying their total area 16 m<sup>2</sup>, 32 m<sup>2</sup>, 64 m<sup>2</sup> mass flow rates are 50 kg/h m<sup>2</sup> and heat storage tank of 1000 l and 2000l only for the 64 m<sup>2</sup> collector area. Collectors are tilted 40° toward south – azimuth 0° also is installed 200l DHW storage tank heating with the same collector array only in period when the heating storage tank is charged or the condition for the circulation pump is not satisfied.

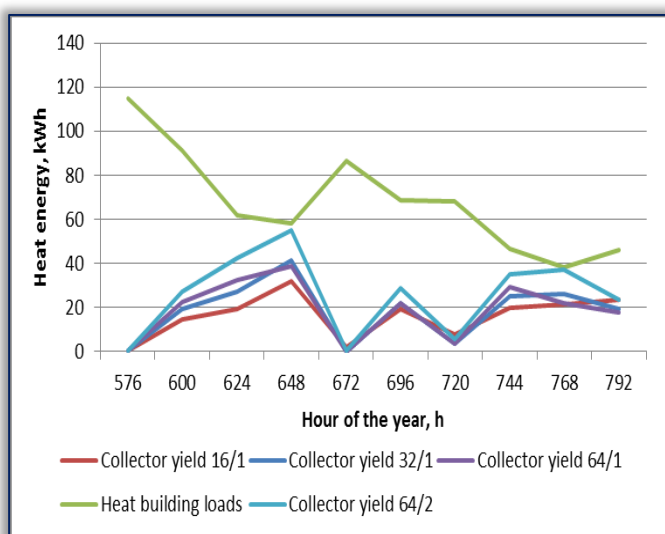


Figure 6. Hourly heating loads and collector energy yield for different areas ten day period

Common for the analysed systems is that in each of them the heat is distributed through the underfloor heating with flow rate of 2000 kg/h, solar collector array mass flow rate depending from the collector area i.e. 50 kg/h m<sup>2</sup>, auxiliary heat energy is provided by heater located at the fluid tank outlet with capacity of 12 kW connected with the generator of the absorption cooling machine and 9 kW for the DHW installed also at the tank hot water outlet set to maintain constant temperature of 45°C.

From the obtained results it is concluded that there are no large differences between the solar collector yield of 32 m<sup>2</sup> and 64 m<sup>2</sup>. This is result of the small storage tank capacity which cannot store the available heat from the 64 m<sup>2</sup> collector array solar/heat yield resulting in storage temperature increase thus decrease in solar fraction and collector efficiency.

On Figure 6 are also presented collector yields only for ten days.

### OPTIMIZATION METHODOLOGY

In solar system energy design the collector area is considered as the primary parameter for a given load and system configuration. The collector area is also the optimization parameter i.e. the aim is to find the collector area that gives the highest life cycle savings.

A method for the economic optimization is considered in which life cycle savings are plotted against collector area  $A_c$ , to find the area that maximises the savings. The optimization procedure is simplified if life cycle savings (LCS) are expressed mathematically in terms of the collector area. Therefore the optimum is obtained when:

$$\frac{\partial LCS}{\partial A_c} = 0 \quad (1)$$

The maximum savings are obtained when the relationships between the collector area and solar fraction satisfies the following relation:

$$\frac{\partial F}{\partial A_c} = \frac{P_2 C_A}{P_1 C_{F1} L} \quad (2)$$

where :  $P_1$  – ratio of life cycle fuel cost savings to first year fuel savings,  $P_2$  – ratio of life cycle expenditure incurred from additional investment to the initial investment,  $L$  – load (GJ),  $C_{F1}$  – first year unit energy cost delivered from fuel,  $C_A$  – area independent costs

The economic evaluation of a solar application includes factors such as the capacity cost of delivering solar energy, the optimum sizing of collectors and other equipment the costs of competing technologies and financial analyses. There figures of merit that are used to accept or reject particular solar application including simple payback, cash flow, capital cost per unit of energy saved, life cycle cost, net present value and levelized energy cost.

For a range of economic assumptions, an analysis considering a 5 or 7 year simple payback is assumed to be an adequate figure of merit to establish cost goals for active solar cooling

and heating technologies. For residential applications, a payback period of 5–7 years may consider as acceptable.

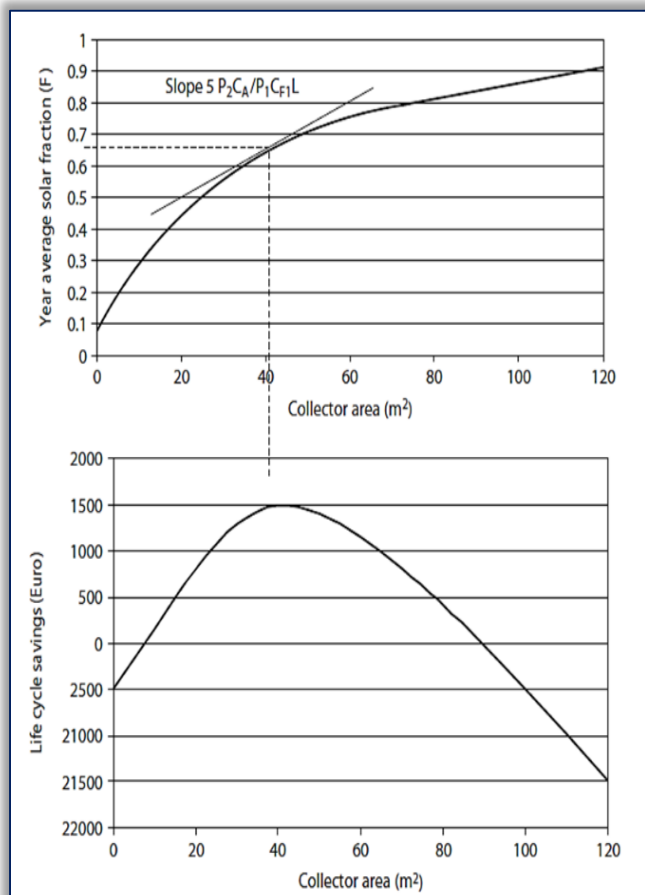


Figure 7. Optimum collector area determination from the slope of the F versus  $A_c$  curve

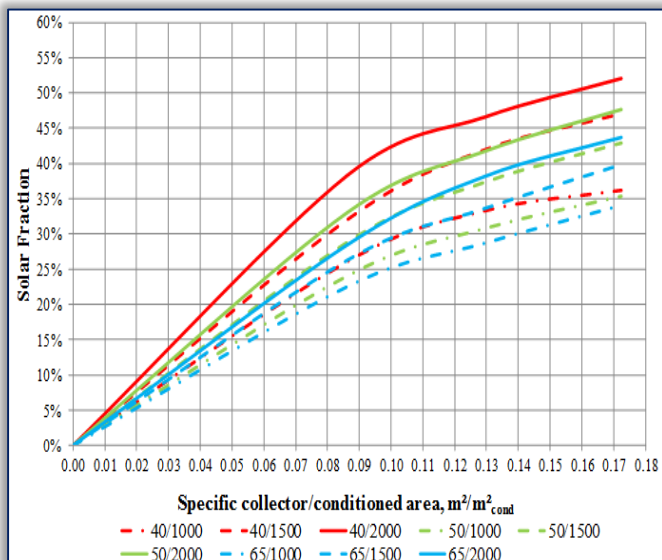


Figure 8. Function dependence between solar fraction in regard of ration solar collector area and building specific heat energy consumption

Comparison is performed between different combinations of solar thermal systems and auxiliary heating devices in regard of conventional heating system with electrical boiler. The analyzed solar systems have total solar collector area of 16 m<sup>2</sup>,

32 m<sup>2</sup> and 64 m<sup>2</sup> combined with storage tanks of 1000 l, 1500 l and 2000 l, and auxiliary heating energy provided by electric heater or heat pump air–water with E.V.I compressors with nominal capacity of 15 kW product of Hidros model Lzti 10.

On the next Figure 8 are presented simulation results for the solar fraction savings regarding solar collector area, accumulator storage volume and type of building i.e. specific heat consumption.

### CONCLUSION

In this paper were assessed the thermal performance of solar assisted air–conditioning system for residential buildings for weather conditions in Macedonia. Within the analysis are covered several solar thermal systems varying the collector area, hot water storage tank and the auxiliary heat source. It is performed verification on the model for solar assisted air conditioning system which provides reliable results i.e. can be used for further analyses.

Methodology is derived according to which can be determined optimal solar collector area and buffer tank in regard of building energy performance generating maximum life cycle cost savings. From the simulation results is generated diagram according to which can be derived the specific savings–solar fraction in regard of the solar collector area, buffer tank and building energy performance.

### Note

This paper is based on the paper presented at 13th International Conference on Accomplishments in Mechanical and Industrial Engineering – DEMI 2017, organized by University of Banja Luka, Faculty of Mechanical Engineering, in Banja Luka, BOSNIA & HERZEGOVINA, 26 - 27 May 2017.

### References

- [1] Mateus, T. and A.C. Oliveira, Energy and economic analysis of an integrated solar absorption cooling and heating system in different building types and climates. *Applied Energy*, 2009. 86(6): p. 949–957.
- [2] Risto Ciconkov, Refrigerating and air–conditioning systems in Republic of Macedonia regarding the use of CFC fluids, *Proc. Fac. Mech. Eng.–Skopje*, Vol.19, No. 2, pp.103–110, 2000
- [3] Risto Ciconkov, TEWT concept for estimating of the global warming from the refrigerating and air–conditioning systems, *Proc. Fac. Mech. Eng.–Skopje*, Vol.21, No.1, pp. 17–28,2002
- [4] (ESTIF), E.S.T.I.F., The Spanish Technical Building Code (Royal Decree 314/2006). 2006. p. 42.
- [5] (ESTIF), E.S.I., Best practice regulations for solar thermal. 2007. p. 61.
- [6] Al–Ali, A., Y. Hwang, and R. Radermacher, Review of solar thermal air conditioning technologies. *International Journal of Refrigeration*, 2014. 39(0): p. 4–22.
- [7] Jan Albers, F.S., Heat transfer calculation for absorption heat pumps under variable flow rate conditions, in *International Sorption Heat Pump Conference*. 2011: Italy. p. 9.
- [8] H.–M. Hellman, C.S., F. Ziegler, The characteristics equations of absorption chillers, in *International sorption heat pump conference*. 1999: Germany.

- [9] A.Napolitano, W.S., Monitored installation and results, report of Subtask B Task 38 IEA SHC, AIT Austrian Institute of Technology. 2010, Institute for Renewable Energy, EURAC: Italy.
- [10] I.Seso, D.Tasevski, Developing simulation application using graphical programming language for optimization of solar collector position, Mechanical Engineering – Scientific Journal, Vol. 31, No. 1–2, pp. 63–75 (2013)
- [11] Standardization, E.c.f., Energy performance of buildings – Overall energy use and definition of energy ratings, in Primary energy factors; Carbon dioxide emissions. 2008, European Committee for standardization: Brussels. p. 62.



ISSN: 2067-3809

copyright © University POLITEHNICA Timisoara,  
Faculty of Engineering Hunedoara,  
5, Revolutiei, 331128, Hunedoara, ROMANIA  
<http://acta.fih.upt.ro>

<sup>1</sup>Srbislav ALEKSANDROVIĆ, <sup>2</sup>Slavisa ĐAČIĆ, <sup>3</sup>Milentije STEFANOVIĆ,  
<sup>4</sup>Milan ĐORĐEVIĆ, <sup>5</sup>Vukic LAZIC, <sup>6</sup>Dusan ARSIC

## INFLUENCE OF PROCESS PARAMETERS ON THE FRICTION COEFFICIENT IN ONE AND MULTI PHASE STEEL STRIP DRAWING IRONING TEST

<sup>1,3,5,6</sup>University of Kragujevac, Faculty of Engineering, Kragujevac, SERBIA

<sup>2</sup>Coal Mine, Pljevlja, MONTENEGRO

<sup>4</sup>University of Pristina, Faculty of Technical Sciences, Kosovska Mitrovica, SERBIA

**Abstract:** Part of the experimental results of influence on friction in the stripe ironing process with double thinning are presented in this paper. Applied was Schlosser model for evaluating influence of lateral force, contact pressure, average absolute roughness height and thinning strain on friction coefficient. Applied was classical model because of sufficient intensity of drawing and lateral force. If a lateral and drawing forces are small, classical model is not suitable and give unreal negative friction coefficient values. 20 mm wide and 2.5 mm thick strips of mild steel DC04 sheets were used in the single, three and four-phase process with a maximum thinning deformation of about 29%. Appropriate lubricant, mineral oil, was used in conditions of lower speed of 20 mm/min. Three and four phase process was realized with variable lateral force of 5, 10, 15 and 20 kN. The applied experimental test procedure enables the precise quantification of lateral force, contact pressure, thinning strain and roughness influence on friction to be established. Test also enables evaluation of lubricants quality.

**Keywords:** strip ironing test, mild steel, friction coefficient

### INTRODUCTION

Process of ironing is metal forming process which combine features of sheet metal forming and massive (bulk) forming. Thinning strain reach over 25%, and contact pressure over 1000 MPa [1]. It is well known application of the ironing process in manufacturing different kinds of thin walled cans. World annual production (especially for beverage cans) are more than billion pieces. In the tribological sense, ironing process is one of the most severe, owing to the high surface expansion, large plastic strains and high normal pressure at the tool-workpiece interface. Considering previous notice more researchers still interested in ironing. During the last decade significant attention is paid on investigation of environmentally friendly lubricants application [1, 2, 3].

Mostly in order to quantify the performance of the individual lubricants, a different experimental test methods has been developed. Wide applying have double (or single) sided thinning stripe ironing test in different variations [4, 5, 6, 7, 8]. Following mathematical model is mainly, so called Schlosser model [4]. Despite its evident deficiency or inaccuracy was indicated yet in article [5], and in [9] detailed motivated, however that model is applying even in recent extensive researches [8]. In author's investigations [9, 10, 11] proposed was different, or corrected mathematical model usable in all conditions with real results. In this paper presented is experimental investigation of process parameters (lateral force, thinning strain, nominal pressure, and roughness) influence on friction coefficient in double sided ironing of DC04 steel sheet stripes. Applied was classical, less accurate but simpler Schlosser model because of convenient conditions.

### EXPERIMENT

#### — Device description, physical and mathematical model

The special device for physical modeling the symmetrical contact between the sheet strip and die was used for experimental investigation (Figure 1 and Figure 2). The sheet metal sample (strip 2) is placed in the jaws (1) vertically. In the initial phase the thinning makes such that the right-hand sliding tool element (6 right) acts upon the strip by lateral force  $F_D$  (Figure 2). Due to the fixed left side tool element (6 left) and the action of right element, the even double sided ironing of the strip is realized.

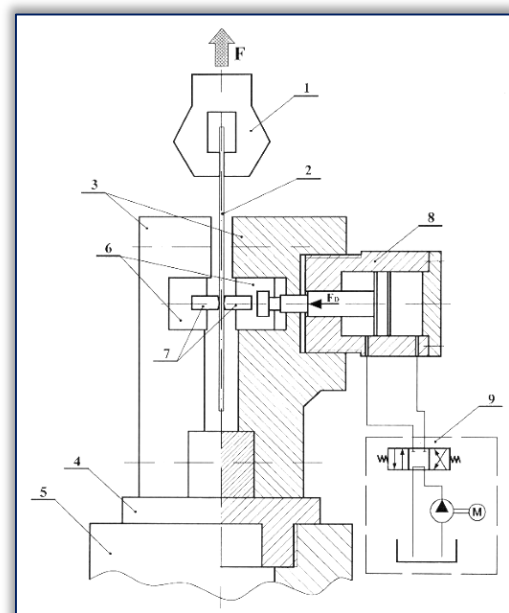


Figure 1. Experimental device scheme

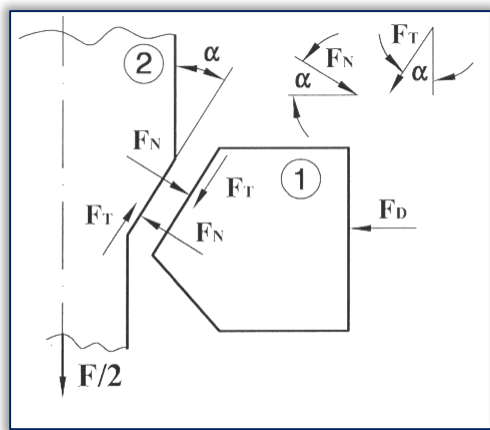


Figure 2. Force acting scheme

After the initial thinning deformation was realized, the tensile force  $F$  begins to act, and the ironing process continues until the sample length is executed. The main action of the ERICHSEN 142/12 laboratory hydraulic press is used as the tensile force across the range of 0-20 kN at speed of 20 mm/min. The lateral force is realized by the hydro-cylinder (8, Figure 1). The maximum range of the lateral force is 0-50 kN. The piston pushes right hand element (6) which is coupled to the sliding element (7). The hydro cylinder (8) is powered by the independent hydraulic aggregate (9), which contains the filter, electric motor, pump, two position directional control valve, adjustable control valve for lateral force and manometer. The data acquisition system measures drawing force dependence on the sliding length or time and the constant intensity of lateral force [10, 11, 12].

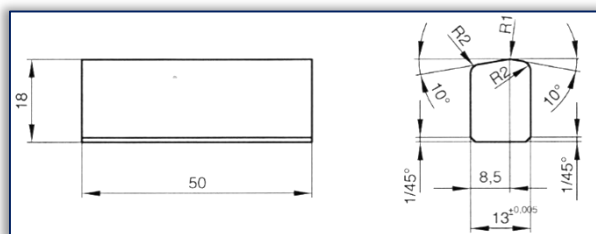


Figure 3. Tool elements geometry

Geometry of the tool elements are shown at Figure 3. Physical appearance of elements and assembly can be seen at Figure 4.

For the contact elements material chosen was alloyed tool steel X160CrMoV12 with 62 HRC hardness after thermal treatment. Active surfaces are fine ground and polished with average absolute roughness height  $R_a \approx 0,06 \mu\text{m}$ .

According to chosen model [4, 8, 10] following formulas for friction coefficient and average calculated (nominal) pressure was used:

$$\mu = \frac{\frac{F}{2F_D} - \text{tg}\alpha}{\frac{F}{2F_D} \text{tg}\alpha + 1} = \frac{F - 2F_D \text{tg}\alpha}{F \text{tg}\alpha + 2F_D} \quad (1)$$

$$\bar{p} = \frac{F \sin^2 \alpha + F_D \sin 2\alpha}{b(s_0 - s_1)} \quad (2)$$

Formulas (1) and (2) with current data for this experiment, are:

$$\mu = \frac{F - 0,3526 \cdot F_D}{0,1763 \cdot F + 2 \cdot F_D} \quad (3)$$

$$\bar{p} = \frac{0,03015 \cdot F + 0,34202 \cdot F_D}{20,3(2,49 - s_1)} \quad (4)$$



Figure 4. View of tool elements and tool assembly

#### — Strip material properties

Geometry of the strip is shown in Figure 5 and Table 1.

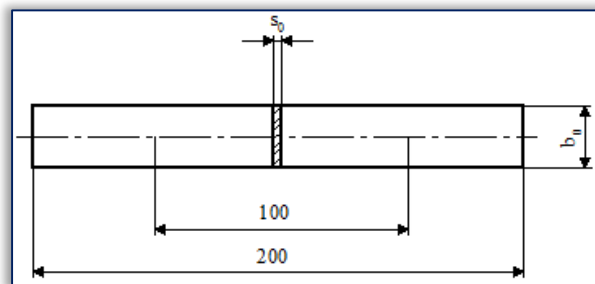


Figure 5. Strip geometry

Table 1. Strip dimensions

Material		$l_0$ [mm]	$b_0$ [mm]	$s_0$ [mm]
Č 0148 (DC04)	min	100	20.2	2.47
	sred.	100	20.3	2.49

For experimental investigations in this paper chosen was the low carbon steel sheet DC04. Specimens for mechanical properties were prepared according to standards SRPS EN ISO 6892 - 1.2012. Determined material characteristics are shown in Table 2.

Table 2. Mechanical properties

Material		$R_{p0,2}$ [MPa]	$R_M$ [MPa]	$R_{p0,2}/R_M$	A [%]	n
Č 0148 (DC04)	min	184.53	283.77	0.65	57.90	0.215
	sred.	185.16	284.54	0.65	57.95	0.216

In Table 2  $R_{p0.2}$  is yield strength,  $R_M$  is tensile strength,  $A$  is percentage elongation at moment of fracture and "n" is strain hardening exponent.

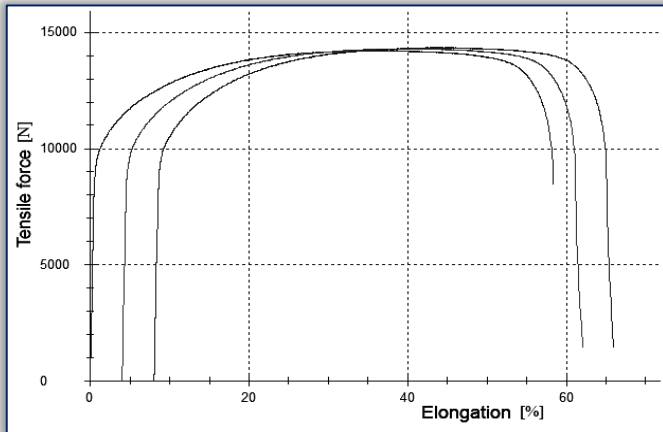


Figure 6. Tensile force - strain curves

Experimental tensile force – strain curves (Figure 6) were obtained for three specimens with excellent repeatability. As can be seen, force curves have smooth dependence on strain which is common for such a material.

### RESULTS AND DISCUSSION

Within results of this experiment, diagrams of tensile forces are presented first (Figure 7, Figure 8, Figure 9 and Figure 10). In the first case (Figure 7) used are one phase process. Each stripe sliding process needs separate specimen with appropriate lateral force ( $F_D$ ). Values are chosen according to empirical recommendation (5kN; 10 kN and 15 kN). Lateral force of 15 kN is below the limiting intensity and process reached full sliding length of about 60 mm.

Figure 8 represents severe conditions. There is three phase process realized on the single specimen. First sliding is performed with lateral force of 5 kN at the path length of about 56 mm. Second phase is performed on the same specimen but ironing starts 21 mm after stripe path beginning. Lateral force was higher: 10 kN. Third sliding passage take place on the same strip also, after 37 mm path. Conditions was severe but no brake occurred.

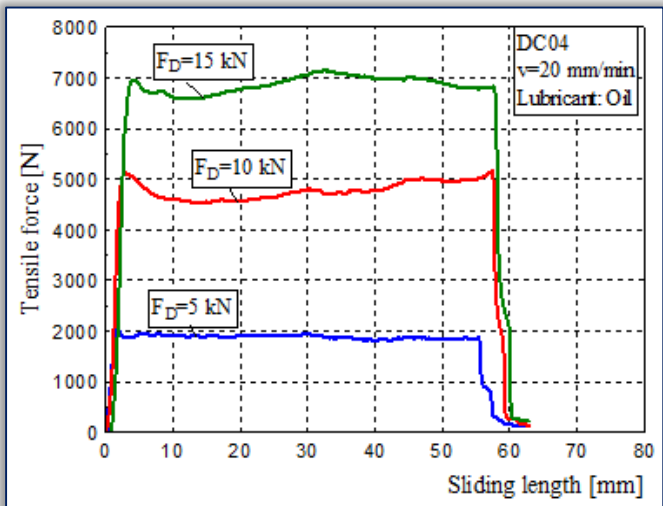


Figure 7. Tensile force vs. sliding length curves

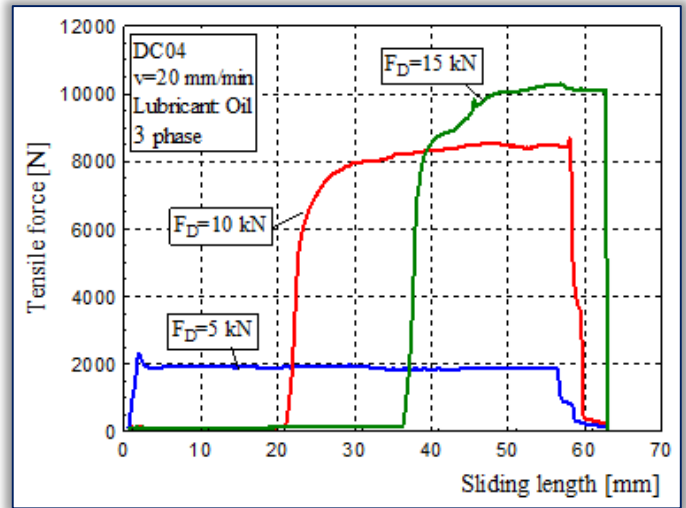


Figure 8. Tensile force vs. sliding length curves  
Lubricant in the process was mineral oil (signed PRESS 509 EP) of domestic producer, intended to drawing operations. Kinematic viscosity of that lubricant is  $170 \text{ mm}^2/\text{s}$  at  $40^\circ\text{C}$ , and density of  $0.950 \text{ g/cm}^3$  at  $20^\circ\text{C}$ .

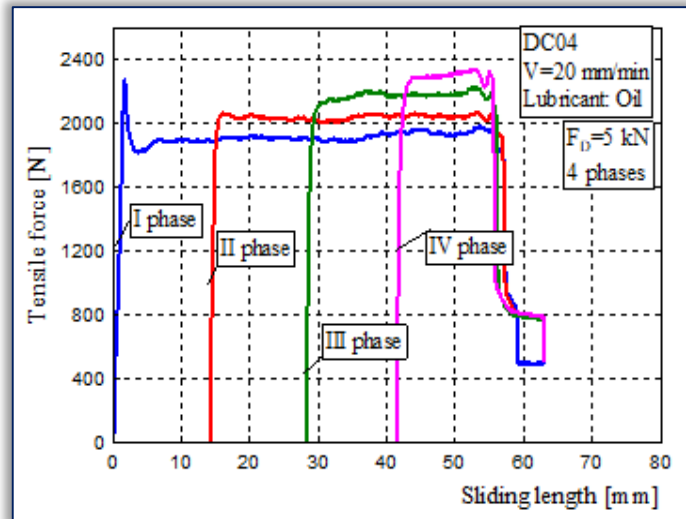


Figure 9. Tensile force vs. sliding length curves

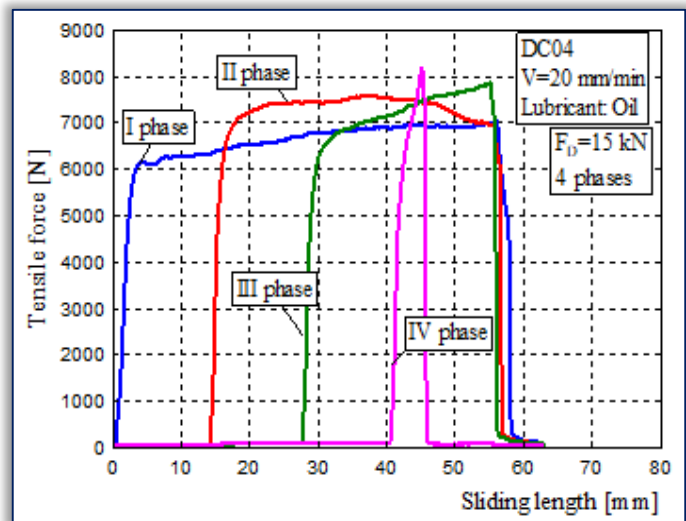


Figure 10. Tensile force vs. sliding length curves

Figure 9 shows tensile force diagrams for four phase ironing process with constant lateral force of 5 kN in each phase. Second, third and four phase starts with about 14 mm offset like in previous case. Sliding process is relatively smooth and no brake occurs.

Figure 10 shows tensile force diagrams for four phase ironing process with constant lateral force of 15 kN in each phase. Conditions are more severe. Second, third and four phase starts with about 14 mm offset like in previous case. Sliding process is relatively stable from first to third phase and no brake occurs, but in fourth phase brake happend after only 6 mm of sliding length.



Figure 11. Strips after multi-phase ironing

In this study investigated are the influences of lateral force, calculated (nominal) pressure, thinning strain and average roughness on the friction coefficient (Figure 12, 13, 14 and 15).

Dependences given at the. Figure 12 determined are according to terms (1) and (3). For tensile force  $F$  intensities was adopted average values. For one phase process friction coefficient ( $\mu$ ) have relatively small values, even in case of 15 kN lateral force.

Diagrams for three phase processes clearly shows that  $\mu$  increase, and it is in accordance with heavier process conditions. Especially in the three phase process with lateral force increasing (Figure 12),  $\mu$  reached maximum value.

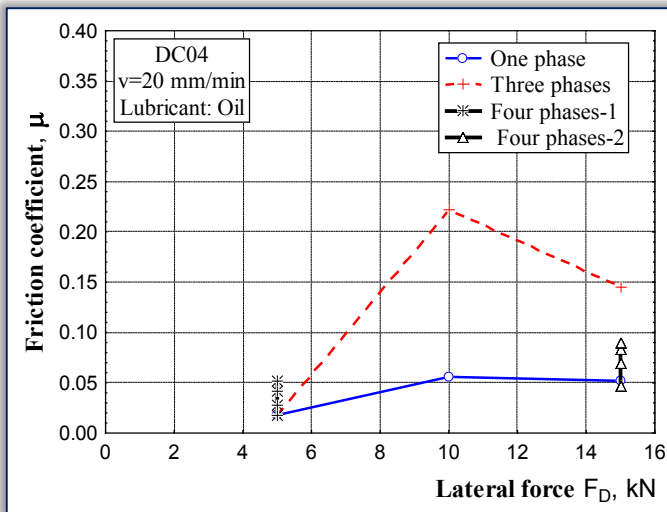


Figure 12. Friction coefficient dependence on lateral force

Figure 13 shows friction coefficient dependence on calculated pressure according to terms (2) and (4). For that

parameter must be noticed that it is only calculated or nominal parameter, which inversely depends on strip thinning strain (Figure 14). Because of that, pressure values are reached unreal intensities for very small thinning. So, calculated pressure need to be considered like parameter related to thinning strain, rather than real pressure.

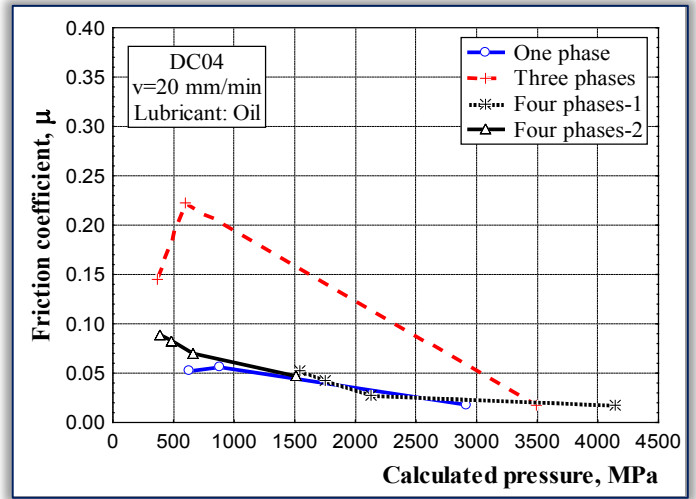


Figure 13. Friction coefficient dependence on calculated pressure

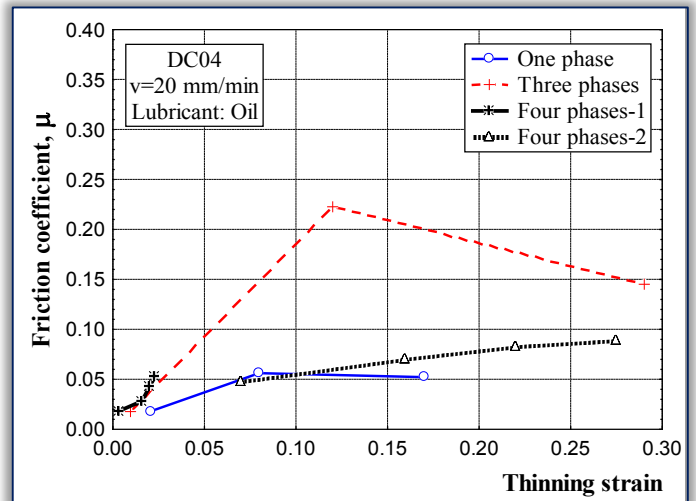


Figure 14. Friction coefficient dependence on thinning strain

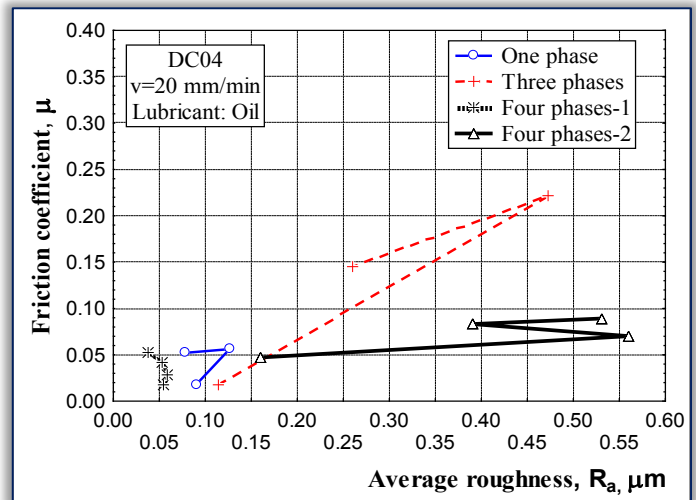


Figure 15. Friction coefficient vs. average roughness



For diagrams at Figure 13 need to be notice that the process starts at the high calculated pressure values and goes to lower values (from right to left side of diagram). As can be seen from Figure 13 and Figure 14, friction coefficient increasing with thinning strain increasing, or calculated pressure decreasing. Relation between friction coefficient and average roughness  $R_a$  (Figure 15) gives somewhat unexpected values in four phase (process 2) cases. In third stage  $\mu$  slightly increases while  $R_a$  decreases. Expectation is opposite. Possible explanation is in the way of  $\mu$  calculation and  $R_a$  determination.  $\mu$  is calculated according to formulas (2 and 4) and depends only of tensile force  $F$  and lateral force  $F_D$ . In other side  $R_a$  is determined experimentally, by measuring. Also, it is possible to occur polishing effect in the all cases (except in four phase-1 process with low lateral force intensity) with decreasing  $R_a$  and the calculated lower  $\mu$  values at the same time.

### CONCLUSIONS

Experimental analysis was accomplished in this study. Intention was to evaluate process parameters influence on the friction coefficient. Results shows the following annotations:

- increasing of lateral and drawing forces both in three phase process strongly influence on friction coefficient increasing,
- thinning strain increasing, i.e. calculated (nominal) pressure decreasing, caused friction coefficient increasing,
- known relationship of average roughness  $R_a$  on friction coefficient is confirmed, but polishing effect occurred in the some stages of processes where  $R_a$  and friction coefficient decreasing.

For further evaluations of different influences on the steel ironing process (especially multi phase) needs to continue extensive experiments in different conditions.

### Acknowledgement

The work reported in this paper was partially supported by the Serbian Ministry of Education, Science and Technological development, through contract TR34002.

### Note

This paper is based on the paper presented at 13th International Conference on Accomplishments in Mechanical and Industrial Engineering – DEMI 2017, organized by University of Banja Luka, Faculty of Mechanical Engineering, in Banja Luka, BOSNIA & HERZEGOVINA, 26 - 27 May 2017.

### References

- Bay N. et al. (2010). Environmentally benign tribo-systems for metal forming, CIRP Annals - Manufacturing Technology, Vol. 59, No. 2, pp. 760 – 780.
- Sagisaka Y. et al. (2012). Evaluation of Environmentally Friendly Lubricants for Cold Forging, Journal of Materials Processing Technology, Vol. 212, No. 9, pp. 1869–1874.
- Đorđević M., Arsić D., Aleksandrović S., Lazić V., Milosavljević D., Nikolić R. (2016). Comparative study of an environmentally friendly single-bath lubricant and conventional lubricants in a strip ironing test, Journal of

- Balkan Tribological Association, Vol. 22, No.1A-II, pp. 947-958.
- Schlosser D. (1975). Beeinflussung der Reibung beim Streifenziehen von austenitischem Blech: verschiedene Schmierstoffe und Werkzeuge aus gesinterten Hartstoffen, Bänder Bleche Rohre, No. 7/8, pp. 302-306
- Deneuille P., Lecot R. (1994). The study of friction in ironing process by physical and numerical modelling, Journal of Materials Processing Technology, Vol. 45, No. 1-4, pp. 625–630.
- Andreasen J.L., Bay N., Andersen M., Christensen E., Bjerrum N. (1997). Screening the performance of lubricants for the ironing of stainless steel with a strip reduction test, Wear, Vol. 207, No. 1-2, pp. 1-5, 1997.
- Van der Aa H.C.E., Van der Aa M.A.H., Schreurs P.J.G., Baaijens a F.P.T., Van Veenen W.J. (2000). An experimental and numerical study of the wall ironing process of polymer coated sheet metal, Mechanics of Materials, Vol. 32, No. 7, pp. 423-443.
- Adamovic D., Stefanovic M., Mandic V. (2012). Modelling of ironing process, Faculty of Engineering, University of Kragujevac. (In Serbian)
- Aleksandrovic S., Stefanovic M., Lazić V., Adamovic D., Djordjevic M., Arsić D. (2013). Different ways of friction coefficient determination in stripe ironing test, in Proceedings of the International conference on Tribology SERBIATRIB 2013, Kragujevac, Serbia, pp. 359-363.
- Djadic S. (2016). Metal forming with double sided ironing, Master thesis, Faculty of Engineering, University of Kragujevac. (In Serbian)
- Djordjević M., Aleksandrović S., Lazić V., Stefanović M., Nikolić R., Arsić D. (2013). Experimental analysis of influence of different lubricants types on the multi-phase ironing process, Materials Engineering - Materijalové inžinierstvo, Vol. 20, No. 3, pp. 147-152, 2013.
- Djordjević M., Aleksandrović S., Arsić D., Lazić V. (2016). Experimental-numerical analysis of contact conditions influence on the ironing strip drawing process, Industrial lubrication and tribology, the article DOI (10.1108/ILT-10-2015-0156), 2016.



ISSN: 2067-3809

copyright © University POLITEHNICA Timisoara,  
Faculty of Engineering Hunedoara,  
5, Revolutiei, 331128, Hunedoara, ROMANIA  
<http://acta.fih.upt.ro>

# Fascicule 2

## [ April - June ]

### t o m e

# [2018] XI

**ACTA**Technica**CORVINIENSIS**  
BULLETIN OF ENGINEERING



**ISSN: 2067-3809**

copyright © University POLITEHNICA Timisoara,  
Faculty of Engineering Hunedoara,  
5, Revolutiei, 331128, Hunedoara, ROMANIA  
<http://acta.fih.upt.ro>

<sup>1</sup>Milan ŠLJIVIĆ, <sup>2</sup>Milija KRAIŠNIK, <sup>3</sup>Jovica ILIĆ, <sup>4</sup>Jelica ANIĆ

# DEVELOPMENT OF SMALL BATCHES OF FUNCTIONAL PARTS USING INTEGRATION OF 3D PRINTING AND VACUUM CASTING TECHNOLOGY

<sup>1,3</sup>Faculty of Mechanical Engineering, University of Banja Luka, BOSNIA & HERZEGOVINA

<sup>2,4</sup>Faculty of Mechanical Engineering, University of East Sarajevo, BOSNIA & HERZEGOVINA

**Abstract:** In conditions of dynamic market environment there is an increasing requirement for rapid development and production of complex and functional parts from different materials. In this paper, we present the process of development and production of small batches of functional parts in the integrated system of additive and vacuum casting technology. All advantages of this integrated approach were used during the research. Data obtained from the manufacturer were used for the proper selection of materials and they relate to the value of mechanical characteristics.

**Keywords:** Additive Manufacturing, Vacuum casting, Functional parts, 3D Printing

## INTRODUCTION

The more time spent on the product development, the more opportunities for profit are lost. It is this philosophy that drives many industries during the development of new products. Especially, as more and more often the need for rapid design, development, testing and production of the final product, i.e., a small batch of functional parts which would be expensive to develop with conventional tools and accessories as it would not be economically justifiable. Technologies of rapid prototyping and rapid tooling provide an answer to these requirements, in this particular case technology of material extrusion and technology of vacuum casting, the integration of which are used all their advantages in the production of small batch of specific gear [1].

## 3D PRINTING TECHNOLOGY AND ITS ROLE IN THE INTEGRATED PROCESS

The RP technique, which was used in a specific case for making master models of gear, is a 3D printer based on FDM principle (Stratasys - Dimension Elite), which plays a key role in the integrated process [2]. Of great importance is the accuracy that is achieved in this 3D printer. It is necessary to pay special attention to the positioning and orientation of the master model on the platform during the printing process. The procedure that has been necessary to obtain a master model or prototype of gear is as follows [3]:

- Product design in one of the CAD software packages,
- Conversion of CAD models in STL format that is recognized by a 3D printer,
- Transfer of STL files to the computer that controls the three-dimensional printer,
- Processing of STL files within the CatalystEX program in which all the parameters are set and adjusted according to the required model,
- Creating a three-dimensional model using additive technology and
- Further processing of created prototypes.

The layout of the gear model designed in SolidWorks software package is shown in Figure 1 and parameter adjustment within the CatalystEX, where the selection of the orientation of models, processing of layers and layout of models on a base on which printing on a "Dimension Elite" 3D printer will be performed, is shown in Figure 2.

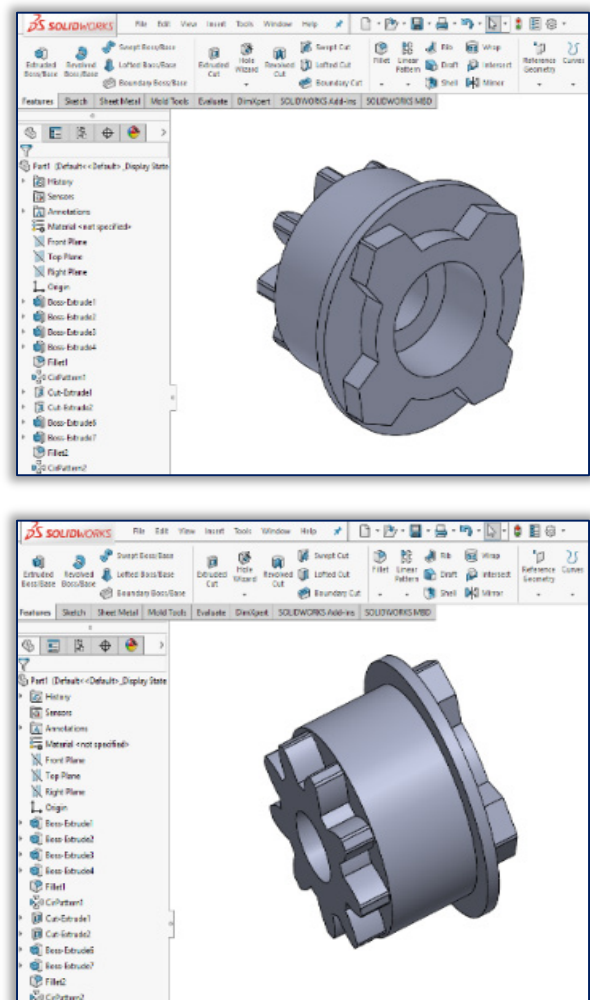


Figure 1. A gear model in Solid Works software package

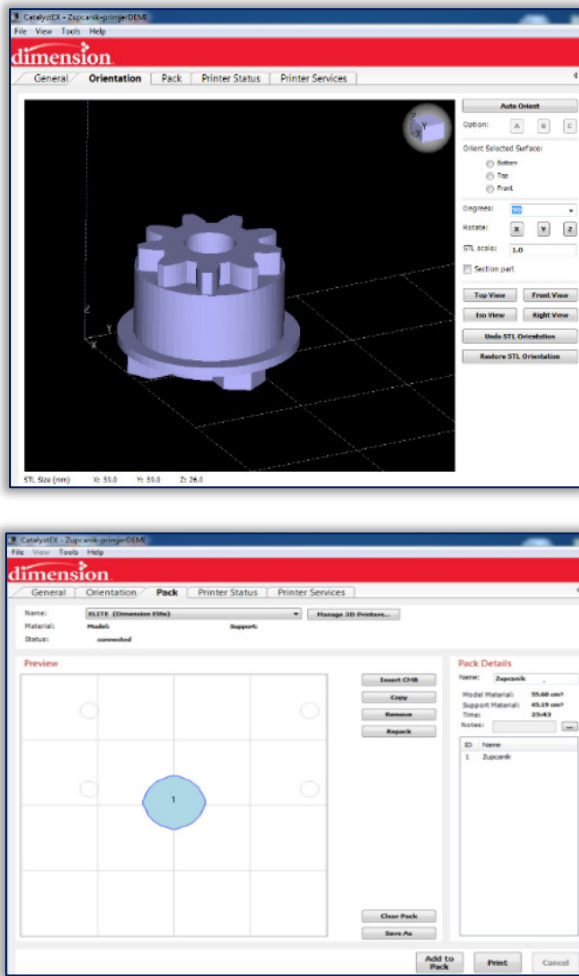


Figure 2. Orientation and processing of models in CatalystEX  
**VACUUM CASTING TECHNOLOGY AND ITS ROLE IN THE INTEGRATED PROCESS**

Vacuum casting has become a widely accepted method of soft tooling, replacing traditional methods such as investment casting [4]. Vacuum casting is a newer version of investment casting with changes to the process of creating the mold. Several needs are addressed by vacuum casting which make it extremely popular.

Most importantly, vacuum casting reduces the time for part production when compared to traditional methods. This, in turn, significantly reduces costs.

The additional following characteristics offered by vacuum casting justify the choice of this technology for the integrated process:

- 1) Accurate Castings: Textures, fine details, and complex surfaces are exactly reproduced from the master model due to the replicating nature of the silicone rubber mold.
- 2) Consistent Quality: Vacuum casting produces dimensionally stable and accurate castings. The technique allows castings of thin wall and void-free sections as well. Furthermore, vacuum casting in silicone molds allows producing parts with undercuts because the pliable silicone molds do not present problems when removing cast parts, even with undercuts, from the mold.

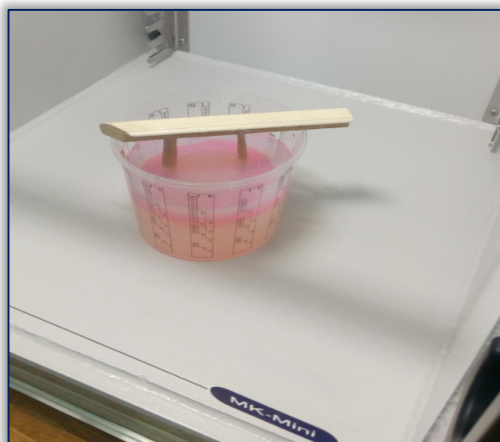
- 3) Up to 95% Saving in Time: After the silicone mold has been created, replicas of the master model may be fabricated within a few hours, depending on the number of parts required.
- 4) Fit and Function Testing: The cast parts are sufficiently accurate so that fit and function testing may be conducted to determine which modifications must be made.
- 5) Cost Savings: Using vacuum casting offers reductions in cost when compared to rapid prototyping or traditional hard tooling.
- 6) Material Choices: Vacuum casting resins simulate production thermoplastics, rubber, and glass. Additionally, the resins sustain high impact and resist elevated temperatures. With vacuum casting, users have the options to create clear or colored parts as well.

The process of vacuum casting consists of the following steps:

1. Preparation of gear negatives produced on a 3D printer for the casting process. Setting the parting tape on the gear negative that will facilitate the separation of silicone mold.
2. Bonding plastic gates on the gear negative which has a role to form an inlet channel in the silicone mold and to facilitate the positioning and fixation of the negative in the silicone casting frame, according to Figure 3a.



a)



b)

Figure 3 a) Casting silicone into the frame with the negative, and b) removing the residual air from the silicon in a vacuum chamber

3. Calculation of the necessary quantity of silicone mixture to form a silicone mold to be used for molding the gear. The silicone mixture is poured into the frame with fixed gear negatives and then the frame with the negative submerged in silicone is placed in a vacuum chamber in order to remove the residual air bubbles from silicon, according to Figure 3b.
4. Positioning of the silicone mold in a vacuum chamber (Figure 3a.). After solidification of silicone, silicone mold is cut to parting line, during which we relieve the negative and get a silicone mold for casting a replica of a given negative (Figure 3b).
5. The molding halves are then combined and the next step is to calculate necessary quantities of resin for molding of the gear. The amount of resin is commonly determined by weighing the individual master model which is increased by 20-30%, taking into account the loss of material in vessels and inlet channels.

Table 1. Mechanical characteristics of components used for casting of the gear

MECHANICAL PROPERTIES AT 23°C			
Flexural modulus of elasticity	ISO 178 :2001	MPa	2.300
Flexural strength	ISO 178 :2001	MPa	80
Tensile strength	ISO 527 :1993	MPa	60
Elongation at break in tension	ISO 527 :1993	%	11
Charpy impact resistance	ISO 179/2D :1994	kJ/m <sup>2</sup>	> 60
Hardness at 23°C	ISO 868 :1985	Shore D1	80
Hardness at 120°C	ISO 868 :1985	Shore D1	> 65

In this case, to cast the gear, components made by Axson Technologies were used, thus by mixing them in the casting process the parts with physical and mechanical characteristics according to Table 1 are obtained.

6. After a certain quantity of the material needed for molding and the proportion of the individual components of the material in a total amount are determined, then vacuum casting process follows. The casting process takes place in a vacuum chamber under conditions that are recommended for corresponding elements and components of the material, according to Figure 6.
7. After solidification of the molded material in a vacuum chamber, mold halves are separated and, if necessary, post-processing of the molded item follows.

Small batches of gears, made in the integrated process of additive manufacturing technology and vacuum casting in the Laboratory for Plasticity and Processing Systems at the Faculty of Mechanical Engineering in Banja Luka as a result of this study are shown in Figure 7.

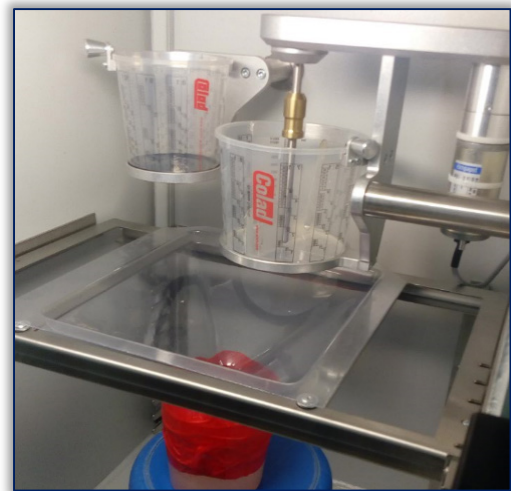


Figure 6. The casting process in a vacuum chamber MK-mini



Figure 7. Small batches of gears made in the integrated process of additive manufacturing technology and vacuum casting

## CONCLUSIONS

The development of a gear case study through the integration process of 3D printing and vacuum casting shows an example of a very successful application of modern technology in the rapid development of functional parts and production replicas of identical part.

Replicas can be made from different materials that can be very broad spectrum in terms of physical, technical and mechanical properties. Replicas fully meet the requirements in terms of dimensional accuracy and functionality, i.e. all the

details from the master model have been faithfully reproduced on its replicas.

This only confirms the importance and benefits that is provided by the integration of 3D printing and vacuum casting technologies in the rapid development and production of small series of prototypes and functional parts.

#### **Acknowledgment**

This investigation on the application of advanced technologies for sustainable Additive manufacturing methods and technologies has been realized as part of Tempus WIMB No. 543898 project implementation, a project co-funded by the European Union.

#### **Note**

This paper is based on the paper presented at 13th International Conference on Accomplishments in Mechanical and Industrial Engineering – DEMI 2017, organized by University of Banja Luka, Faculty of Mechanical Engineering, in Banja Luka, BOSNIA & HERZEGOVINA, 26 - 27 May 2017.

#### **References**

- [1] ASTM F2792-12a: Standard Terminology for Additive Manufacturing Technologies
- [2] Šljivić M., Pavlović A., Ilić J., Stanojević M., Todorović S. (2017): Comparing the Accuracy of Professional and Consumer Grade 3D Printers in Complex Models Production, FME Transactions, Vol.45, No.3, pp. 348-353
- [3] Wohlers Report 2014: 3D Printing and Additive Manufacturing, State of the Industry, Annual Worldwide Progress Report, WOHLERS ASSOCIATES, INC. Colorado 80525, USA.
- [4] Grenda E.: Printing the future, The 3D printing and rapid prototyping source book, Third Edition, CASTLE ISLAND CO. ARLINGTON, MA 02474, USA
- [5] Pavlovic A., Šljivić M., Kraišnik M., Ilić J., Anić J. (2017): Polymers in Additive Manufacturing: the Case of a Water Pump Impeller, FME Transactions, Vol.45, No.3, pp. 354-359, doi:10.5937/fmet1703354P
- [6] Despeisse M., Ford S. (2015): The Role of Additive Manufacturing in Improving Resource Efficiency and Sustainability, Institute for Manufacturing, University of Cambridge, UK, No.3, ISSN 2058-8887
- [7] Jacobus Dippenaar D., Schreve K. (2012): 3D printed tooling for vacuum assisted resin transfer moulding, The International Journal of Advanced Manufacturing Technology,



ISSN: 2067-3809

copyright © University POLITEHNICA Timisoara,  
Faculty of Engineering Hunedoara,  
5, Revolutiei, 331128, Hunedoara, ROMANIA  
<http://acta.fih.upt.ro>

<sup>1</sup>Ile MIRCHESKI, <sup>2</sup>Tashko RIZOV

# NONDESTRUCTIVE DISASSEMBLY PROCESS OF TECHNICAL DEVICE SUPPORTED WITH AUGMENTED REALITY AND RFID TECHNOLOGY

<sup>1-2</sup>Ss. Cyril and Methodius University in Skopje (UKIM), Faculty of Mechanical Engineering, Skopje, MACEDONIA

**Abstract:** This paper presents nondestructive disassembly process of technical device supported with augmented reality system and RFID technology. During the last few decades, the rapid development of automobiles, electric and electronic equipment, resulted in creation of billions tons of waste. For instance, “around 3 billion tons of waste are generated in the EU each year - over 6 tones for every European citizen. The new recycling/reuse concept uses the nondestructive disassembly process of technical device supported with augmented reality and RFID technology. System includes marking the products with components of interest by using a RFID tag. The products can be marked with a RFID tag that will contain the ID of the product design in the centralized database. The recycling/reuse facilities use this ID to download data relevant for nondestructive disassembly of the product and obtaining the components of interest. The system is modular and extensible in terms of the services and re-manufacture offered. The overall system has a forum that is helpful in communication between recycling/reuse facilities and product designers. Augmented reality system offers video presentation when possible to visualize the disassembly process. The database contains valuable data for the product regarding the materials and component of interest used for each of the components in the product. Main objective of this paper is developing of a new recycling/reuse concept by using the nondestructive disassembly process supported with augmented reality and RFID technology.

**Keywords:** disassembly, reuse, augmented reality, RFID

## INTRODUCTION

Waste created by obsolete equipment and other machine assemblies and white goods becomes actual problem in the modern society. This problem is interesting for investigation for a lot of institutions and scientists. The problem arises from the nature of these products. For some reason some of the parts inside the assemblies should or must not be destroyed along with the whole product. Some parts from the product are valuable for reuse, remanufacturing or recycling and should not be deposited, this means that the component can be reused avoiding the whole refabricating of the component. Other products cannot be discarded along with the other materials because they are toxic and need to be discarded in specialized facilities. During the last few decades, the rapid development of automobiles, electric and electronic equipment, resulted in creation of billions tons of waste. For instance, “around 3 billion tons of waste are generated in the EU each year - over 6 tones for every European citizen [1].” The extensive usage of personal computers arises the question for the privacy of the data discarded along with the device. Some companies acquire certificate for proper data destruction. The list goes on and every product may or may not have some part that needs to be extracted by hand before it is all discarded or recycled for reuse of the materials. Facilities for proper recycling of this assemblies are created that will discard or obtain these parts in a proper manner. Because of the different nature of different products there are facilities specialized for each of the products. For example facility for batteries, facility for recycling of computers and other IT equipment, facilities for

recycling refrigerators because of the environmentally hazardous CFC-12 or other materials used in the cooling process etc. We believe that there is place for improvement in this process.

Current legal regulations clearly indicate that the technical products should be designed considering the recovery of the product at the end-of-life stage. In Europe, the designers have to follow European directives for environment protection such as Directive 2000/53/EC for end-of-life vehicles [2] and 2002/96/EC for waste electrical and electronic equipment (WEEE) [3]. The designers have to incorporate the directives into the product design in order not to pollute the environment or reduce the impact of pollution to a minimum level.

## BACKGROUND

This paper deals with problems on how to reduce hazardous substances in products, to prevent pollution of the environment and to incorporate design for the environment early in the product design stage in order to facilitate product dismantling and recovery, and to achieve the quantified targets for reuse, recycling and total recovery.

Augmented Reality (AR) points out to be a good technology for training in the field of maintenance, assembly and disassembly, as instructions or rather location-dependent information can be directly linked and/or attached to physical objects. The products contain a large number of components, such us screws, plugs, etc., and their location is important from aspect of the product assembly and disassembly. AR-based training takes place with the real physical devices of the training scenario [4]. Based on the

principle of perspective projection, the 3D virtual scene in AR-based assembly and disassembly guiding system is positioned into the virtual world and displayed the specified viewpoint on the specified screen area. All algorithms proposed in this paper [5] are utilized by automatically extracted CAD feature's bounding box model of part as input data so they could be implemented for online planning of 3D assembly guiding scenes. One of the most industrial applications in which augmented reality can be applied is disassembly process. In the paper [6], the authors introduce the possibilities of the implementation of augmented reality concept in the disassembly process with goal of shortening the overall duration of the disassembly process of heating circulation pump assembly.

Zhang et al. [7] proposed a RFID-assisted assembly guidance system in an augmented reality environment. The paper presented a novel research aiming at providing just-in-time information rendering and intuitive information navigation, methodologies of applying RFID, infrared-enhanced computer vision, and inertial sensor. Stankovski et al. in the paper [8,9] presented a new way for identification of products/parts and their tracking during the whole life cycle, from the manufacture and assembly phase to the disassembly phase. RFID technology is applied on a chosen product, an in-mould labelling (IML) robot. RFID-based integrated method for electromechanical products disassembly decision-making was presented in the paper [10]. Chen et al. shows how RFID technology can be utilized to record and trace the lifecycle information, hence optimizing disassembly process and improving recovery efficiency. This integrated method is highly extensible, and it can be applied to various types of electromechanical products. Mircheski et al. in the paper [11] presented a method for improving the process and cost of nondestructive disassembly of a final product. The method analyzes the nondestructive disassembly by determining a disassembly interference matrix, feasible disassembly sequences, and improved nondestructive disassembly sequences. The innovative element of the nondestructive disassembly method proposed in the paper is integrating the generated conceptual design solutions for a given technical device with a software package developed for determining its improved disassembly sequence embedded within a 3D CAD platform. In this article, a nondestructive disassembly process of a technical device supported with augmented reality and RFID technology is proposed. Different from other methods and strategies, this method uses system which marks the components of interest from the product by using a RFID tag which contains the ID of the product design in the centralized database. The system is modular and extensible in terms of the services and re-manufacture offered. The overall system has a forum that is helpful in communication between recycling/reuse facilities and product designers. Augmented reality system offers video presentation when possible to visualize the disassembly process. Main objective of this

paper is the development of a new recycling/reuse concept by using the nondestructive disassembly process supported with augmented reality and RFID technology.

### THE STRUCTURE OF THE MODEL

The research presented in this paper is oriented into creating and implementing of useful novel model for easy nondestructive disassembly process of technical device supported with augmented reality and RFID technology. In this context, the novel model is intended for end-of-life products which consist valuable components or component of interest. The novel model for nondestructive disassembly includes innovative elements such as: planning of nondestructive disassembly process in the early stages of the design process; connecting with the production process and product marking with RFID tag which will indicate that the product consists a valuable component of interest; and into the end-of-life stage of the product will give procedure and order for nondestructive disassembly supported with augmented reality. The overall model is an iterative process that improves the product structure and some valuable components will be reused or recycled. As depicted in Figure 1, the proposed model is performed in three main phases.

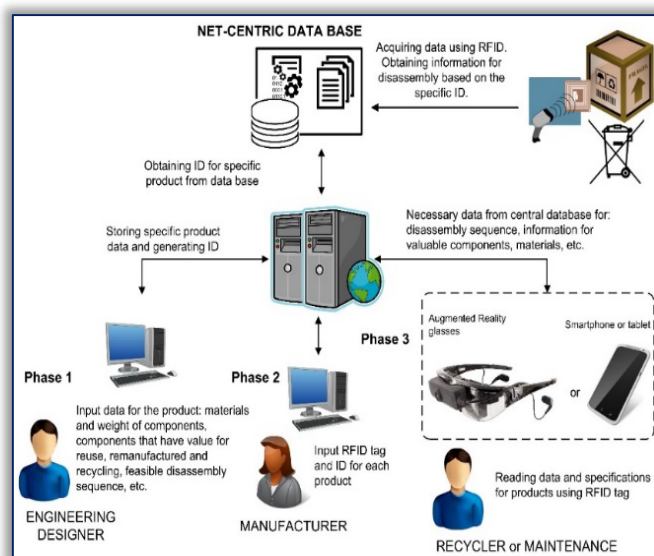


Figure 1. Flowchart of the proposed model for nondestructive disassembly using augmented reality and RFID technology

— **Phase 1:** Planning of the nondestructive disassembly process in the early stages of the design process which includes identification of fastener, component, contacts between parts, materials and weight for the parts by using of 3D CAD file as an input in SolidWorks assembly file of product with extension ".SLDASM". Also, this phase includes the automatic determination of the contact matrix between fasteners and components (FC), automatic determination of the contact matrix between components (CC) for all subassemblies (SA) within the product assembly (A), the disassembly operations, the disassembly interference matrix, all possible disassembly sequences, the improved disassembly sequence by using of developed software presented in the paper [11].



In order to demonstrate the proposed model, the product hair-dryer is used as an example. The main goal of the model is the presentation of the improved non-destructive disassembly sequence supported with augmented reality and RFID technology. Constituent components of the hair-dryer are:  $C_1$ =Holder,  $C_2$ =Exit part, housing which is consisted of two components (called  $C_3$ =Body part and  $C_4$ =Back part),  $C_5$ =Propeller,  $C_6$ =Electric motor,  $C_7$ =Heating element. A discrete fasteners in the hair dryer are:  $F_1$ =F-Bolt M2x8-3,  $F_2$ =F-Bolt M2x8-1,  $F_3$ =F-Bolt M2x8-2,  $F_4$ =F-Bolt M2x28-1, and non-discrete fasteners are:  $F_5$ =F5-Virtual (between  $C_1, C_3$ ),  $F_6$ =F6-Virtual ( $C_1, C_6$ ) and  $F_7$ =F7-Virtual ( $C_2, C_3$ ). In the Figure 2, the CAD model of the product assembly for hair-dryer and its constituent elements is shown with exploded view. For simplicity of calculations the abbreviation names for components and fasteners ( $C_1, C_2, \dots$  and  $F_1, F_2, \dots$ ) are applied.

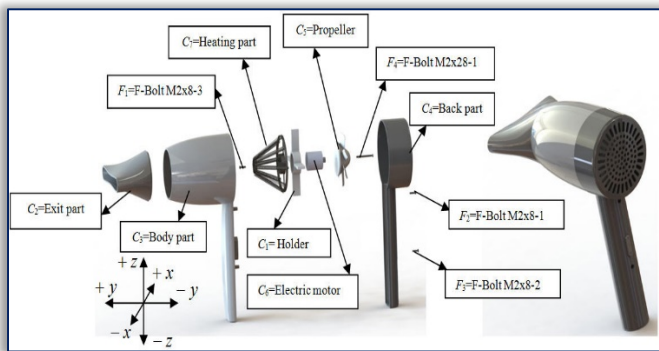


Figure 2. Exploded view and assembly of hair-dryer

The electric motor as valuable component of interest for reuse is aim for the disassembly process. The optimal disassembly sequences in according with methodology presented in the paper [11] are:

$F_2(-y), F_3(-y), C_4(-y), F_4(-y), C_5(-y), C_6(-y)$

$F_3(-y), F_2(-y), C_4(-y), F_4(-y), C_5(-y), C_6(-y)$

The optimal nondestructive disassembly sequence is usually a partial disassembly sequence, because not all disassembly operations return profit. The optimal nondestructive disassembly sequence gives insight into the disassembly cost, the percent of recovered material and other characteristics of the product. The lower the disassembly cost, the higher is the economic effect of the product recovery. The higher is the weight and volume of the recovered materials, the higher is the environmental benefit. These criteria can give important information to the designer in order to compare the design variants and select those that return higher value at product end-of-life and have lower negative effect to the environment.

— **Phase 2:** The model for nondestructive disassembly process of technical device utilizes RFID technology. Radio Frequency Identification (RFID) is a wireless identification technology consisted of a RFID tag, RFID reader/writer, a RFID antenna and related software. The key advantages of this technology compared to other identification technologies, like for example the barcode are:

noncontact identification; long-distance reading of tags; simultaneous reading of multiple tags; high automation of the procedure; huge quantity of data can be processed very fast. The main disadvantages of the RFID technology is the limited amount of data that can be stored on a single tag and the price of a tag compared to a barcode sticker.

The developed model operates using a Neology Ultra High Frequency (UHF) Class-1 Gen-2 96 bit RFID tag containing a code in XML format. The products are marked with the appropriate RFID tag. The system is based on the software package of Inner Circle Logistics using the software Circus<sup>SM</sup>, Jester<sup>SM</sup>, Ringmaster<sup>SM</sup> and Scarborough Fair<sup>SM</sup> as is presented in Figure 3.

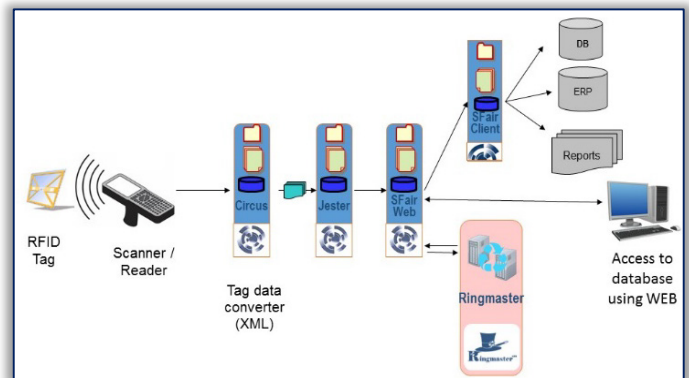


Figure 3. Diagram of the RFID software system architecture  
Circus<sup>SM</sup> is a RFID interface software that provides the ability to tie passive RFID tag data to the database utilizing next generation security protocols. Jester<sup>SM</sup> is an automated data exchange application designed to post data to a net-centric virtual relational database. In the same way that Scarborough Fair<sup>SM</sup> makes data available to a variety of audiences, Jester<sup>SM</sup> runs in the background and enables smart data transfer capabilities that tie directly to virtually any database. Ringmaster<sup>SM</sup> provides the authentication and control functions for the systems as well as the domain name system (DNS) lookup and other web services. It guarantees the security of the system, ensuring that only those with proper authority can access the information.

When the RFID tag is read by a RFID reader (Figure 4), the read information is transformed in order to access the centralized database and obtain the product ID code and the product design datasheet, such as shown in the Figure 1. The database can be designed in a way to satisfy the needs of each member of the product lifecycle chain. At this point, the product design sheet contains data elements for the product name, manufacturer, dimensions, number of parts, materials of parts, whether the product contains hazardous materials, components of interest, and the most important the disassembly sequence. The recycling facilities can use this ID to download data relevant for nondestructive disassembly of the product and obtaining the components of interest. The manufacturer inputs the necessary data in the database. The design of the database can be adopted to various requirements.

The proposed model is modular and extensible in terms of the services offered. The system may have forums that will be helpful in communication between recycling facilities and product designers.

This form of the system design provides the necessary security of the proposed model. The RFID tag contains only non-sensitive information that can be utilized after accessing a secure database. In that way, reading the information written on the tag during the lifecycle of the product does not present a security risk for the any of the involved parties.

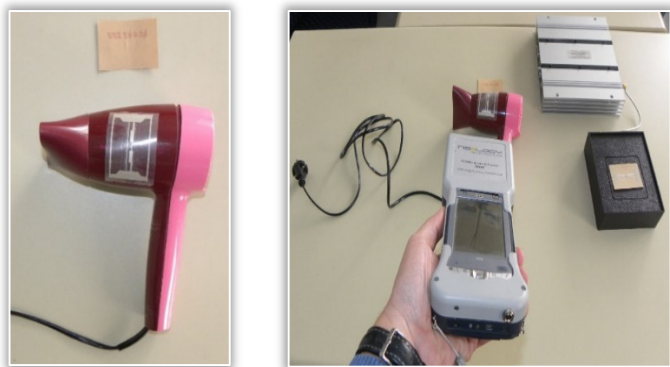


Figure 4. Placement of RFID tag and tag reading

— **Phase 3:** The system offers interactive video tutorials of nondestructive disassembly process and disassemble of valuable components of interest with visualization of the disassembly process supported with augmented reality.

Augmented reality (AR) is a technology that enables digitally stored spatial information to be overlaid graphically on views of the real world [12]. AR allows the user to see the real world, with virtual objects superimposed upon or composited with the real world. Ideally, it would appear to the user that the virtual and real objects coexisted in the same space. Augmented Reality enhances a user's perception of and interaction with the real world [13]. The virtual objects display information that the users cannot directly detect with their own senses. The information conveyed by the virtual objects helps a user perform real-world tasks.

The usual 2D technical drawings or 3D video animations of the disassembly process are difficult to understand and challenging to follow. The proposed model uses an interactive video guide superimposed on the real product. The system requires a hand-held device equipped with rear mounted camera, Android or iOS operating systems and access to internet. An animation of the disassembly process is created for the defined optimal nondestructive disassembly sequence from phase 1.

Using the Augment software platform the animation is uploaded to the Augment Manager providing the necessary information and tags. Using the data read from the RFID tag, a link to the 3D model in Augment Manager is generated and the animation is loaded on the hand-held device. The superimposed model in augmented reality is displayed on the screen.

The animation guides the recycler in the process of the nondestructive disassembly step-by-step as shown in Figure

5. The system provides with corresponding views as the user changes the viewing angle and position relative to the product with real motion. The component of interest is highlighted and the corresponding information is displayed. In case of presence of hazardous materials, the animation will provide the procedures for secure disposal. The systems is designed to operate using a hand-held device or a Head-Mounted Display (HUD).

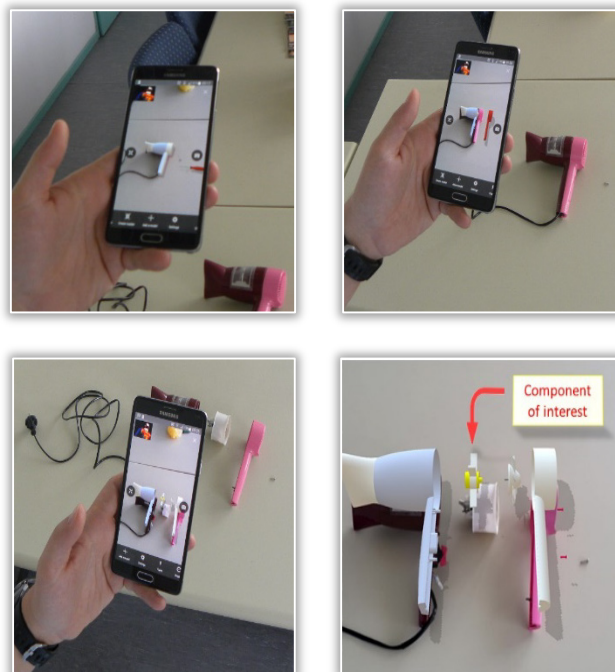


Figure 5. Step-by-step visual guide for nondestructive disassembly operations in Augmented Reality

## CONCLUSION

In this paper, a novel model for nondestructive disassembly process of end-of-life product supported with augmented reality and RFID technology is proposed. Using this model, the information about the nondestructive disassembly process of end-of-life product and information regarding the valuable component of interest can be delivered directly via net-centric database by using of RFID tag and the nondestructive disassembly process will be shown with video presentation in augmented reality.

The model provides the necessary security of the product information by not storing real information to the RFID tag. As a result, this proposed model can improve the percent of recovered material, recovered valuable functional component of interest for reuse, lower negative effect to the environment, biggest recovery profits, easy disassembly process by using of video presentation and augmented reality.

## Note

This paper is based on the paper presented at 13th International Conference on Accomplishments in Mechanical and Industrial Engineering – DEMI 2017, organized by University of Banja Luka, Faculty of Mechanical Engineering, in Banja Luka, BOSNIA & HERZEGOVINA, 26 - 27 May 2017.

## References

- [1] European Commission, Brussels, Belgium, Life Cycle Thinking and Assessment for Waste Management. From [http://ec.europa.eu/environment/waste/publications/pdf/Making\\_Sust\\_Consumption.pdf](http://ec.europa.eu/environment/waste/publications/pdf/Making_Sust_Consumption.pdf), accessed on Aug. 6, 2016.
- [2] Directive 2000/53/EC. End-of-life vehicles. European Parliament.
- [3] WEEE Directive 2002/96/EC. Waste Electrical and Electronic Equipment (WEEE). European Parliament.
- [4] Webel, S., Bockholt, U., Engelke, T., Peveri, M., Olbrich, M., Preusche, C. (2011). Augmented Reality Training for Assembly and Maintenance Skills. BIO Web of Conferences, p. 97.1-97.4.
- [5] Chen, C.J., Hong, J., Wang, S.F. (2015). Automated positioning of 3D virtual scene in AR-based assembly and disassembly guiding system. Int J Adv Manuf Technol, vol. 76, no. 5, p. 753–764.
- [6] Tegeltija, S., Lazarevic, M., Stankovski, S., Cosic, I., Todorovic, V., Ostojic, G. (2016). Heating circulation pump disassembly process improved with augmented reality. Thermal Science, vol. 20, no. 2, p. S611-S622.
- [7] Zhang, J., Ong, S.K., Nee, A.Y.C. (2010). RFID-assisted assembly guidance system in an augmented reality environment. International Journal of Production Research, vol. 49, no. 13, p. 3919-3938.
- [8] Ostojic, G., Lazarevic, M., Stankovski, S., Cosic, I., Radosavljevic, Z. (2008). Radio Frequency Identification Technology Application in Disassembly Systems. Strojniški vestnik - Journal of Mechanical Engineering, vol. 54, no. 11, p. 759-767.
- [9] Stankovski, S., Lazarevic, M., Cosic, I., Puric, R., (2009). RFID technology in product/part tracking during the whole life cycle., Assembly Automation, vol. 29, no. 4, p.364-370, doi: 10.1108/01445150910987781
- [10] Shaoli, C., Yi, J., Zhu, X., Jiang, H., Ju, W. (2016). RFID-based integrated method for electromechanical products disassembly decision-making. International Journal of Computer Integrated Manufacturing, vol. 30, no. 2-3, p. 229-254.
- [11] Mircheski, I., Pop-Iliev, R., Kandikjan, T. (2016). A Method for Improving the Process and Cost of Nondestructive Disassembly. Journal of Mechanical Design, vol. 138, no. 12, p. 121701-121701-15., doi: 10.1115/1.4034469
- [12] Rizov, T. (2014). Application of Augmented Reality in Interactive Pedestrian Navigation Systems. American Journal of Science and Technology. vol. 1, no.1, p. 11-16.
- [13] Azuma, R (1997). A Survey of Augmented Reality. Teleoperators and Virtual Environments, vol. 6, issue 4. p. 355–385.



ISSN: 2067-3809

copyright © University POLITEHNICA Timisoara,  
Faculty of Engineering Hunedoara,  
5, Revolutiei, 331128, Hunedoara, ROMANIA  
<http://acta.fih.upt.ro>

# Fascicule 2

## [ April - June ]

### t o m e

# [2018] XI

**ACTA**Technica**CORVINIENSIS**  
BULLETIN OF ENGINEERING



**ISSN: 2067-3809**

copyright © University POLITEHNICA Timisoara,  
Faculty of Engineering Hunedoara,  
5, Revolutiei, 331128, Hunedoara, ROMANIA  
<http://acta.fih.upt.ro>

<sup>1</sup>Jasna GLIŠOVIĆ, <sup>2</sup>Jovanka LUKIĆ, <sup>3</sup>Blaža STOJANOVIĆ, <sup>3</sup>Nadica STOJANOVIĆ

# AIRBORNE WEAR PARTICLES FROM AUTOMOTIVE BRAKE SYSTEMS IN URBAN AND RURAL AREAS

<sup>1</sup> University of Kragujevac, Faculty of Engineering, SERBIA

**Abstract:** Non-exhaust vehicle emissions are currently thought to be tyre wear, brake wear, clutch wear, road surface wear, corrosion of other vehicle components, corrosion of street furniture and crash barriers, and the resuspension of road dust. Among non-exhaust sources, brake wear can be a significant particulate matter (PM) contributor, particularly within areas with high traffic density and braking frequency. Regulations for brake pad performance are influenced by many bodies across the world, including the Particle Measurement Programme by the United Nations Economic Commission for Europe (UNECEPMP). In order to continuously improve their products and ensure regulatory compliance, brake pad manufacturers conduct brake performance tests and they can be carried out on vehicles and on dynamometers. The main topic of this paper regards the potential impact of the emitted PM on the human health, depending on the mechanisms of formation and toxicity of the particles. On-going European projects dealing with this important problem will also be discussed in the paper.

**Keywords:** Brake system; wear particles; legal requirements; health

## INTRODUCTION

The pollutants present in the ambient air, primarily respirable particles (particulate matter-PM), draw a lot of attention of researchers, regulatory bodies and the general public because of its negative effects on human health. The legislation of the European Union for many years, and since 2010 also the Serbian regulations, prescribe monitoring of two fractions of particles present in the air, with aerodynamic diameter less than 2.5  $\mu\text{m}$ , so-called fine particles, and smaller than 10  $\mu\text{m}$ ,  $\text{PM}_{10}$ , which includes fine particles and the coarse particles that are in the range of 2.5-10  $\mu\text{m}$ . In addition to natural sources, the most important anthropogenic air pollution sources include power plants and traffic. Fine particles and gases from power plants and transport often come from the combustion process. The literature indicates that industrial processes are the biggest sources of pollution, followed by emissions from installations for the collective and local heating and all forms of transport that represents the process of burning fossil fuels that are not directly tied with industry. In urban areas, road traffic is marked as the biggest source of air pollution [1].

The particulate matter generated by road transport activity can be categorised according to its mechanism of formation. It is often assumed that diesel exhaust is the main source of particulate matter from road vehicles. However, there are a number of non-exhaust processes which can also result in particulate matter being released directly to the atmosphere. The main abrasion processes leading to the direct emission of particulate matter are tyre wear, brake wear and road surface wear. In addition to direct non-exhaust emissions, material previously deposited on the road surface can be suspended or resuspended in the atmosphere as a result of tyre shear, vehicle-generated turbulence, and the action of the wind. In the case of road transport, it is commonly assumed that most

primary fine particles ( $\text{PM}_{2.5}$ ) are emitted from the exhaust, whereas many of the coarse particles ( $\text{PM}_{2.5-10}$ ) are considered to originate from non-exhaust sources. This oversimplifies the situation somewhat; there is evidence to suggest that non-exhaust particles contribute to both the fine and coarse modes [2].

The composition of the friction material influences the brake wear factor. The three types of brake lining tend to be used for conventional applications. NAO linings are relatively soft and create less noise, but they generally wear faster and create more dust than the other types. Low-metallic linings are made from an organic formula mixed with small amounts (10 to 30 %) of metal to help with heat transfer and provide better braking. With the added metal, there is more brake dust, and they may be slightly noisier. Semi-metallic linings have a metal content of around 30 to 65%. These pads are more durable and have excellent heat transfer, but also wear down rotors faster, have intrusive noise characteristics, and may not perform as well under low-temperature conditions [3].

Driving behaviour, in particular the frequency and severity of braking events, is also an important determinant of brake wear. Because the brake wear only occurs during forced decelerations, the highest concentrations of brake wear particles should be observed near busy junctions, traffic lights, pedestrian crossings, and corners. However, particles may also be released from the brake mechanism or wheel housing sometime after the primary emission event [2].

The aim of the present study is to present the different aspects regarding PM resulting from brake wear and provide all the necessary information in terms of physicochemical characteristics, emission factors and possible adverse health effects. On-going European projects dealing with this important problem will also be presented.

## BRAKE WEAR PARTICLES

The results of the recently published study conducted in three European countries, Austria, Switzerland and Germany where 75 million people live, estimated that exposure to respirable particles responsible for about 40,000 deaths per year. Half the number of these deaths is attributed to particles from traffic, which is equal to the number of people who annually die in the European Union in traffic accidents. The introduction of limit values of concentrations of pollutants in the ambient air, in particular, those relating to respirable particles, contributes to improve the health of populations, which certainly has positive economic effects too [4].

Respirable particles are characterized by a number of characteristics including size, density, shape and composition. Generally, the impact on human health, effects on the environment and the fate of particles depend on their size. Particulate matter is frequently classified according to its size, i.e.  $PM_{10}$ ,  $PM_{2.5}$  and  $PM_{0.1}$  for particulates with an aerodynamic diameter  $D$  smaller than, respectively,  $10\ \mu\text{m}$ ,  $2.5\ \mu\text{m}$  and  $0.1\ \mu\text{m}$ . Very coarse particles ( $D > 10\ \mu\text{m}$ ) are generally filtered in the nose and throat. Coarse particles ( $2.5\ \mu\text{m} < D < 10\ \mu\text{m}$ ) can settle in the bronchi and lungs. Fine particles ( $0.1\ \mu\text{m} < D < 2.5\ \mu\text{m}$ ) can easily penetrate into the lungs gas exchange regions, and they might cause vascular inflammation related diseases and possibly lung cancer. Ultrafine particles ( $D < 0.1\ \mu\text{m}$ ) or nanoparticles might be even more dangerous, as they can reach intimate structure of tissues and organs and act as nucleations sites for cancer and degenerative pathologies.

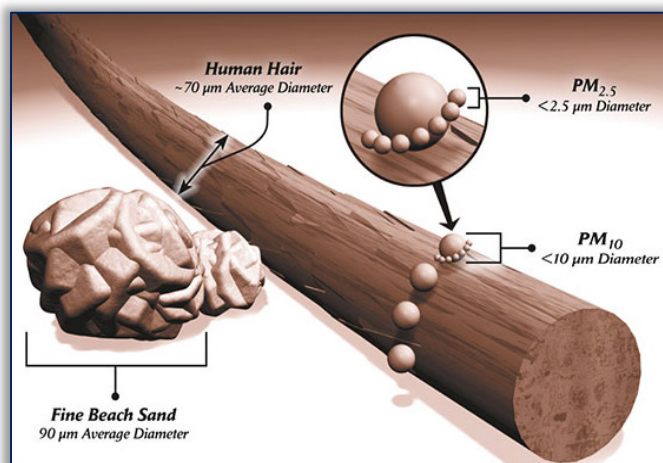


Figure 1. Relative Size of Particulate Matter

Despite the emissions of  $PM_{2.5}$  and  $PM_{10}$  decreased by 16% and 21% respectively between 1999 and 2009, PM limits were exceeded widely across the EU area, a quite discouraging result. Whilst exhaust gases in the road transport are monitored and are the object of the European directives, less is known about the particulates originating from the wear of e.g. brakes and tyres. A recent study for the city of London regarding 2011 and 2015 PM emissions, estimated a consistent increase of the PM wear emissions (brakes and tyres) with respect to the overall PM emissions: from 35% to 47% for  $PM_{10}$  and from 40% to 55% for  $PM_{2.5}$ .

During rapid deceleration, brakes are subject to large frictional heat generation, which leads to the wear of linings and disc. Brake wear emissions tend to occur at junctions, traffic lights, corners and other sites where rapid deceleration occurs. For light-duty vehicles (LDV) and heavy-duty vehicles (HDV), total brake wear factors are around 10-20 mg/vkm and 50-80 mg/vkm (vehicles kilometres) respectively. Around 50% of the particles generated normally enter the atmosphere, and 80% of the emission appears to be  $PM_{10}$ . The proportion originating from the wear of the brake linings compared with wear of the disc or drum is uncertain [2].

## EUROPEAN PROJECTS RELATING TO EMISSION OF BRAKE WEAR PARTICLES

Compliance with air quality standards for  $PM_{10}$  requires control of both fine and coarse particles. As the two modes tend to have different sources and formation mechanisms, different types of control are required. Primary fine particles from combustion sources are subject to regulation. As a result of the changes in legislation, and following the development and application of new technologies, the mass concentration of particles in the exhaust of diesel engines has reduced steadily over the last 20 years. There are currently no legal requirements for the control of the road vehicle non-exhaust particle emissions in the EU. Certain regulations, which are designed for other purposes, could influence nonexhaust PM emissions indirectly. Such regulations include restrictions on the use of studded tyres in certain countries to reduce damage to the road surface, and road/tyre noise standards [2]. There are several on-going research projects, some funded by the EU (e.g. REBRAKE) some by other organizations, that address different issues and very often are not known outside the involved groups or organizations.

Rebrake's project twofold objectives aim at on the one hand bringing a deeper comprehension of the physical and chemical phenomena underlying the brake wear process, including higher comprehension and analysis of characteristics coarse, fine and ultra-fine particles (UFP) and on the other of reducing at least 50% particulate matter ( $PM_{10}$ ) from brake wear, in compliance with the EU2020 thematic strategy of 47% reduction of particulate matter by 2020. The Rebrake project is articulated in four phases. In the first phase of the project, the experimental brake tests consist in setting up experimental tests and elaborating PM collection methodologies. In the second phase, the collected particles, from conventional and, newly developed materials, are chemically and morphologically characterized and compared with literature results regarding human health impacts. In the third phase of the project wear mechanisms are modeled and correlated to the actual brake system parameters and to the ingredients of the linings under investigation. In the fourth phase, novel brake systems will be engineered, in order to cut down the PM emissions by 50%. Knowing the influencing factors on brake dust emissions and how to measure the impact of changed parameters, it is possible systematically to search for measures to reduce the particle emission e.g.

change in formulation, collect the particles or change their physical properties in a way that makes them less harmful [5]. The LOWBRASYS project aims at demonstrating a novel and low environmental impact brake system that will reduce micro and nanoparticles emissions by at least 50%. The measurement and understanding of micrometer-sized and ultrafine particles and their effects on health and the environment will be improved and whilst providing recommendations to policy makers. The LOWBRASYS challenge is to develop a new generation of transport technologies able to push innovation towards a cleaner and more efficient road transport, improving air quality with positive effects on both environment and human life. At the same time LOWBRASYS matches the requirement to comply with possible future stricter legislations on vehicles emissions (both exhaust and non-exhaust) and EU air quality [6].

COBRA will demonstrate a completely novel brake pad production technology that will be based on an innovative hydraulic binder composition instead of phenolic resins, at comparable braking performance. State-of-the-art brake pads are constituted by thermo setting phenolic resins, which are suitable for friction and relatively high contact temperature applications. In addition, the novel technology will avoid the emission of aerosols and secondary ultrafine particulate (PM<sub>0.1</sub>) generated during braking by traditional phenolic-resin-made pads.

Since the phase out of asbestos brakes, brake lining material contains 1–14% Cu with an average Cu content of 5–10% in current brake linings. This makes brake wear from vehicles an important source of atmospheric copper concentrations. It is the dominating source of copper in ambient air in Western Europe. The history of changing regulations governing chemical compounds used in automotive brake pads in North America is shown in Figure 2 [7]. In March 2010, Washington became the first state to pass legislation in an effort to protect its waterways from the runoff of toxic copper brake dust. California also passed a bill, which became law in September 2010. The California law mandates that brakes contain no more than 5 percent copper beginning in 2021. By 2025, the limit will be reduced to 0.5 percent.

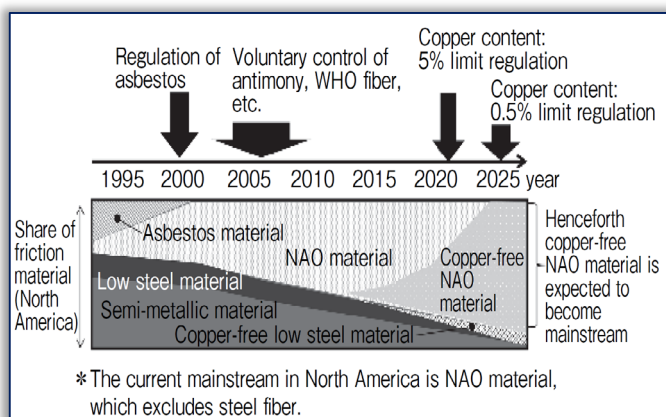


Figure 2. Change in the Regulation of Chemical Substances for Brake Pads [7]

## DEVELOPMENT OF A STANDARDIZED METHOD FOR MEASURING BRAKE WEAR PARTICLES

All involved parties agree that a standardized test procedure for sampling and investigating brake wear particles, both in terms of mass and number, would be beneficial for the research and the development of low emitting brake systems. Brake wear particles generation and sampling can be performed in the laboratory by means of a roller chassis bench (Full Chassis Dynamometer), a brake dynamometer or a pin-on-disc configuration. In one case the attention is focused on particles generated at brake system level while in the other case at vehicle level. While measuring brake particle emissions from a whole vehicle would better reflect real world conditions and would enlarge the range of possible technologies for particle emission reduction (vehicle-to-vehicle communication, hybridization, etc.), this represents a very complex challenge from a scientific and technical point of view. Issues like the representativeness of sampled particles and contribution from other sources (tyres, road, exhaust gas) appear very difficult to resolve.

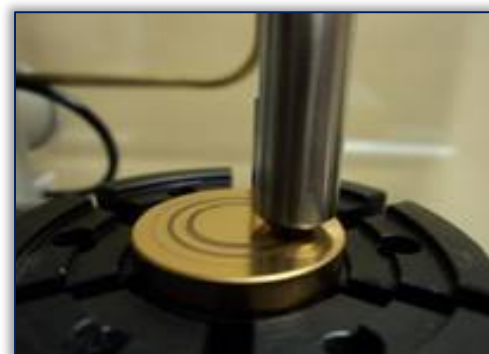


Figure 3. Measuring of brake particles

Test rigs are considered a much simpler solution to investigate particle emissions from brake systems. Brake system suppliers as well as instrument manufacturers is actively working on the development of test rigs based on a brake dynamometer to generate, sample, and characterize particles.

## CONCLUSIONS

Even though a hazardous effect of emissions from friction brakes on humans has not been proven, future regulations are expected to cover total vehicle emissions including those from friction brakes. Overall brake emissions are highly

depending on the applied drive cycles and braking conditions. The quantitative measurement of brake emissions is difficult and complex as the observed system around the brakes has no defined boundaries and cannot be closed without interfering with the particle flow and influencing the measuring results. It is predicted that the relative contribution of non-exhaust sources to traffic related emissions will increase in the forthcoming years due to stricter control in exhaust emissions.

**Acknowledgment:**

Research presented in this paper was supported by Ministry of Education, Science and Technology Development of the Republic of Serbia, Grant TR 35041.

**Note:**

This paper is based on the paper presented at 13th International Conference on Accomplishments in Mechanical and Industrial Engineering – DEMI 2017, organized by University of Banja Luka, Faculty of Mechanical Engineering, in Banja Luka, BOSNIA & HERZEGOVINA, 26 - 27 May 2017.

**References**

- [1] Grigoratos, T. and Martini, G.(2014). Non-exhaust traffic related emissions. Brake and tyre wear PM, Report EUR 26648 EN
- [2] Boulter, P. G. (2007). A review of emission factors and models for road vehicle non-exhaust particulate matter, TRL Limited, Published Project report PPR065
- [3] Kennedy, K. and Gadd, J. (2003). Preliminary examination of trace elements present in tyres, brake pads and road bitumen in New Zealand
- [4] Künzli, N et al. (2000). Public-health impact of outdoor and traffic-related air pollution: a European assessment, The Lancet, vol.356, no.9232, p.795-801
- [5] Ciudin, R., Verma, P.C., Gialanella, S. & Straffelini, G. (2014). Wear debris materials from brake systems: environmental and health issues. WIT Transactions on Ecology and the Environment-The Sustainable City IX, vol.2, p.1423-1434
- [6] The LOWBRASYS project, from <http://www.lowbrasys.eu/en/>, accessed on 2016-09-07
- [7] Ito, T. (2013). Automotive Parts for "Environment, Safety and Comfort Performance", Hitachi Chemical Technical Report, vol.55, p.46-49



ISSN: 2067-3809

copyright © University POLITEHNICA Timisoara,  
Faculty of Engineering Hunedoara,  
5, Revolutiei, 331128, Hunedoara, ROMANIA  
<http://acta.fih.upt.ro>



<sup>1</sup>.Ahmed Abdel Hamid A. ABDALLAH

# MODERN TECHNOLOGY AND ECONOMICAL DEVELOPMENTS IN DESALINATION ON EMPHASIS OF NUCLEAR METHODOLOGY

<sup>1</sup>. Faculty of Engineering at the Civil Engineering Department, Giza Higher Institute of Engineering and Technology, Giza, EGYPT

**Abstract:** Fresh water resources are rapidly being exhausted in many regions in the world. The worst-affected areas are the arid and semiarid regions of Middle East and North Africa. It is estimated that about 20-25% of the world's population are suffering from adequate and safe water supply. This proportion will increase due to population growth relative to water resources. During past decades, more interests are paid to the desalination of sea and brackish water resources. Desalination technologies have been now well established, and the total world capacity in mid-2012 was 80 million m<sup>3</sup>/day of potable water, in some 15,000 plants, majority of these are in the Middle East and North Africa. Nowadays using nuclear energy for fresh water production from seawater (nuclear desalination) has been drawing broad interests in many countries. These interests are driven by the expanding global demand for fresh water, by concern about global heating emissions and pollutions from fossil fuels and developments in small and medium sized reactors that might be more suitable than large power reactors. Several international organizations, like the IAEA, adopted cooperative active programs for supporting the activities on demonstration of nuclear seawater desalination worldwide. These include optimization of the coupling of nuclear reactors with desalination systems, economic research and assessment of nuclear desalination projects, development of software and training for the economic evaluation of nuclear desalination as well as fossil fuel based plants. In this paper, recent technical and economic developments in nuclear desalination and its future prospects have been reviewed and evaluated.

**Keywords:** Nuclear desalination; Potable water needs; Water resources scarce areas

## INTRODUCTION

The purpose of this paper is to provide an overview of various nuclear desalination plant design concepts, which are being proposed, evaluated, or constructed in countries with the aim of demonstrating the feasibility of using nuclear energy for desalination applications under specific conditions. Recent technical and economic developments in nuclear desalination and its future prospects have been reviewed and evaluated. Future potential applications of a variety of nuclear reactor designs in nuclear desalination are being proposed for examination. These include: high- temperature gas reactors (HTGRs), liquid metal cooled reactors (LMRs) such as lead-bismuth cooled or sodium cooled reactors, and other innovative reactor design concepts. The paper also focuses on advanced designs in the small category, i.e. those now being built for the first time or still on the drawing board, and some larger ones which are outside the mainstream categories. Many of the designs described here are not yet actually taking shape. Three main options are being pursued: light water reactors, fast neutron reactors and also graphite-moderated high temperature reactors. The first has the lowest technological risk, but the second (FNR) can be smaller, simpler and with longer operation before refueling.

## DESALINATION TECHNIQUES

Seawater desalination is the process to obtain “pure” water through the separation of the seawater feed stream into:

- » a product stream that is relatively free of dissolved substances, and
- » a concentrate brine discharge stream.

As depicted in Figure 1, desalination processes can be broadly categorized into two main types: processes using heat and process using electricity. The first types of processes are mainly the distillation processes, multi-stage flash (MSF) or multi effect distillation (MED). Vapour compression (VC) is a distillation process but it uses electricity, just as the membrane based processes like the reverse osmosis (RO) and the electro- dialysis (ED). Of these, the most commonly used processes are MSF, MED and RO. VC is often combined with MED.

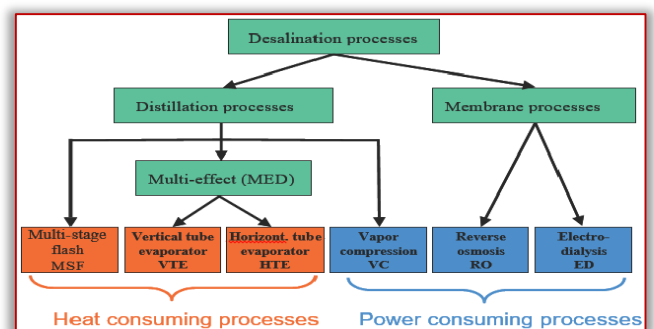


Figure 1. Types of desalination techniques

In distillation processes, (MSF or MED) seawater is heated to evaporate pure vapour that is subsequently condensed. The heat energy required for distillation is usually supplied as low pressure saturated steam, which may be extracted from the exhaust of a back pressure turbine, from a crossover steam duct or from a dedicated, heat only plant. The amount and quality of steam, required to produce the desired amount of pure water, depends on the seawater

temperature, the maximum brine temperature and the type, design and performance of the distillation plant. Usually, the efficiency of distillation plant is expressed in kg of pure water produced per kg of steam used in the first effect: this ratio is called the gain output ratio (GOR).

Desalination is an energy intensive process. For the MED and MSF plants, the principal energy is in the form of heat but some electrical energy is required for the pumps and auxiliaries. RO uses only electrical energy to create the required pressure. The total energy consumption of these two processes is a function of many variables: heating fluid temperature and flow rate, seawater temperature and salinity, desalination plant capacity etc. Indicative values are given in Table 1. Desalination processes are described from technical point of view in many literatures. [1-3]

### STATUS AND DEVELOPMENTS IN NON-NUCLEAR DESALINATION.

#### — Technical Status and Developments

In mid-2012, the total world capacity of potable water was 80 million m<sup>3</sup>/day (29,200 GL/yr), in some 15,000 plants. A majority of these are in the Middle East and North Africa. The largest plant – Jubail 2 in Saudi Arabia - has 948,000 m<sup>3</sup>/day (346 GL/yr) capacity, operated by Saudi Water Conversion Corporation. Two thirds of the world capacity is processing seawater, and one third uses brackish artesian water. The major technology in use and being built today is reverse osmosis (RO) driven by electric pumps which pressurize water and force it through a membrane against its osmotic pressure. (About 27 Bar, 2700 kPa. Therefore RO needs compression of much more than this).

This accounted for 60% of 2011 world capacity. A thermal process, multi-stage flash (MSF) distillation process using steam, was earlier prominent and it is capable of using waste heat from power plants. It accounted for 26% of capacity in 2011. With brackish water, RO is much more cost-effective, though MSF gives purer water than RO. A minority of plants use multi-effect distillation (MED - 8% of world capacity) or Multi-effect Vapour Compression (MVC) or a combination of these. MSF-RO hybrid plants exploit the best features of each technology for different quality products.

In Israel, some 10% of Israel's water is desalinated, and one large RO plant provides water at 50 cents per cubic meter. Malta gets two thirds of its potable water from RO. Singapore in 2005 commissioned a large RO plant supplying 136,000 m<sup>3</sup>/day - 10% of needs, at 49 cents US per cubic meter. Malta gets two thirds of its potable water from RO, and this takes 4% of its electricity supply. Singapore in 2005 commissioned a large RO seawater desal plant supplying 136,000 m<sup>3</sup>/day - 10% of needs, at 49 cents US per cubic meter, and has contracted for a 318,500 m<sup>3</sup>/d RO plant on a build-own-operate basis, costing US\$ 700 million, to provide water at US 36 c/m<sup>3</sup>. The same company is building a 500,000 m<sup>3</sup>/d seawater desal plant in Algeria [4].

The UAE operates the 820,000 m<sup>3</sup>/day Jebel Ali MSF plant in Dubai, Fujairah producing 492,000 m<sup>3</sup>/day, Umm Al Nar

394,000 m<sup>3</sup>/day, and Taweelah A1 power and desal plant producing 385,000 m<sup>3</sup>/day. In February 2012 China's State Council announced that it aimed to have 2.2 to 2.6 million m<sup>3</sup>/day seawater desalination capacity operating by 2015[5]. The Kwinana desalination plant near Perth, Western Australia, has been running since early 2007 and produces about 140,000 m<sup>3</sup>/day (45 GL/yr) of potable water, requiring 24 MWe of power for this, hence 576,000 kWh/day, hence 4.1 kWh/m<sup>3</sup> overall, and about 3.7 kWh/m<sup>3</sup> across the membranes. The plant has pre-treatment, then 12 seawater RO trains with capacity of 160,000 m<sup>3</sup>/day which feed six secondary trains producing 144,000 m<sup>3</sup>/day of water with 50 mg/L total dissolved solids. The cost is estimated at a \$ 1.20/m<sup>3</sup>. Discharge flow is about 7% salt. Future WA desalination plants will have more sophisticated pre-treatment to increase efficiency. In August 2011 the state government decided to double the size of its new Southern Water Desal Plant at Binning up plant near Perth to 100 GL/yr, taking the cost to about \$1.45 billion. Stage 1 of 50 GL/yr was within the A\$ 955 million budget. At the April 2010 Global Water Summit in Paris, the prospect of desalination plants being co-located with nuclear power plants was supported by leading international water experts.

#### — Energy Consumption and Economics

Desalination is energy-intensive process. As seen from Table 1, Reverse Osmosis (RO), needs up to 6 kWh of electricity per cubic meter of water (depending on its original salt content), hence 1 MWe will produce about 4000 to 6000 m<sup>3</sup> per day from seawater. MSF and MED require heat at 70-130°C and use 25-200 kWh/m<sup>3</sup>, though a newer version of MED (MED-MVC) is reported at 10 kWh/m<sup>3</sup> and competitive with RO. A variety of low-temperature and waste heat sources may be used, including solar energy, so the above kilowatt-hour figures are not properly comparable.

Table 1. Average energy consumption and water cost in desalination processes (modified after Ref. [2])

Process	World installed capacity (%)	Specific Heat Consumption (kWth.h/m <sup>3</sup> )	Specific Electricity Consumption (kWth.h/m <sup>3</sup> )	Water Cost (\$ / m <sup>3</sup> )
MSF	44	50-110	4-6*	0.8-1.86
MED	4	60-110	1.5-2.5*	0.27-1.49
RO	42	none	3-5.5	0.45-1.62
ED	6	none	-	0.58
VC	4	-	-	0,46-1.21

\* Some electricity is required to run the pumps and other auxiliary systems in MSF and MED

For brackish water and reclamation of municipal wastewater RO requires only about 1 kWh/m<sup>3</sup>. The choice of process generally depends on the relative economic values of fresh water and particular fuels, and whether cogeneration is a possibility. Approximately, it could be concluded that, in order to produce about 300 000 m<sup>3</sup>/day, MED process would require about 550 MW (th) and 15 MW (e). To produce the same amount of water, RO would require only about 60 MW (e). The thermal energy requirements for MSF could be twice as much as those for the MED plant.

## NUCLEAR DESALINATION

### — Economical and Environmental Incentives

Nuclear desalination is defined to be the production of potable water from seawater in a facility in which a nuclear reactor is used as the source of energy for the desalination process. Electrical and/or thermal energy may be used in the desalination process. The facility may be dedicated solely to the production of potable water, or may be used for the generation of electricity and production of potable water, in which case only a portion of the total energy output of the reactor is used for water production. Nuclear power is a proven technology, which has provided more than 16% of world electricity supply in over 30 countries. More than ten thousand reactor-years of operating experience have been accumulated over the past 5 decades. In recent years, the option of combining nuclear power with seawater desalination has been explored to tackle water shortage problem. Over 175 reactor-years of operating experience on nuclear desalination have been accumulated worldwide. Several demonstration programs of nuclear desalination are also in progress to confirm its technical and economical viability under country-specific conditions, with technical coordination or support of IAEA.

In this context, nuclear desalination now appears to be the only technically feasible, economically viable and sustainable solution to meet the future water demands, requiring large scale seawater desalination:

- » Nuclear desalination is economically competitive, as compared to desalination by the fossil energy sources,
- » Nuclear reactors provide heat in a large range of temperatures, which allows easy adaptation for any desalination process.
- » Some nuclear reactors furnish waste heat (normally evacuated to the heat sink) at ideal temperatures for desalination.
- » Desalination is an energy intensive process. Over the long term, desalination with fossil energy sources would not be compatible with sustainable development: fossil fuels reserves are finite and must be conserved for other essential uses whereas demands for desalted water would continue to increase.

Furthermore, the combustion of fossil fuels would produce large amounts of greenhouse gases and toxic emissions. Basing the estimations to only the Mediterranean region, it can be shown that around 2020, there will be additional need of water production of about 10 million m<sup>3</sup>/day. If nuclear instead of fossil fueled option is chosen, then one could avoid about:

- » 200 000 000 t/year of CO<sub>2</sub>,
- » 200 000 t/year of SO<sub>2</sub>,
- » 60 000 t/year of NO<sub>x</sub>, and
- » 16 000 t/year of other hydrocarbons.

These extrapolated to the world desalination capacities would lead to more than double the amounts given above [6].

### — Current Experience and Developments in Nuclear Desalination

Table 2 summarizes past experience as well as current developments and plans for nuclear-powered desalination based on different nuclear reactor types.

Japan now has over 150 reactor-years of nuclear powered desalination experience. Kazakhstan had accumulated 26 reactor-years before shutting down the Aktau fast reactor at the end of its lifetime in 1999. The experience gained with the Aktau reactor is unique as its desalination capacity was orders of magnitude higher than other facilities.

Most of the technologies in Table 2 are land-based, but the Table also includes a Russian initiative for barge-mounted floating desalination plants. Floating desalination plants could be especially attractive for responding to temporary demands for potable water [7].

Table 2. Current nuclear reactor types and adopted desalination processes

Reactor type	Location	Desalination process	Status
LMFR	Kazakhstan (Aktau)	MED, MSF	In service till 1999
PWRs	Japan (Ohi, Takahama, Ikata, Genkai)	MED, MSF, RO	In service with operating experience of over 125 reactor-years.
	Rep. of Korea, Argentina, etc.	MED	Under design
	Russian Federation	MED, RO	Under consideration (floating unit)
BWR	Japan (Kashiwazaki-Kariva)	MSF	Never in service following testing in 1980s, due to alternative freshwater sources; dismantled in 1999.
HWR	India (Kalpakkam)	MSF/RO	Under commissioning
	Pakistan (KANUPP)	MED	Under construction
NHR-200	China	MED	Under design
HTRs	France, The Netherlands, South Africa, USA	MED, RO	Under development and design

LMFR: liquid metal fast reactor; PWR: pressurized water reactor; BWR: boiling water reactor; HWR: heavy water reactor, NHR: nuclear heat producing reactor; HTR: high temperature reactor MED: multi-effect distillation; MSF: multi stage flash distillation; RO: reverse osmosis

### — Technical and Economic Feasibility of Nuclear Desalination

The following sections provide additional details on the new developments listed in Table 3.

- » Argentina has identified a site for its small reactor (CAREM), which could be used for desalination. A related initiative on safety aspects of nuclear desalination addresses practical improvements and implementation and shares advances around the world.
- » China is proceeding with several conceptual designs of nuclear desalination using NHR type heating reactor for coastal Chinese cities. A test system is being set up at INET (Institute of Nuclear Energy Technology, Tsinghua University, and Beijing) for validating the thermal-hydraulic parameters of a multi-effect distillation process.

- » Egypt has completed a feasibility study for a nuclear co-generation plant (electricity and water) at El-Dabaa. Construction of a pre-heat RO test facility at El Dabaa is nearing completion. The data generated will be shared with interested Member States.
- » France has recently concluded several international collaborations: one with Libya designed to undertake a techno-economic feasibility study for a specific Libyan site and the adaptation of the Libyan experimental reactor at Tajoura into a nuclear desalination demonstration plant using both MED and RO processes in a hybrid combination. The other collaboration is with Morocco (The AMANE project) for a techno-economic feasibility study of Agadir and Laayoun sites. Under a bilateral collaboration signed between India and France, it has also been agreed that the two partners will collaborate on the development of advanced calculation models, which will then be validated at Indian nuclear installations (the experimental reactor CIRUS and the Kalpakkam plant, with hybrid MSF-RO systems).
- » Israel continues to regularly provide technical and economic information on low cost desalination technologies and their application to large-scale desalination plants.
- » Japan continues with its operation of nuclear desalination facilities co-located inside many nuclear power plants.
- » The Republic of Korea is proceeding with its SMART (System-integrated Modular Advanced Reactor) concept. The project is designed to produce 40 000 m<sup>3</sup>/day of potable water.
- » Morocco continues the process of establishing an adequate legal and institutional legislative and regulatory nuclear framework while staying abreast of technical developments in general and nuclear desalination.
- » Tunisia has completed its techno-economic feasibility study, in collaboration with France, for the la Skhira site in the southeast part of the country. The final report, presented in March 2005 was very favorably received by the Tunisian authorities who have already announced their willingness to go for the nuclear desalination option.
- » USA will include in its Generation IV roadmap initiative a detailed discussion of potential nuclear energy products in recognition of the important role that future nuclear energy systems can play in producing fresh water.
- » Further R&D activities are also underway in Indonesia and Saudi Arabia. In addition, interest has been expressed by Algeria, Brazil, Islamic Republic of Iran, Iraq, Italy, Jordan, Lebanon, Philippines, Syrian Arab Republic and United Arab Emirates in the potential for nuclear desalination in their countries or regions.
- » India is building a demonstration plant at Kalpakkam using a 6300 m<sup>3</sup>/day hybrid desalination system (MSF-RO) connected to an existing PHWR. The RO plant, with a production capacity of 1800 m<sup>3</sup>/day, was set up in 2004

and is since operating. The MSF plant (4500 m<sup>3</sup> /day) is to be commissioned in 2006.

- » Libyan Arab Jamahiriya is considering, in collaboration with France, to adapt the Tajoura experimental reactor for nuclear desalination demonstration plant with a hybrid MED-RO system. The MED plant, of about 1000 m<sup>3</sup>/day production capacity, will be manufactured locally.
- » Pakistan is constructing a 4800 m<sup>3</sup>/day MED thermal desalination plant coupled to a PHWR at Karachi. It is expected to be commissioned towards the end of 2006.
- » The Republic of Korea is exploring a possibility of using a co-generating integral type reactor SMART combined with a multi-effect distillation (MED) plant producing 40000 m<sup>3</sup>/day of fresh water. The basic design of 330 MW (th) SMART is completed. In parallel with out-pile tests, a one-fifth scale pilot plant SMART-P is being planned to construct along with a MED unit by 2008.
- » The Russian Federation continues its R&D activities in the use of small reactors for nuclear desalination and has invited partners to participate in an international nuclear desalination project based on a nuclear floating power unit (FPU) equipped with two KLT-40s reactors. The co-generation plant, foreseen for construction in 2006, will be sited at the shipyard in Severodvinsk, Arkhangelsk region in the western North Sea area where the FPU is being manufactured [8].

#### ADVANCES IN REACTOR DESIGN FOR NUCLEAR DESALINATION

There are no specific nuclear reactors for desalination. Any reactors, capable of providing electrical and/or thermal energy can be coupled to an appropriate desalination process. These reactors can operate as dedicated systems (producing only the desalted water) or as co-generation systems producing both water and electricity.

Dedicated nuclear systems are considered more suitable for remote, isolated regions. Many developing countries may face both power and water shortages. In this case, IAEA studies have shown that the small and medium sized reactors (SMRs), operating in the cogeneration mode, could be the most appropriate nuclear desalination systems for several reasons:

- » SMRs have lower investment costs.
- » Almost all SMR concepts appear to show increased availability ( $\geq 90\%$ ).
- » Because of inherent safety features, most SMRS have a larger potential for being located near population centers, hence lowering the water transport costs.

This section is thus mainly devoted to a very brief description of SMRS. These reactors have been discussed in detail in [3]. For the purposes of updating the information, two innovative, generation-4 SMRs (IRIS and ANTARES) are also described. CAREM-D, The NHR-200 and The AP-600 are the most important advanced reactor systems used for modern nuclear desalination plants as described in Table 3.

Table 3. Some technical characteristics of different nuclear reactors proposed for desalination [9]

	CAREM	NHR-200	AP-600	GT-MHR*	PBMR*
Net thermal/ electrical power (MW(th)/MW(e))	100/27	200/NA	610/1932	600/286	266/115
Fuel	Enriched UO <sub>2</sub>	Enriched UO <sub>2</sub>	Enriched UO <sub>2</sub>	Enriched UO <sub>2</sub> particles	Enriched UO <sub>2</sub> particles
Coolant	Water	Water	Water	He	He
Moderator	Water	Water	Water	Graphite	Graphite
Coolant circuit pressure (MPa)	12.25	2.5	15.5	71.5	69.6
Coolant circuit in/out temperature (°C)	284/386	153/210	288/322	493.2/854.6	525/892
Secondary circuit feed water pressure (MPa)	4.7		57.5	-	-
Secondary circuit feed water (fluid) temperature (°C)	200			-	-
Intermediate (or tertiary) circuit pressure (MPa)		3.0		7	7
Intermediate (or tertiary) circuit in/out temperature (°C)		135/170		100	100
Plant life time (years)		40	40	60	60
Net thermal/ electrical power (MW(th)/MW(e))	743/240	330/90	2 X 150/35	335/1002	600/280
Fuel	Nt. UO <sub>2</sub>	Enriched UO <sub>2</sub>	Enriched UO <sub>2</sub>	Enriched UO <sub>2</sub>	Enriched UO <sub>2</sub> particles
Coolant	D <sub>2</sub> O	Water	Water		He
Moderator	D <sub>2</sub> O	Water	Water		Graphite
Coolant circuit pressure (MPa)	10.3	15	12.7	15.5	5.5
	PHWR	SMART	KLT-40C	IRIS	ANTARES
Coolant circuit in/out temperature (°C)	249/293.4	270/310		292/328.4	395/850
Secondary circuit feed water pressure (MPa)	4.2	5.2		6.4	(N <sub>2</sub> /He) 5.5
Secondary circuit feed water (fluid) temperature (°C)	170	180		224	(350/800)
Intermediate (or tertiary) circuit pressure (MPa)					
Intermediate (or tertiary) circuit in/out temperature (°C)			130		30/550
Plant life time (years)	40	60	40	60	60

\* Calculated characteristics for MED couplings based on waste heat utilization

### TECHNICAL AND ECONOMIC DEVELOPMENTS

Considerable advances have been recently made in several countries on the development of improved or innovative nuclear reactors. These include:

- » Advanced PWRs such as CAREM (integral PWR, Argentina), SMART (integral PWR, Republic of Korea), NHR-200 (dedicated heat only reactor, being developed by INET, China), AP-600 (Westinghouse, USA and ANSALDO, Italy) and the barge-mounted KLT-40 class of reactors, derived from Russian Ice-breakers[10].

» HWRs, being modified for nuclear desalination in India and Pakistan. HTRs such as the GT-MHR (developed by an international consortium, led by General Atomics) and the PBMR (planned to be constructed soon in South Africa by the PBMR Company).

» Other advanced reactors such as the integral PWR, IRIS (being developed by an international consortium, led by Westinghouse) and the innovative HTR, ANTARES (under development by Framatome, ANP, France)[11,12].

Desalination technologies have, in parallel, also known considerable technological innovations:

» an almost exponential increase in production capacity of the plants: thus, for example, between the years 1980 and 2005, multi-effect distillation (MED) unit plant capacities have increased from 1 000 to 31 000 m<sup>3</sup>/day and multi-stage flash (MSF) unit sizes have increased from 31 000 to 80 000 m<sup>3</sup>/day.

» choice of high performance materials, (e.g. carbon-steel in place of simple, painted steel), development of high heat transfer alloys for the tubes, increasing use of non-metallic evaporator materials.

» improvement in corrosion resistance (e.g. utilization of anti-scaling organic products in place of conventional acid treatment).

» improvements in availability and thermodynamic efficiencies, due to the incorporation of on-line cleaning procedures.

» modular construction, with improvements in fabrication procedures, reducing construction lead times.

» development of efficient and more precise process control systems and procedures.

The most rapid and significant advances have been reported in membrane based processes, in particular reverse osmosis (RO):

» increase of salt rejection efficiency (from 98 to 99.8 %).

» increase in permeate flux (86 %).

» enhanced chlorine tolerance.

» reduction of the costs of cleaning and pre-treatment due to ever increasing resistance against fouling.

» development of longer life membranes.

Many countries have undertaken nuclear desalination studies in their specific conditions. Analysis of the results leads to the following conclusions: Whatever the nuclear reactor, the desalting capacity and the site-specific conditions, nuclear desalination is by far economically the most interesting option as compared to the gas turbine, combined cycle plant as long as gas prices remain higher than about 21 \$/bbl, if nuclear can achieve capital costs at or below the 1500 \$/kWth range. In this context, the IAEA has received 8 reports summarizing site- studies from Argentina (CAREM + RO), China (NHR-200 + MED), Egypt (PWR-1000 + RO, PWR- 1000 + MED), France (PWR-900 and AP-600, coupled to RO and MED, GT-MHR and PBMR, coupled to MED, with waste heat utilization), India (PHWR + MED, PHWR + RO and PHWR + hybrid MSF-RO), Republic of Korea (SMART + MED),

Pakistan (CANDU + MED) and Syrian Arab Republic (PBMR coupled to MED, MED/VC and RO) [13].

Because of very diverse site conditions, production capacities, economic hypotheses, variety of nuclear reactors and even calculation methods, it is very difficult to arrive at specific conclusions regarding different nuclear desalination systems. One may however, obtain a range of values for different combinations:

- » For the RO based systems, desalination costs vary from 0.6 to 0.94 \$/m<sup>3</sup>.
- » In all cases where the nuclear desalination costs are compared with those from the combined cycle plant, it is observed that the nuclear desalination costs are much lower.
- » For the MED based systems, the nuclear desalination costs vary from 0.7 to 0.96 \$/m<sup>3</sup>.
- » In one study, the MED /VC, coupled to a PWR leads to a cost of 0.5 \$/m<sup>3</sup>.
- » As for RO, wherever comparisons have been made, the desalination cost of nuclear reactors coupled to MED are systematically more than 20% lower than the corresponding cost by the combined cycle MED systems.
- » In a hybrid MSF-RO system, the desalination cost of MSF, coupled to a PHWR is 1.18 \$/m<sup>3</sup>, compared to 0.95 \$/m<sup>3</sup> for RO but that of the hybrid MSF-RO system is 1.1 \$/m<sup>3</sup>. This cost is likely to be further reduced as hybrid system capacity is increased [14].

With identical economic hypotheses, used for three cases, DEEP-3 results show that nuclear reactors, coupled to RO would lead to a desalination cost of 0.6 to 0.74 \$/m<sup>3</sup>. Corresponding cost for MED would be about 0.89 \$/m<sup>3</sup>.

Nuclear desalination costs can still be further reduced by adopting certain cost reduction strategies involving the use of waste heat from nuclear reactors and normally evacuated to the sea or river, the launching of optimized hybrid systems and the extraction of strategic and costly minerals from the brine rejected by desalination plants, accompanied by zero brine discharge to the sea.

The most crucial problem for the launching of full-fledged nuclear desalination systems remains the financing of projects. However, studies have shown that the project financing method (in which instead of financing the local utility, an independent structure for project financing is created and which seeks to reduce the risks through multiple government and/or international credits) coupled to the leasing (instead of buying all the project equipment, a part is leased) would be a very suitable approach for most developing countries [14].

## CONCLUSIONS

This paper provides information and recalls some of the advances made both in the nuclear reactor and desalination technologies. It is expected that the information contained in this report would be of use to decision makers in the Member States considering nuclear desalination options. Desalination technologies are mainly of two types:

- » thermal processes, based on the utilization of heat energy for distillation (also requiring some electrical energy for the pumps and other auxiliary systems) and
- » membrane based processes using only electrical (or mechanical) energy.

Among the thermal processes, the most commonly used are MSF and MED Vapour compression (VC) is a distillation process which uses electrical energy. Reverse Osmosis (RO) and Electro-dialysis (ED) are membrane based processes. There are no specific nuclear reactors for desalination. Any reactors capable of providing electrical and/or thermal energy can be coupled to an appropriate desalination process. These reactors can operate as dedicated systems (producing only the desalted water) or as co-generation systems producing both water and electricity. Dedicated nuclear systems are considered more suitable for remote, isolated regions. Many developing countries may face both power and water shortages. In this case, many studies have shown that the small and medium sized reactors (SMRs), operating in the cogeneration mode, could be the most appropriate nuclear desalination systems.

## References

- [1] T.Younos, Economics of desalination, *Journal of Contemporary Water Resources & Education*, 132, (2015) 39-45
- [2] IAEA, Use of Nuclear Reactors for Seawater Desalination, IAEA-TECDOC-574, IAEA, Vienna (2012)
- [3] IAEA, Optimization of the Coupling of Nuclear Reactors and Desalination Systems, IAEA-TECDOC-1444, IAEA, Vienna (2015)
- [4] S. Nisan, S. Dardour, Y. Dumont, N. Reguigui, Inter-regional collaborative nuclear desalination studies by France and Tunisia, *Int. J. Nuclear desalination*, 1, 3, 308–324 (2014).
- [5] T.M. Pankratz, Advances in desalination technologies. Nuclear desalination: Challenges and options, *International Conference Marrakech, Morocco* (2011).
- [6] IAEA, Desalination Economic Evaluation Program (DEEP 3.0) User's Manual, Computer Manual Series 19, Vienna (2016).
- [7] M.Methnanp, Recent model developments for the Desalination Economic Evaluation Program DEEP, *International Desalination Association Congress*, Singapore (2015).
- [8] S. Nisan, B. Commercon, S. Dardour, A new method for the treatment of a reverse osmosis process with preheating of the feed water, *Desalination*, 182, 485–49 (2005).
- [9] S. Dardour, S. Nisan, F. Charbit, Utilisation of waste heat from GT-MHR and PBMR type of reactors for nuclear desalination, *EUROMED 2006 Conference*, Montpellier, France (2006).
- [10] GT-MHR CONSORTIUM, *International GT-MHR Project Design Review*, St Germain-en- Laye, France (1999).
- [11] J.R. Humphries, K. Davies, J. Ackert, An advanced reverse osmosis technology for applications in nuclear installations, *ICAPP Meeting*, Hollywood, Florida, USA (2002)
- [12] J.Le Dirach, S.Nisan, C. Poletiko, Extraction of strategic materials from the concentrated brine rejected by integrated nuclear desalination systems, *Desalination*, 182, (2005), 451–462
- [13] Massachusetts Institute Of Technology, MIT Report, *The future of nuclear energy* (2003)
- [14] N.Bozgiemda, S. Nisan, M. Albouy, Financing of nuclear desalination projects in developing countries, *EUROMED 2006 Conference*, Montpellier, France (2006)

# FIVE-LEVEL DTC BASED ON ANN OF IM USING 13-LEVEL HYSTERESIS CONTROL TO REDUCE TORQUE RIPPLE COMPARING WITH CONVENTIONAL CONTROL

<sup>1</sup>. Ecole Nationale Polytechnique d'Oran-Maurice Audin, Oran, ALGERIA

**Abstract:** In this paper, the author proposes a novel strategy of direct torque control (DTC) of induction machine (IM) fed by five-level NPC inverter using the Artificial neural network (ANN) applied in switching select voltage. I used the torque hysteresis by using the 13-level hysteresis controller. The DTC control proposed in this paper can reduce the torque ripple, stator flux ripple and the THD value of stator current. The validity of the proposed control scheme is verified by simulation tests of an induction machine.  
**Keywords:** Induction machine; DTC; Five-level NPC inverter; artificial neural network; 13-level hysteresis controller; THD

## INTRODUCTION

In recent years, many studies have been carried out to develop different solution for the induction motor control having the features of precise and quick torque response and reduction of complexity of the field-oriented algorithms. The direct torque control technique has been recognized as viable solution to achieve these requirements [1]. The DTC method has been proposed in the mid 1980's, the DTC method for AC machines is prevalently utilized in many variable speed drive [2]. It is based on the errors between the reference and the estimated values of torque and flux for to directly control the inverter states in order to reduce the torque and flux errors within the prefixed band limits to this end, it uses tables to select the switching procedure based on the inverter states and reduces the influence of the parameter variation during the operation. The DTC drive contains a pair of hysteresis comparators, a flux, torque estimator and a voltage vector selection table. The torque and flux are controlled simultaneously by applying suitable voltage vectors and by limiting these quantities within their hysteresis bands [3]. DTC provides very quick response with simple control structure and hence, this technique is gaining popularity in industries [4]. The disadvantages of conventional DTC are high torque ripple and slow transient response to the step changes in torque during start-up. For that reason the application of fuzzy logic and artificial neural network attracts the attention of many scientists from all over the world [5]. This paper is devoted to multilevel DTC and DTC-ANN of IM.

The reason for this trend is the many advantages which the architecture of ANN have over traditional algorithmic methods. Among the advantages of ANN are the ease of training and generalization, simple architecture, possibility of approximating nonlinear functions, insensitivity to the distortion of the network, and inexact input data [5].

In this paper, I'm present the performance of the DTC control with 13-level hysteresis of IM fed by five-level NPC inverter using ANN. The ANN then replaces the switching table of the

five-level DTC. Neural DTC is used to improve dynamic response performance and decrease the torque and stator flux ripples.

## FIVE-LEVEL DTC CONTROL

The multilevel DTC block diagram is shown in Figure 1. In every sampling time of the inverter stator voltages and currents are sampled. Using these sampled inputs stator flux, speed, torque and flux angle are estimated in the adaptive motor model. Estimated torque and flux are compared with their respective reference values through hysteresis comparators. Based on torque, flux errors and flux angle apt switching state is generated through the optimal switching table [6]. For speed control based on the DTC, a proportional-integral (PI) controller is used to generate the reference torque from the difference between the reference and measured speeds [7].

DTC does not need a pulse width modulator and a position encoder, which introduce delays and requires mechanical transducers respectively. DTC based drives are controlled in the manner of a closed loop system without using the current regulation loop.

The stator flux components are estimated using the measured stator voltage and current components:

$$\begin{cases} \Phi_{s\alpha} = \int_0^t (v_{s\alpha} - R_s i_{s\alpha}) dt \\ \Phi_{s\beta} = \int_0^t (v_{s\beta} - R_s i_{s\beta}) dt \end{cases} \quad (1)$$

The stator flux amplitude is given by [9]:

$$\Phi_s = \sqrt{\Phi_{s\alpha}^2 + \Phi_{s\beta}^2} \quad (2)$$

The stator flux angle is calculated by:

$$\theta_s = \arctg\left(\frac{\Phi_{s\beta}}{\Phi_{s\alpha}}\right) \quad (3)$$

Electromagnetic torque equation is given by:

$$T_e = \frac{3}{2} p [\Phi_{s\alpha} i_{s\beta} - \Phi_{s\beta} i_{s\alpha}] \quad (4)$$

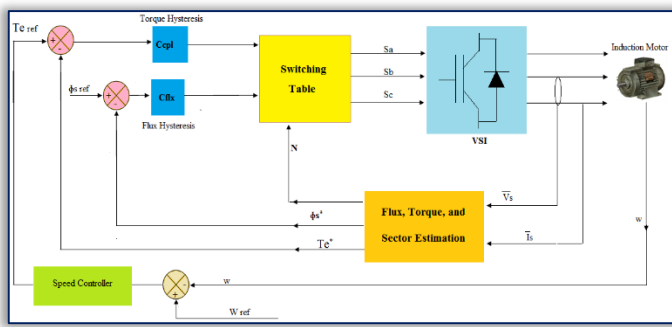


Figure 1. Block diagram of DTC of IM drives

Figure 2 shows the circuit of a five-level diode clamped inverter (NPC) and the switching states of each leg of the inverter. Each leg is composed of two upper and lower switches with anti-parallel diodes. Four series DC-link capacitors split the DC bus voltage in half, and 18 clamping diodes confine the voltage across the switches within the voltage of the capacitors, each leg of the inverter can have five possible switching states, 4, 3, 2, 1 or 0. The NPC can be able to minimize the harmonic distortion of the stator current. Further the active switches of the converter are operated at low frequency [10]. The five-level NPC inverter derived from three-level NPC inverter.

The representation of the space voltage vectors of a five-level inverter for all switching states is given by Figure 3 [11].

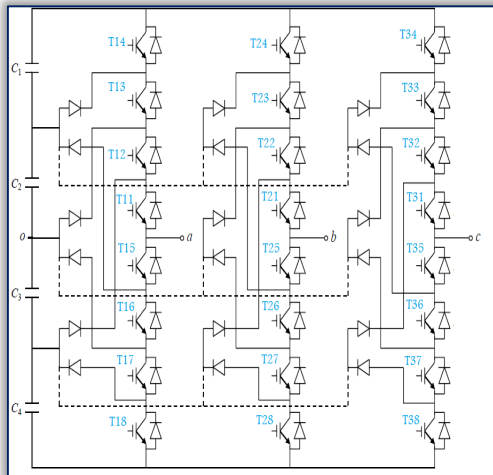


Figure 2. Schematic diagram of a five-level inverter

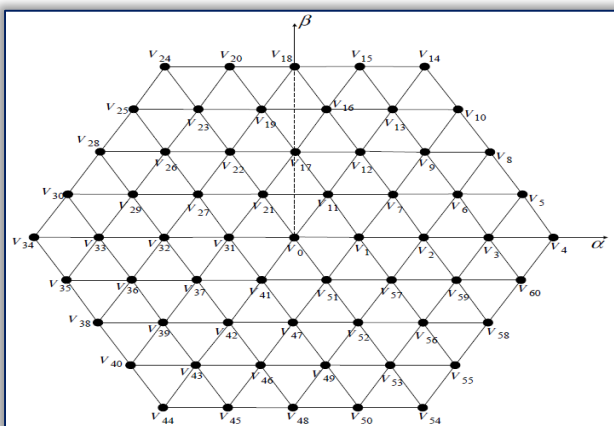


Figure 3. Space vector diagram of five-level inverter

The switching selection block in Figure 1 receives the input signals  $C_{cpl}$ ,  $C_{cflx}$  and  $N$  generate the desired control voltage vector as given in look-up table shown in Table 1.

Table 1. Switching Table of five-level inverter

	$C_{cflx}$	$C_{cpl}$	N											
			1	2	3	4	5	6	7	8	9	10	11	12
1	6	14	14	24	24	34	34	44	44	54	54	4	4	
	5	15	20	25	30	35	40	45	50	55	60	5	10	
	4	18	18	28	28	38	38	48	48	58	58	8	8	
	3	13	13	23	23	33	33	43	43	53	53	3	3	
	2	9	19	16	26	19	29	36	39	46	49	59	6	
	1	12	12	22	22	32	32	42	42	52	52	2	2	
	0	0	0	0	0	0	0	0	0	0	0	0	0	
	-1	52	52	2	2	12	12	22	22	32	32	42	42	
	-2	56	59	6	9	16	19	26	29	36	39	46	49	
	-3	53	53	3	3	13	13	23	23	33	33	43	43	
	-4	58	58	8	8	18	18	28	28	38	38	48	48	
	-5	55	60	5	10	15	20	25	30	35	40	45	50	
	-6	54	54	4	4	14	14	24	24	34	34	44	44	
0	6	17	17	27	27	37	37	47	47	57	57	7	7	
	5	17	17	27	27	37	37	47	47	57	57	7	7	
	4	17	17	27	27	37	37	47	47	57	57	7	7	
	3	11	11	21	21	31	31	41	41	51	51	1	1	
	2	11	11	21	21	31	31	41	41	51	51	1	1	
	1	11	11	21	21	31	31	41	41	51	51	1	1	
	0	0	0	0	0	0	0	0	0	0	0	0	0	
	-1	0	0	0	0	0	0	0	0	0	0	0	0	
	-2	41	41	51	51	1	1	11	11	21	21	31	31	
	-3	47	47	57	57	7	7	17	17	27	27	37	37	
	-4	42	42	52	52	2	2	12	12	22	22	32	32	
	-5	46	49	56	59	6	9	16	19	26	29	36	39	
	-6	43	43	53	53	3	3	13	13	23	23	33	33	
-1	6	24	24	34	34	44	44	54	54	4	4	14	14	
	5	25	30	35	40	45	50	55	60	50	10	15	20	
	4	28	28	38	38	48	48	58	58	8	8	18	18	
	3	23	23	33	33	43	43	53	53	3	3	13	13	
	2	19	26	29	36	39	46	49	56	59	6	9	16	
	1	22	22	32	32	42	42	52	52	2	2	12	12	
	0	0	0	0	0	0	0	0	0	0	0	0	0	
	-1	42	42	52	52	2	2	12	12	22	22	32	32	
	-2	46	49	56	59	6	9	16	19	26	29	36	39	
	-3	43	43	53	53	3	3	13	13	23	23	33	33	
	-4	48	48	58	58	8	8	18	18	28	28	38	38	
	-5	45	50	55	60	5	10	15	20	25	30	35	40	
	-6	44	44	54	54	4	4	14	14	24	24	34	34	

### FIVE-LEVEL DTC CONTROL WITH ANN

In order to improve the five-level DTC performance a complimentary use of neural network is proposed. ANN is part of the family of statistical learning methods inspired by biological nervous system and are used to estimate and approximate functions that depends only on a large number of inputs [12].

ANN's have been proven to be universal approximations of non-linear dynamic systems. They are able to emulate any complex non-linear dynamic system by using an appropriate multilayer neural network. Many applications have been reported in power electronics, including fault detection and diagnosis in electrical machines, power converter control and the high performance control of electrical drives [13]. The general structure of the IM with DTC-ANN using a five-level inverter is represented by Figure 4. The Artificial neural network replaces the switching table selector block. He uses a dense interconnection of computing nodes to approximate nonlinear function [14].



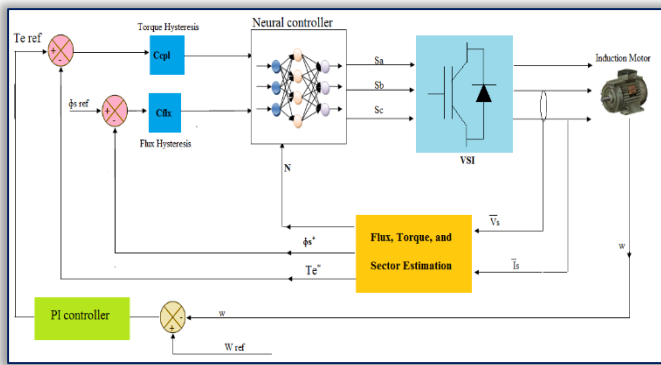


Figure 4. Block diagram of DTC-ANN of IM drives  
The structure of the neural network to perform the five-level DTC applied to IM satisfactorily was a neural network with 3 linear input nodes, 64 neurones in the hidden layer, and 3 neurones in the output layer, as shown in Figure 5.

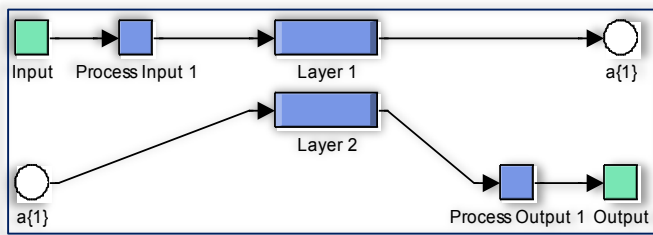


Figure 5. Neural network structure for five-level DTC

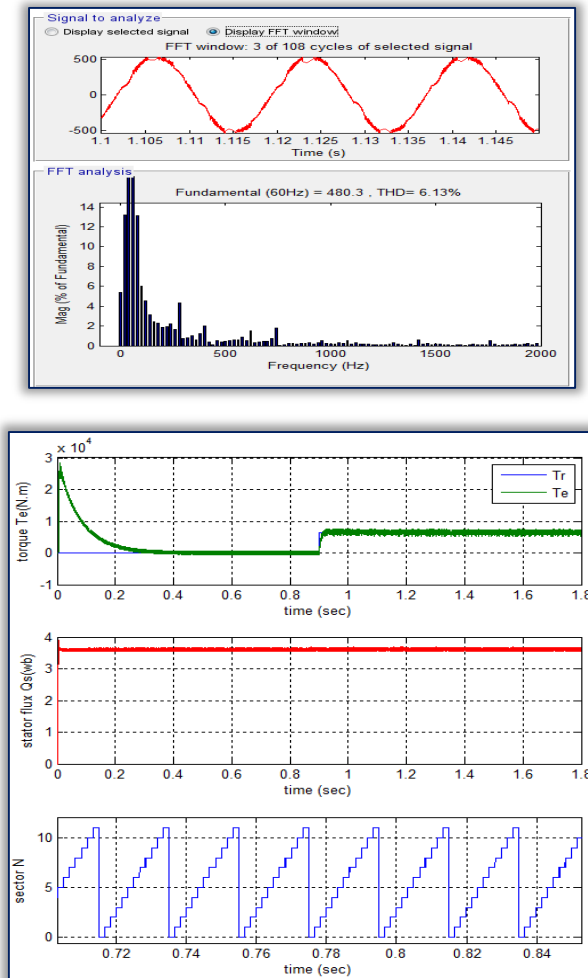


Figure 6. Dynamic responses of five-level DTC

## SIMULATION RESULTS

The simulation results of five-level DTC-ANN of IM are compared with conventional five-level DTC. The performance analysis is done with stator current, stator flux and torque plot. The dynamic performance of the five-level DTC for IM is shown Figure 6. The dynamic performance of the five-level DTC-ANN control is shown Figure 7.

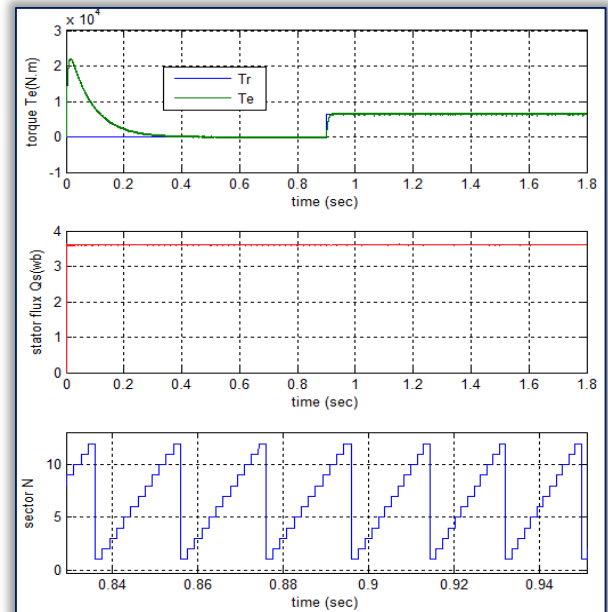
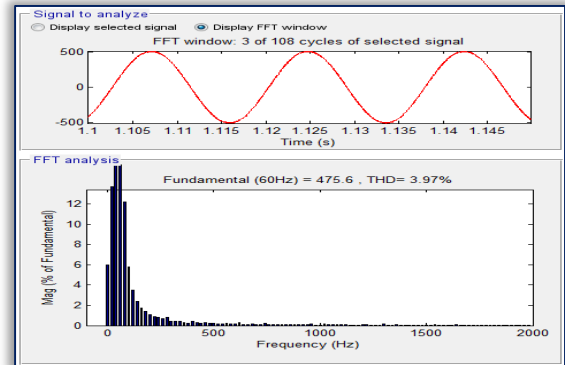


Figure 7. Dynamic responses of five-level DTC-ANN

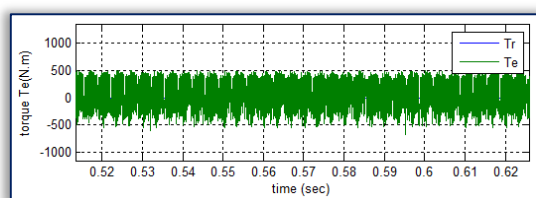
Figures 6-7 show that the THD value of stator current in the five-level DTC-ANN scheme has been reduced significantly. Table 2 shows the comparative analysis of THD value of stator current.

Table 2. Comparative analysis of THD value of stator current

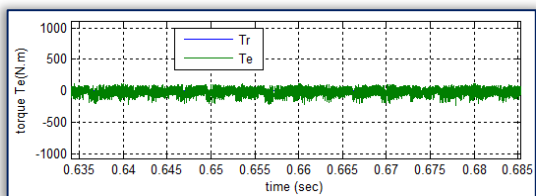
Five-level DTC	Five-level DTC-ANN
6.13%	3.97%

The use of ANN has improved the band electromagnetic torque are shown in Figure 8.

From the simulation results presented in Figure 9, it is apparent that the stator flux ripple for the five-level DTC-ANN is considerably reduced. In other hands, the stator flux was restored correctly its reference.



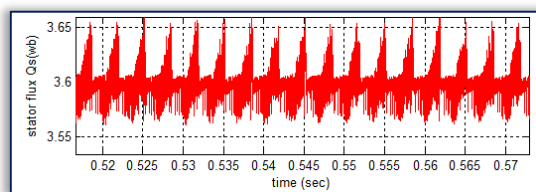
a)



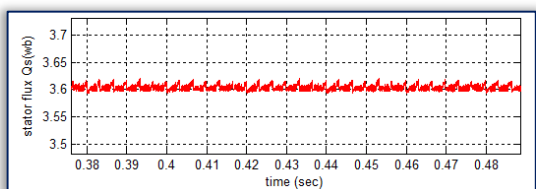
b)

Figure 8. Zoom in the torque.

a) Five-level DTC; b) Five-level DTC-ANN



a)



b)

Figure 9. Zoom in the stator flux.

a) Five-level DTC; b) Five-level DTC-ANN

## CONCLUSIONS

In this paper, the five-level DTC principle is presented and it is shown that with ANN technique for induction machine. The simulation results obtained for the five-level DTC with ANN illustrate a considerable reduction in torque ripple, stator flux ripple and THD value of stator current compared to the conventional five-level DTC.

## References

- [1] E. Hassan, D. A. Khaburi, "DTC-SVM scheme for induction motors fed with a three-level inverter," *International Journal of Mechanical, Aerospace, Industrial, Manufacturing Engineering*, Vol. 2, No. 8, 2008, pp: 958-962.
- [2] O. Hemakesavulu, C. Ganesh, M. Manasa, "Simulation of fuzzy logic controller based matrix converter DTC-SVM method for induction motor drive," *International Journal of Computer Engineering and Applications*, Vol. 7, Issue 3, Parte 1, 2014, pp: 98-111.
- [3] L. Salima, B. Tahar, S. Youcef, "Direct torque control of dual star induction motor," *International Journal of Renewable Energy Research*, Vol. 3, No. 1, 2013, pp: 121-125.
- [4] A. Idir, M. Kidouche, "Direct torque control of three phase induction motor drive using fuzzy logic controllers for low torque ripple," *Proceedings Engineering & Technology*, Vol. 2, 2013, pp: 78-83.

- [5] A. Abbou, H. Mahmoudi, "Performance of a sensorless speed control for induction motor using DTFC strategy and intelligent techniques," *Journal of Electrical Systems*, Vol. 6, No. 3-5, 2009, pp: 64-81.
- [6] G. Kumara Swamy, Y. P. Obelusu, "Modified SVPWM algorithm for 3-level inverter fed DTC induction motor drive," *International Journal of Power Electronics and Drive System*, Vol. 7, No. 4, 2016, pp: 1134-1145.
- [7] A. A. Hassan, A. M. EL-Sawy, Y. S. Mohamed, E. G. Shehata, "Sensorless sliding mode torque control of an IPMSM drive based on active flux concept," *Alexandria Engineering Journal*, Vol. 51, 2012, pp: 1-9.
- [8] H. G. Zaini, M. K. Metwally, M. Ahmed, "Direct torque control of induction motor drive fed from hybrid multilevel inverter," *International Journal of Electrical & Computer Sciences*, Vol. 14, No. 3, 2014, pp: 6-11.
- [9] H. Benbouhenni, "Comparateur à hysteresis à sept niveaux pour la commande DTC basée sur les techniques de l'intelligence artificielle de la MAS," *Journal of Advanced Research in Science and Technology*, Vol. 4, No. 2, 2017, pp: 553-569.
- [10] P. Rajasekaran, V. Jawahar Senthilkumar, "An improved DTFC based five-levels NPC inverter fed induction motor for torque ripple minimization," *International Journal of Power Electronics and Drive System*, Vol. 7, No. 2, 2016, pp: 531-542.
- [11] E. Benyoussef, A. Meroufel, S. Barakat, "Three-level DTC based on Fuzzy logic and neural network of sensorless DSSM using extended kalman filter," *International Journal of Power Electronics and Drive System*, Vol. 5, No. 4, 2015, pp: 453-463.
- [12] D. Narasimha Rao, T. Surendra, S. T. Kalyani, "DPFC performance with the comparison of PI and ANN controller," *International Journal of Electrical and Computer Engineering*, Vol. 6, No. 5, 2016, pp: 2080-2087.
- [13] A. Miloudi, E. AL-radadi, A. Draou, "A simple hysteresis PI based neural controller used for speed control of an indirect field oriented induction machine drive," *Journal of Electrical Engineering*, Vol. 58, No. 1, 2007, pp: 10-18.
- [14] A. Abbou, H. Mahmoudi, "Performance of a sensorless speed control for induction motor DTFC strategy and intelligent techniques," *Journal of Electrical Systems*, Vol. 6, No. 3-5, 2006, pp: 64-81.



ISSN: 2067-3809

copyright © University POLITEHNICA Timisoara,  
Faculty of Engineering Hunedoara,  
5, Revolutiei, 331128, Hunedoara, ROMANIA  
<http://acta.fih.upt.ro>

<sup>1</sup>Malik Muhammad ZAID, <sup>1</sup>Muhammad NAUMAN,  
<sup>2</sup>Mudasser RAHIM, <sup>3,4</sup>Muhammad Usama MALIK

## DSP BASED ENERGY MONITORING WITH ONLINE DAQ SYSTEM

<sup>1,2</sup> University of Engineering and Technology, Lahore, PAKISTAN

<sup>3</sup> University of Engineering and Technology, Taxila, PAKISTAN

<sup>4</sup> Technical Education and Vocational Training Authority (TEVTA), Jhelum, PAKISTAN

**Abstract:** This work manifests a low-cost three phase digital signal processing (DSP) based energy monitoring with online data acquisition (DAQ) system. In this endeavor, multifarious parameters are measured. All these parameters are displayed on the TFT LCD of the microcontroller in the real-time domain. Along with the measurement of miscellaneous parameters from the microcontroller, these parameters are directed over the internet via Wi-Fi module. On the internet, there is a succinct, vivid and pithy data log of these measured parameters which show their respective instantaneous values and accumulates them on the internet. This data log interprets energy monitoring over a period of the day, week, month or year. This energy meter can measure voltage (RMS), current (RMS), apparent power (S), real power (P), frequency, displacement factor, distortion factor and total harmonic distortion (THD) of current and voltage using a STM32F429 microcontroller.

**Keywords:** three phase energy monitoring, thin film transistor, digital signal processing, online monitoring, load duration curve

### INTRODUCTION

The measurement of electrical energy plays an essential role in monitoring the usage of electricity. Electric supply companies usually set up an electric meter to measure electrical energy. These companies usually collect data at the end of the month and deliver the bills to consumers. But still, in the modern age, there is a possibility of error in it. There might be the possibility of electricity theft. For these possible errors, there needs a device that will keep the record of the consumer's usage of electricity, from which a consumer can compare his utilization or can improve his electrical energy consumption habits. There should be a device that collects all the data and store it and whenever consumer want to go through it is available.

In the modern age, almost everything is executed online, the energy is also measured online for this purpose. Digital signal processing technique is one of the most frequently used technique nowadays. Mathematical manipulations are usually used in this technique. The measuring algorithms like digital filtering and Fourier transform [1] require the very frequent use of mathematical operation. Furthermore, daily life physical signals can be transformed into digital form through an analog to digital converters (A/D). The voltage and current signals are transformed to digital form and are used for energy measuring purpose. So, there must be an asunder A/D for the measurement of voltage and current. Moreover, this device is portable, can easily communicate, can display results on LCD & the internet and of low-cost.

Online energy measuring instruments are usually characterized by their data processing time. Data processing time usually depends on adopted algorithms and processors. One of the best things to implement all these applications is a microcontroller which has A/D, timers and all the necessary things which are required. Due to the presence of a non-

linear load in power system, it affects the power quality of system especially power factor by producing harmonics in current waveform. So, it is necessary to measure the degree of harmonics which causes the distortion of current waveform [2]. For this various power, quality monitors developed.

In power system, various parameters play the very important role that effects the power quality. For measuring these parameters fluke meter is used which measures power factor, three phase voltages and current, THD etc. But, it is quite expensive on an academic level. In this paper microcontroller based energy meter, with online DAQ system is bestowed. Other than regular quantities that traditional meters measure, it also has an apex importance to measure energy quality factors.

### WORK GOALS

This meter is used to measure three phase voltages, current, power factor, real and reactive power, frequency, THD of current & voltage, displacement factor and distortion factor. All the measured parameters are shown in real time on the TFT LCD of the microcontroller along with this all the parameters are also sent on the internet, where the graphs showing the energy consumption patterns are displayed. Using this meter, the status of energy consumption can be known worldwide by accessing only the internet. If energy consumption in any building exceeds the allowable limit then the alarm will ring on the mobile or laptop on which energy consumption pattern is monitoring.

This meter can be installed in homes or in any commercial building. Energy consumption of a day, week, month or a year can be easily analyzed. This meter is entirely based on digital signal processor (DSP) in which signal computations are done to achieve work goals.

## SYSTEM ARCHITECTURE

This meter is composed of the three-phase voltage sensor, current sensor comprising of three CTs having a ratio of 450:5 Amps and zero crossing detector. Along with this the small and valuable circuitry named “signal conditioning circuit” is also present, which plays a vital role in signal computations in the hardware. This signal conditioning circuit is composed of 1-volt D.C shift. The microcontroller used in this meter is STM32F429-Disco with TFT LCD. In this energy meter built in A/D of the microcontroller is used. Online monitoring uses the ESP8266 Wi-Fi module to send data over the internet. All energy consumption patterns are seen on the website thingspeak.com.

### A. Voltage Sensor

It consists of three voltage transformers (VTs) and each VT is used for one phase. It steps down 230 volts A.C to 13 volts. These 13 volts are not in the range of A/D converter which is 0 to 3.3 volts [3] until these 13 volts are passed through the potential divider to get 0.619047 volts across the resistor and this voltage is further used to measure voltage. In this sensor, such low value of the voltage is used to be measured by the microcontroller because if transient occurs in the three-phase system then the voltage taken by the microcontroller will not exceed 3.3 volts [3]. Figure 1 shows the schematic of the voltage sensor's connection.

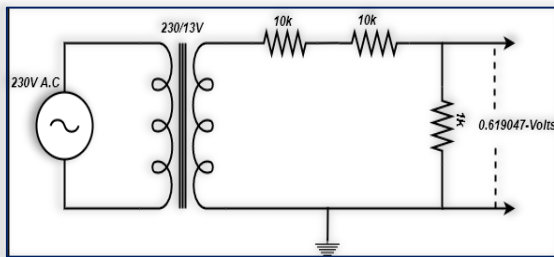


Figure 1. Schematic of voltage sensor's connection

### B. Current Sensor

This sensor is composed of three current transformers (CTs). It steps down the current at a ratio of 450:5 amps. The burden used for this CT is 0.47 ohms. The current is passed through the CT and to measure this current, voltage is taken across the burden. The CT used in the sensor is shown in figure 2 and how this sensor is deployed in the hardware is shown in figure 3.



Figure 2. Current transformer (CT)

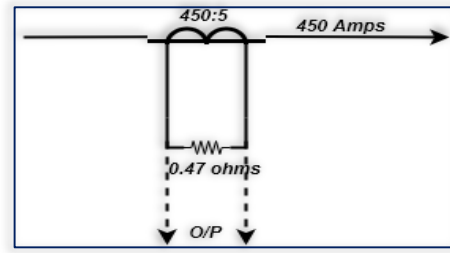


Figure 3. Schematic of current sensor's connection

### C. Zero Crossing Detector

System frequency is measured by using zero crossing detector. In this circuit, 230 volts AC is stepped down to 13 volts and after passing through the potential divider it is sent to zero-crossing IC LM358 which gives digital logic on the output, working as a comparator. When the sinusoidal waveform falls below the zero axis it gives high logic and when sinusoidal waveform goes above zero axis then afore-said IC gives low logic and this output is given to the microcontroller and the frequency is measured using the timer interrupt. The output waveform of zero-crossing is shown in fig 5.

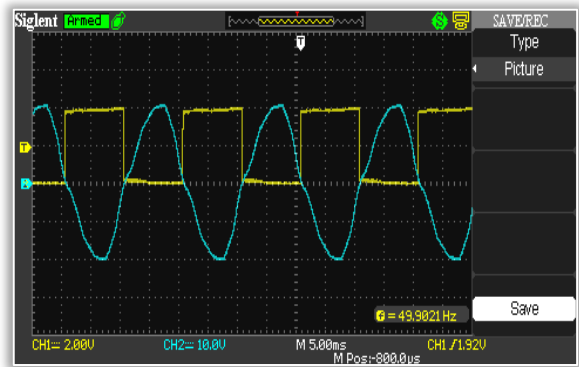


Figure 4. Output of zero crossing detector

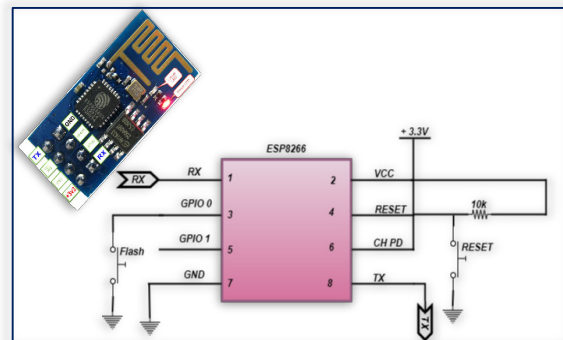


Figure 5. Schematic of ESP8266 Wi-Fi module

### D. Wi-Fi Module

The critical part is the design of the data log system for the acquisition of AC parameters. Although the understandable GUI on the TFT LCD of STM32F429 is developed for the instant monitoring purpose of electrical power being used. But this data log will enable to draw a load duration curve on the daily, monthly, weekly or annual basis. For this, IOT Module ESP8266 is used, it is a Wi-Fi operated the device. It accepts commands to work. There are some sites that give free space to view data sent by ESP8266 to the Internet. To

make ESP8266 work properly with a microcontroller, it is very necessary to match their baud rates. The module is configured in station mode and has nearby Wi-Fi access to facilitate data transmission and reception. Figure 5 shows the circuit diagram of ESP8266 Wi-Fi module.

### E. Signal Conditioning Current

This is the smallest but very important part of the meter. This meter works on the STM32F429IZ-Disco microcontroller while the A/D of this microcontroller is unipolar but our signals are bipolar. The microcontroller is unable to read these bipolar signals. For this purpose, signal conditioning circuit is designed to adapt the signal which gives DC offset to the voltage and current signal so that these signals are centered across 1 volt. The voltage and current signals are passed through signal conditioning circuit [4] to give them a shift of 1 volt to make all signals within the range of A/D which is 0 to 3.3 volts [3]. All these shifted signals are then sent to the microcontroller for further progress.

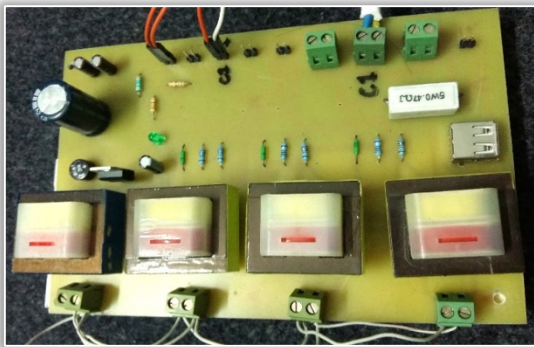


Figure 6. Voltage sensor's hardware PCB

## SOFTWARE IMPLEMENTATION

The below list shows some of the major techniques of software implementations.

### A. External Memory (SDRAM)

Define To store all the data external SDRAM of 64-Mbit is used. Which consists of 4-banks of 16 Mbit each. The bank consists of 4096 rows with 256 columns and 16 bits. This external SDRAM has different modes of operation comprising of auto-refresh, power-saving and power-down. In this, the values are captured on the positive edge of the clock signal. The DMA controller has direct access to memory and can trigger transactions such as peripheral to memory, memory to peripheral and memory to memory.

In this energy meter, six independent channels of the ADC-3 are used for power system and is attached with APB-2. The default frequency of ADC-3 is 90 MHz but the prescaler is accordingly set in such a way that frequency of the ADC-3 becomes 45 MHz, which is the sampling frequency of ADC. In this, samples are taken at the timer interrupt and the frequency of this timer interrupt is 25.6 kHz. Therefore, in the end, the sampling frequency of this energy meter becomes 25.6 kHz in which 512 samples are taken in one cycle for signal computation.

All these samples are stored in the internal buffer and when the internal buffer is near to its full capacity all this data is

immediately transferred to address in the external memory through DMA. Samples are taken without any loss and the better accuracy is obtained by using this technique. When the DMA is in the mode of data transfer, reading or writing, microcontroller performs other calculations.

### B. System's Algorithm

In this ADC is configured in an independent mode with five-cycles and two sampling delay. For the acquisition of samples, a timer interrupt of 25.6 KHz is introduced which collects 512 samples in a 50Hz AC cycle. Samples are stored in the memory space using direct memory access (DMA) to avoid data loss. After the collection of 512 samples, RMS of the signal is calculated using given formula and this signal is the shifted signal obtained after the addition of 1-volt DC shift. The flowchart showing all the steps of software implementations is shown in figure 7.

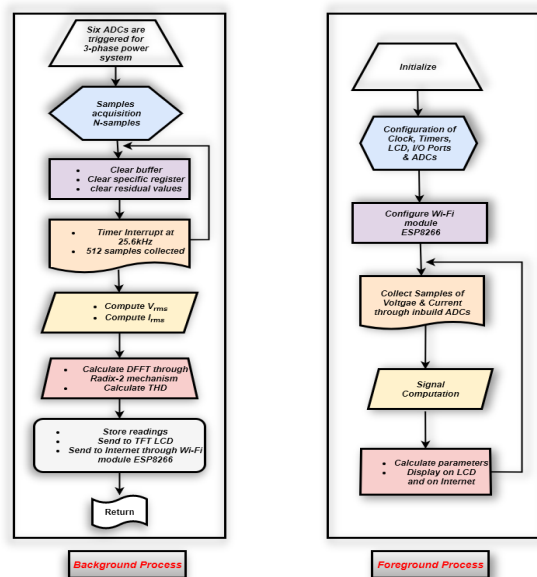


Figure 7. Flow chart of software implementation

$$V_{\text{rms,shifted a.c}} = \sqrt{\frac{\sum_{i=1}^n (X_i)^2}{n}} \quad (1)$$

$$I_{\text{rms,shifted a.c}} = \sqrt{\frac{\sum_{i=1}^n (X_i)^2}{n}} \quad (2)$$

$n$  = number of samples  $X_i$  = Instant sample

The number of samples is calculated by using the given formula as described below:

$$\text{Number of samples} = \frac{\text{Timer frequency}}{\text{A.C signal frequency}}$$

$$\text{Number of samples} = \frac{25.6 \text{ KHz}}{50 \text{ Hz}} = 512 \text{ samples}$$

In this case,  $n = 512$  samples.

The average value of the shifted signal having DC shift of 1-volt is calculated by using following formula:

$$V_{\text{mean,shifted signal}} = \frac{\sum_{i=1}^n (X_i)}{n} \quad (3)$$

$$I_{\text{mean,shifted signal}} = \frac{\sum_{i=1}^n (X_i)}{n} \quad (4)$$

$n$  = number of samples  $X_i$  = Instant sample

The RMS value of AC signal excluding the DC shift is calculated as:

$$AC^2 = RMS^2 - DC^2 \quad (5)$$

$$AC = \sqrt{RMS^2 - DC^2} \quad (6)$$

$$V_{rms,ac} = \sqrt{V_{rms,shifted\ ac}^2 - V_{mean,shifted\ ac}^2} \quad (7)$$

$$I_{rms,ac} = \sqrt{I_{rms,shifted\ ac}^2 - I_{mean,shifted\ ac}^2} \quad (8)$$

For the calculation of apparent power, following formula is used

$$S = V_{rms} * I_{rms} \quad (9)$$

Since load can be unbalanced on all three phases, so apparent power of each phase must be calculated separately. Total apparent power will be the sum of apparent power of all three phases such as

$$S_{total} = S_a + S_b + S_c \quad (10)$$

Similarly, the real power is also calculated for each phase. The real power is average utilized power over a complete cycle as

$$P = \frac{\sum_{i=1}^N (V_i * I_i)}{N} \quad (11)$$

The input displacement factor (IDF) is:

$$IDF = \frac{P}{S} = \frac{Real\ Power}{Apparent\ Power}$$

While the true power factor becomes:

$$PF = Input\ Displacement\ factor * Distortion\ Factor$$

The distortion in the signal is calculated using Fast Fourier Transform (FFT) technique [5]. With the help of FFT, different frequency components are calculated using the radix-2 algorithm. Radix-2 is the fast process for the calculation of FFT. In this method samples are divided into two parts of equal number of samples then these resulting samples are present in two parts and each part consists of the same number of samples as the other part then each part is further divided into equal number of samples and this process goes on until we get each part which has 2 samples then FFT of such number of samples is trivial and can easily be calculated. For example, when we have eight number of samples then it is divided into two FFT's of size 4 and then this is divided into four FFT's of size 2 and then it is easy to find the FFT's of size two through the radix-2 mechanism. This mechanism for eight number of samples is also shown below in figure 9.

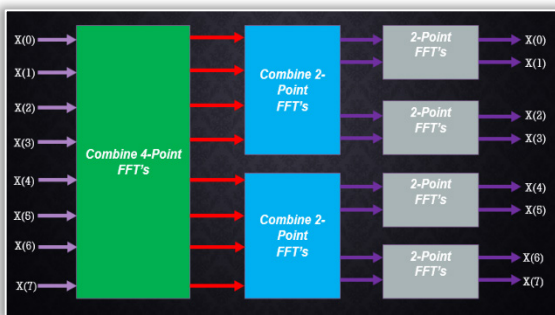


Figure 8. Radix-2 mechanism of FFT

For the calculation of THD factor first, thirteen frequency components are taken. Distortion factor and total harmonic distortion are calculated for each phase using the formula:

$$THD_F = \sqrt{\frac{V_2^2 + V_3^2 + V_4^2 + \dots + V_n^2}{V_1^2}} \quad (12)$$

$$THD_F = \sqrt{\frac{I_2^2 + I_3^2 + I_4^2 + \dots + I_n^2}{I_1^2}} \quad (13)$$

$$Dist.\ fact.\ in\ V_a = \frac{V_1}{V_{rms}} \quad (14)$$

where  $V_1$  is the first harmonic component in the signal. The power factor for each phase is calculated separately. For the sake of better Information, the average power factor is calculated.

The calculated data is then sent to a website for monitoring and plotting of load duration curve. For this purpose, ESP8266 Wi-Fi module is used. It is configured in station mode and connected to local Wi-Fi. The data is sent to thingspeak.com using internet protocol. USART (Universal Synchronous/Asynchronous Receiver Transmitter) is configured to send AT commands to Wi-Fi module at the baud rate of 115200 bits/second. Along with uploading of data, all measurements are also displayed on a built-in TFT LCD of the microcontroller.

## RESULTS AND DISCUSSIONS

This meter is attached with three phase variable supply of 0-300V (10A each phase) and the results are compared with the Yokogawa meter, 2013 model. Figure 9 shows the voltage measurements.

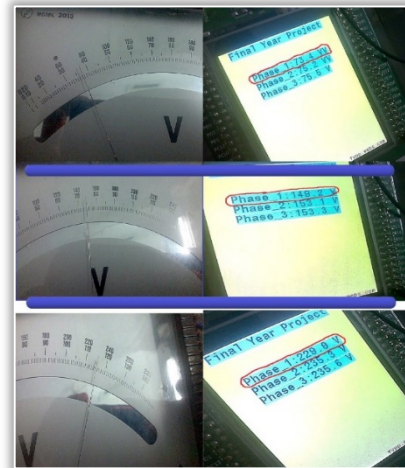


Figure 9. Voltage reading on microcontroller

The graph of voltage reading is shown in figure 10.

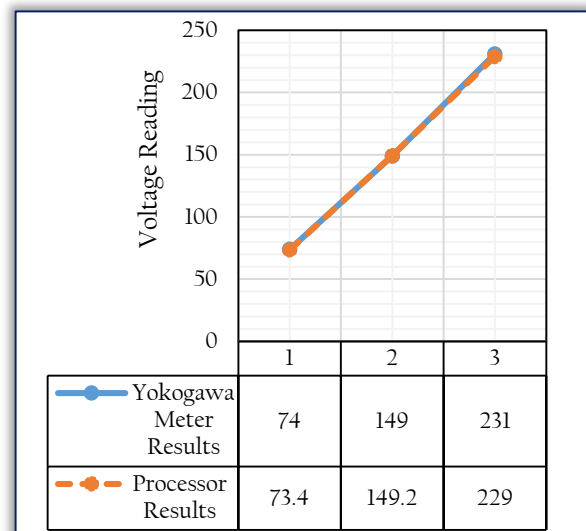


Figure 10. Voltage comparison between microcontroller and meter reading

For the measurement of the current non-linear load is connected and the results are compared with the Yokogawa current meter. Figure 11 shows the results of current measurement.

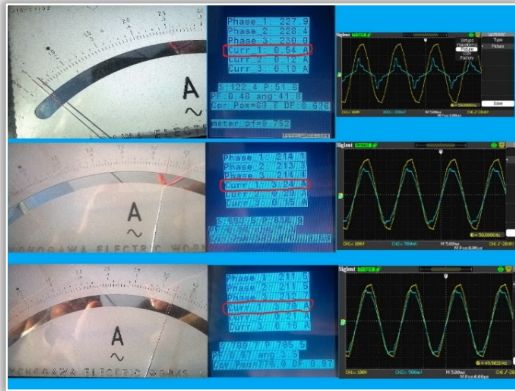


Figure 11. Current Measurement on microcontroller  
The graph of current reading is shown in figure 12.

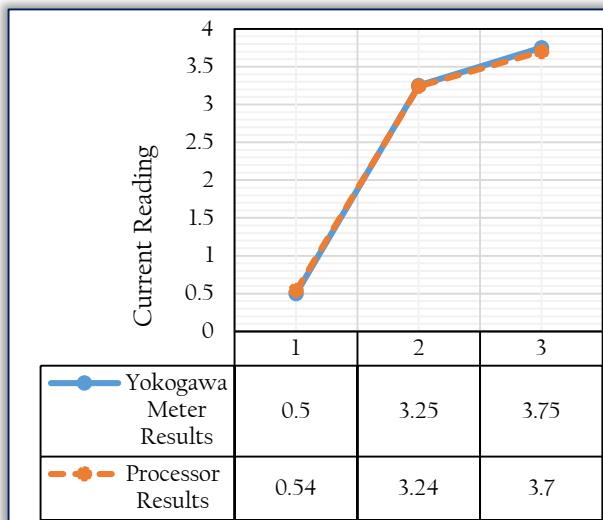


Figure 12. Current comparison between microcontroller and meter reading

Percentage error calculated from these measurements are shown below in figure 13.

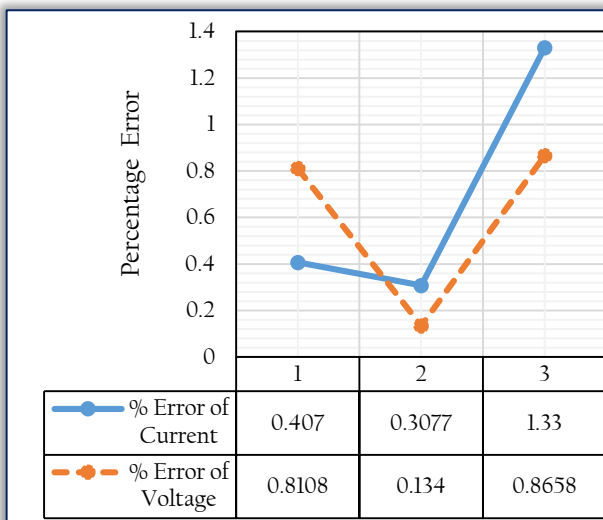


Figure 13. Percentage error of voltage and current readings

In this work, the square waveform is given to the meter with D.C shift of 1 volt. Fourier analysis is performed on the square waveform and Fourier coefficients are calculated from the radix-2 mechanism. These Fourier coefficients are compared with theoretical Fourier coefficients calculated as shown below:

$$V_0(t) = a_0 + \sum_{n=0}^{\infty} [a_n \cos(n\omega_s t) + b_n \sin(n\omega_s t)]$$

$$V_0(t) = \sum_{n=1,3,5,\dots}^{\infty} [b_n \sin(n\omega_s t)]$$

$$\text{while } \omega = \frac{2\pi}{T_s}$$

$$b_n = \frac{2}{T_s} \int_0^{T_s} V_0(t) \sin(n\omega_s t) \cdot dt$$

$$V_0(t) = \sum_{n=1,3,5,\dots}^{\infty} \left[ \frac{4V_s}{n\pi} \sin(n\omega_s t) \right] + a_0 \quad (15)$$

RMS value of fundamental voltage:

$$V_n = \frac{4V_s}{\sqrt{2} n \pi}$$

$$V_1 = \frac{4(1)}{\sqrt{2} (1) \pi} = 0.9003163162$$

Harmonics:

$$V_3 = \frac{4(1)}{\sqrt{2} (3) \pi} = 0.3001054387$$

$$V_5 = \frac{4(1)}{\sqrt{2} (5) \pi} = 0.1800622632$$

$$V_7 = \frac{4(1)}{\sqrt{2} (7) \pi} = 0.1286166166$$

$$V_9 = \frac{4(1)}{\sqrt{2} (9) \pi} = 0.1000351462$$

The microcontroller results are shown in figure 14 while the theoretical computations are shown in figure 15.

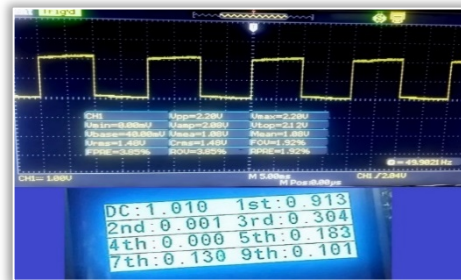


Figure 14. Harmonics calculations of square waveform on the microcontroller

The theoretical results which calculated from the analysis of square waveform are:

$V_n = \frac{4V_s}{n\pi}$	
Theoretical Calculations	FFT measurement (Microcontroller)
$V_1 = 0.900316316$	0.913
$V_3 = 0.300105439$	0.304
$V_5 = 0.180062263$	0.183
$V_7 = 0.128616617$	0.13
$V_9 = 0.100035146$	0.101

Figure 15. Harmonics of square waveform calculated theoretically

The results which get from the microcontroller are compared with theoretical results as shown in figure 16.

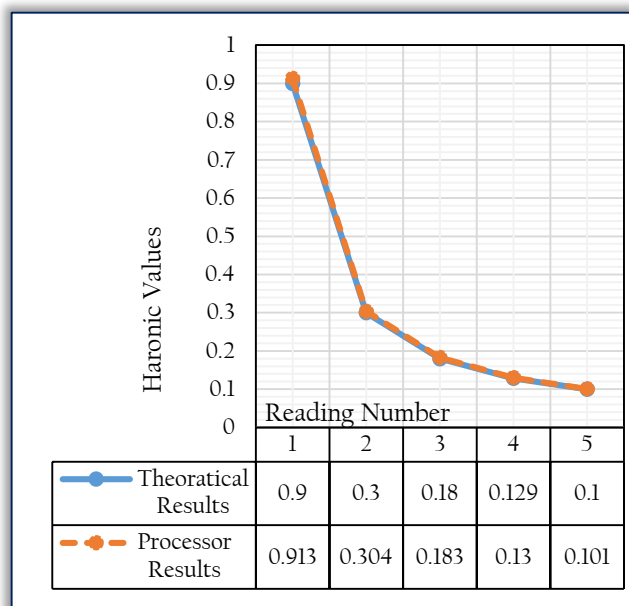


Figure 16. Comparison of harmonics calculation between microcontroller and theoretical results

All data is sent to the internet using Wi-Fi module and how to display data over the Internet is displayed. Figure 17 shows the comprehensive graphical user interface for online monitoring.

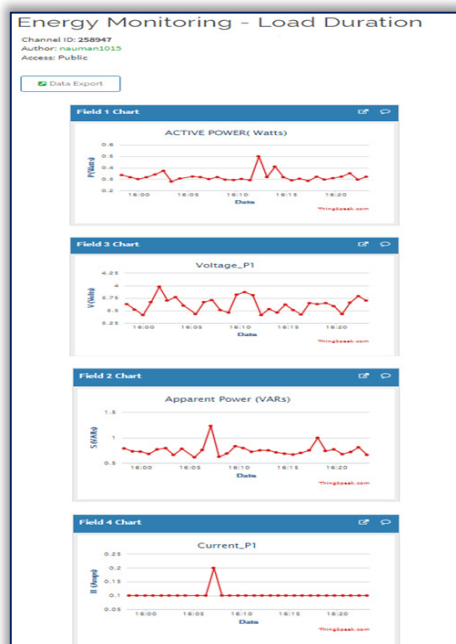


Figure 17. GUI for online energy monitoring

## CONCLUSION

The development of low-cost DSP based energy monitoring with online data acquisition and its implementation is described in detail. This meter is scrutinized on artificial disturbances and tests are performed on the single and three-phase power system in real time. Therefore, it is culminating for real time monitoring. This is fast, robust, and efficient and gives meticulous results and all the signal computations are totally based on digital signal processing by using STM32F429-disco microcontroller.

This data acquisition will also be very constructive for future researchers and can easily be installed anywhere. It is extremely low-cost, portable and very easy to handle.

## References

- [1] Tomas Radil. "PQ Monitoring System for RealTime Detection and Classification of Disturbances in a Single-Phase Power System", IEEE Transactions on Instrumentation and Measurement, August 2008.
- [2] Pedro M. Ramos, "On the Use of Multi Harmonic Least-Squares Fitting for THD Estimation in Power Quality Analysis", Metrology and Measurement Systems, January 2012.
- [3] T. Saravanakumar, G. Sainarayanan and K. Porkumar, "Design of a Cost Effective Optimized Power Factor Measurement Device for Nonlinear Single Phase Home Appliances", Research Journal of Applied Sciences, Engineering and Technology, 10(4): 454-463, June 2015.
- [4] S. Parthasarathy and Dr. N.V. Anandkumar, "Development of Low-Cost Data Acquisition System for Photo Voltaic Systems", International Journal of Innovative Research in Science, Engineering and Technology, July 2016.
- [5] Mirosław Szmajd, Krzysztof Górecki and Janusz Mroczka, "DFT algorithm analysis in low-cost power quality measurement systems based on a DSP processor", 9th International Conference Electrical Power Quality and Utilization Barcelona, October 2007.



ISSN: 2067-3809

copyright © University POLITEHNICA Timisoara,  
Faculty of Engineering Hunedoara,  
5, Revolutiei, 331128, Hunedoara, ROMANIA  
<http://acta.fih.upt.ro>



<sup>1</sup>Gagandeep KAUR, <sup>2</sup>Sunaina SAINI

# DISTRIBUTED GENERATION PLACEMENT IN DISTRIBUTION NETWORK USING SELECTIVE PARTICLE SWARM OPTIMIZATION

<sup>1-2</sup> Department of Electrical Engineering, I.K. Gujral Punjab Technical University, Punjab, INDIA

**Abstract:** The lack of synchronization of power supply and demand in distribution network leads to poor voltage profile on lines and increase of real power loss. The integration of Distribution Generation (DG) unit in these networks offers consistent supply of electrical power which accordingly recovers system voltage profile and consequently reduces real power losses. Placement of DG units at optimized location with optimal DG rating participate a vital role in distribution network to synchronize power supply and demand. This study demonstrates the identification of optimized DG placement and optimal DG rating through optimization techniques which were accomplished in MATLAB'13. In minimization of multi-objective function, the technical hitches were resolved using weight factor within the operating limits of network. Three techniques were accomplished on IEEE 33-bus and IEEE 69-bus standard distribution networks. Among these implemented techniques, Selective Particle Swarm Optimization (SPSO) has given the best result thereby minimizing the real power loss up to 48.09% for standard IEEE 33-bus system and 63.02% for IEEE 69-bus system.

**Keywords:** voltage profile, real power loss, distributed generation (DG), SPSO, distribution network

## INTRODUCTION

In most of the developing countries, the centralized placed power plants supply to a multifaceted interconnected transmission and distribution networks. These networks are to transfer the power over long or short distances with an efficient manner at customer end [1]. In recent times a revolution of deregulation and restructured environment in centralized power system has confronted a challenge for power generating units to work independently and to meet the increasing power demand. This becomes a favorable opening to the dispersed generations such as distributed generators (DG) to present sufficient and dependable power release. Modernization of power system is enhancing the access of generated electricity & storage of power at distribution end. For consistent supply of power, placement of DG and demand organization is vital features as in [2]. For management of ever increasing challenge the most important deciding factor is the penetration level of DG units [3]. Several researchers have presented and examined the DG placement and DG rating problems by applying different optimization techniques. The instant variation in demand and probably higher demand and less supply leads to worsening of voltage profile or black outs in electric system networks. In year 1997, S/Se Brazil felt a major blackout due to voltage instability in power distribution network [4]. Hence, DG placement and DG rating in distribution network needs the must consideration of voltage profile constraints. Real power losses have major impact on the power quality, power transfer expenses and profits of electric companies. To improve power quality and reduce technical or non-technical losses, placement of DG units in distribution network has been approached as an attractive power source [5]. An optimization technique of Optimal Coordinated Voltage

Control (OCVC) has been implemented to investigate multi-objective problem to lessen voltage inaccuracies at DGs and pilot buses and reactive power deviations [6]. For improving voltage stability in distribution network, a multi objective performance index (MOPI) under several operating limits through Chaotic Artificial Bee Colony (CABC) has been introduced in [7]. For voltage profile increment and reduction of power losses through DG placement, Basu et.al has applied other methods such as fuzzy approach and Harmonic Search Algorithm (HSA) [8]. A simple fast load flow method has been applied for achievement of real power losses and voltage profile as in [9]. Here, with the installation of DG units of range of sizes at different site has been performed with backward forward sweep algorithm (BFSA). A researcher revealed a technique to offer solution through selection of candidate buses for DG location and rating. In this technique, prioritization of those candidate buses was done which were susceptible to voltage level and consequently, voltage stability margin were enhanced [10]. Placement of DG units on priority basis for power compensation in power deficiency period has been handled by continuous load flow and nodal analysis techniques [11]. Analysis of system performance on the basis of power reliability has been done with network reconfiguration in the continuation of DG units. Optimal DG placement has been identified with sensitivity analysis as in [12].

## PROBLEM FORMULATION

### — Power Loss Reduction Index

To lessen the power loss in distribution network system, power loss reduction index (PLRI), has been introduced and utilized to investigate the minimization of power loss in distribution network. The representation of PLRI is as below:

$$PLRI = \frac{PL(WDG)}{PL(WODG)} \quad (1)$$

where, PL (WDG) is loss of power while placing DG and PL (WODG) is loss of power when no DG in network.

#### — Voltage Profile Improvement Index

Voltage Profile is a primary feature of consideration while analyzing about power quality and power transfer in power distribution system. Voltage collapse sensitive buses are observed and DG is selected arbitrarily. Voltage profile improvement index (VPII) is another index to observe system voltage for continuity of power supply. VPII is represented as below:

$$VPII = \frac{VP(WDG)}{VP(WODG)} \quad (2)$$

Where, VP (WDG) & VP (WODG) are voltage profile with DG and without DG respectively.

#### — Objective Function for DG Integration

For integration of DG unit in power distribution system, several objective functions have been utilized by researchers to recover power quality of network. Here, grouping of two independent indexes i.e PLRI and VPII to minimize the multi-objective function defined below:

$$F = \text{minimization}(w_1 \times f_1 + w_2 \times f_2) \quad (3)$$

The function  $f_1 = PLRI$  and function  $f_2 = 1/VPII$ ,

To simplify the calculation and to decide the importance of primary parameter in multi-objective function, weights  $w_1$  and  $w_2$  are used. Here the weights have a sum in range of 0-1, and equal weight of 0.5 has been taken. Thus the objective function 'F' has been formed to achieve the optimal solution. The optimal DG rating and DG placement at optimal location has been obtained only on that candidate bus, where overall distribution network power loss is less.

#### OPTIMIZATION TECHNIQUES

##### — Repeated Load Flow

For repeated load flow (RLF) a standard procedure has been followed for integration of optimum DG rating in distribution system [13]. Load flow analysis has been done iteratively using forward backward method until optimum results has come out. First of all DG ratings has been defined and load flow for each candidate bus was made to flow. For the defined DG ratings, a power loss for every participating bus has been reported. The bus location having minimum power loss was the optimum DG placement and the equivalent DG rating size was the optimum size.

##### — Particle Swarm Optimization (PSO)

A stochastic search evolution computational procedure is again a popular population based and named Particle Swarm Optimization (PSO). Kennedy and Eberhart developed this technique by critically analyzing the activities of group of fishes and flock of birds. In PSO algorithm, a number of particles in population presents in search space having n-dimensions and shift from their location as per information w.r.t time. On the basis of this enough information, particle modifies its direction and shift on the way to best position called *pbest*. The overall best position based on shift of neighboring particles is called as *gbest*. The updating of

position by particle is according to best position faced by them and their neighbors [14].

In n-dimensional search space, the particle position as:

$$Zm = (zm_1, zm_2, \dots, zm_n) \quad (4)$$

Based on it, the current position of particle as:

$$Sk_{iD+1} = (Sk_{iD}) + (Sk_{iD+1}) \quad (5)$$

$i = 1, 2, \dots, n$  and  $D = 1, 2, \dots, m$

where,  $Sk$  is the present particle position and  $(Sk+1)$  the new position. The particle velocity in n-dimensional search space is:

$$Vm = (vm_1, vm_2, \dots, vm_n) \quad (6)$$

The updated velocity of particle is shown below:

$$vk_{iD+1} = wi \times viDk + c_1 \times rand \times (pbest_{iD} - Sk_{iD}) + c_2 \times rand \times (gbest_{iD} - Sk_{iD}) \quad (7)$$

where  $vk+1$  = updated velocity,  $vk$  = present velocity, *pbest* = individual best velocity, *gbest* = overall best velocity, *n* = particles number in a population, *m* = participants number in a particle, *rand* = random values generated, *c* = acceleration coefficient of particle, *wi* = inertia weight for each particle

The inertia weight is given by the equation:

$$w = \frac{w(\max) - w(\min)}{k(\max)} \times k$$

where, *wmax* = maximum inertia weights, *wmin* = minimum inertia weights, *k* = current inertia weight, *kma* = iterations count (max)

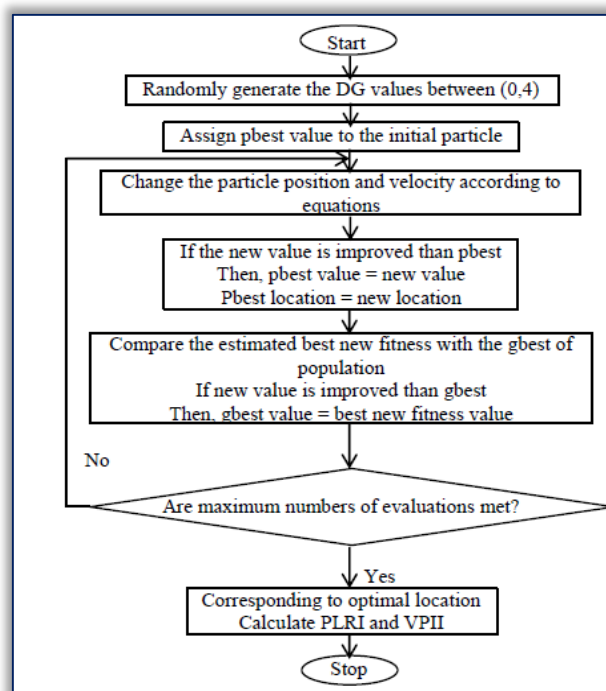


Figure 1. PSO Algorithm

The range random lies between 1 & 2 and suitable value for  $c_1$  and  $c_2$  is 2. The selection of *wmax* and *wmin* values is by hit and trial method [15]. Figure 1 depicts the flow chart for optimal placement of DG and DG rating size in distribution system through PSO. DG rating or size has been limited (0, 4) when PSO techniques was applied in MATLAB. The DG values were selected as particles to be optimized to minimize the value of objective function.

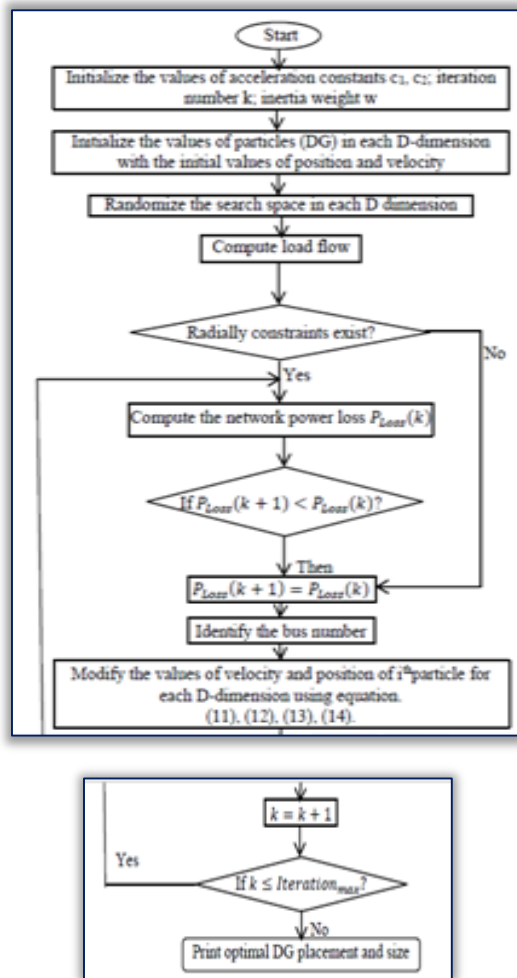


Figure 2. SPSO Algorithm

### — Selective Particle Swarm Optimization (SPSO)

In recent years, the improved versions of PSO technique have been proposed and used by researchers with objectives to increase usage of this technique with fast convergence speed and better optimal solutions. An advanced version of PSO is binary PSO (BPSO) through modulating search space to be binary. This technique has been developed by Kennedy and Eberhart and is a discrete version of PSO [16]. Again the advanced version of BPSO is SPSO, proposed by Khalil and Gorpnich [17], where solution quality is improved by adopting sigmoid transformation of velocity function for selection of search space. In SPSO technique, for search space a set of DN positions is  $SD = [SD_1, SD_2, \dots, SD_N]$  for each D dimension, where DN are the selected positions in dimension D.

$$\begin{aligned}
 (v \ iDk+1) &= DN \ 11 + \exp(-viDk+1) & (9) \\
 xiDk+1 &= \{SD1 \ \text{if} \ sig(viDk+1) < 1 \\
 & \quad SD2 \ \text{if} \ (viDk+1) < 2 \\
 & \quad SDN \ \text{if} \ (viDk+1) < N\} & (10)
 \end{aligned}$$

where,  $SD_1, SD_2, \dots, SD_N$  are the selected values for each particle in dimension D.

Velocity constraints  $[Vmin, Vmax]$  can be calculated using the following equation:

$$\begin{aligned}
 viDk+1 &= \{Vmax, \text{if } viDk+1 > Vmax \\
 & \quad viDk+1, |viDk+1| \leq Vmax
 \end{aligned}$$

$$Vmin, iDk+1 < Vmin \dots (11)$$

$$\begin{aligned}
 viDk+1 &= \{rand \times viDk+1, \text{if } |viDk+1| = |viDk| \\
 & \quad viDk+1 \ \text{otherwise}
 \end{aligned}$$

The invariability of  $i^{th}$  particle velocity value in a D-dimension at the minimum or maximum values can be ignored using the equation given below and push the particles going through the selected space.

To find out the solution for optimal DG placement and DG rating or size there would be key steps distribution system:

1. Indicate the number of dimensions
2. Identification of search space for all dimensions
3. To select an optimal solution from the search spaces by implementing SPSO

The buses of the network represent the search space of a specific dimension. For standard IEEE systems the candidate buses represents search space for a system dimension. The random selection of the DG size is for a particular bus of one dimension at a time. The SPSO after identification of search space of each dimension employs an optimal solution for enhancement of power quality.

### RESULTS AND DISCUSSIONS

The optimization techniques implemented for this study has been largely analyzed on standard radial networks consist of IEEE 33 & IEEE 69 bus systems. Both the test systems have been gone through load flow, optimal DG placement and DG rating have been identified using above proposed optimization techniques with simultaneously minimizing the objective function. How the simultaneous optimal placement of DG and optimal DG rating improve the power quality in terms of loss reduction and enhanced voltage profile have been compared and discussed in both test systems.

#### — IEEE -33 Test System

To minimize the objective function in IEEE 33 test system, the two main parameters of concern i.e reduction of power loss and improved voltage profile have been analyzed. For the system base voltage taken was 12.6 KV, the power losses (real & reactive) before DG placement has been found 210 KW and 143.0 KVAR respectively.

Table 1: Outcome after DG Integration

IEEE 33- Bus System	RLF	PSO	SPSO
Real Power Loss (KW)	111.02	111.07	109
Minimum Voltage Profile	0.94251 Bus 18	0.94324 Bus 18	0.94900 Bus 18
Optimum DG Rating (MW) & Placement	2.6 Bus 6	2.6509 Bus 6	2.5173 Bus 6

The total apparent power loss was 254.065 for the base case. The minimum voltage profile was at bus-18 which was 0.90377 before DG placement in distribution network. With the implementation of these techniques bus having minimum real power loss has been identified. In correspondence of that, optimal DG rating, power loss and voltage profile were calculated. The outcome after DG integration is displayed in table 1 and voltage profile & power loss against these techniques is shown in figure 3 & 4 respectively. Indexes VPll and PLRI were also computed

which shows the impact of DG location by optimization with these techniques.

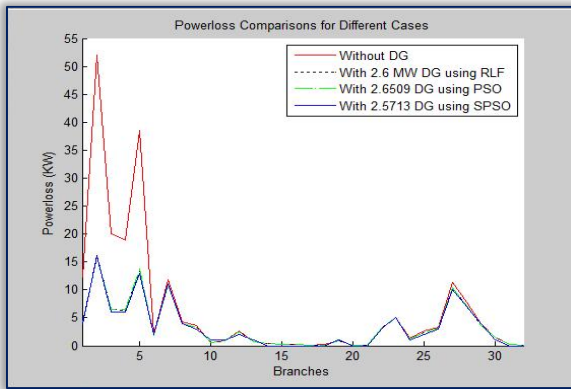


Figure 3. Voltage Profile Improvement

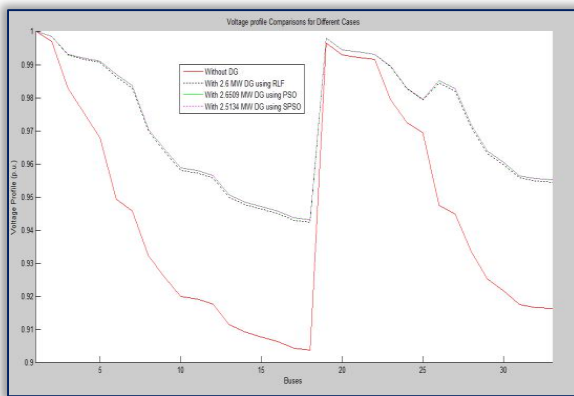


Figure 4. Power Loss Reduction

Figure 5 and Figure 6 illustrates about VPIL and PLRI with DG installation for RLF, PSO, and SPSO. After optimizing the indexes, the table-2 demonstrates the values of objective function "F",  $f_1$ , &  $f_2$  and function is minimized up to 0.5. The comparison of results of techniques revealed that PSO has better findings than RLF, but overall SPSO has given best results.

Table 2. Minimization of Objective Function

Objective Function	RLF	PSO	SPSO
$f_1$	1.0	1.0	1.0
$f_2$	0.31026	0.30584	0
F	0.65513	0.65292	0.5

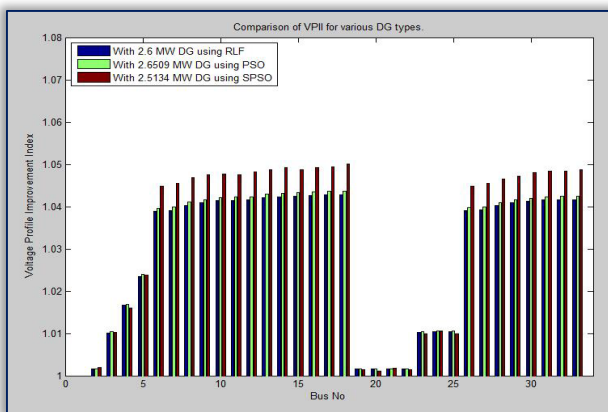


Figure 5. Comparison of VPIL

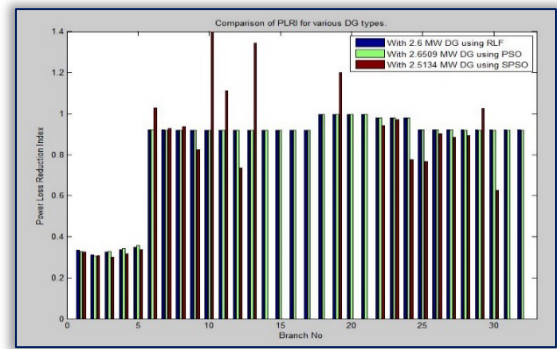


Figure 6. Comparison of PLRI

### — IEEE-69 Test Systems

These optimization techniques have been implemented on IEEE-69 radial distribution network for minimization of objective function. The base case voltage value has been taken as 12.66 KV, apparent power loss of 247.36 KVA with the real and reactive power losses of 225 KW and 102.53 KVAR respectively before DG integration in distribution network.

Table-3 presents the results after DG integration in 69- bus distribution networks. Results present that minimum power loss is 83.02 KW by integrating 1.857 MW DG at bus number 61. Simultaneously voltage profile of 0.968 has also been improved while using SPSO, better than other cases. Figure 7 and figure 8 shows the comparison of voltage profile and power loss for all implemented techniques.

Table 3. Outcome after DG Integration

69- Radial Bus System	RLF	PSO	SPSO
Real Power Loss (KW)	84.065	84.117	83.20
Minimum Voltage Profile	0.96259 Bus 27	0.96253 Bus 27	0.968 Bus 27
Optimum DG Rating (MW) & Placement	1.8 Bus 61	1.79 Bus 61	1.857 Bus 61

The determination of VPIL and PLRI were also done for all approaches which presents change in voltage profile and power losses. Figure 9 and Figure 10 shows VPIL & PLRI for RLF, PSO, and SPSO techniques with DG placement. The multi-objective function has been minimized by using these three approaches. Table-4 displays the values for objective function  $F'$  for different cases and maximum minimization is up to 0.50021 with SPSO.

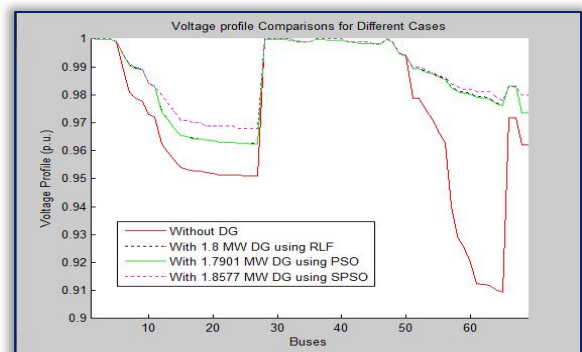


Figure 7. Comparing Voltage Profile

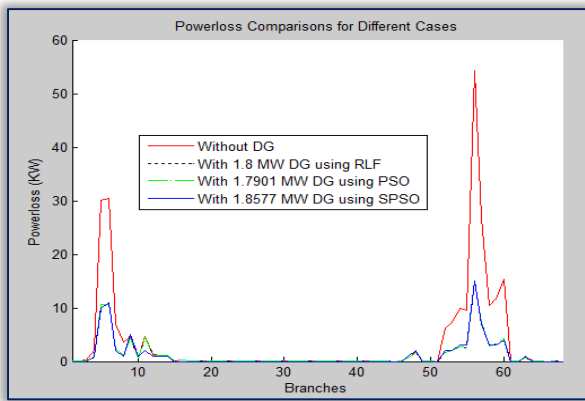


Figure 8. Comparing Power Loss

Table 4. Objective Function for IEEE 69-Test System

Objective Function Value	RLF	PSO	SPSO
f 1	1	1	1
f 2	0.27212	0.27201	0
F	0.63606	0.636	0.50021

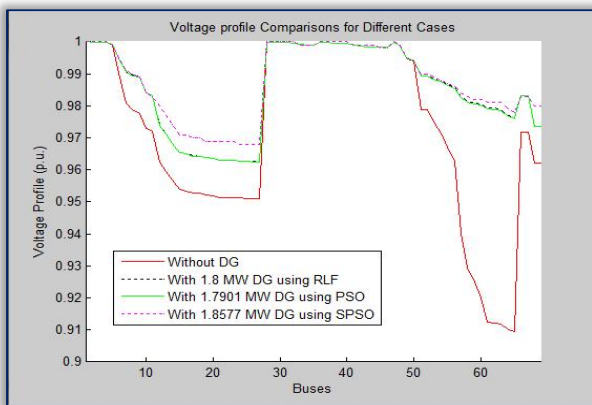


Figure 9. VPIL for RLF, PSO and SPSO

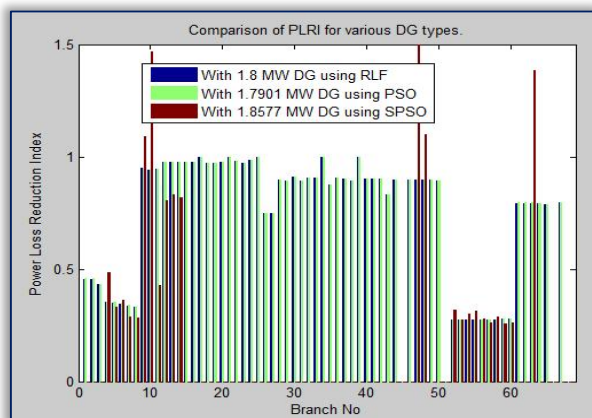


Figure 10. PLRI for RLF, PSO and SPSO

## CONCLUSIONS

In this study, minimization of multi-objective function for two networks has been done which further calculates VPIL and PLRI indexes for better voltage profile and less power loss. For 33-bus network the reduction in real power loss was observed to be 47.13% for RLF, 47.10% for PSO and 48.09% in case of SPSO. On the other side for 69-bus system, 62.637 %, 62.614% and 63.02% of power loss has been reduced by RLF,

PSO and SPSO respectively. Voltage profile has been improved while placing DG unit. Study concludes that SPSO technique has given best results in both test systems.

## References

- [1] S. Safigianni, G. N. Koutroumpetis, and V. C. Poulis, Mixed Distributed Generation Technologies in a Medium Voltage Network, *Electric power Systems Research*, vol. 96, pp. 75-80, 2013.
- [2] P. Chiradeja, Benefit of Distributed Generation: A Line Loss Reduction Analysis, *IEEE/PES Transmission and Distribution Conference & Exhibition: Asia and Pacific Dalian, China*, pp. 1-5, 2005.
- [3] Poornazaryan, P. Karimyan, G. B. Gharepetian, and M. Abedi, Optimal Allocation and Sizing of DG Units Considering Voltage Stability, Losses and Load Variations, *Electrical Power and Energy Systems*, vol. 79, pp.42-52, 2016.
- [4] R. B. Prada, and L. J. Souza, Voltage Stability and Thermal Limit: Constraints on the Maximum Loading of Electrical Energy Distribution Feeders, *Proceeding of Inst. Electr. Eng. - Gen. Trans. Distrib.*, vol. 145, pp. 573-577, 1998.
- [5] D. Q. Hung, N. Mithulanathan, R. C. Bansal, Analytical Expressions for DG Allocation in Primary Distribution Networks, *IEEE Trans Energy Conv.*, vol. 25, no. 3, pp. 814-820, 2010.
- [6] J. R. Castro, M. Saad, S. Lefebvre, D. Asber, and L. Lenoir, Optimal Voltage Control in Distribution Network in the Presence of DGs, *Electrical Power and Energy Systems*, vol.78, pp. 239-247, 2016.
- [7] N. Mohandas, R. Balamurugan and L. Lakshmi N., Optimal Location and Sizing of Real Power DG Units to Improve the Voltage Stability in the Distribution System using ABC Algorithm United with Chaos, *Electrical Power and Energy Systems*, vol.66, pp. 41-52, 2015.
- [8] P. S. Babu and R. M. Mohan, Optimal Performance Enhancement of DG for Loss Reduction using Fuzzy and Harmonic Search Algorithm, *IEEE International Conference on Electrical Electronics Signals, Communication & Optimization*, Jan 24-25, Vishakhapatnam, India, 2015.
- [9] E. K. Bindumol and C. A. Babu, A Simple and Fast Load Flow Algorithm for Sizing and Placement of DG in Radial Distribution System, *IEEE International Conference on Electrical Electronics Signals, Communication & Optimization*, Jan 24-25, Vishakhapatnam, India, 2015.
- [10] R. S. Al Abri, E. F. El-Saadany, and Y. M. Atwa, Optimal Placement and Sizing Method to Improve the Voltage Stability Margin in a Distribution System using Distributed Generation, *IEEE Tranaction on Power System*, Vol. 28, No.1, pp. 326- 334, Feb 2013. 2015.
- [11] M. Ettehad, H. Ghasemi, and S. Vaez-Zadeh, Voltage Stability-Based DG Placement in Distribution Networks, *Electrical Transaction on Power Delivery*, vol.28, No.1, pp. 171-178, Jan 2013.
- [12] R. S. Rao, K. Ravindra, K. Satish, and S. V. L.Narasimham, Power Loss Minimization in Distribution System using Network Reconfiguration in the presence of Distributed Generation, *IEEE Transaction on Power System*, vol.28, No.1, 2013.

- [13] N. Acharya, P. Mahat, and N. Mithulananthan, An Analytical Approach for DG Allocation in Primary Distribution Network, *Electrical Power and Energy Systems*, vol.28, pp. 669-678, 2006.
- [14] J. Kennedy and R. Eberhart, Particle Swarm Optimization, *Proceeding of IEEE International Conference on Neural Network (ICNN'95)*, vol. 5, pp. 1942-1948, Perth, Australia, Nov 29-Dec 1, 1995.
- [15] R. C. Eberhart , and Y. Shi, Comparing Inertial Weights and Constriction Factor in Particle Swarm Optimization, *Proceeding of International Congress on Evaluating Computation*, pp. 84-88, San Diego California, Piscataway, NJ: IEEE Service Center, 2000.
- [16] J. Kennedy and R. Eberhart, A Discrete Binary Version of the Particle Swarm Algorithm, *IEEE International Conference on Systems, Man and Cybernetics(SMC 97)*, Vol.5, pp. 4104-4108, 1997.
- [17] T. M. Khalil and A.V. Gorpinich, Optimal Conductor Selection and Capacitor Placement for Loss Reduction of Radial Distribution Systems by Selective Particle Swarm Optimization, *IEEE Seventh International Conference on Computer Science & Systems*, Nov. 27-29, Cairo, Egypt, pp. 215-220, 2012.



ISSN: 2067-3809

copyright © University POLITEHNICA Timisoara,  
Faculty of Engineering Hunedoara,  
5, Revolutiei, 331128, Hunedoara, ROMANIA  
<http://acta.fih.upt.ro>

<sup>1</sup>Igor MIKLÓŠIK, <sup>2</sup>Peter KELLO, <sup>3</sup>Juraj SPALEK

## FIRE DETECTION IN TuSim BY FibroLaser

<sup>1</sup> ELTODO SK, a.s, Žilina, SLOVAKIA

<sup>2</sup> University of Žilina, Faculty of Electrical Engineering, Department of Control and Information Systems, Žilina, SLOVAKIA

**Abstract:** Road tunnels are important part of traffic infrastructure not only for shortening the paths in mountainous regions or in towns but also they increase economical effectiveness. Occurrence of traffic accidents in the tunnel is less common, but consequences can be more serious. The contribution shows the simulation of fire in a road tunnel through programmable logic controller (PLC) based simulator. Fire detection in the tunnel model is realized by FibroLaser. Influence of the pressure difference for various fire scenarios, types of vehicle on the air speed, etc. is counted by evaluation of the average temperature in the fire section.

**Keywords:** Simulation, application programming interface, programmable logic devices, fire, FibroLaser

### INTRODUCTION

Road tunnels are important part of traffic infrastructure not only for shortening the paths in mountainous regions or in towns but also they increase economical effectiveness. Occurrence of traffic accidents in the tunnel is less common, but consequences can be more serious. A lot of technological equipment is necessary to provide the tunnel system safe in any circumstances. There are not many chances to simulate malfunctions of selected components in real 24-hour operation to see all consequences. Therefore, Tunnel simulator (TuSim) has been developed to simulate the technological equipment of the tunnel. Models can be used to simulate expected process behaviour with a proposed control system.

#### TuSim

TuSIM is PLC based system running on the B&R Automation industrial PC (PLC) with uninterruptible power supply (UPS) unit. TuSIM hardware is displayed on Figure 1 from top to bottom: Masterview Liquid-crystal-display (LCD) switch, Bernecker and Rainer (B&R) industrial PC on the bottom right part of the figure, visualization server and UPS unit on the bottom left part of the figure.



Figure 1. TuSim Hardware

All devices of the tunnel technological equipment are simulated by the software inside the PLC [1]. Equipment of three tunnels is implemented: City tunnel, Motorway 2 tubes and Motorway 1 tube tunnel. TuSim supports in addition to the simulation of the technological equipment also the control of the traffic sequences. Each tunnel tube can operate in following traffic sequences: tunnel tube open, left lane closed, right lane closed, speed limit 60 km/h, adaptation lighting failure, tunnel tube closed. Switching from one sequence to another follows the time requirements which allow all vehicles to adapt to the new conditions. TuSim supports several simulated responses of the control system to unexpected events in the tunnel like complete or partial power failure, fire, traffic alarm or pre-alarm, lighting malfunction, SOS button activation, physical measurements alarm or pre-alarm [1]. We implemented models important for simulation of unexpected events analysis into the current version of the software. Whole source code concept from the PLC software to the visualization screens is open for enhancements so models important for the basic functionality e.g. traffic model, evacuation model have been already implemented. There are many graphical screens to visualize the state of each subsystem of the technological equipment – at least one for each subsystem. Handling of the screens and separate connections to the simulator is realized by visualization server and two client PCs with human-machine interface (HMI)/ (SCADA) CIMPLICITY software, which uses client/server architecture. Server is responsible for collection and distribution of the data from the PLC; clients allow interacting with the data distributed by the server and perform control actions.

### SIMULATION OF FIRE

#### — Fire curves

Development of vehicle tunnel fires depends on number of factors: interior material, vehicle cargo, size and location of the fire and ventilation. The time behaviour of fire consists of incipient phase, growth phase, fully developed phase and decay phase [2].

First two phases are most important for simulation of fire detection by technological devices, second and third phases are important for evacuation simulation. Decay phase can be ignored in our case. Fire growth curve can be mathematically counted by linear growth, quadratic growth, or exponential growth [2]. Most common is quadratic growth and exponential decay, so we have selected them for the simulation.

$$Q(t) = \alpha \cdot t^2 \text{ for } 0 < t < t_{\max}$$

$$Q(t) = Q_{\max} \text{ for } t_{\max} < t < t_{\text{decay}}$$

$$Q(t) = Q_{\max} \cdot e^{-b \cdot (t - t_{\text{decay}})} \text{ for } t > t_{\text{decay}}$$

Figure 2 shows the growth of fire, where ultrafast rate is defined like  $\alpha = 0.1876 \text{ kW/s}^2$ , fast is  $\alpha = 0.0469 \text{ kW/s}^2$  medium is  $\alpha = 0.01172 \text{ kW/s}^2$ , and slow rate is  $\alpha = 0.00293 \text{ kW/s}^2$  [2].

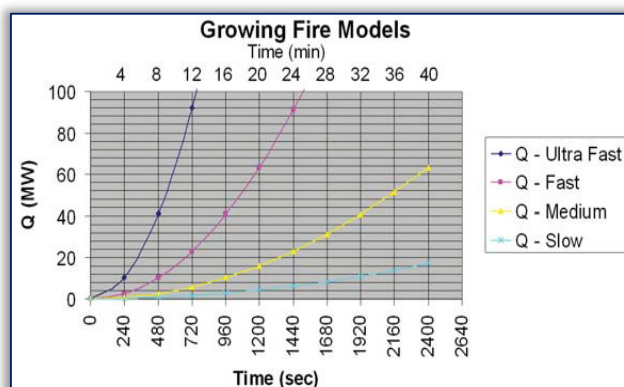


Figure 2. Quadratic fire growth [2]

Our simulations work with following fire scenarios from which everyone has specified Heat Release Rates (HRR) of the fire [3]: Car 5 MW, Van 10 MW, Bus 20 MW, Truck 50MW [3]. Figure 3 shows generated fire curves used for our simulation.

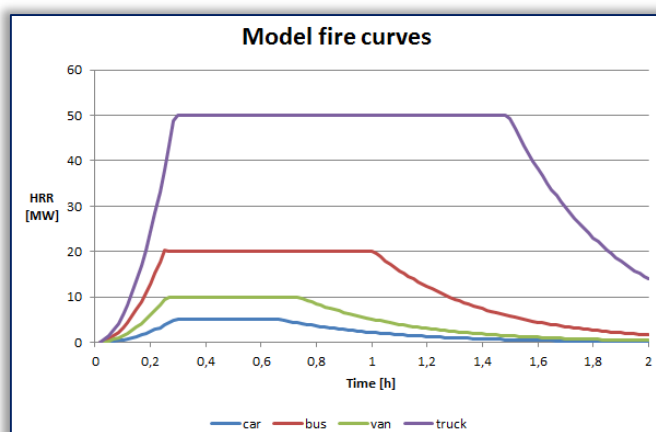


Figure 3. HRR curves for selected scenarios

#### — Air temperatures

TuSim models have been also enhanced for estimation of the safety of people in the tunnels. High temperature and smoke in the tunnel are dangerous for the people because they can block evacuation doors. Following equations have been used for estimation of the air temperature in the place of fire [4][6]:

$$T_f = T_0 + \frac{0.7Q}{v\rho A c_p}$$

where:  $T_0$  - initial temperature in the tunnel [K],  $v$  - air speed in the tunnel [m/s],  $\rho$  - air density [kg/m<sup>3</sup>],  $c_p$  - air thermal capacity [kJ/kgK],  $A$  - tunnel sectional area [m<sup>2</sup>],  $Q$  - heat release rate [W].

The HRR of the fire is reduced, since not all heat from the fire is consumed for heating the air, part is also radiated into the wall. Model of the heating is one dimensional, so the value of the temperature obtained from the equation is an average temperature of the temperature cut. Detailed comparison of the temperatures from the model with three dimensional models can be found in [6]. Comparison shows that best results (1% accuracy) are obtained when airspeed is higher or equal to the critical speed. Critical speed of the air during the fire determines the state when back-layering of the smoke occurs. Figure 4 shows how the smoke diffuses depending on the airspeed. Figure 4a) and 4b) the airspeed is lower than critical speed and in the tunnel occurs back-layering of smoke. Fig 4c) the airspeed is higher than critical speed and in the tunnel does not occur back-layering of smoke.

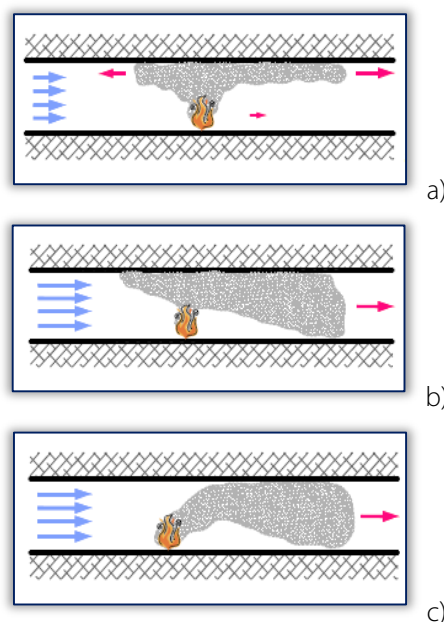


Figure 4. Spreading of smoke depending on the airspeed [7]  
Several equations are available for calculation of the critical speed. We have compared calculation according to Kennedy and analytical calculation, which is preferred for our purpose [5]:

$$(Fr_m \cdot A \cdot c_p \cdot T \cdot \rho) \cdot v_c^3 + (Fr_m \cdot Q)v_c^2 - g \cdot H \cdot Q = 0$$

$$Fr_m = 4.5 \cdot \left(1 + 0.0374|\min(\text{grade}, 0)|^{0.8}\right)^{-3}$$

where:  $Fr_m$  - Froude number,  $v_c$  - critical speed in the tunnel [m/s],  $\rho$  - air density [kg/m<sup>3</sup>],  $c_p$  - air thermal capacity [kJ/kgK],  $g$  - gravitational acceleration [m/s<sup>2</sup>],  $A$  - tunnel sectional area [m<sup>2</sup>],  $H$  - height of the tunnel [m], grade - gradient of the tunnel [%],  $Q$  - heat release rate [W].

Figure 5 shows the both mentioned calculations of the critical speed and HRR for model of the tunnel in the TuSim.

#### FIRE DETECTION

With growing volume of trade and increasing transit cargo transport, the road traffic is taking up a larger part of it in



comparison with rail transport, which has unavoidable negative influence on environment, road traffic density and quality of life - particularly in urban areas. If we want to provide protection to the citizens and create suitable conditions for survival in extraordinary situations, it is necessary to know the risks of transporting dangerous goods. The current situation requires creating an electronic system for monitoring of dangerous cargo replacing the insufficient system of today. This system would contribute to increasing security not only of participants of road traffic but also of citizens living in proximity of road communications where dangerous cargo is transported and also protection of the environment.

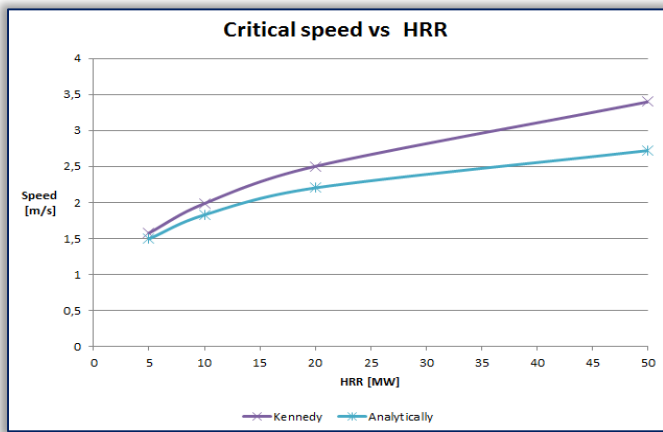


Figure 5. Critical speed vs HRR

#### — Air speed during the fire

Air speed in the tunnel during the unexpected event is not constant. In case of the tunnel with single directional traffic is air speed at the beginning influenced with "piston effect" – cars move the air in the direction of the traffic. In case of bidirectional traffic is this effect not so significant, it depends on the difference of traffic intensities at each portal of the tunnel. At the moment of the traffic stop, air speed decreases and is influenced until the moment of the start of the ventilation by the temperature, pressure and height differences between the portals. This effect is often called "stack effect". Air flow inside the tunnel can be after simplifications considered as one dimensional flow described by Bernoulli's equation. Tunnel is usually approximated as the circular-profile tube with defined hydraulic diameter. The equation for calculation of the hydraulic diameter is as follows:

$$D_h = \frac{4 \cdot A}{P}$$

where: A – tunnel sectional area [m<sup>2</sup>], P – perimeter of the tunnel [m].

There are several tools available to simulate the three dimensional air flow through Navier-Stokes equations such as FDS [8], but TuSim simulates the reactions of the control system and has to be able to count the airflow in real-time. We have to consider also the orientation of the air movement, friction term in the equation should have opposite sign to the direction of the air. Same situation occurs in traffic term when

vehicle speed is smaller than the air speed. Therefore, expression with absolute value of the speed multiplied by the speed is preferred to the power of the speed. Pressure difference for the wall friction, entry and exit of the tunnel can be described [9]:

$$\Delta P_{\text{friction}} = -\frac{1}{2} \rho \cdot v \cdot |v| \cdot \left( \xi_{\text{entry}} + \alpha \cdot \frac{L}{D_H} + \xi_{\text{exit}} + \xi_{\text{local}} \right)$$

where: v – air speed in the tunnel [m/s], ρ – air density [kg/m<sup>3</sup>], D<sub>H</sub> – hydraulic diameter [m], L – tunnel length [m], ξ<sub>entry</sub> – loss coefficient tunnel entry, ξ<sub>exit</sub> – loss coefficient tunnel exit, ξ<sub>local</sub> – other local losses, λ – friction coefficient.

Pressure difference term for the movement of the vehicles [10][11]:

$$\Delta P_{\text{traffic}} = \frac{\rho}{2 \cdot A} \cdot \sum_{i=1}^N C_i \cdot |v_i - v| \cdot (v_i - v) \cdot A_i$$

where: v – air speed in the tunnel [m/s], v<sub>i</sub> – speed of the i-th vehicle [m/s], ρ – air density [kg/m<sup>3</sup>], C<sub>i</sub> – drag factor, A – tunnel sectional area [m<sup>2</sup>], A<sub>i</sub> – front area of the i-th vehicle [m<sup>2</sup>].

Pressure difference term for the stack effect [9][11]:

$$\Delta P_{\text{stack}} = \left( 1 - \frac{T_a}{T_b} \right) \cdot \rho \cdot g \cdot L \cdot \frac{s}{100}$$

where: T<sub>a</sub> – ambient temperature [K], T<sub>m</sub> – average temperature in the tunnel [K], ρ – air density [kg/m<sup>3</sup>], L – tunnel length [m], g – gravitational acceleration [m/s<sup>2</sup>], s – tunnel gradient [%].

Pressure difference term for the fans [9]:

$$\Delta P_{\text{fans}} = \frac{\eta \cdot I_{\text{fan}}}{A} \cdot \left( 1 - \frac{v}{v_{\text{fan}}} \right)$$

where: η – fan efficiency, I<sub>fan</sub> – fan power [N], A – tunnel sectional area [m<sup>2</sup>], v – air speed in the tunnel [m/s], v<sub>fan</sub> – fan speed [m/s].

We have several possibilities to include the fire influence on the air movement in the tunnel. The problem is that the fire divides the tunnel in the two sections: section upward the fire and section downward the fire. The average temperature in the section, where most of the smoke remains, is significantly higher than in the other section. We can use table values for temperature differences of each fire type according to [6] such as 25 K for 5 MW fire, 65 K for 30 MW and 90 K for 50 MW fire. Disadvantage is that also length of the fire section is fixed and that's not usable for our simulation, since we simulate different positions of fire in the tunnel. Better attempt is to use the average temperature in the section [6][9]:

$$T_m = T_0 + (T_f - T_0) \exp\left(-\frac{hP}{\nu \rho A c_p} x\right)$$

where: T<sub>m</sub> – initial temperature in the tunnel [K], T<sub>f</sub> – average fire temperature [K], v – air speed in the tunnel [m/s], ρ – air density [kg/m<sup>3</sup>], c<sub>p</sub> – air thermal capacity [kJ/kgK], A – tunnel sectional area [m<sup>2</sup>], x – distance from the fire [m], h – heat conduction coefficient [W/m<sup>2</sup>K].

Problem is that heat conduction coefficient depends on several factors and analytical solution is more complex.

Analytical solution for the average temperature can be found in [9]. We can use fixed suggested value 25 W/m<sup>2</sup>K or linearized expression from [6]. Average temperature obtained from the equation can be directly used in pressure difference term for the stack effect. Or we can include additional fire pressure difference term for the air speed between in interval 1,5 – 3,5 m/s [12]:

$$\Delta P_{\text{fire}} = c \cdot \frac{Q}{v \cdot D_H}$$

where:  $v$  – air speed in the tunnel [m/s],  $D_H$  - hydraulic diameter [m],  $Q$  – heat release rate [W],  $c$  – correction coefficient.

Figure 6 shows the comparison of pressure differences counted from all mentioned ways: fixed temperature difference according the tables, own pressure difference term  $\Delta P_{\text{fire}}$ , average temperature  $T_m$  in the fire section for different speeds and different lengths of the section.

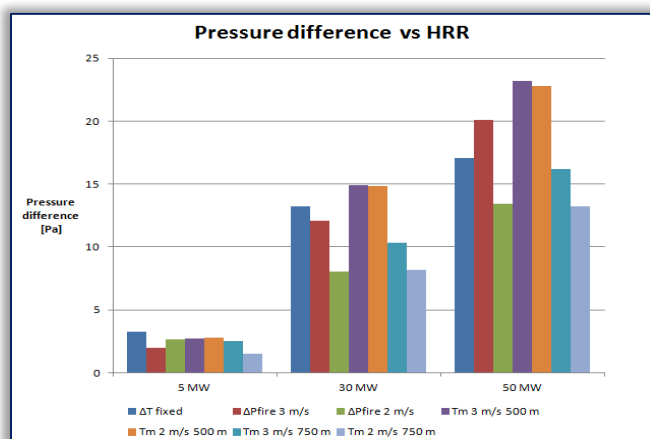


Figure 6. Comparison of fire pressure differences

Most of the pressure terms influence the final equation with similar pressure differences,  $\Delta P_{\text{fire}}$  outputs higher pressure with lower air speed. The effect of the air speed is not so significant with average temperature  $T_m$ . Average temperature term demonstrates also the differences between the different length of fire sections. We decided to use the average temperature term in the fire section, because it can consider both air speed and length of fire section. Final differential equation for the air speed in the tunnel [13]:

$$\frac{dv}{dt} = \frac{\sum_{i=1}^N \Delta P_i}{L \cdot \rho}$$

where:  $v$  – air speed in the tunnel [m/s],  $\rho$  – air density [kg/m<sup>3</sup>],  $L$  – tunnel length [m],  $\Delta P_i$  - pressure difference term [Pa].

We have solved the equation for the air speed in the simulator numerically with Euler method and time step one second. We have used following data for the simulation experiment: traffic intensity 1000 veh/h, traffic stop (fire) in the fifth minute of the simulation. We assumed that both lanes with single direction traffic stopped in the same time and traffic congestion occurred immediately. Other cases for example stop of the vehicles only in one lane were not simulated. Tunnel model used for the simulation was 1000 m long; fire section was 500 m long, gradient was 1 %, hydraulic diameter

equal to 7.83 m, sectional area 57.26 m<sup>2</sup>, perimeter 29.22 m. Fans were turned on in the tenth minute (five minutes after the fire) of the simulation of every fire scenario. This does not correspond to the reality, since control system of the tunnel should react dynamically to the conditions, which depend on the vehicle fire type. Therefore, we should include also fire detection time estimation into our simulation.

#### — FibroLaser detection of fire

Video detection is the only technological subsystem today that can give immediate response to unexpected event in the tunnel. The disadvantage of video detection subsystem is that it is used as multi-purpose: automatic stop detection, low/high speed warning, traffic flow analysis, wrong vehicle direction, smoke detection. Fire detection is only one of the tasks of the subsystem and it can trigger false alarms because of combustion products, light reflections, fog and wet road. Vehicle stop detection can trigger alarm immediately but control system should not perform tunnel close traffic sequence in every vehicle stop situation. Therefore, operator should consider individual situation and perform the control action such as close the lane, limit the speed, or close the tunnel. Therefore, fire detection systems without human influence should also be included in the tunnel.

Heat detection subsystem is nowadays in tunnels realized by FibroLasers. They consist of control unit and laser sensor cables. Laser beam is sent into the cable from control unit and light reflection is obtained and analysed. Light is scattered into "Stokes" and "Anti-Stokes" signals (Raman Effect) [14]. Temperature change in the cable can be detected from the signal strength difference between Stokes and Anti-Stokes signals.

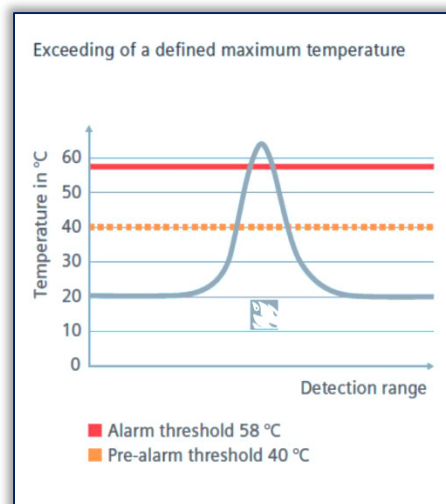


Figure 7. Rule 1 – threshold temperature 40 °C [14]

We decided to implement this subsystem into the simulator according the Siemens FibroLaser datasheet [14]. We implemented and compared all the rules for several fire scenarios. Figure 7 shows the rule 1 for triggering the pre-alarm and alarm in case of exceeding the defined maximum temperature. FibroLaser from Honeywell [15] uses also value 60°C for triggering the alarm. Figure 8 shows the rule 2 for triggering the pre-alarm and alarm in case of exceeding the

average temperature. FibroLaser from Honeywell [15] uses also value 15 °C for triggering the alarm.

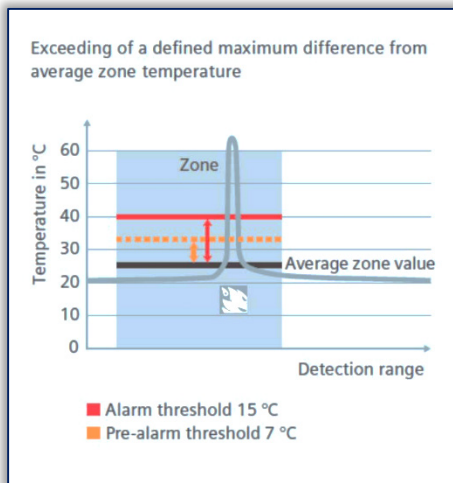


Figure 8. Rule 2 – average temperature 7 °C threshold [14]

Figure 9 shows the rule 3 for triggering the pre-alarm and alarm in case of exceeding the defined temperature gradient. FibroLaser from Honeywell [15] uses value  $\Delta 13^{\circ}\text{C}/40\text{ s}$  for triggering the alarm. All FibroLaser rules according the values from the Siemens datasheet were implemented with logical OR statement to trigger the alarm or pre-alarm. We have used standard values from the datasheet and one minute time step for the evaluation of the rules.

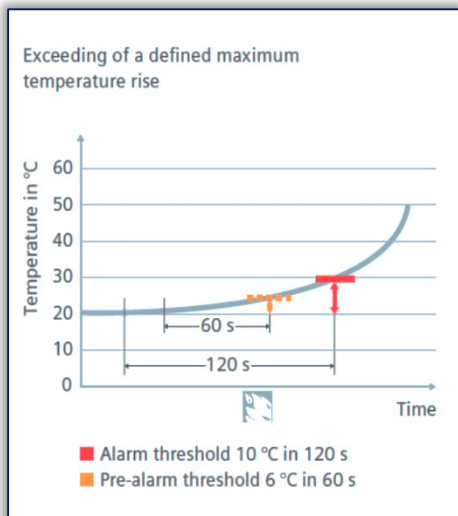


Figure 9. Rule 3 – threshold  $\Delta 6^{\circ}\text{C} / 60\text{ s}$  [14]

We cannot use the average air temperature as the input for the FibroLaser detection, since temperature close to the fire is significantly higher and is three-dimensional. We have used calculation for estimation of the heat radiated into the tunnel wall [13]:

$$Q_{\text{wall}} = P \cdot L_f \cdot [h \cdot (T_{\text{SM}}^4 - T_{\text{Wall}}^4) + \epsilon \cdot \sigma \cdot (T_{\text{SM}}^4 - T_{\text{Wall}}^4)]$$

where:  $T_{\text{wall}}$  - wall temperature [K],  $T_{\text{SM}}$  - hot air/smoke temperature [K],  $h$  – heat conduction coefficient [W/m<sup>2</sup>K],  $\epsilon$  – emissivity,  $\sigma$  – Stefan-Boltzmann constant [W/m<sup>2</sup>K<sup>4</sup>],  $P$  – perimeter of the tunnel [m],  $L_f$  - length of fire [m].

We have used constant value of heat conduction coefficient; even it depends on the air speed and other parameters, such

as Reynolds number. The equation has been solved numerically to obtain estimated wall temperature. We have applied all FibroLaser rules for simulated wall temperature, estimated times for pre-alarm and alarm triggering for each fire scenario were:

- Car: Pre-alarm 3.min, alarm 5.min,
- Van : Pre-alarm 2.min , alarm 3.min,
- Bus : Pre-alarm 2.min, alarm 2.min,
- Truck: Pre-alarm 1.min, alarm 1.min.

Two pairs of jet fans were automatically turned on after triggering the alarm as the reaction of the control system. One pair created the air flow with the speed 3 m/s, which was according the Figure 4 on the edge for safety in all fire scenarios. Figure 10 shows the average temperature in the middle of 500 m fire section. This temperature is used for the simulation of the air speed during the fire in the tunnel. It can be seen that the temperature difference in the car and van scenarios is not so high to influence the air speed significantly.

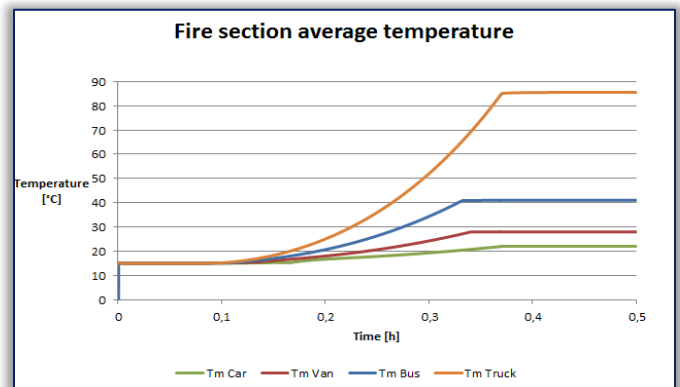


Figure 10. Fire section average temperature

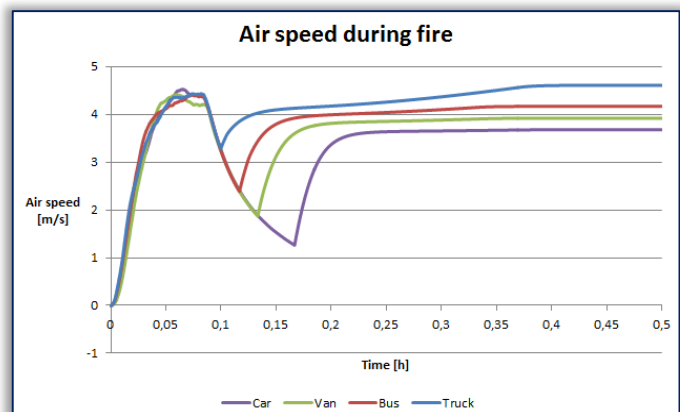


Figure 11. Air speed during fire

Figure 11 shows the air speed in the tunnel with automatic fire detection by the FibroLaser. The average temperature influences most the speed in truck fire scenario. Reaction to the fires with high HRR is faster and therefore reaction of the control system is also faster and raising the air speed in the tunnel can be more prompt.

### CONCLUSIONS

We have successfully implemented equation for the air speed with fire influence into the TuSim. We applied FibroLaser detection rules and estimated wall temperature for triggering

the fire alarm scenarios and we simulated the reaction of the control system. Therefore we obtained dynamical detection time for each vehicle fire scenario. We haven't considered all fire detection subsystems and all possibilities of traffic situations in the tunnel during the fire. We have specified own HRR curves and we have not used complex fire model with solving of the chemical reactions. FibroLasers are installed on the ceiling of the tunnels so comparison with three dimensional simulation tools would be necessary to use the absolute value of fire detection times. Even alternative principles such as fuzzy models [16] are used to estimate the fire detection time [17] by FibroLasers and smoke sensors. Producers of FibroLasers often provide own software tools for estimation of this time with better knowledge of FibroLaser characteristics. Additional comparison and adjustment of our simulation outputs with estimations based on other principles should also be performed

#### Acknowledgement

The paper has been written with the support of the ERDF project "ITMS 26220120050 Centre of excellence for systems and services of intelligent transport II."



#### References

- [1] J. Kopásek, "SW for simulation of functionality of road tunnel technology equipment", User Manual., ELTODO EG, 2013, pp.68–73
- [2] National Cooperative Highway Research Program, "Design Fires in Road Tunnels", A Synthesis of Highway Practice, 2011, pp. 72-75
- [3] NFPA 502, "Standard for Road Tunnels, Bridges, and Other Limited Access Highways", 2011, pp. 26-29
- [4] M. Persson, "Quantitative Risk Analysis Procedure for the Fire Evacuation of a Road Tunnel – An illustrative Example", Department of Fire Safety Engineering, Lund University, Sweden, 2002, pp. 32-33
- [5] F. Tarada, "New Perspectives on the Critical Velocity for Smoke Control", Fourth International Symposium on Tunnel Safety and Security, Frankfurt am Main, 2010
- [6] Bundesministeriums für Verkehr, Innovation und Technologie, "Betrachtung der Wärmefreisetzung im Brandfall", 2010,
- [7] SATRA, Větrání tunelu Sitina při požáru, Národní dálničná společnost, a.s., 2006.
- [8] National Institute of Standards USA and Technology and VTT Technical Research Centre of Finland, Fire Dynamics Simulator (FDS), IN: [http://www.nist.gov/el/fire\\_research/fds\\_smokeyview.cfm](http://www.nist.gov/el/fire_research/fds_smokeyview.cfm) (12.1.2016)
- [9] H. Ingason, A. Lönnemark, Y. Z. Li, "Model of ventilation flows during large tunnel fires", Tunneling and Underground Space Technology, 2012
- [10] L. Kurka, L. Ferkl, O. Sládek, J. Pořízek, "Simulation of Traffic, Ventilation and Exhaust in a complex Road Tunnel", IFAC, 2005
- [11] Bundesamt für Strassen ASTRA, "Luftung der Strassentunnel – Systemwahl, Dimensionierung und Ausstattung v2.03", pp.27-30, 2008
- [12] J. Pořízek, "Fire Test in the Mrazovka Tunnel", ITA-AITES Tunnel Magazine 1/2007
- [13] I. Riess, M. Bettelini, "The Prediction of Smoke Propagation due to Tunnel Fires", ITC Conference Tunnel Fires and Escape from Tunnels, 1999
- [14] Siemens Ltd, "FibroLaser III – reliable fire protection for long and widespread systems", 2010, pp. 6
- [15] Honeywell, "Linear heat detector DTS", "Lineární tepelný detektor DTS" (in Slovak), Honeywell Life Safety Austria GmbH, pp. 7
- [16] Cigánek, Ján - Noge, Filip - Kozák, Štefan. Modeling and control of mechatronic systems using fuzzy logic. In International Review of Automatic Control. Vol. 7, No. 1 (2014), s. 45-51. ISSN 1974-6059.
- [17] P. Přibyl, O. Přibyl, "Effect of tunnel technological systems on evacuation time", Tunneling and Underground Space Technology vol. 44, 2014, pp.88-96



ISSN: 2067-3809

copyright © University POLITEHNICA Timisoara,  
Faculty of Engineering Hunedoara,  
5, Revolutiei, 331128, Hunedoara, ROMANIA  
<http://acta.fih.upt.ro>

<sup>1</sup>I.O. OLADELE, <sup>2</sup>O.T. BETIKU, <sup>3</sup>A.M. OKORO, <sup>4</sup>O. EGHONGHON

# MICROSTRUCTURE AND MECHANICAL PROPERTIES OF 304L AND MILD STEEL PLATES DISSIMILAR METAL WELD JOINT

<sup>1-4</sup>Department of Metallurgical and Materials Engineering, Federal University of Technology, Akure, NIGERIA

**Abstract:** Weldment of dissimilar metals has been of increasing demand and importance in many structural and industrial applications to optimize properties combination, reduce weight of component and cost. In this research, the microstructural and mechanical properties of dissimilar metal welded joint (DMWJ) of austenitic stainless steel (304L; 18/8) and mild steel plates of 5 mm thickness were experimentally investigated. A single V butt joint was prepared and the plates were welded using Gas Tungsten Arc Welding (GTAW) process with ER308L as filler metal. The mechanical properties were examined by tensile, hardness and bending tests while the microstructural characteristics were studied using the Scanning Electron Microscope (SEM). From the results, it was observed that tensile and hardness properties of the dissimilar weld fall between that of the austenitic stainless steel and the mild steel base metals while the bending strength emerges as the best. Austenitic stainless steel possesses bending strength property that was next to the welded sample as well as the best tensile and hardness properties.

**Keywords:** dissimilar metal weld, austenitic stainless steel, mild steel, mechanical properties, microstructure

## INTRODUCTION

Welded dissimilar metals have emerged as structural materials for various industrial applications which provide good combination of mechanical properties like strength, corrosion resistance with lower cost. They have found widespread application in power generation, electronic, nuclear reactors, petrochemical and chemical industries mainly to get tailor-made properties in a component and reduction in weight [1-3].

Austenitic stainless steels possess good mechanical properties and corrosion resistance which account for its application in many equipment and environments like low and high pressure boilers and vessels, fossil-fired power plants, flue gas desulphurization equipment, food processing plants and surgical implants [4].

Gas tungsten arc welding (GTAW), also known as tungsten inert gas (TIG) welding is an arc welding process that uses a non-consumable tungsten electrode to produce the weld. The weld area is protected from atmospheric contamination by an inert shielding gas (argon or helium), and a filler metal is normally used.

GTAW is most commonly used to weld thin sections of stainless steel and non-ferrous metals such as aluminum, magnesium, and copper alloys. The process grants the operator greater control over the weld than competing processes such as shielded metal arc welding and gas metal arc welding, allowing for stronger and higher quality welds. However, GTAW is comparatively more complex and difficult to master, and furthermore, it is significantly slower than most other welding techniques [5].

Conversely, due to difference in thermo-mechanical and chemical properties of the materials to be joined under a common welding condition, it causes a steep gradient of the thermo-mechanical properties along the weld. Also when

joining dissimilar metal welds, diffusion in the weld pool often results in the formation of inter-metallic compound in the welded region. These inter-metallic compounds can be deleterious to the mechanical properties, especially particles of primary crystals, which represent strong stress concentrators and promote the initiation of sharp microcracks [6]. The growth of microcracks may cause brittle fracture thereby reducing the ductility of the joint [3].

Tanaka et al., [7] showed that the mechanical properties of the joints are greatly influenced by the formation of inter-metallic compounds. Therefore, inter-metallic compounds should be checked in order to find problems related to crack sensitivity, ductility, corrosion, and many more which makes the study of microstructure significant [8].

Radha et al., [1] studied the tensile strength of MIG and TIG welded dissimilar joints of mild steel and stainless steel. Stainless steel of grades 202, 304, 310 and 316 were welded with mild steel by Tungsten Inert Gas (TIG) and Metal Inert Gas (MIG) welding processes.

The results were compared for different joints made by TIG and MIG welding processes and it was observed that TIG welded dissimilar metal joints have better properties than MIG welded joints. Jamaludin et al., [9] studied the mechanical properties of welded joint by tension test. It was observed that, the yield strength and tensile strength of welded samples using mild steel welding electrode were slightly lower than welded samples using stainless steel welding electrode.

Giridharan et al., [5] carried out an experimental work to study the mechanical properties of a dissimilar welding joint between IS 2062GrC mild steel and AISI 316L stainless steel, using AISI 309L filler rod. Tensile test, bend test and the microstructural characteristics were studied. The result showed good bending behavior, and improved tensile

strength in the weld area. Electron microscopy showed the dilution of base metals in the weld zone.

In this work, dissimilar welding of austenitic stainless steel (304L; 18/8) and mild steel plates of 5 mm thickness was carried out using GTAW process. Assessment of the microstructural characteristics and mechanical properties of the dissimilar joints were investigated and the formation of dissimilar joints produced by GTAW based on the experimental results was discussed.

### EXPERIMENTAL PROCEDURE

#### — Chemical Analysis

The major materials used for this experiment were austenitic stainless steel (ASS) (304L/18.8; that is 18% Cr and 8% Ni) and mild steel in the form of a rectangular plate both with thickness of 5 mm. The chemical compositions of the base metals under study were obtained by spectrometry and were as shown in Table 1.

Table 1: Chemical composition of austenitic stainless steel (ASS) and mild steel (wt.%)

Elements	C	Si	Mn	P	S
ASS	0.091	0.430	1.310	0.039	0.011
Mild Steel	0.071	0.327	1.155	<0.001	<0.001
Elements	Ni	Cr	Mo	N	Cu
ASS	8.050	18.09	0.220	0.038	0.350
Mild Steel	0.169	0.062	0.013	0.008	0.022

#### — Welding and Sample Preparation

The base metals were cut into the desired length of 150 x 60 mm and a single-V butt joint was prepared for better root penetration. The welding operation was carried out afterwards using the Gas Tungsten Arc Welding (GTAW) and a stainless steel filler metal (ER308L) was used. Direct Current Electrode Negative (DCEN) was employed with welding speed of 150 mm/min and welding current of 110 A.

The arc length, filler tip angle, filler type and size are; 2.0 mm, 60°, ER308L and 3.2 mm, respectively. Pure argon gas was used as the shielding gas to prevent oxidation of molten steel. After completion of the welding process, tensile test samples with dumbbell shapes were cut transversely from the welded joint and the base metal. Machining was also done for the hardness test and microstructural samples which were sectioned from the Weld metal (WM), Heat affected zone (HAZ) and the Base metal (BM).

### PROPERTY TESTS

#### — Determination of Tensile Properties of the Samples

Tensile test samples were prepared in accordance with ASTM A370-08A [10] and the test was carried out using Su Zhou Long Sheng universal testing machine. Three samples were tested with a load of 300 KN and crosshead speed of 5 mm/min correlating with an initial strain rate of 0.98 s<sup>-1</sup> respectively. The specimen was mounted by its ends into the holding grips of the test apparatus. The tensile testing machine was designed to elongate the specimen at a constant rate, and to continuously and simultaneously measure the instantaneous applied load and the resulting

elongations. The applied load permanently deformed and fractured each sample into two parts.

#### — Determination of Bending Properties of the Samples

The bending test was carried out by using Testometric universal testing machine in accordance with ASTM E190-92 [11] standard test method for bending properties of welded samples. The bending test was performed at the speed of 100 mm/min. Three samples were tested for each representative samples from where the average values for the test samples were used as the illustrative values.

#### — Determination of the Hardness of Samples

This method consists of indenting the test material with a hardened steel ball indenter using Indentec hardness testing machine. Rockwell hardness test produces a much smaller indentation more suited for hardness traverses. The hardness samples were separated into three parts- Base metals (BM) for mild steel and stainless steel, HAZ for mild steel and stainless steel and the weld metal (WM).

The test samples were cut into 9 x 9 mm for the different zones and were used for the hardness as well as the microstructural characterization using the Scanning Electron Microscope (SEM). The indenter was forced into the test material under a preliminary minor load of 60 kgf which gradually increased to 100 kgf and 150 kgf. The test was carried out 3 times at different locations on BM, HAZ and WM and, the readings were recorded as displayed by the hardness testing machine.

### RESULT AND DISCUSSION

#### — Mechanical Properties

The tensile properties such as yield strength, ultimate tensile strength and the tensile modulus were evaluated. All the data were the average of the measured values obtained as shown in Figure 1.

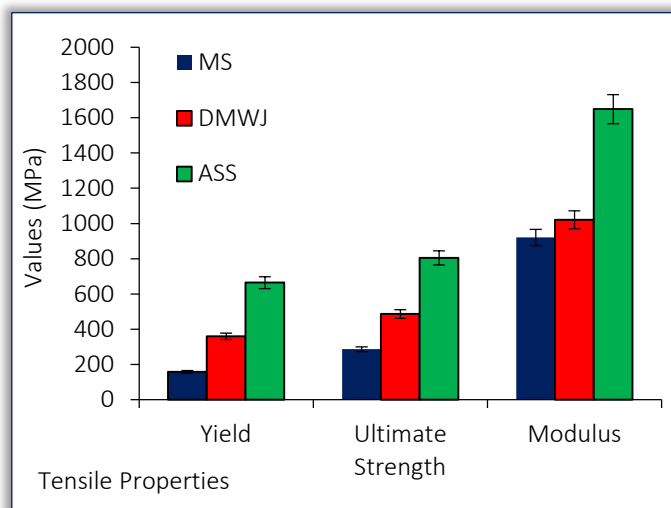


Figure 1: Charts of the tensile properties for the various zones

The charts for the various tensile properties of the welded dissimilar metals were as shown in Figure 1. The plot shows the yield, ultimate tensile strength and tensile modulus of the weld and base metal samples. It was revealed from the results

that similar trends emerged in the response of the materials to these properties. In all the properties examined, austenitic stainless steel gave the optimum performance followed by the weld and mild steel samples, respectively. This trend in terms of materials and values for the properties were ideal for structural integrity where gradual decrease in property from one end to another is essential for effective service performance. The values at the weld joints form the transitional values between that of austenitic stainless steel and the mild steel.

The austenitic stainless steel (ASS) base metal possesses the highest ultimate tensile strength with a value of 805.3 MPa followed by weld sample with a value of about 486.2 MPa while the lowest was the mild steel (MS) base metal with a value of about 286.3 MPa. The results showed that ultimate tensile strength of the weld joint shows an increase of about 38.9% compared to the mild steel base metal. This shows that the weld joint aids balance in transition from low strength mild steel to high strength austenitic stainless steel. The yield strength and tensile modulus also followed the same trend, the highest been 664.31 and 1649.33 MPa, respectively exhibited by the austenitic stainless steel while the lowest was 157.77 and 920.77 MPa, respectively exhibited by the mild steel.

The weld joint shows an increase of about 56.1 % in yield strength and 9.8 % in tensile modulus compared to the mild steel base metal. Part of the reason for this may be the presence of high amount of Chromium and Nickel in the austenitic stainless steel than the mild steel as shown in Table 1. The welded dissimilar metal samples fractured closed to the mild steel due to the low strength possess by the steel compared to the austenitic stainless steel as shown in Figure 2.

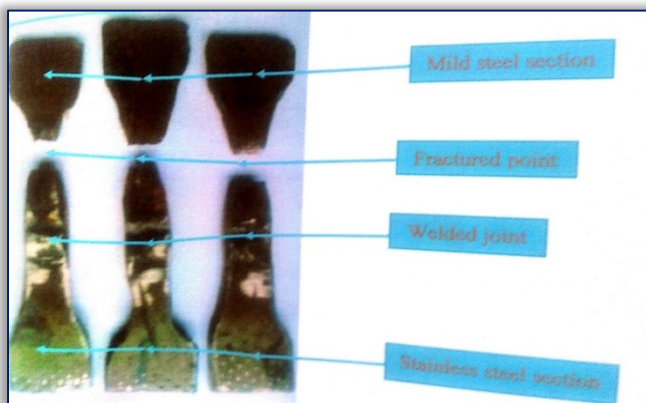


Figure 2: Fractured sample after tensile test showing fracture of sample at mild steel side

Rockwell hardness test was carried out on the samples to measure the variation in hardness across the weld zones of austenitic stainless steel 304L and mild steel. The hardness assessment in Figure 3 shows the average hardness values across the weld interface covering the base metals.

The hardness value obtained is higher for ASS 304L when compared to the mild steel. The highest average hardness value is 37.38 HRC for the austenitic stainless steel base metal

while the lowest hardness value is 27.1 HRC for mild steel heat affected zone. The hardness value obtained at the DMWJ which is lower than that of the stainless steel but higher than that of the mild steel. This implies that, there is diffusion of alloying elements in the weld pool which affects the mechanical properties, hence, an intermediary hardness in the joint.

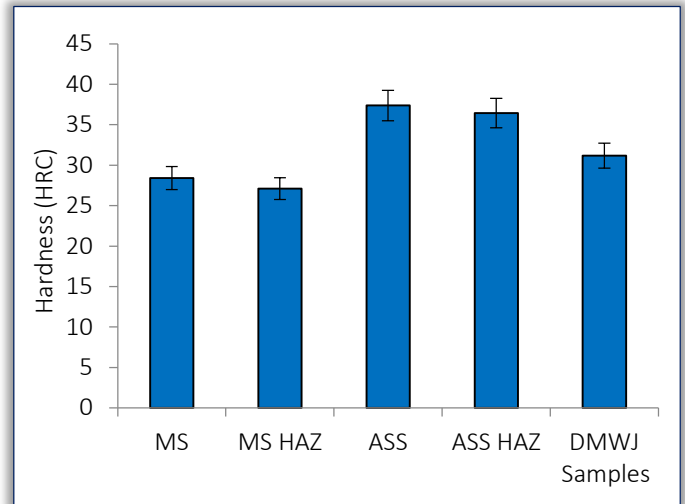


Figure 3: Rockwell hardness values of samples at different regions

In agreement with the findings of Muralimohan et al., [12], it was revealed from the results in Figures 1 and 2 that, there is an analogous tendency in hardness distribution in the various zones like that of the tensile properties. The reason for the variation in hardness can be due to the varying carbon content in the base metals.

The bending test was used to determine the maximum breaking load the materials can withstand before failure as shown in Figure 4.

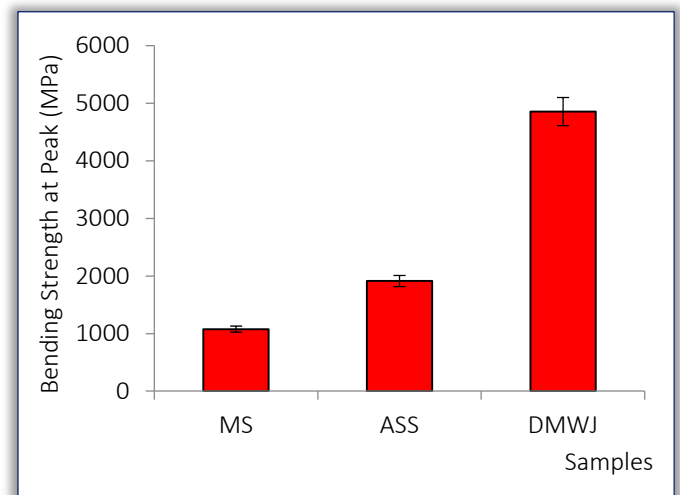


Figure 4: Bending Strengths of base metals and the dissimilar metal welded joint

The bending test result shows that the dissimilar metal weld sample possess the best bending strength due to the highest bending resistance capability. The sample was with a value of about 4857 MPa followed by the austenitic stainless steel base metal with a value of 1913 MPa while the mild steel

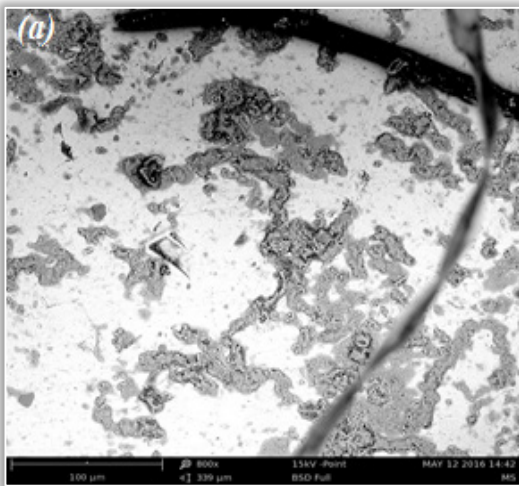
possess the lowest bending strength with a value of 1436 MPa. Considering other mechanical properties, the response of the dissimilar metal weld shows that, it possesses good combination of mechanical properties. The fractured points from the tensile test results as shown in Figure 2 further confirmed this since it occurred at the end close to mild steel and not at the weld joint.

The dissimilar metal welded samples possess intermediate strength and hardness between austenitic stainless steel and mild steel but it possesses the best bending strength. This therefore, implies that by joining these two different metals for applications in areas where changes in structural properties are essential based on environmental effects and cost, this product may be considered for such.

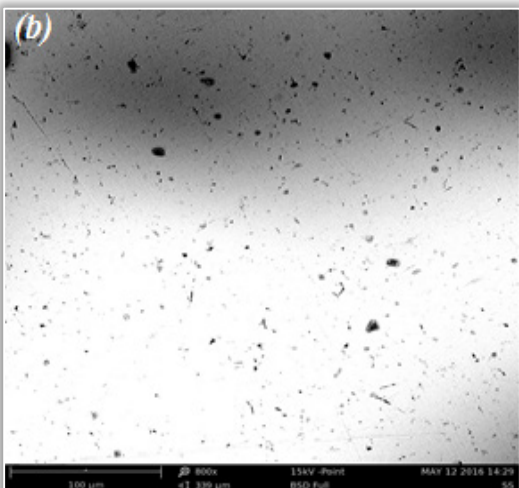
#### — Microstructural Examination

The welded sample, base metal and HAZ of the two dissimilar materials were examined with the Scanning Electron Microscope and the microstructures were analyzed as shown in Figure 5.

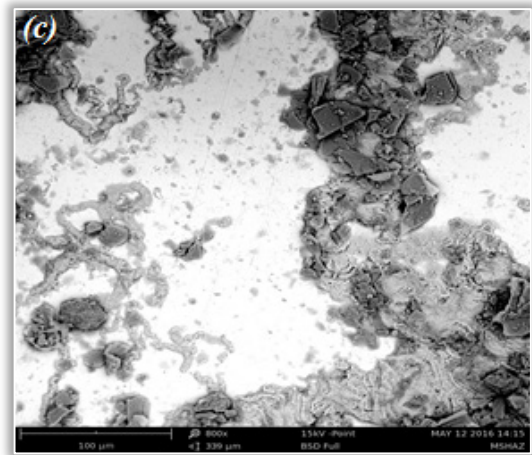
In stainless steel welds, the microstructures were usually related to types of solidification and subsequent transformation behavior. The heat input is handled differently for each welding process and can result in different effects on the dissimilar stainless steel welded joints.



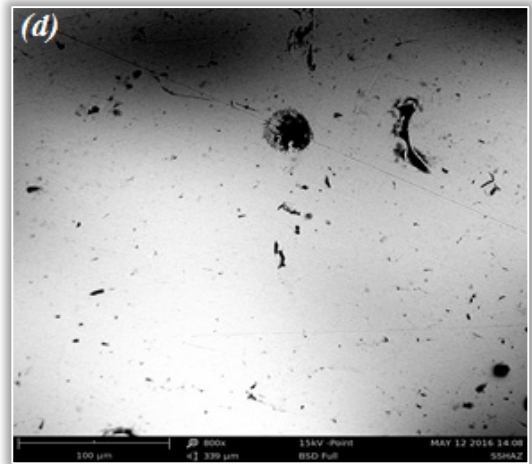
a)



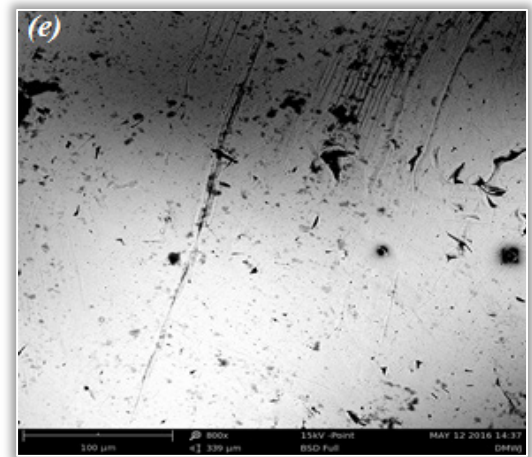
b)



c)



d)



e)

Figure 5: SEM images of a. BM of mild steel b. BM of ASS  
c. HAZ of mild steel d. HAZ of ASS  
e. fusion zone of the dissimilar weld metal

Figures 5 (a-e) showed the various sections of the metals where it became obvious the influence of heat input and solidification on the transformation behavior.

Figures 5 (a) and (c) shows the micrograph of the mild steel BM and HAZ. The mild steel BM reveals a heterogeneous microstructure, consisting of ferrite, and pearlite.

The globular and lamellar pearlite phases are dispersed across the ferrite phase. This corresponds to mild steel HAZ showing fragmentation of pearlite, noticing clearly iron carbide



(cementite) globular dispersed in the ferrite phase as a result of recrystallization occurred by the heat generated during welding.

Figures 5 (b) and (d) shows the micrograph of the ASS BM and HAZ, the HAZ exhibits low level of isolated inclusions similar to Andrés et al., [13] but this increases in the WM. Hsieh et al., [14] studied the microstructure, recrystallization, and mechanical properties in the heat affected and fusion zones of dissimilar stainless steels. Two types of stainless steels, namely 304 (X5CrNi18-10 according to EN 1.4301) (fully austenite containing a few ferrite phases) and 430 (X6Cr17 according to EN1.4016) (fully ferritic microstructure) were welded using GTAW without a filler material.

The recrystallization phenomenon was evident with the second pass heat-affected zone (HAZ-2) and indicated equiaxed grains after second pass welding. The contents of  $\delta$ -ferrite exhibited the highest value of all situations in the first pass fusion zone (FZ-1) during first pass welding. These findings confirm the effect of heat input even when filler is not used. However, it should be pointed out that the filler metal and buttering are unavoidable when the dissimilarity between the base metals cannot result in joints that are free of flaws [15].

#### CONCLUSIONS

This experimental work presents the study on the microstructural and mechanical properties in a dissimilar welding joint between 304L austenitic stainless steel and mild steel using ER308L filler rod. From the study, the following conclusions were made:

- Gas Tungsten Arc Welding process was successfully used to produce the ASS and mild steel dissimilar metal joint
- The tensile strength obtained in dissimilar welded joint was 38.9% higher than parent material of mild steel whose tensile strength was 286.3 MPa. Fracture of the tensile test sample occurred at the mild steel base metal side.
- The hardness value in the ASS side was higher than the mild steel side, this can be attributed to the varying carbon content
- The welded joint possesses the highest bending strength with a value of 4857 MPa. This was followed by the ASS base metal and then the mild steel base metal.

#### References

[1] Radha, R.M.; Visnu, K.T.; and Rajesha, S: A Study of Tensile Strength of Mig and Tig Welded Dissimilar Joints Of Mild Steel And Stainless Steel, *International Journal of Advances in Materials Science and Engineering*, 3(2), 23-32, 2014.

[2] Pouraliakbara, B.H.; Hamedia, M.; Kokabia, A.H.; and Nazarib, A: Designing of CK45 Carbon Steel and AISI 304 Stainless Steel Dissimilar Welds, *Materials Research*, 17(1), 106-114, 2014.

[3] Tayyab, I: Analysis of Dissimilar Metal Welding of 1020 Mild Steel and 304 Stainless Steel, Master Thesis, Department of Mechanical Engineering, National Institute of Technology, Rourkela, 2014.

[4] Oladele, I.O.; Omotoyinbo, J.A.; and Akinwekomi, A.D: The Effect of Weld Goemetry and Post Weld Heat Treatment on the Corrosion Behaviour of Austenitic Stainless Steel Immersed in 1.0 M NaCl Solution, *Material Research*, 13(1), 405- 418, 2010.

[5] Giridharan, S.; Kannan, T.M.; Balamurugan, K.; Kumar, A.; and Vignesh: Experimental Investigation and Analysis of Dissimilar welding of AISI 316L and IS 2062 using GTAW, *International Journal of Innovative Research in Science, Engineering and Technology*, 5(6), 11052-11058, 2016.

[6] Oladele, I.O.; Betiku, O.T.; and Fakoya, M.B: Effect of Post Weld Heat Treatment on the Mechanical and Corrosion Behaviour of Welded Al-Fe-Si Alloy Joints, *Leonardo Electronic Journal of Practice and Technologies*, (30), 75-86, 2017.

[7] Tanaka, T.; Morishige, T.; and Hirata, T: Comprehensive Analysis of Joint Strength for Dissimilar Friction Stir Welds of Mild Steel to Aluminum Alloys, *Scripta Materialia*, 61, 756–759, 2009.

[8] Shahid, F.; Khan, A.A.; and Hameed, M.S: Mechanical and Microstructural Analysis Of Dissimilar Metal Welds, *International Journal of Research and Reviews in Applied Sciences*, 25(1), 6-14, 2015.

[9] Jamaludin, S.B.; Noor, M.M.; Kadir, S.K.; and Ahmad, K.R: Mechanical Properties of Dissimilar Welds between Stainless Steel and Mild Steel, *Advanced Materials Research*, 795, 74-77, 2013.

[10] ASTM A370-08A: Standard Test Methods and Definitions for Mechanical Testing of Steel Products, ASTM international, 2008.

[11] ASTM E190-92: Standard Test Method for Guided Bend Test for Ductility of Welds, ASTM International, Re-approved 2008.

[12] Muralimohan, C.H.; Haribabu, S.; Hariprasada, R.; Muthupandi, V.; and Sivaprasad, K: Evaluation of Microstructures and Mechanical properties of Dissimilar Materials by Friction Welding, *Procedia Materials Science*, 5, 1107-1113, 2014.

[13] Andrés, G.F.; Rafael, S.A.; Leiry, C.B.; and Alberto, V.R: Crack growth study of dissimilar steels (Stainless-Structural) butt-welded unions under cyclic loads, *Procedia Engineering*, 10, 1917–1923, 2011.

[14] Hsieh C.C.; Lin D.Y.; Chen M.C.; and Wu W: Microstructure, Recrystallization, and Mechanical Property Evolutions in the Heat-Affected and Fusion Zones of the Dissimilar Stainless Steels, *Materials Transactions*, 48(11), 2898-2902, 2007.

[15] Mvola, B.; Kah P.; and Martikainen J: Dissimilar Ferrous Metal Welding Using Advanced Gas Metal Arc Welding Processes, *Rev. Adv. Mat. Science*, 38, 125-137, 2014

ISSN: 2067-3809

copyright © University POLITEHNICA Timisoara,  
Faculty of Engineering Hunedoara,  
5, Revolutiei, 331128, Hunedoara, ROMANIA  
<http://acta.fih.upt.ro>

# Fascicule 2

## [ April - June ]

### t o m e

# [2018] XI

**ACTA**Technica**CORVINIENSIS**  
BULLETIN OF ENGINEERING



**ISSN: 2067-3809**

copyright © University POLITEHNICA Timisoara,  
Faculty of Engineering Hunedoara,  
5, Revolutiei, 331128, Hunedoara, ROMANIA  
<http://acta.fih.upt.ro>

<sup>1</sup>Saša VASILJEVIĆ, <sup>2</sup>Nataša ALEKSIĆ, <sup>3</sup>Dragan RAJKOVIĆ,  
<sup>4</sup>Rade ĐUKIĆ, <sup>5</sup>Milovan ŠARENAC, <sup>6</sup>Nevena BANKOVIĆ

# THE BENEFITS OF APPLICATION OF CAD/CAE TECHNOLOGY IN THE DEVELOPMENT OF VEHICLES IN THE AUTOMOTIVE INDUSTRY

<sup>1-6</sup> High Technical School of Professional Studies, Kragujevac, SERBIA

**Abstract:** The development of various software packages enables easier and faster designing and development of the existing systems in the automotive and other industries. CAD technology tests allow faster and much economical designing of different parts and systems in vehicles. With this technology, it is possible to speed up the process of designing and making of the most complicated systems and parts in the vehicle without additional experiments. However, the problem arises with designing parts and systems that do not have a sufficiently developed field of theoretical assumptions. This paper presents different applications on specific complex systems and parts of vehicles and each of them has been given the importance in the research.

**Keywords:** Vehicles, design, development, CAD, CAE

## INTRODUCTION

The development of automotive industry and its products requires a set of challenging and elaborate researches and series of complex experiments. With the development of technology, many software solutions have been created that facilitate and enable faster testing of certain parts and assemblies in vehicles. The use of these software solutions is diverse, and in the automotive industry they have various applications, e.g. determining the load of individual parts or assemblies, examination of a vehicle's design etc. This paper shows the application and importance of CAD technology in this industry, and its advantages in relation to some real experiments.

Even in the earliest age of computer technology, graphic simulation has proven to accelerate all engineering and design processes for several hundred times in relation to "manual" design, and to speed up production of various documents and, consequently, the research. The development has led to creation of a model and research of three-dimensional interpretation. All the technologies rely on the principles of mathematical sciences, descriptive geometry, informatics and applied electronics. ISO standards define computer graphics as a set of methods and techniques for converting data that are sent to or from the graphic display, via computer. Some of the most famous CAD technological processes are CATIA, SolidWorks, AutoCAD, ProENGINEER.

Nowadays, the development of software in the automotive industry and industry in general goes mainly into three directions – design, engineering and production. CAD (Computer-aided design) is the use of computer systems to help in the creation, modification, analysis, or optimization of a design.

Computer-aided engineering (CAE) is a widespread use of computer software to help in engineering analysis tasks. It includes finite element analysis (FEA), computational fluid

dynamics (CFD), multibody dynamics (MBD), and optimization. Software solutions used for production purposes are CAM (Computer-aided manufacturing) technologies [1,2].

In this paper, we will carry out the analysis of benefits of only CAE and CAD technologies in the process of development itself, which represents the very purpose of this paper; as well as the advantages they have in designing and developing the vehicle in relation to experimental methods. One of the main advantages of technologies is faster testing of the development of some parts or the entire vehicle, the reduction of cost of experiments and development (the easier way of checking the weaknesses and disadvantages of a part), and the acceleration of the process of creating technical documentation. The use of technologies has allowed manufacturers to reduce the cost and product development time, and to improve safety, comfort and durability of the vehicles they manufacture.

## GENERAL IMPORTANCE OF THE PHASES OF A VEHICLE DEVELOPMENT

By observing all the phases of the development of one vehicle, and all the products in its life cycle, as can be seen in Figure 1, it can be noticed that there are different tests in all phases of the life cycle and, consequently, different studies. These researches and tests are highly complex and elaborate, therefore, the application of CAD/CAE is of great benefit and importance due to its advantages in relation to the real experiments that would be carried out. Today, the so-called virtual laboratories are developed, and they greatly reduce the cost of testing and the time necessary for researches. Virtual laboratories represent an innovation in the use of information technology for the purpose of education. They represent a unique link between the laboratory test desk from the past and the experiments of the future.

With the use of existing databases, the latest electrical equipment is available from any place at any time. In this

phase, the exactness of technical documentation is of great importance, thus, CAD technology is used for the making of accurate and precise technical documentation.

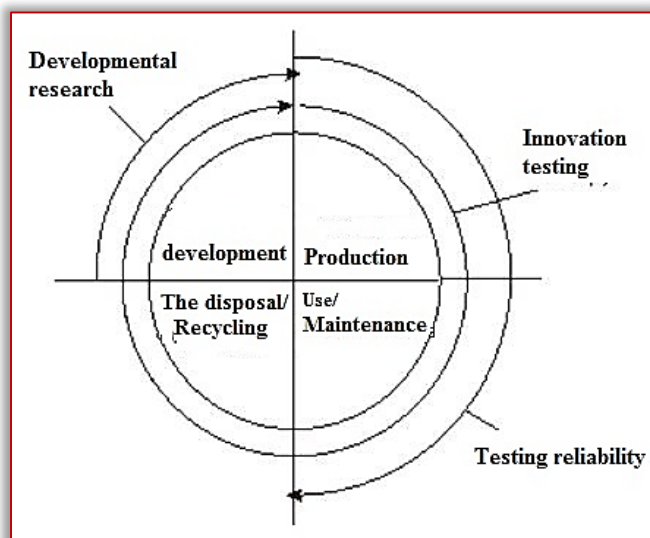


Figure 1. An overview of tests and researches in the product's (vehicle's) life cycle

The next type of vehicle testing is testing of new innovations, which implies possible changes to already existing systems, in this case, on vehicles. The tests regarding the mentioned changes are completed with the help of CAE technologies. With this technology, the characteristics of such an altered system with all these innovations can be freely determined. Such testing, or a research, represents an option that in relation to some physical researches enables the development and testing of these examinations with many changes and possibilities it has provided.

When using a products, in this case a vehicle, its reliability is of great importance – CAE technology allows us to accurately determine the reliability of each vehicle system, even after a longer period of its being used.

#### COMPARISON OF VIRTUAL AND PHYSICAL EXPERIMENTS

Testing was an important part of product development in the past. The weaknesses of a design could be detected by testing before the product came into the customer's hands. However, the ability to carry out a thorough analysis of many aspects of a design using the computer-assisted engineering (CAE) tools has reached the point where "virtual" product development can be considered to be a realistic proposal. Virtual experiments have certain advantages, namely the ability to control the experiment, the repeatability of performance and results, the ability to perform accelerated tests, the safety of the experiment implementation, the ability to simulate real conditions, the ability to optimize the implementation of the experiment, the specific experiment implementation plan. The development of a new product is one of the most powerful and most difficult activities in the industry.

In addition to the mentioned advantages, the use of technologies considerably reduces the cost of testing and the research. The security is very important, as well as the

repeatability of the experiment, because some researches can be extremely expensive; therefore physical testing can be carried once, and with CAE technology it can be repeated.

#### — Cases when it is not possible to apply CAD/CAE technologies

Despite the development of the existing technologies, there are cases when it is not possible to apply modern technology in the development and research of some systems, or in the automotive industry in the development of certain systems in the vehicle.

The reason for this is that certain theories or some phenomena have not been sufficiently explored, thus simulations cannot be properly or at all completed. There are also simulations that are extremely difficult because it is hard to simulate some physical phenomena, therefore the software is not sufficiently developed. For example, the analysis of the fatigue of the hot exhaust system is currently extremely difficult for simulation (due to uncertainties about the properties of the material, the crack propagation at elevated temperatures, the influence of the geometry of the welds and the change in the properties of the material at elevated temperature), but it is relatively easy to set the exhaust system to the engine and perform a test in order to determine whether the exhaust system will develop cracks. Such systems are often better developed using traditional physical testing. Also, if the working conditions are not specified, then it is very difficult to have confidence in the results of the virtual experiment.

#### — Application of CAD/CAE technology in designing a vehicle

Advanced technologies have a major role in designing vehicles in the automotive industry because it is possible to accurately model the desired shape of a vehicle. With the use of these technologies we have an overview in the design phase, because creating 3D parts in the space provides an ideal insight into geometry, keeping in mind that the body of the vehicle itself has a large number of parts, the defined elements are easily grouped into assemblies and sub-assemblies.



Figure 2. An overview of a vehicle design development, [3]

With the help of technologies the creation of vehicle's appearance is accelerated, it is possible to create desired view at the drawing, the expenses of probing the body of the car are reduced, the co-operation of co-workers is simplified etc. These models are significant because they allow the comparison of the quality of all parts of a vehicle. The design phase itself is not so simple – there are several phases that have to be completed and these technologies allow all this to be done virtually, which is much simpler and cheaper. Figure 2 shows the stages in the designing of a vehicle.

— **Benefits of CAD/CAE technology when analyzing vehicle's design**

Not only is CAD technology important in designing vehicles, but its role is substantial in testing of a design, that is, it simplifies the testing of a known design. The importance of aerodynamics, the flow of air over the surface of a vehicle is very well known. Air resistance plays a very important role in all resistances, therefore it is a priority to maximize the aerodynamics of a vehicle.

With the help of these technologies it can be accurately determined which points on the vehicle are critical, and certain parts of a vehicle can be reconstructed if there is a suspicion that air spinning is increased. The use in these cases is very important because it is possible to reconstruct the design of a vehicle without expensive aerotunels and without the prototype, which greatly reduces the cost, and consequently lack of prototype saves time in the vehicle development. Figure 3 shows the look of a test using one of the technologies.

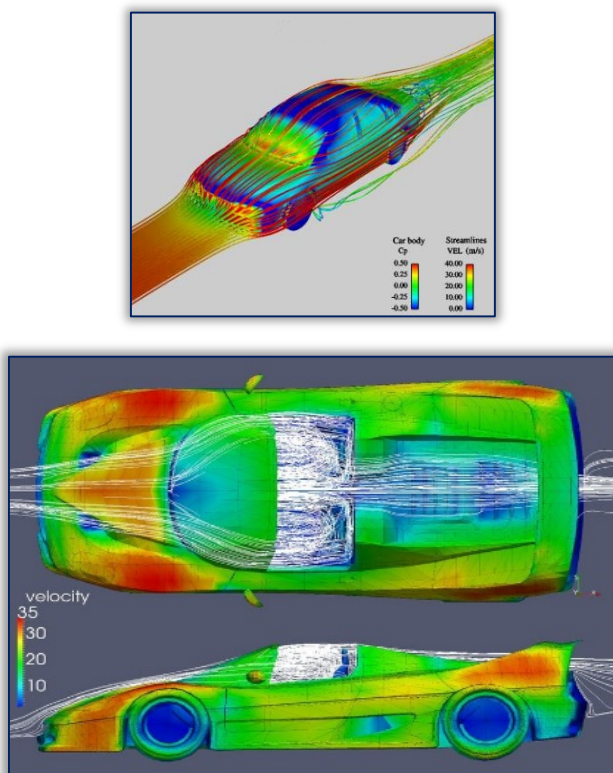


Figure 3. A demonstration of a vehicle's aerodynamic testing, [4]

CAE technology has also been used in the simulation of crash tests or in vehicle's body safety checks. These tests are very expensive and require specialized testing centers. In addition to rigorous and precise testing requirements, as well as prototypes of vehicles being tested, CAE technology produces precise results of vehicle deformation during testing, which is very useful and is possible to perform corrections to the virtual model of the vehicle with reduced cost of testing and time saving. Figure 4 shows an example of this test.

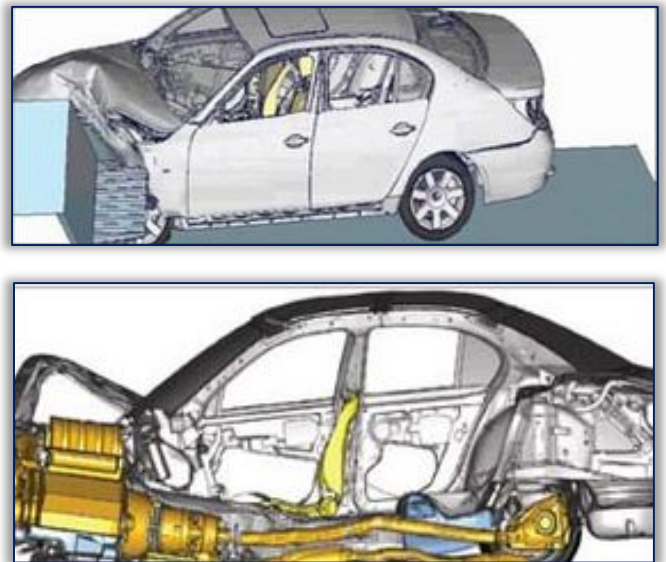


Figure 4. Safety test of the body of a vehicle, [5]

— **Application of CAD/CAE technology to check vehicle's ergonomic characteristics**

Ergonomic characteristics of vehicles are significant for the reduction of fatigue and facilitation of car driving. One of the software that is developed according to the principles of CAE technology is RAMSIS. RAMSIS is the world-leading 3D-CAD-ergonomics tool, designed in cooperation with the German automobile industry for the ergonomic development of vehicles and cockpits.

Ergonomics is increasingly seen as a quality factor by the customer and it is becoming a significant differentiation criteria. RAMSIS is the world's leading CAD tool for the ergonomics design and analysis of vehicle's interior design and analysis of vehicle interior and working places and is used by 70% of the automobile manufacturers [6]. This software package allows you to check the ergonomic characteristics of the vehicle, or the comfort of the driver or other passengers in vehicles. RAMSIS is not only available to the user as a pure CAD application (e.g. integrated into CATIA or as stand-alone version) - as RAMSIS and VR, this ergonomics system can also be used for extensive real-time tests in virtual reality laboratories of automotive manufacturers.

Figure 5 shows the example of a driver in the vehicle and one of the possible analysis of the driver's comfort at a particular driver's position in the vehicle.

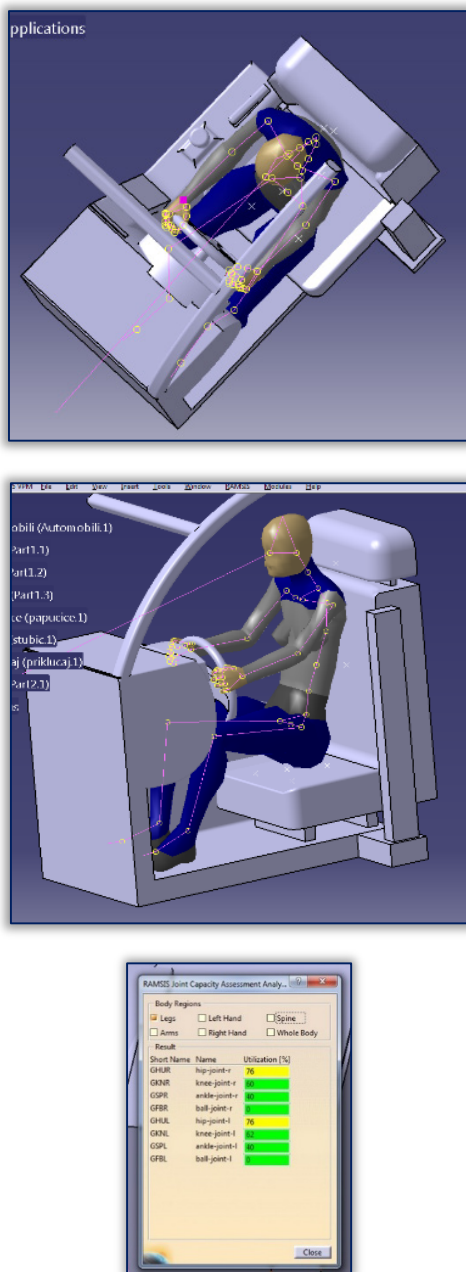


Figure 5. The analysis of the driver's comfort in the vehicle and the analysis in the CAE software

— Significance of CAE technology in examining the elements of passive interior safety

Bearing in mind the previously mentioned concern regarding the ergonomics of the vehicle, which in this case concerns the interior of the vehicle, the application of CAE technology is very important in the examination of the operation of individual elements of passive safety, such as an airbag, which, in the case of a traffic accident, should prevent the driver from hitting the steering wheel or other element of the interior.

Figure 6 shows an example of an analysis of driver's impact in the airbag. This application is very important in the analysis of the position and shape of the airbag, because it replaces long-term and highly complex physical work about driver's impacts in the airbag, as well as analysis of the shape and

position of the impact, bearing in mind that passengers can be found in different positions in a traffic accident.

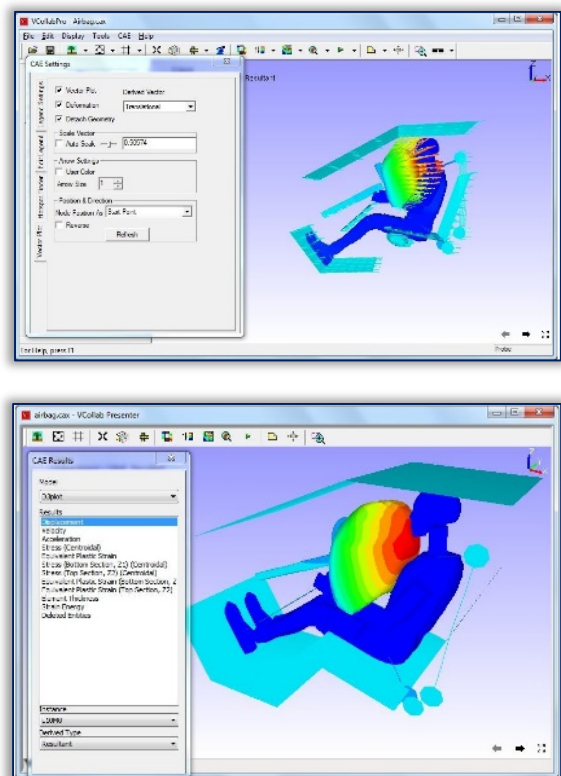


Figure 6. A demonstration of the analysis of driver's impact in the air bag by using CAE technology, [7]

— The importance of CAE technology in testing the performance and efficiency of certain systems in vehicle

In addition to benefits of all previously shown elements regarding ergonomics of the vehicle, CAE technology also enables the display of the flow of certain fluids through the various systems on the vehicle. CAE technology is used for testing air conditioning system (AC).

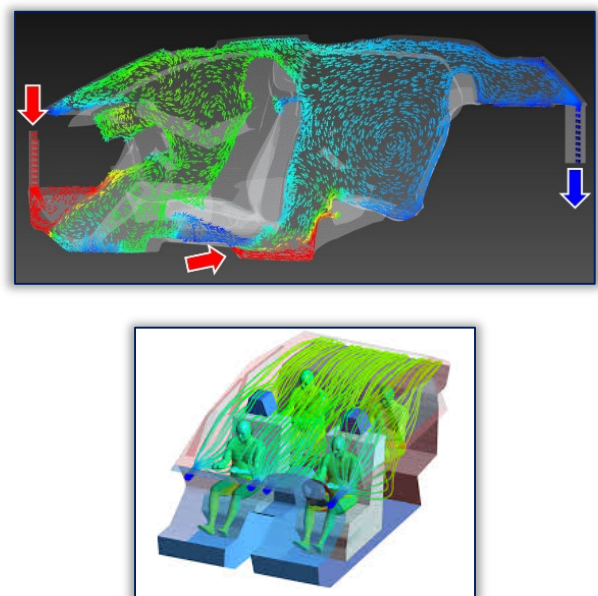


Figure 7. Demonstration of air flow simulation using CAE technology, [8]

Figure 7 shows a simulation of the operation and flow of air using this technology. With CAE, the flow of air in the vehicle is accurately determined as well as the impact on air temperatures in different vehicle zones. CAE simplifies tests of the validity of the operation of this system without complex experiments or expensive equipment. It is also possible to complete a simulation of cooling down of the engine or the air flow in the engine compartment.

— **The importance of CAD/CAE application while projecting vehicle's propulsion unit**

Nowadays, the process of designing and manufacturing internal combustion engines (ICE) cannot begin without an adequate verification of the idea which is the first and most important stage in this business. Modern motors are mostly made by improving the existing ones, that is, by modernizing older solutions using software tools. Captured parameters are put into the appropriate software that through a complex mathematical model mimics complex physical and chemical processes in the engine. When such constructed engine is put into propulsion, the parameters of the monocylinder operation (engine indication) are collected, on which basis a mathematical model is developed and is further processed on the computer.

Mathematical models of the engine are made based on the laws of thermodynamics, fluid mechanics, chemical kinetics and other sciences. Depending on the type of engine on which it is operated (two-stroke, four-stroke, slow-moving, high-speed, diesel, otto-engine, etc.), the appropriate software is selected to mimic the given engine.

Having in mind that most of the processes and phenomena in the engine can be modeled and calculated using a computer, that motor parts can be "made" on the computer and that the engine itself, ie, its assemblies and subassemblies can be successfully simulated on the computer, we come to the concept of "virtual" engine. It means that the engine can be engineered, simulated, and tested on a computer before making the real prototype and testing it. The programs display the gas temperature during the operation of the virtual engine, as well as the temperature assumptions that certain mechanical parts of the engine are subjected to.

Thus, the constructor is able to monitor the flow of temperature, pressure and flow rate of gas, and to optimize it with various interventions on the virtual engine. After the thermodynamic calculation and the first modeling stage provide the approximate dimensions and shapes of the motor parts, thorough examination is performed on several types of strains, which during the modeling give an insight about overloads and possible destruction of elements. Finite Element Methods (FEMs) are used today.

On the basis of these calculations, computers perform complicated analyzes, solve problems straight away and allow easy change of engine performance parameters, saving both time and money.

**CONCLUSIONS**

Nowadays, product development is a very complex process because modern products are more elaborate since there is a demand to maximize efficiency with minimal consumption of certain means. The development in the automotive industry follows this trend, given the characteristics of today's vehicles. There are several stages in which it is possible to develop them.

The use of various modern software such as CAD and CAE technology, enables us to perform various researches very effectively and efficiently, and it is possible to test different modifications in order to improve the characteristics and develop them. The benefit of these systems is that they enable faster and cheaper research and development of the vehicle.

The adoption of this technology allows better communication between all members of the vehicle development team, because each problem can be graphically displayed, better production of technical documentation, possible repetition of each simulation or research with the possibility to change the model itself, at minimal cost, the possibility to test one vehicle or its elements several times under different conditions, it is not necessary to create a prototype for testing, it eliminates the need for expensive test equipment, allows designers to inspect all faults on a vehicle or system.

Compared to physical experiments, which are carried out in real conditions and environment, the virtual experiments may have certain disadvantages, however, they are quite developed and can simulate real conditions, and they will continue to develop and eliminate their drawbacks.

**Note**

This paper is based on the paper presented at 7th International Conference Industrial Engineering and Environmental Protection 2017 – IIZS 2017, organized by University of Novi Sad, Technical Faculty "Mihajlo Pupin", in Zrenjanin, SERBIA, 12 – 13 October 2017.

**References**

- [1] Wang, Donghui; Hu, Fan; Ma, Zhenyu; Wu, Zeping; Zhang Weihua, A CAD/CAE integrated framework for structural design optimization using sequential approximation optimization, *Advances in Engineering Software*, Volume: 76 Issue 1 (2014)
- [2] Letić, D., Davidović, B., Radulović, B., Berković, I., Desnica, E., The high-performance algorithm of the computer methods at the establishing of the states of stress of the brake mechanism by the finite element method (fem), *Metalurgija* 51 (4) 2012., pp. 513– 517, ISSN 0543-5846
- [3] Tovey M., Concept design CAD for the automotive industry, *Journal of Engineering Design*. Mar2002, Vol. 13 Issue 1, p5-18. 14p, ISSN: 0954-4828, 2002.
- [4] Aerodinamičnost, <https://www.google.rs/imgres?imgurl=http://www2.mech.kth.se/courses/5C1211/>

- [5] Ispitivanje bezbednosti vozila,  
<http://www.digitaleng.news/de/improving-product-development-with-cae/> , 29.07.2017
- [6] RAMSIS,  
<http://www.intrinsys.com/software/ramsis?src=applied>  
, 30.07.2017.
- [7] Ispitivanje vazdušnog jastuka,  
[http://training.vcollab.com/CAE\\_Display\\_VectorPlot\\_Pro.html](http://training.vcollab.com/CAE_Display_VectorPlot_Pro.html) , 30.07.2017.
- [8] A/C, <http://www.theseus-fe.com/application-areas/automotive/electromobility> . 31.07.2017.



ISSN: 2067-3809

copyright © University POLITEHNICA Timisoara,  
Faculty of Engineering Hunedoara,  
5, Revolutiei, 331128, Hunedoara, ROMANIA  
<http://acta.fih.upt.ro>



<sup>1</sup>S. ABDULKAREEM, <sup>1</sup>E.J. EDACHE, <sup>1</sup>I.I. OLOWOSULE,  
<sup>2</sup>M.Y. KOLAWOLE, <sup>3</sup>I.I. AHMED, <sup>1</sup>T.K. AJIBOYE

## EFFECT OF DATE SEED PARTICULATES ON MECHANICAL PROPERTIES OF ALUMINIUM ALLOY

<sup>1</sup>Department of Mechanical Engineering, Faculty of Engineering & Technology, University of Ilorin, NIGERIA

<sup>2</sup>Department of Mechanical Engineering, Kwara State University, Malete, Ilorin, NIGERIA

<sup>3</sup>Department of Materials and Metallurgical Engineering, Faculty of Engineering & Technology, University of Ilorin, NIGERIA

**Abstract:** The results of an experimental investigation of mechanical properties of date seed particles reinforced aluminium alloy composites, processed by stir casting method are reported in this paper. Two sets of composites with date seed of 300 and 500 µm particle sizes were used. The ranges of particle size used were based on the weight fraction when sieve analysis was conducted on the sample collected for the work. Each grain size had four types of composite samples with the reinforcement weight fractions of 5, 10, 15 and 20%. The mechanical properties considered were the tensile strength, Impact and hardness behaviors. Unreinforced aluminium alloy samples were also tested for the same properties. It was found that the hardness and tensile strength increases with the increase in the weight fraction and the fracture toughness decreases with increase in the weight fraction of reinforced date seeds particles. It was concluded that the improvement in the mechanical properties can be well accredited to the high dislocation density.

**Keywords:** aluminium alloy; date seed particle late; mechanical properties; metal matrix composites; reinforcement

### INTRODUCTION

Metal matrix composites (MMCs) have found application in many areas of daily life for quite some time these materials are produced *in situ* from the conventional production and processing (Karl 2006). According to Chaudhary et al, 2015, the growth of MMCs has been one of the main innovations in the field of material development in the past 2 decades. MMCs is a new generation of engineering materials in which particle reinforcement is incorporated into a metal matrix to improve its strength, specific stiffness, wear resistance, excellent corrosion resistance and high elastic modulus. MMCs are the forerunners amongst different classes of composites. Over the past two decades metal matrix composites have been transformed from a topic of scientific and intellectual interest to a material of broad technological and commercial significance (Ron and Alcan 1994, Kok and Ozdin 2006). Aluminium based metal matrix composites have received increasing attention in recent years as engineering materials with most of them possessing the advantages of high strength, hardness and wear resistance (Kok and Ozdin 2006). Particulate reinforced aluminium alloy composites have shown a significant improvement in tribological properties, including sliding and abrasive wear resistance and seizure resistance (Kok 2003). In aluminium alloy matrix composites reinforced with ceramic particles, it has been generally agreed that increasing the particle content can enhance wear resistance (Kok 2003, Kok and Ozdin 2006). Al<sub>2</sub>O<sub>3</sub> and SiC particles are the most commonly used reinforcements in MMCs and the addition of these reinforcements to aluminium alloys has been the subject of a considerable amount of research work (Udomphol 2007).

(Anilkumar, H.S. et al. 2010) studied mechanical properties of fly ash reinforced aluminium alloy (Al6061) composites using stir casting technique. It was reported that the tensile strength, compression strength and the material hardness increased with increase in the weight fraction of reinforced fly ash and decreased with increase in particle size of the fly ash. The alloy ductility decreased with increase in the weight fraction of reinforced fly ash and decreased with increase in particle size of the fly ash (Kok and Ozdin 2006). (Charles and Arunachalam 2004) and (Anilkumar, H.S. et al. 2010) studied the properties of aluminium alloy hybrid composites (Al-alloy/Silicon carbide (SiC)/fly ash). They reported that the wear and hardness were enhanced by increasing volume fraction of SiC. They also reported that the tensile strength was high at 10 volume fraction of SiC and decreased as the volume fraction increased. A further study was carried out by (Manoj, Deepak et al. 2009) on the development of aluminium based silicon carbide particulate metal matrix composite, where stir casting method was used to form metal matrix composite. Their result shows that an increase in the composition of SiC, increased the hardness and impact strength of the composite. It was also reveal that the best results was obtained at 25% weight fraction of 320 grit size SiC particles (Saravanana and Senthil 2013). The mechanical properties of aluminum alloy (Al2024) reinforced with SiC and graphite particles ware investigated by (Basavarajappa, Chandramohan et al. 2004). Their results revealed that the mechanical properties such as hardness, yield strength, ultimate tensile strength and compressive strength of the composite increased predominantly with the increase in volume fraction of the reinforcement. However,

the investigation of the abrasive wear behavior of an Al-4.0Cu-0.75Mg alloy composites reinforced with SiC, Si<sub>3</sub>N<sub>4</sub>, Al<sub>2</sub>O<sub>3</sub> produced by stir casting techniques by (Sato and Mehrabian 1976) showed that the wear rates of particulate composites were lower than those of the matrix aluminium alloy by a factor of 4. (Kok and Ozdin 2006) investigated the wear resistance of aluminium alloy reinforced with Al<sub>2</sub>O<sub>3</sub> particles fabricated by a vortex method, their result reveal that the abrasion wear resistance and wear resistance increased with increase in Al<sub>2</sub>O<sub>3</sub> particle size and content. The effect of Al<sub>2</sub>O<sub>3</sub> particle size on the wear resistance was more significant than that of the particle content.

The work of (Kok 2003) on the effect of Al<sub>2</sub>O<sub>3</sub> particle content and size on the porosity and mechanical properties of Al<sub>2</sub>O<sub>3</sub> particle-reinforced 2024 aluminium alloy composites and examination of the wettability problem during the incorporation of Al<sub>2</sub>O<sub>3</sub> particles into the aluminium alloys. The result of the investigation shows that the density of the composites increased with increasing weight percentage and size of particles, whereas the porosity of the composites increased with decreasing size and increasing weight percentage of the particles. The wettability and the bonding force between Al alloy/Al<sub>2</sub>O<sub>3</sub> particles were improved by the applied pressure after the casting. The tensile strength and hardness of MMCs increased while elongation decreased with decreasing size and increasing weight percentage of the particles (Udomphol 2007). The work of Ramesh et al, (2014) titled "Effect of reinforcement of natural residue (Quarry Dust) to enhance the properties of AMMCs, reported that here is significant improvement in the tensile strength and the hardness with addition of quarry dust particulates, having the tensile strength of matrix alloy and Al-quarry dust composites improved from 150 MPa to 172 MPa

(Ameh, Isa et al. 2015) worked on "Effect of particle size and concentration on the mechanical properties of polyester/date palm seed particulate composites". They achieved optimum tensile strength of 16.7619 N/mm<sup>2</sup> and elastic modulus of 343.8 N/mm<sup>2</sup> at 15wt% and 10wt% loading respectively with 0.5mm particles. The percent water absorption was found to be least for 0.5mm particle size while hardness was enhanced to the maximum of 74 HRF (Rockwell Hardness Factor) by 2mm particle size at 25wt% loading. In a related work of (Alaa 2015) titled "Investigation of tensile and impact of composite materials reinforced with natural materials." He concluded that the composite specimens reinforced with olive seeds powder gives high mechanical than composites specimens reinforced with dates seeds powder. He recorded value of modulus of elasticity and tensile strength at 18 wt% and grain size of 300µm for two types of powder. Effects of MoSi<sub>2</sub> reinforcement and aging treatment on hardness and wear properties of AA 2024-MoSi<sub>2</sub> nanocomposites were investigated by Sameezadeh et al, 2011. They reported that, with increased volume fraction of nano MoSi<sub>2</sub> up to 3-4%, the hardness of the composites continuously increased and that the particle agglomeration

reduced the amount of effective nano particulate available and the particle strengthening effect diminished.

It can be observed from the aforementioned literature reported that addition of date seed as reinforcement in aluminium alloy is rarely available. Hence there is need to investigate the effect addition of date seed particles in aluminium composite. According to (Souhail, Christophe et al. 2004), date fruit has been an important crop in arid and semiarid regions. This fruits plays an important part in the economic and social lives of the people of these regions. The fruit of the date palm is well known as a staple food composing of a fleshy pericarp and seed. The pits of date palm (seed) are a waste product of many industries, after transformation of the date fruits. It has been reported by (Mohammad, Mostafa et al. 2014) and (Mohamed, Souhail et al. 2013) that in some date-processing countries, such as Tunisia, date seeds are discarded as wastes or used as fodder for domestic farm animals.

In most parts of northern Nigeria where date fruit is been heavily consumed, the seed is usually discarded as wastes after the fleshy pericarp of the date has been eaten. More importantly, these date seeds turn out to be wastes after the date fruit has been consumed (eaten). Furthermore, the aluminium alloy used as melt in this work is off-cuts from the production of aluminium doors and windows. The addition of date seeds particles as reinforcement in aluminium composites was achieved through stir casting process with various weight fractions and grain sizes of date seeds particles. The effect of the reinforcing material on mechanical property of the aluminium composite was investigated and reported in this work.

## MATERIALS AND METHOD

### — Reinforcement Material

The materials (date seeds) used in this work (Figure 1) was sourced from local vendor, with fleshy pericarp of the date fruits removed to obtain the seeds (Figure 1a). The seeds were sundried for one week to reduce and maintain the moisture content in other to aid the pulverizing process. After drying, local grinding machine was used to pulverize the date seeds, the pulverized seed particles (Figure 1b) were sieved using standard sieve sizes of 600, 500, 420 and 300 µm successively.



Figure 1. Date Seed Used in this Work (a) Raw Date Seeds and (b) Pulverized Date Seed

— Matrix Material

In this work, the matrix phase of the composite is aluminium alloy. The aluminium was cast from aluminium scrap. The scraps (Figure 2) that was used for the melt were sourced from aluminium window frame and door fitters as off-cuts from aluminium alloy 6063 commonly referred to as architectural alloy which are normally used in window frames and doors as well as extrusions of parts. To minimize the level of impurity in the melt, the scraps were cleaned using steam and hand towel to removed dirt and colored inscriptions on the aluminium scraps. Table 1 gives the elemental composition of the aluminium scrap used.



Figure 2. The Scrap (off-cuts) from Aluminium Alloy 6063

Table 1. Elemental Compositions of the Aluminium Used

Element	Mg	Si	Fe	Cr	Cu
wt. %	0.45-0.9	0.2-0.6	0.35	0.10	0.10
Element	Ti	Mn	Zn	Al	
wt. %	0.10	0.10	0.10	Bal	

EXPERIMENTAL PROCEDURE

— Sample Preparation

The quantity of Aluminium scrap and date seeds particles required to produce composites having 5, 10, 15, and 20% weight of date seeds particles were evaluated using charge calculations. The date seeds particles were initially preheated at a temperature of 180°C for 20 minutes to help improve wettability with the aluminium alloy. Aluminium alloy was weighed and charged into the crucible. The loaded crucible was put into the heating chamber of the electric furnace and the temperature of the furnace was set to 850°C (150°C above the liquidus temperature of aluminium).

The preheated date seeds particles was added at this temperature and stirring of the slurry was performed manually for 2 minutes. The composite slurry was then reheated to 850°C and a further stirring was carried out for another 2 minutes to help improve the distribution of the date seeds particles in the molten aluminium alloy. The molten composite was then cast into prepared sand molds. Unreinforced aluminium alloy was also prepared by casting for control experimentation.

— Testing for Mechanical Properties

≡ Tensile Test

The tensile test was conducted according to ASTM E8/(E8M) (ASTM 2016) on each of the cast sample using Testometric Universal Testing Machine (TUTM) model FS50AT, with maximum load capacity of 50KN. The tensile test samples (Figure 3) were 10mm diameter and gauge length of 100mm, machined from the cast aluminium composites. Average of three readings was taken for each sample prepared from the cast aluminium alloy. Analyses of the tensile results were generated and obtained from the machine.

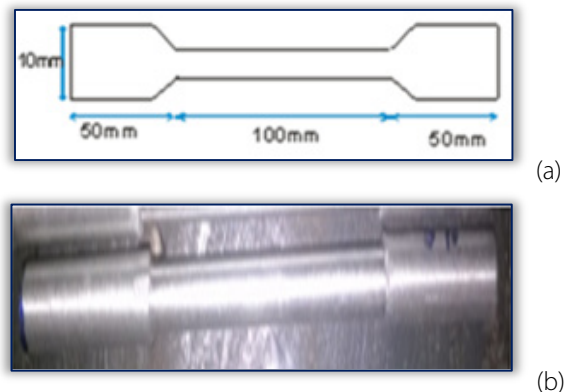


Figure 3. Prepared Samples for Tensile Test (a) Schematic and (b) Sample Piece

Figure 4 shows the impact test workpiece sample. In line with the ASTM E23-16b, the test was carried out on Avery-Denison Izod impact testing machine (model: 6705U/33122). The samples were prepared with gauge length of 55mm, diameter of 10mm, and notch depth and angle of mm and 45° respectively machined from the cast aluminium composites.

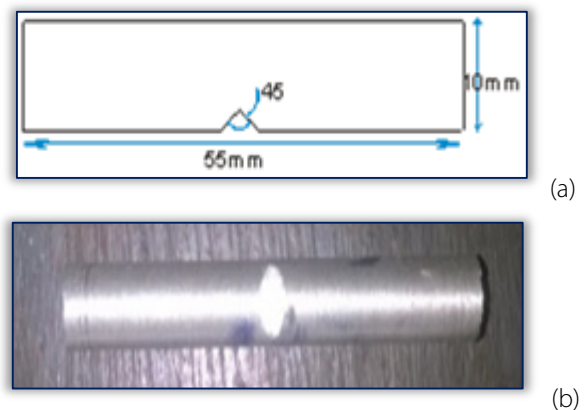


Figure 4. Sample for Izod Impact Test (a) Schematic and (b) Sample piece

≡ Hardness Test

The permanent depth of indentation was carried out on 30 mm height samples (Figure 5) cut out of the as-cast aluminium composite for hardness test according to ASTM B647-10. The sample surfaces were prepared by grinding on emery paper of 400 grits thereafter polished to obtain flat and smooth surface before setting the samples on Rockwell hardness machine of model MCT-381DS. Average of three readings was taken for each sample.



Figure 5. One of the Prepared Samples with Indentations

## RESULTS AND DISCUSSIONS

### ≡ Tensile Test

Figure 6 shows the variation of tensile strength of the composites with different weight fractions of date seeds particles. It can be noted that the stress at upper yield increased with increase in the weight percentage of date seeds particles. Therefore the date seeds particles act as barriers to the dislocations when taking up the load applied (Basavarajappa, Chandramohan et al. 2004). The date seed particles obstruct the advancing dislocation front, thereby strengthening the matrix (Anilkumar, H.S. et al. 2010). Also, as the size of the date seeds particles increased, there was increase in tensile strength. Poor bonding of smaller size date seeds particles with the matrix could be the reason for this behavior. The observed improvement in tensile strength of the composite is attributed to the fact that the filler date seeds particles possess higher strength. The decrease in the tensile strength of the samples with date seeds particles weight fraction beyond 10% is due to the poor wettability of the reinforcement with the matrix.

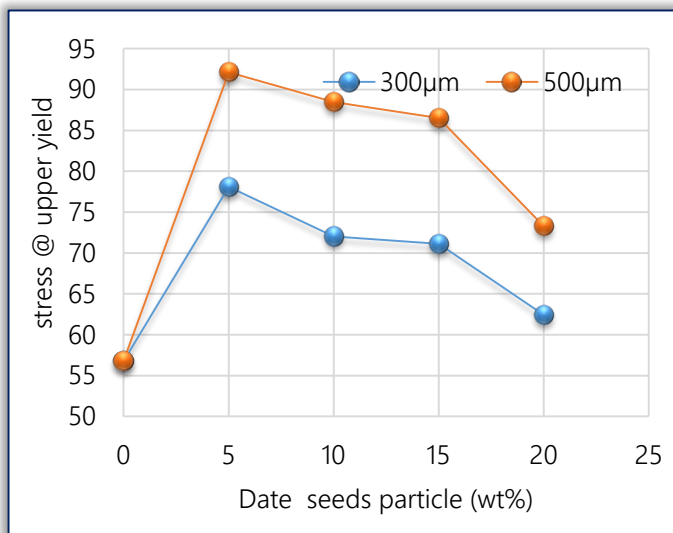


Figure 6. Variation of Tensile Strength with Weight Fraction of Date Seeds Particles

### — Impact Test

The relation between weight fraction of date seeds particles reinforcement and impact energy of cast aluminium alloy composites at different grain sizes of 300µm and 500µm is

shown in Figure 7. The fracture toughness (which is a measure of the composites resistance to crack propagation) was observed to decrease with increase in weight fraction of date seeds particles which is consistent with the trend in most hard particle reinforced metal matrix composites (Saravanan and Senthil 2013). The increased sites (particles, particle/matrix interfaces, and particle clusters) for crack nucleation with increasing weight fraction of the date seed particles were likely to be responsible for this observed trend, similar to the work of (Saravanan and Senthil 2013). Also as it was observed in tensile test result (Figure 6), increase in date seed particles size from 300 to 500 µm (Figure 7) gave a corresponding increase in impact energy of the aluminum composite.

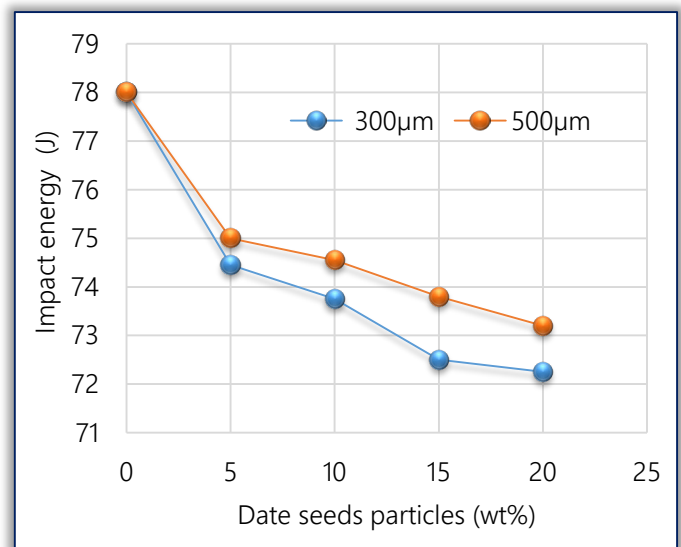


Figure 7. Variation of Impact Energy (J) with Weight Fraction of Date Seeds Particle

### — Hardness

The behaviour of weight percentage of date seeds particles reinforcement on hardness of cast aluminium alloy composites at different grain sizes of 300 and 500 µm is shown in Figure 8.

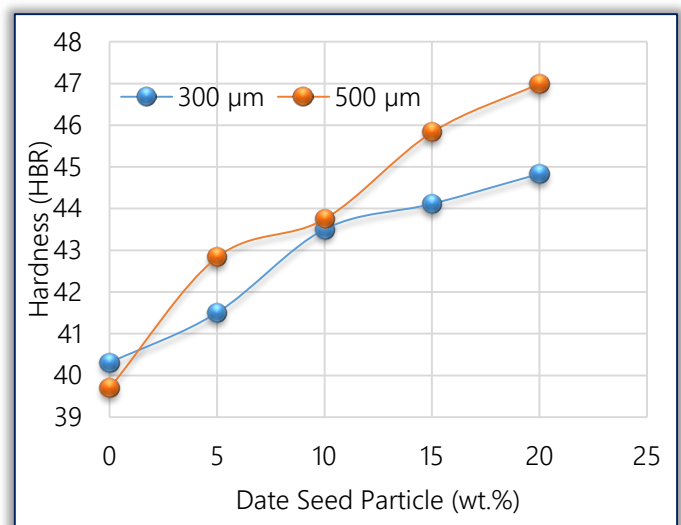


Figure 8. Variation of Hardness with Weight Fraction of Date Seeds Particles

It can be observed that the hardness of the composite increase steadily with increase in weight fraction of the date seeds particles up to 10%wt before the two size particles show a slight reduction in their hardness.

However, the particle size of 500  $\mu\text{m}$  has higher hardness values of 47 HBR as against that of 300 $\mu\text{m}$  particle size that has 44.83 HBR. This hardness behavior occurs due to increases in surface area of the matrix as a result of reduced grain size of the aluminium. Thus the presence of such hard surface area offers more resistance to plastic deformation which leads to increase hardness. Similar finding was reported by Saravanan, et al, 2015; Saravanana and Senthil 2013 and Swamy, et al, 2011 Miracle 2005.

### CONCLUSIONS & FUTURE WORK

The conclusions drawn from the present work can be summarized as follows:

- The date seeds particulate as reinforcement in aluminium alloy composite can be used to improve the mechanical properties of aluminium alloy composite.
- The hardness and tensile strength increase with increase in the weight fraction while the impact strength of the aluminium alloy decrease with increase in the weight fraction of reinforced date seeds particles.
- It can also be concluded that the improvement in the mechanical properties can be accredited to high dislocation density of the material

The following future works have been planned for this research: The effects of heat treatments on the various weight fractions (5, 10, 15 and 20%) of the compositions and the microstructural analysis of the various weight fraction of the compositions

### Acknowledgement

The authors would like to appreciate the following staff of the University for their assistance during the research work. Mr. M. Ndagi of the department of Mechanical Engineering, Mr. O. S. Awojobi of the Department of Materials and Metallurgical Engineering, Mr. Ibraheem Lateef of central workshop and Mr. R.O. Olaoye of the Department of Geology.

### References

[1] Alaa, A. M, Investigation of Tensile and Impact of Composite Materials Reinforced with Natural Materials. *Journal of Engineering and Technology* 33(4): 919-933, 2015.

[2] Ameh, O. A; Isa, T.M and Sanusi, I, "Effect of Particle Size and Concentration on the Mechanical Properties of Polyester Date Palm Seed Particulate Composites." *Journal of Practices and Technologies* (26): 65-78, 2015

[3] American Society for Testing and Materials. *Standard Test Methods for Tension Testing of Metallic Materials*. West Conshohocken, PA, ASTM International 2016.

[4] American Society for Testing and Materials, (2014). *Standard test method for Material Hardness*. ASTM International 2014.

[5] American Society for Testing and Materials, (2014). *Standard test methods for Impact Loading* ASTM International, 2013.

[6] Anilkumar, H. C; Hebbar, H. S and Ravishankar, K. S. *Mechanical Properties of Fly Ash Reinforced Aluminium Alloy (Al6061) Composites*. *International Journal of Mechanical and Materials Engineering* 6 41-45, 2010.

[7] Basavarajappa, S; Chandramohan, G and Dinesh, A. *Mechanical Properties of MMC's- An Experimental Investigation*. *International Symposium of Research on Materials and Engineering*. Madras: 1-8. 2004

[8] Charles, S. and V. P. Arunachalam, V.P, *Property Analysis and Mathematical Modeling of Machining Properties of Aluminium Alloy Hybrid (Al-Alloy/Sic/Flyash) Composites Produced by Liquid Metallurgy and Powder Metallurgy Techniques*. *Indian Journal of Engineering and Materials Science* 11: 473-480, 2004.

[9] Chaudhary, S. P; Singh, P. K; Rai, S; Patel, H and Kumar, B. A *Review on Effect of Reinforcement Particles on the Mechanical Properties of Aluminium Based Composites*. *International Journal of Innovative Research in Science, Engineering and Technology*, 4, (9), 8377-8382, 2015

[10] Karl, U. K. (2006). "Custom-made Materials for Automotive and Aerospace Engineering." *Journal Materials and Manufacturing Processes* 23 (3), 327-335, 2008

[11] Kok, M. *Production and Mechanical Properties Of Al2O3 Particle-Reinforced 2024 Aluminium Alloy Composites*. *Journal of Materials Processing Technology* 161, 381–387, 2003.

[12] Kok, M. and Ozdin, K. *Wear Resistance of Aluminium Alloy and its Composites Reinforced by Al2O3 Particles*. *Journal of Materials Processing Technology* Vol. 183 (2), 301-309, 2006

[13] Manoj, S; Deepak, D; Lakhvir S and Vikas, C. *Development of Aluminium Based Silicon Carbide Particulate Metal Matrix Composite*. *Journal of Minerals and Materials Characterization and Engineering* 8: 455-467, 2009.

[14] Miracle, D. B. *Metal Matrix composites;-From Science to Technological Significance*. *Composites Science and Technology* 65, 2526-2540, 2005.

[15] Mohamed, A. B; Souhail, B; Christophe, B and Hamadi, A. *Chemical Composition and some Functional Properties of Soluble Fibro-Protein Extracts from Tunisian Date Palm Seeds*. *African Journal of Biotechnology* 12(10): 1121-1131, 2013.

[16] Mohammad, Z. H; Mostafa, I. W; Vandita, S. V. S and Mohammad, S. R. *Chemical Composition of Date-Pits and Its Potential for Developing Value-Added Product – a Review*. *Polish Journal of Food Nutrition Science* 64(4), 215–226, 2014.

[17] Ramesh, M; Karthikeyan, T and Kumaravel, A. *Effect of Reinforcement of Natural Residue (Quarry Dust) to Enhance the Properties of Aluminium Metal Matrix Composites*. *Journal of Industrial Pollution Control* 30 (1), 109-116, 2014

[18] Ron, C. and Alcan, B. *Aluminium: Physical Properties, Characteristics and Alloys*, Talat, 2015.

[19] Sameezadeh, M; M. Emamy, M and Farhangi, H. *Effects of particulate reinforcement and heat treatment on the hardness and wear properties of AA 2024-MoSi2 nanocomposites*. *Materials and Design* 32, 2157-2164, 2011

- [20] Saravanan, C; Subramanian, K; Ananda, K; V and Sankara, N., R. Effect of Particulate Reinforced Aluminium Metal Matrix Composite –A Review. Mechanics and Mechanical Engineering, 19, (1), 23–30, 2015
- [21] Saravanana, S. D and Senthil, K. M. Effect of Mechanical Properties on Rice Husk Ash Reinforced Aluminum alloy (AlSi10Mg) Matrix Composites. Procedia Engineering 64, 1505 – 1513, 2013.
- [22] Sato, A and Mehrabian, R. Aluminum Matrix Composites: Fabrication and Properties. Metallurgical Transactions B 7(3): 443-451 1976.
- [23] Souhail, B; Christophe, B; Claude, D; Nour-Eddine, D and Hamadi, A. Date seeds: Chemical Composition and Characteristic Profiles of the Lipid Fraction. Journal of Food Chemistry 84: 577-584, 2004.
- [24] Suraya, S; Shamsuddin, S; Munira, A and Fazilah, A. A. Effect of TiC Particulates on the Microstructure and Mechanical Properties of Aluminium-Based Metal Matrix Composite. Journal of Advanced Materials Research, 903, 145-150, 2014.
- [25] Swamy1, A. R. K; Ramesha, A; Veeresh Kumar, G. B and Prakash, J. N. Effect of Particulate Reinforcements on the Mechanical Properties of Al6061-WC and Al6061-Gr MMCs. Journal of Minerals & Materials Characterization & Engineering, 10 (12), 1141-1152, 2011
- [26] Udomphol, T. Aluminium and its alloys
- [27] [http://www.sut.ac.th/engineering/metal/pdf/Nonferrous/02\\_Aluminium and aluminium alloy.pdf](http://www.sut.ac.th/engineering/metal/pdf/Nonferrous/02_Aluminium%20and%20aluminium%20alloy.pdf) May-Aug 2007, Access on July 19, 2011



ISSN: 2067-3809

copyright © University POLITEHNICA Timisoara,  
Faculty of Engineering Hunedoara,  
5, Revolutiei, 331128, Hunedoara, ROMANIA  
<http://acta.fih.upt.ro>

# DYNAMIC MODELING OF 3 DoF ROBOT MANIPULATOR

<sup>1,2</sup> University of Prishtina / Faculty of Mechanical Engineering, Prishtina, KOSOVO

**Abstract:** Dynamical Modeling of robots is commonly first important step of Modeling, Analysis and Control of robotic systems. This paper is focused on using Denavit-Hartenberg (DH) convention for kinematics and Newton-Euler Formulations for dynamic modeling of 3 DoF - Degree of Freedom of 3D robot. The process of deriving of dynamical model is done using Software Maple. Derived Dynamical Model of 3 Dof robot is converted for Matlab software use for future analysis, control and simulations.

**Keywords:** Modelling, dynamics, robot, analysis

## INTRODUCTION

Dynamics is a huge field of study devoted to studying the forces required to cause motion. The dynamic motion of the manipulator arm in a robotic system is produced by the torques generated by the actuators. This relationship between the input torques and the time rates of change of the robot arm components configurations, represent the dynamic modeling of the robotic system which is concerned with the derivation of the equations of motion of the manipulator as a function of the forces and moments acting on. So, the dynamic modeling of a robot manipulator consists of finding the mapping between the forces exerted on the structures and the joint positions, velocities and accelerations. A good model has to satisfy two conflicting objectives.

A robot manipulator is basically a positioning device. To control the position we must know the dynamic properties of the manipulator in order to know how much force to exert on it to cause it to move: too little force and the manipulator is slow to react; too much force and the arm may crash into objects or oscillate about its desired position.

Deriving the dynamic equations of motion for robots is not a simple task due to the large number of degrees of freedom and nonlinearities present in the system. This part is concerned with the development of the dynamic model for 3 Dof robot and their kinematics and dynamics equations.

## ROBOT STRUCTURE OF 3 DOF AND COORDINATE SYSTEMS

Based on structure of 3 Dof robot (Figure 1), is created Table 1 of Denavit-Hartenberg parameters for 3 DoF robot.

Table 1. Denavit-Hartenberg parameters for 3 DoF robot

Link #	$a_i$	$\alpha_i$	$d_i$	$\theta_i$
1	0	0	$d_1$	$q_1^*$
2	0	$-\beta$	$d_2^*$	0
3	0	0	$L_{3a}$	$q_3^*$

\* Joint variable

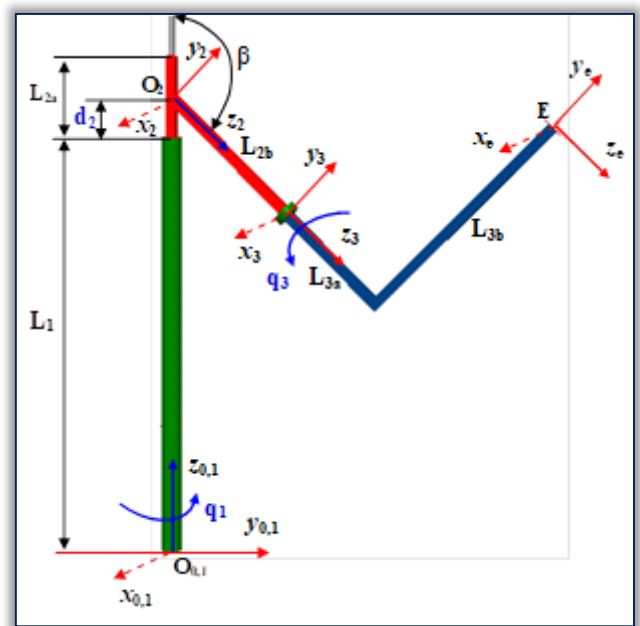


Figure 1. Symbolic representation - Axes rotations for Denavit-Hartenberg parameters

Denavit-Hartenberg transformation matrix for adjacent coordinate frames,  $i$  and  $i - 1$ .

$$A_i = \begin{bmatrix} \cos(\theta_i) & -\cos(\alpha_i) \cdot \sin(\theta_i) & \sin(\alpha_i) \cdot \sin(\theta_i) & a_i \cdot \cos(\theta_i) \\ \sin(\theta_i) & \cos(\alpha_i) \cdot \cos(\theta_i) & -\sin(\alpha_i) \cdot \cos(\theta_i) & a_i \cdot \sin(\theta_i) \\ 0 & \sin(\alpha_i) & \cos(\alpha_i) & d_i \\ 0 & 0 & 0 & 1 \end{bmatrix}$$

Orthogonal rotation matrix  $R_i$  which transforms a vector in the  $i$ -th coordinate frame to a coordinate frame which is parallel to the  $(i-1)$ -th coordinate frame is first 3x3 sub-matrices of  $A_i$ :

$$R_i = \begin{bmatrix} \cos(\theta_i) & -\cos(\alpha_i) \cdot \sin(\theta_i) & \sin(\alpha_i) \cdot \sin(\theta_i) \\ \sin(\theta_i) & \cos(\alpha_i) \cdot \cos(\theta_i) & -\sin(\alpha_i) \cdot \cos(\theta_i) \\ 0 & \sin(\alpha_i) & \cos(\alpha_i) \end{bmatrix}$$

for  $i=1,2, \dots, N$ , where  $R_{N+1} = E = \text{diag}(1)$

## DYNAMIC EQUATIONS – NEWTON-EULER FORMULATION

Dynamics of robot is the study of motion with regard to forces (the study of the relationship between forces/torques and

motion). A dynamic analysis of a manipulator is useful for the following purposes:

- It determines the joint forces and torques required to produce specified end-effector motions (the direct dynamic problem).
- It produces a mathematical model which simulates the motion of the manipulator under various loading conditions (the inverse dynamic problem) and/or control schemes.
- It provides a dynamic model for use in the control of the actual manipulator.

Dynamic modelling of mechanical structures can be a complex problem. In robotics, more specifically, in manipulators, there are two methodologies used for dynamic modelling.

### NEWTON-EULER FORMULATION

The Newton-Euler formulation [1] shown in equations (1)-(9) computes the inverse dynamics (ie., joint torques/forces from joint positions, velocities, and accelerations) bases on two sets of recursions: the forward and backward recursions. The forward recursions (1)-(3) transform the kinematics variables from the base to the end-effector. The initial conditions (for  $i=0$ ) assume that the manipulator is at rest in the gravitational field. The backward recursions (4)-(9) transform the forces and moments from the end-effector to the base, and culminate with the calculation of the joint torques/forces.

Angular velocity of the  $i$ -th coordinate frame

$$\omega_{i+1} = \begin{cases} R_{i+1}^T \cdot \begin{bmatrix} \omega_{i+1} + z_{i+1} \cdot \dot{\theta}_{i+1} \\ \omega_i \end{bmatrix} & \text{if joint is rotational} \\ R_{i+1}^T \cdot \omega_i & \text{if joint is translational} \end{cases} \quad (1)$$

where:  $z_0 = [0 \ 0 \ 1]^T$

Angular acceleration of the  $i$ -th coordinate frame

$$\dot{\omega}_{i+1} = \begin{cases} R_{i+1}^T \cdot \begin{bmatrix} \dot{\omega}_{i+1} + z_{i+1} \cdot \ddot{\theta}_{i+1} + \omega_{i+1} \times (z_{i+1} \cdot \dot{\theta}_{i+1}) \\ \dot{\omega}_i \end{bmatrix} & \text{if joint is rotational} \\ R_{i+1}^T \cdot \dot{\omega}_i & \text{if joint is translational} \end{cases} \quad (2)$$

Linear acceleration of the  $i$ -th coordinate frame

$$\dot{v}_{i+1} = \begin{cases} R_{i+1}^T \cdot \begin{bmatrix} \dot{v}_{i+1} + \omega_{i+1} \times p_{i+1} + \omega_{i+1} \times (\omega_{i+1} \times p_{i+1}) \\ \dot{v}_i \end{bmatrix} & \text{if joint is rotational} \\ R_{i+1}^T \cdot \begin{bmatrix} \dot{v}_{i+1} + z_{i+1} \cdot \ddot{d}_{i+1} + 2\omega_{i+1} \times (z_{i+1} \cdot \dot{d}_{i+1}) \\ \dot{v}_i \end{bmatrix} & \text{if joint is translational} \end{cases} + \begin{bmatrix} \omega_{i+1} \times p_{i+1} \\ \omega_{i+1} \times (\omega_{i+1} \times p_{i+1}) \end{bmatrix} \quad (3)$$

where:  $p_i = [a_i \ d_i \cdot \sin(\alpha_i) \ d_i \cdot \sin(\alpha_i)]^T$  is position of the  $i$ -th coordinate frame with respect to the  $(i - 1)$ -th coordinate frame.

Initial conditions:  $\omega_0 = \dot{\omega}_0 = v_0 = 0$ ; Gravitational

acceleration:  $\dot{v}_0 = [g_x \ g_y \ g_z]^T$ .

Linear acceleration of the center-of-mass of link  $i$

$$a_i = \dot{\omega}_i \times s_i + \omega_i \times (\omega_i \times s_i) + \dot{v}_i \quad (4)$$

where:  $s_i$  is position of center-of-mass of link  $i$

Net force exerted on link  $i$ :

$$F_i = m_i \cdot a_i \quad (5)$$

Net moment exerted on link  $i$

$$N_i = I_i \dot{\omega}_i + \omega_i \times (I_i \cdot \omega_i) \quad (6)$$

where  $I_i = \begin{bmatrix} I_{ixx} & 0 & 0 \\ 0 & I_{iyy} & 0 \\ 0 & 0 & I_{izz} \end{bmatrix}$

$I_i$  is moment of inertia tensor of link  $i$  about the centre-of-mass of link  $i$  (parallel to the  $i$ -th coordinate frame), with only principal inertias  $I_{ixx}$ ,  $I_{iyy}$  and  $I_{izz}$ . Because of symmetry of link frames, cross-inertias can be used zero.

Force exerted on link  $i$  by link  $i - 1$ :

$$f_i = R_{i+1}^T \cdot f_{i+1} + F_i \quad (7)$$

Moment exerted on link  $i$  by link  $i - 1$

$$n_i = R_{i+1}^T \cdot n_{i+1} + p_i \times f_i + N_i + s_i \times F_i \quad (8)$$

Joint torque/force at joint  $i$ :

$$\tau_i = \begin{cases} n_i \cdot (R_{i+1}^T \cdot z_{i+1}) & \text{if joint is rotational} \\ f_i \cdot (R_{i+1}^T \cdot z_{i+1}) & \text{if joint is translational} \end{cases} \quad (9)$$

### DERIVING OF DYNAMICAL MODEL FOR 3 DOF ROBOT

Based on Newton-Euler formulation (1-9), rotation matrices for links of robot ( $i=1,2,3$ ) are:



$$R_1 = \begin{bmatrix} \cos(q_1) & -\sin(q_1) & 0 \\ \sin(q_1) & \cos(q_1) & 0 \\ 0 & 0 & 1 \end{bmatrix}$$

$$R_2 = \begin{bmatrix} 1 & 0 & 0 \\ 0 & \cos(\beta) & \sin(\beta) \\ 0 & -\sin(\beta) & \cos(\beta) \end{bmatrix}$$

$$R_3 = \begin{bmatrix} \cos(q_3) & -\sin(q_3) & 0 \\ \sin(q_3) & \cos(q_3) & 0 \\ 0 & 0 & 1 \end{bmatrix}$$

Initial conditions are:

$$z_0 = \begin{bmatrix} 0 \\ 0 \\ 1 \end{bmatrix}, \omega_0 = \begin{bmatrix} 0 \\ 0 \\ 0 \end{bmatrix}, \dot{\omega}_0 = \begin{bmatrix} 0 \\ 0 \\ 0 \end{bmatrix}, v_0 = \begin{bmatrix} 0 \\ 0 \\ 0 \end{bmatrix}, \dot{v}_0 = \begin{bmatrix} 0 \\ 0 \\ 0 \end{bmatrix}$$

Forward recursions, for 3 DoF robot, (i=1,2,3).

Angular velocity of the i-th coordinate frame:

$$\omega_1 = R_1^T \cdot (\omega_0 + z_0 \cdot \dot{q}_1)$$

$$\omega_2 = R_2^T \cdot \omega_1$$

$$\omega_3 = R_3^T \cdot (\omega_2 + z_0 \cdot \dot{q}_3)$$

Angular acceleration of the i-th coordinate frame:

$$\dot{\omega}_1 = R_1^T \cdot (\dot{\omega}_0 + z_0 \cdot \ddot{q}_1) + \omega_0 \times z_0 \cdot \dot{q}_1$$

$$\dot{\omega}_2 = R_2^T \cdot \dot{\omega}_1$$

$$\dot{\omega}_3 = R_3^T \cdot (\dot{\omega}_2 + z_0 \cdot \ddot{q}_3) + \omega_2 \times z_0 \cdot \dot{q}_3$$

Position of the i-th coordinate frame with respect to the (i-1)-th coordinate frame:

$$p_1 = \begin{bmatrix} 0 \\ 0 \\ L_1 \end{bmatrix}, p_2 = \begin{bmatrix} 0 \\ 0 \\ d_2 \end{bmatrix}, p_3 = \begin{bmatrix} 0 \\ 0 \\ L_{2b} \end{bmatrix}$$

Linear acceleration of the i-th coordinate frame:

$$\dot{v}_1 = R_1^T \cdot \dot{v}_0 + \dot{\omega}_1 \times p_1 + \omega_1 \times (\omega_1 \times p_1)$$

$$\dot{v}_2 = R_2^T \cdot \dot{v}_1 + z_0 \cdot \dot{q}_2 + (2\dot{\omega}_1 \times z_0 \cdot \dot{q}_2) + (\omega_1 \times p_1)$$

$$\dot{v}_3 = R_3^T \cdot \dot{v}_2 + \dot{\omega}_3 \times p_3 + \omega_3 \times (\omega_3 \times p_3)$$

Linear acceleration of the center-of-mass of link i:

$$\dot{a}_1 = \dot{\omega}_1 \times s_1 + \omega_1 \times (\omega_1 \times s_1) + \dot{v}_1$$

$$\dot{a}_2 = \dot{\omega}_2 \times s_2 + \omega_2 \times (\omega_2 \times s_2) + \dot{v}_2$$

$$\dot{a}_3 = \dot{\omega}_3 \times s_3 + \omega_3 \times (\omega_3 \times s_3) + \dot{v}_3$$

Moment of inertia tensor of link i about the center of mass of link i (parallel to the i-th coordinate frame), with only principal inertias  $I_{ixx}$ ,  $I_{yy}$  and  $I_{zz}$ . Because of symmetry of link frames, cross-inertias are used zero.

$$I_1 = \begin{bmatrix} I_{1xx} & 0 & 0 \\ 0 & I_{1yy} & 0 \\ 0 & 0 & I_{1zz} \end{bmatrix}, I_2 = \begin{bmatrix} I_{2xx} & 0 & 0 \\ 0 & I_{2yy} & 0 \\ 0 & 0 & I_{2zz} \end{bmatrix},$$

$$I_3 = \begin{bmatrix} I_{3xx} & 0 & 0 \\ 0 & I_{3yy} & 0 \\ 0 & 0 & I_{3zz} \end{bmatrix}$$

Net force and moment exerted on link i = 1,2,3:

$$F_1 = m_1 \cdot \dot{a}_1$$

$$F_2 = m_2 \cdot \dot{a}_2$$

$$F_3 = m_3 \cdot \dot{a}_3$$

$$N_1 = I_1 \cdot \dot{\omega}_1 + (\dot{\omega}_1 \times I_1 \cdot \dot{\omega}_1)$$

$$N_2 = I_2 \cdot \dot{\omega}_2 + (\dot{\omega}_2 \times I_2 \cdot \dot{\omega}_2)$$

$$N_3 = I_3 \cdot \dot{\omega}_3 + (\dot{\omega}_3 \times I_3 \cdot \dot{\omega}_3)$$

Backward recursion (i=3,2,1); Force and moment exerted on link i by link i-1.

By supposing that there are no outside load for end-effector are:

$$f_4 = \begin{bmatrix} 0 \\ 0 \\ 0 \end{bmatrix}, n_4 = \begin{bmatrix} 0 \\ 0 \\ 0 \end{bmatrix}, R_4 = \begin{bmatrix} 1 & 0 & 0 \\ 0 & 1 & 0 \\ 0 & 0 & 1 \end{bmatrix}$$

For link #3:

$$f_3 = R_4 \cdot f_4 + F_3$$

$$n_3 = R_4 \cdot n_4 + p_3 \times f_3 + N_3 + s_3 \times F_3$$

Torque at joint 3:

$$\tau_3 = n_3^T \cdot (R_3 \cdot z_0)$$

For link #2:

$$f_2 = R_3 \cdot f_3 + F_2$$

$$n_2 = R_3 \cdot n_3 + p_2 \times f_2 + N_2 + s_2 \times F_2$$

Force at joint 2:

$$\tau_2 = f_2^T \cdot (R_2 \cdot z_0)$$

For link #1:

$$f_1 = R_2 \cdot f_2 + F_1$$

$$n_1 = R_2 \cdot n_2 + p_1 \times f_1 + N_1 + s_1 \times F_1$$

Torque at joint 1:

$$\tau_1 = n_1^T \cdot (R_1 \cdot z_0)$$

In the end the vector of Forces-Torques for 3 DoF robot is:

$$\tau = \begin{bmatrix} \tau_1 \\ \tau_2 \\ \tau_3 \end{bmatrix}$$

Modeling-Calculations of 3 DoF robot is done using Maple software, equations are converted for Matlab use.

## CONCLUSION

Based on presented paper can be concluded that Newton-Euler formulation is very useful for dynamical modeling of systems generally and robotic systems especially.

Use of Maple software is very useful for modelling of complex systems and representations of results symbolically –

representation of expressions of dynamical model with many characters (until 100000).

Opportunity of Maple software to convert derived expressions for Matlab use is very helpful for future analyses and simulations of systems.

#### Acknowledgements

The first author is profoundly thankful to the corresponding author Rame Likaj (email: rame.likaj@uni-pr.edu) which has paid attention to fulfill all requirements about this research work.

#### References

- [1] Luh, J. Y. S., Walker, M. W. and Paul, R. P.; On-Line Computational Scheme for Mechanical Manipulators. Journal of Dynamic Systems, Measurement, and Control 102(2):69-76, June, 1980.
- [2] Brady, M., et al. (editors). Robot Motion: Planning and Control. MIT Press, Cambridge, MA, 1982.
- [3] Khosla, Pradeep, "Estimation of Robot Dynamics Parameters: Theory and Application". Institute for Software Research. Paper 651. <http://repository.cmu.edu/isr/651>, Carnegie Mellon University, 1987.
- [4] A. Shala, R. Likaj; Design of Genetic Algorithm for optimization of Fuzzy Neural Network Controller, 8th International Conference Modern Technologies in Manufacturing, Cluj-Napoca, Romania, 2007.
- [5] H.J. Sommer: Vector loops facilitate simple kinematic analysis of planar mechanisms, either closed-chain or open-chain, Mechanical & Nuclear Engineering Faculty, USA, [www.mne.psu.edu/sommer/me50/](http://www.mne.psu.edu/sommer/me50/)
- [6] J. M. McCarthy and G. S. Soh, 2010, Geometric Design of Linkages, Springer, New York.
- [7] B. Paul, Kinematics and Dynamics of Planar Machinery, Prentice-Hall, NJ, 1979
- [8] L. W. Tsai, Robot Analysis: The mechanics of serial and parallel manipulators, John-Wiley, NY, 1999.
- [9] K. J. Waldron and G. L. Kinzel, Kinematics and Dynamics, and Design of Machinery, 2nd Ed., John Wiley and Sons, 2004.
- [10] Torby, Bruce (1984). "Energy Methods". Advanced Dynamics for Engineers. HRW Series in Mechanical Engineering. United States of America: CBS College Publishing. ISBN 0-03-063366-4.



ISSN: 2067-3809

copyright © University POLITEHNICA Timisoara,  
Faculty of Engineering Hunedoara,  
5, Revolutiei, 331128, Hunedoara, ROMANIA  
<http://acta.fih.upt.ro>

<sup>1</sup>Zorica DJORDJEVIĆ, <sup>2</sup>Saša JOVANOVIĆ, <sup>3</sup>Milan STANOJEVIĆ, <sup>4</sup>Mirko BLAGOJEVIĆ, <sup>5</sup>Sandra VELIČKOVIĆ

## OPTIMIZATION OF FIBER ORIENTATION ANGLE OF A HYBRID Al / COMPOSITE CARDAN SHAFT

<sup>1,2,4,5</sup>University of Kragujevac, Faculty of Engineering Kragujevac, SERBIA

<sup>3</sup>FCA Serbia d.o.o., Kragujevac, SERBIA

**Abstract:** One important property of composite materials is the possibility to change their characteristics by changing the fiber orientation angle. By determining the optimal fiber orientation, the resistance to the torque effect, as well as the value of the critical rotational speed, can significantly be increased. In this paper, using the finite element method, we have examined the effects of fiber orientation angle on the basic static and dynamic characteristics of the shaft (twist angles, natural frequency). The shaft is composed of a combination of aluminum and composite layers of carbon and aramid fibers. In the conclusion section of the paper, optimal variants of the shaft have been identified.

**Keywords:** shaft, twist angles, natural frequency, aramid fiber, carbon fiber

### INTRODUCTION

The modern development of technology and industry calls for more rigid requirements in terms of characteristics of materials used for manufacturing of various mechanical elements and constructions. For the purpose of getting better mechanical characteristics of certain products, over the last decades, there has been a growing tendency for using artificial materials. The advantage of composites as artificial materials over conventional materials is in the fact that in their case the best characteristics of materials they are made of are used. Composite materials are the ones in which it is possible to optimize the mechanical features, machining and forming abilities, environmental effect, material and production costs, since they are made by combining two or more materials with complementary characteristics.

Resistant and fiber-reinforced composite materials of high rigidity and relatively low specific weight are convenient for manufacturing of shafts. Composite shafts, when compared to steel shafts, are attributed with less mass, less value of tension and deformation, extremely harmonic absorption of vibrations and higher values of its own frequencies.

Numerous studies have dealt with optimal design of cardan shafts as well as with types of materials shafts are made of and of course with fiber orientation. The paper [1] presents an experimental and simulation studies to investigate the behaviour of composite hollow shafts, with a specific focus on the maximum torsion capacity of the composite hollow shaft for different winding angles. The maximum static torsion capacity of kenaf yarn fibre reinforces unsaturated polyester composite shaft at a winding angle of 45° was higher strength than 90° orientation.

In paper [2] examines the effect of fiber orientation angles and stacking sequence on the torsional stiffness, natural frequency, buckling strength, fatigue life and failure modes of composite tubes. FEA results showed that the natural

frequency increases with decreasing fiber orientation angles. On the other hand, the critical buckling torque has a peak value at 90° and lowest at a range of 20–40° when the angle of one or two layers in a hybrid or all layers in non-hybrid changed similarly.

In this study [3], a finite element analysis was used to design composite drive shafts incorporating carbon and glass fibers within an epoxy matrix. The results show that, in changing carbon fibers winding angle from 0° to 90°, the loss in the natural frequency of the shaft is 44.5%, while, shifting from the best to the worst stacking sequence, the drive shaft causes a loss of 46.07% in its buckling strength, which represents the major concern over shear strength in drive shaft design.

A hybrid aluminum/composite is an advanced composite material that consists of aluminum tube wound onto outside by layers of composite material. This paper [4] investigates the maximum torsion capacity of the hybrid aluminum/composite shaft for different winding angle, number of layers and stacking sequences. The hybrid shaft consists of aluminum tube wound outside by E-glass and carbon fibers/epoxy composite. The results show that the static torque capacity is significantly affected by changing the winding angle, stacking sequences and number of layers.

### DESIGN PROCEDURE

The lamina is thin it is considered as the plane stress problem. Hence, it is possible to reduce the 3-D problem into 2-D problem. For unidirectional 2-D lamina, the stress-strain relationship in terms of physical material direction is given by [3]:

$$\begin{Bmatrix} \sigma_1 \\ \sigma_2 \\ \tau_{12} \end{Bmatrix} = \begin{bmatrix} Q_{11} & Q_{12} & 0 \\ Q_{12} & Q_{22} & 0 \\ 0 & 0 & Q_{66} \end{bmatrix} \begin{Bmatrix} \epsilon_1 \\ \epsilon_2 \\ \gamma_{12} \end{Bmatrix}. \quad (1)$$

The matrix [Q] is referred as the reduced stiffness matrix for the layer and its terms are given by:

$$\begin{aligned} Q_{11} &= \frac{E_{11}}{1 - \nu_{12}\nu_{21}}; & Q_{12} &= \frac{\nu_{12}E_{22}}{1 - \nu_{12}\nu_{21}} \\ Q_{22} &= \frac{E_{22}}{1 - \nu_{12}\nu_{21}}; & Q_{66} &= G_{12} \end{aligned} \quad (2)$$

where: E is modulus of elasticity, G is modulus of rigidity and  $\nu$  is Poisson's ratio.

In Descartes rectangular coordinate system x-y-z (x-axis is the axial shaft axis), whereas the angle of fibers is measured in reference to the positive direction of x-axis, the relation between tension and deformation may be presented as follows:

$$\begin{Bmatrix} \sigma_x \\ \sigma_y \\ \tau_{xy} \end{Bmatrix} = \begin{bmatrix} \bar{Q}_{11} & \bar{Q}_{12} & \bar{Q}_{16} \\ \bar{Q}_{12} & \bar{Q}_{22} & \bar{Q}_{26} \\ \bar{Q}_{16} & \bar{Q}_{26} & \bar{Q}_{66} \end{bmatrix} \begin{Bmatrix} \varepsilon_x \\ \varepsilon_y \\ \gamma_{xy} \end{Bmatrix}. \quad (3)$$

The lowest natural frequency expression is given as:

$$f_n = \frac{\pi}{2} \sqrt{\frac{gE_x I}{WL^4}}. \quad (4)$$

where g is the acceleration due to gravity, W is the weight per unit length, L is the shaft length and I is the second moment of inertia given, for a thin-walled tube, as:

$$I = \frac{\pi}{4} (r_0^4 - r_i^4) \approx \pi r^3 t. \quad (5)$$

here,  $r_0$  is an outer radius, and  $r_i$  is an inner radius.

#### FINITE ELEMENT ANALYSIS COMPOSITE CARDAN SHAFT

This paper analyses a real shaft of the truck TURBO ZETA 85.14B, which is not made of steel, but of aluminium/composite material [5]. Two different types of composite materials were used: carbon fibre/epoxy resin and aramid fibre/epoxy resin. Table 1 shows the basic properties of these composite materials.

Table 1. Basic properties of composite materials

Material	$E_1$ , GPa	$E_2$ , GPa	$G_{23}$ , GPa	$G_{12}$ , GPa	$\nu$	$\rho$ , kg/m <sup>3</sup>	$t_{ply}$ , mm
Carbon fibres/epoxy composite	131.6	8.20	3.5	4.5	0.281	1550	0.125
Aramid fibres/epoxy composite	81.8	5.10	1.82	1.51	0.31	1380	0.125

In Table 1, the following notation are used:  $E_1$ - longitudinal modulus;  $E_2$  – transverse modulus;  $G_{12}$ ,  $G_{23}$  – shear modulus;  $\nu$  – Poisson's ratio;  $\rho$  – density;  $t_{ply}$  – composite layer thickness.

The basic dimensions of the analyzed shaft [5] are: shaft length 1.35 m, mean radius of the shaft 0.041 m, wall thickness of the ring shaped cross section of the shaft 0,003 m. The shaft was tested under the action of maximum value of the static torsion moment of 5000 Nm.

The analyzed shaft was modelled by linear isoparametric square shell finite elements. The model of the analyzed shaft can be seen in Figure 1. In the numerical analysis, the shaft is

fixed at one end while the other is free and under the effect of the torque. The NX Nastran software was used for the analysis. The composite part of the shaft consists of 8 layers (carbon fibers/epoxy resin and aramid fibers/epoxy resin).

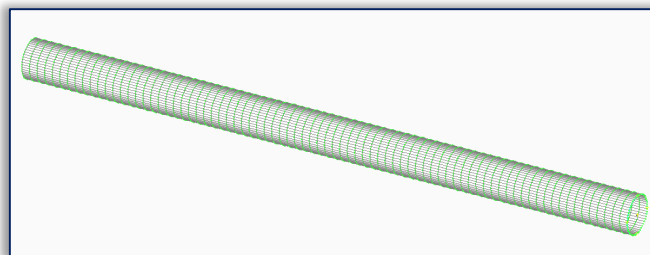


Figure 1. Finite element model of the aluminium/composite shaft

Values of shaft torsion angles resulting from numerical calculation for both analyzed composite materials (carbon and aramide), at different values of fiber orientation angles, are indicated in Figure 2.

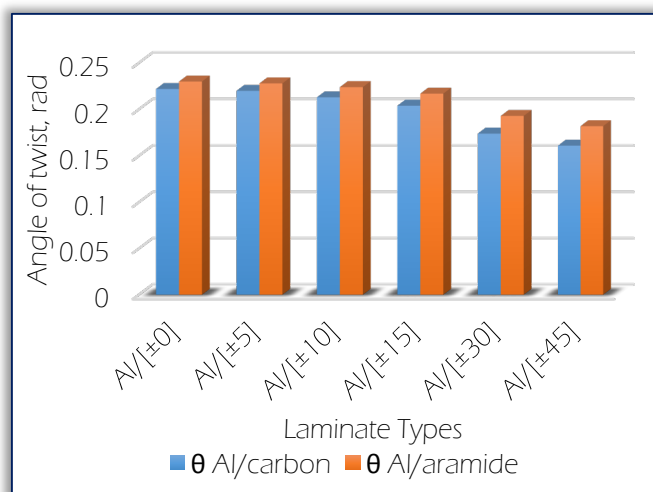


Figure 2. Influence of fiber angle orientation to torsion angle value for hybrid Al/carbon and Al/aramide shafts

As indicated in Figure no. 2 the values of torsion angles are somewhat lower in case of carbon versus aramide fibres. Also, one may see that in case of both materials, the highest values of shaft torsion angles are at fibre orientation angle of 0°, and the lowest with fiber orientation of ±45°.

By using NX Nastran software, the numerical values of natural frequencies of hybrid Al/carbon and Al/aramide shafts have been determined. On grounds of acquired values of natural frequencies  $f_s$ , in the first oscillation critical numbers of rotations of analyzed shafts may be set applying the following expression:

$$n_{kr} = 60 \cdot f_s. \quad (6)$$

It is well known that the values of natural frequencies depend on ratio  $E_1/\rho$ . In case of composite materials, that ratio varies and depends on fiber orientation. The ratio has the maximum value for the fiber angle of 0°, and it decreases as the orientation angles of fibers increase. In reference to that, Figure no. 3 shows that in case of carbon and aramide fibers of natural frequency, the critical number of shaft rotations have the highest value at angle of 0°, whereas the value drops

down with fiber orientation angle getting closer to  $\pm 45^\circ$ . Also, Figure 3 indicates that carbon fibers show significantly better results (higher values of critical number of rotations) than aramide fibers.

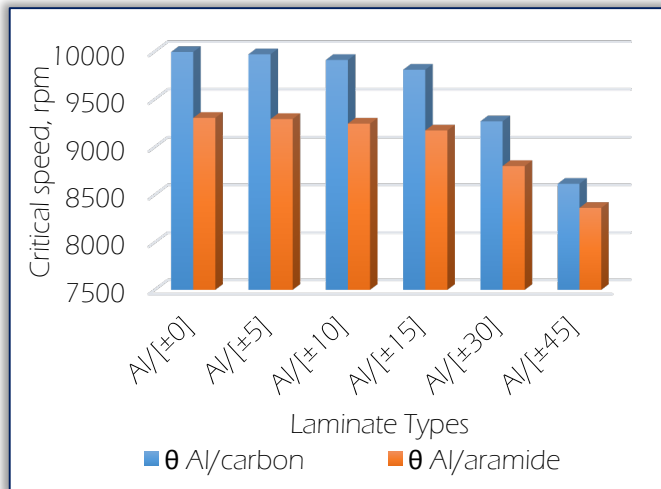


Figure 3. Influence of fiber orientation angle upon values of critical number of rotations for hybrid Al/carbon and Al/aramide shafts

### CONCLUSION

In this paper we have analyzed the relation between types of fiber and fiber orientation angles on one side and parameters such as shaft torsion angle and critical number of rotations on the other. The results show that orientation of fibers has a significant influence upon statistical and dynamic shaft characteristics.

By way of analyzing shaft torsion angles, we got the best results for hybrid Al/carbon shafts with fiber orientation angle of  $\pm 45^\circ$ . For getting the highest possible values of critical number of rotations, carbon fibers with the least possible angles of fiber orientation should be used.

Finding the optimal orientation of fibers helps in discovering the optimal design of composite shaft which would result also in reduction of production costs.

### Acknowledgement

This investigation is a part of the project TR 33015 of Technological Development of the Republic of Serbia and the project III 42006 of Integral and Interdisciplinary investigations of the Republic of Serbia. We would like to thank to the Ministry of Education and Science of Republic of Serbia for the financial support during this investigation.

### Note

This paper is based on the paper presented at 13th International Conference on Accomplishments in Mechanical and Industrial Engineering – DEMI 2017, organized by University of Banja Luka, Faculty of Mechanical Engineering, in Banja Luka, BOSNIA & HERZEGOVINA, 26 - 27 May 2017.

### References

[1] Misri, S., Sapuan, S.M., Leman, Z., Ishak, M.R. (2015). Torsional behaviour of filament wound kenaf yarn fibre reinforced unsaturated polyester composite hollow shafts. *Materials and Design*, vol. 65, p. 953-960.

- [2] Badie, M.A., Mahdi, E., Hamouda, A.M.S. (2011). An investigation into hybrid carbon/glass fiber reinforced epoxy composite automotive drive shaft. *Materials and Design*, vol. 32, p. 1485-1500.
- [3] Abu Talib, A.R., Ali, A., Badie, M.A., Nur Azida C.L., Golestaneh A.F. (2010). Developing a hybrid, carbon/glass fiber-reinforced, epoxy composite automotive drive shaft. *Materials and Design*, vol. 31, p. 514-521.
- [4] Mutasher, S.A. (2009). Prediction of the torsional strength of the hybrid aluminum/composite drive shaft. *Materials and Design*, vol. 30, p. 215-220.
- [5] Djordjevic, Z. (2008) Dynamic conduct composite shafts, PhD Thesis, Faculty of Mechanical Engineering, Kragujevac, Serbia.



ISSN: 2067-3809

copyright © University POLITEHNICA Timisoara,  
Faculty of Engineering Hunedoara,  
5, Revolutiei, 331128, Hunedoara, ROMANIA  
<http://acta.fih.upt.ro>

# Fascicule 2

## [ April - June ]

### t o m e

# [2018] XI

**ACTA**Technica**CORVINIENSIS**  
BULLETIN OF ENGINEERING



**ISSN: 2067-3809**

copyright © University POLITEHNICA Timisoara,  
Faculty of Engineering Hunedoara,  
5, Revolutiei, 331128, Hunedoara, ROMANIA  
<http://acta.fih.upt.ro>

<sup>1</sup>B. O. AKINNULI, <sup>2</sup>S. P. AYODEJI, <sup>3</sup>O.O. OJO

# RECLAMATION OF BASE OIL FROM OIL WELLS DRILL CUTTINGS AND ITS DISPOSAL ECOLOGICAL HAZARD CONTROL

<sup>1,2,3</sup>Department of Mechanical Engineering, Federal University of Technology, Akure, Ondo State, NIGERIA

**Abstract:** The discharge of oil-based drill cuttings to open sea has been adjudged to cause acute and sub-lethal toxic effects such as smothering of seabed life (due to the formation of cuttings piles), poisoning of aquatic life (due to the presence of toxins), and eventual ecological disruption/eco-toxicological disturbances of offshore environment. Equally, oil based drilling fluids are desirable for drilling explorations but they are generally expensive; as a result, their recovery from drill cuttings has the outlook of offering economic benefit to oil and gas industries. In order to circumvent the possible dangers of drill cuttings and to recover oil based drilling fluid for reuse purposes, the treatment of oil-contaminated drill cuttings becomes indispensable. Thermal desorption facility of Warri Refinery in Delta State, Nigeria was employed for this study. Drill cuttings are removed by circulating the drilling fluid over mechanically controlled equipment such as shale shakers, high speed centrifuge, vortex dryers and thermal desorption system. The composition analysis of materials after treatment reveals 80% solids and 10% recovered base oil which is of high economic value. The Thermal Desorption Unit (TDU) process recovers between 10-12 m<sup>3</sup> of oil in every treated 100 tons of oily cuttings.

**Keywords:** investigation, reclamation, oil base cuttings, composition analysis, hazard control

## INTRODUCTION

The Delta Basin of Nigeria is significantly rich in paraffinic and low sulphur crude oil; and this has encouraged oil explorations in the deepwater and continental shelves of low Niger parts (Niger-Delta expanses) of Nigeria. As a result, petroleum hazardous wastes come with the oil exploration activities in this region. However, drilling operations have been adjudged as the major source of these wastes. Apart from produced water, drill cuttings represent the greatest amount of discharges from petroleum related drilling activities [1].

As it is well known, oil and gas explorations and drilling operations require the use of drilling fluids as the drill bit is advanced to the preferred earth depth. This is to facilitate proper cutting process. Thus, when the fluid is introduced through the drill string and injected under high pressure through nozzles at the drill bit, it cools and lubricates the drill bit, maintains hydrostatic pressure on the formation and stabilizes the borehole wall [2]. As the drill bit rotates and advances into the formation, small pieces of rock are broken off and they are then flushed from the borehole along the annulus between the drill string and borehole wall. Drilled muds which are viscous and complex formulation are ejected out of the borehole as well. The ejected mud includes finely divided materials such as ground ilmenite, bentonite, various clays, barite, lead ore, fibers, hulls and others in a liquid medium which may be aqueous (water or brine) or an oil (diesel oil) [3].

In general, three types of mud are currently used or produced during drilling operations; they include oil-based mud (OBM), this is primarily composed of diesel oil or mineral oil and additives; water based mud (OBM) which consists of base salt

water or fresh water containing additives; and the third is synthetic-based mud (SM) which has oil-like base materials [4]. The water-based muds are not able to perform in high temperature conditions. Synthetic-based muds generally perform better than water-based muds but less than oil-based muds. Oil-based muds are well suited for high temperature conditions because oil-based muds are paraffinic in nature with a relatively high boiling range [5, 6]. At the earth's surface, the drill cuttings are separated from the drilled mud through the use of various mechanical solids control equipment such as shakers, high speed decanter or centrifugal mud cleaners and vortex dryer [7]. As a result, the separated drill cuttings consist of mixtures of base oil, pulverised material, speciality chemicals, sediment and reservoir/basin rock fragments [8] [9] [10] [11]. In addition, hydrocarbons and higher concentration of metals such as Ba, Cr, Cu, Ni, Pb, and Zn [9] are major constituents of the drill cuttings. Therefore, there is a need to decontaminate the cuttings and recover base oil from them.

However, oil-based drill cuttings (OBDC) are hazardous solid wastes generated from drilling operations [12].

The deposition of solid drill cuttings forms hydrocarbon contaminated cuttings piles (distinct anthropogenic legacy) underneath hundreds of oil platforms/sea beds as a result of oil exploration and production activities [10] [13]. This occurrence smothers seabed life and most importantly reduction in oxygen and anoxia development within the sediment piles occur due to microbial mediated diagenetic reactions in organic-rich cutting piles [10].

Likewise, drill cuttings initiated weaker faunal response in the works of Hilde et al. [14] while Hilde et al. [15] investigated the role of physical disturbance in effects of water-based drill

cuttings on benthic ecosystems. It was revealed that drill cuttings caused significant reduction in the number of taxa, abundance, biomass and diversity of macrofauna. Katsiaryna et al. [16] conducted laboratory investigation on phytoplankton aggregates and it was observed that drill cuttings significantly affected the physical characteristics of phytodetritus.

These drilling waste/cuttings must be treated because it cannot be discharged directly into a disposal site, not only because of their adverse effect upon the environment, but additionally because of the great value of oil contained in them. It has been a common practice to treat the oil drill cuttings in order to produce a solid material that can be disposed into the environment without injury to it.

Few works have been carried out on the treatment of drill cuttings. Marina et al. [17] carried out microwave radiation treatment of drill cuttings contaminated with synthetic drilling fluid. It was reported that n-paraffin was successfully removed from the contaminated cuttings. Likewise, Robinson et al. [18] reported that drill cuttings can be efficiently microwave-treated under optimized conditions. Robinson et al. [19] revealed that higher microwave power and electric field strength influenced the mechanism of oil removal from drill cuttings. However, total decontamination of oil from the cuttings was achieved during microwave dry remediation of oil contaminated drill cuttings by Irineu et al. [20].

On the other hand, Reginald et al. [21] worked on the stabilization/solidification of drill cuttings for forage production (elephant grass) in acidic soils. The stabilized/solidified drill cuttings were observed to improve the height and leaf lengths of the forage.

Also, supercritical water oxidation of oil-based drill cuttings is also another approach of treating contaminated drill cuttings [12]. Chaillan et al. [22] revealed that the efficiency of bioremediation process of contaminated soil with drill cuttings is dependent on the inherent degradability of HC compounds. However, remediation of oil-based drill cuttings through a biosurfactant-based washing and biodegradation treatment was achieved by Ping et al. [23].

Basically, thermal/mechanical technologies are preferred and used to ensure proper treatment and recovery of base oil from drill cuttings. Although, there are other technologies involving chemical processing as highlighted above but thermal/mechanical processing has proven to be the best over time. Thermal technologies use high temperature to reclaim or destroy hydrocarbon-contaminated drill cuttings. It is the most efficient treatment for destroying organics, and it also reduces the volume and mobility of inorganics such as metals and salt [24].

Thermal treatment can be an interim process to reduce toxicity and volume and prepare a waste stream for further treatment or disposal (such as landfill, land farming and land spreading), or it can be final treatment process resulting in inert solids, water and recovered base oil; the latter is the case with drill cuttings [25]. The thermal treatment technology is

usually set up in a fixed land based installation, but can be made to be mobile to fit uses in an offshore rig platform if necessary but nonetheless large size and weight coupled with limited processing capacity have limited its use off shore. The cost for thermal treatment ranges from \$75 to \$150/ ton, with labor being a large component [26]. George and Smith [27] grouped thermal treatment technologies into two. The first group uses incineration (such as rotary kilns, and cement kilns) to destroy hydrocarbons by heating them to very high temperatures in the presence of air. Incineration is not commonly used for drilling cuttings because there is literally no good recovery for the base oil. The second uses the thermal desorption principle, in which heat is applied directly or indirectly to the drill cuttings to vaporize, volatile and semi volatile components (base oil, water) without incinerating the oil.

In some thermal desorption technologies the off-gases are combusted but in the case of drill cuttings where the base oil has to be recovered, the thermal phase is separated to recover the hydrocarbon (base oil) [28]. Pierce and Wood [29] and Ritter [30] state that the attachments of thermal desorption technologies include direct/indirect rotary kilns and hot oil processors, thermal phase separation, thermal plasma volatilization, and modular thermal processors. In the case of drill cuttings treatment, thermal phase separation is the type of thermal desorption unit used.

The treatment of drill cuttings with thermal desorption unit has both economic and ecological benefits. For instance, thermal desorption process will facilitate the protection of the environment from hazardous oil-base drill cutting deposition and the recovery of water which can be retreated and put to use especially in arid regions. Similarly, the recovered soil with an oil residue of less than 0.5% can be sold to construction companies and used for road construction and building of houses or used for land filling and land spreading. Consequently, this paper examines the thermal desorption processing of drill cuttings obtained from the Delta-Basin of Nigeria. The recovered oil from the TDU was analyzed and compared to untreated base oil in order to identify the effect of TDU process on the reclaimed oil.

## METHODOLOGY

Containment of drill cuttings such as synthetic (pseudo) oil based cuttings and other drilling waste in skips at the drilling/well sites is the first major operation.

However, the process for separating drill cutting from the oil-based drilling fluid starts from the well site with the use of mechanical solids control equipment prior to the transportation of the resultant residue to the waste management facility where thermal desorption technology is applied to recover the base oil from the contaminated drill cuttings.

A typical sample of drill cuttings observed under microscope is shown in Figure 1.



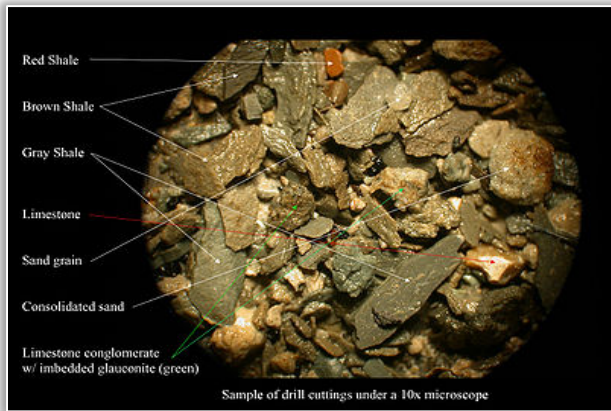


Figure 1: Sample of drill cuttings observed under microscope (drill cuttings)

The overall methodology employed for the waste treatment and oil recovery process is grouped into two which are primary and secondary treatments respectively. The primary treatment system involves the use of drilling platform solids-control systems to initiate solid separation at the well site. These systems employ shale shaker and centrifuge in their solid separation processes. Afterward, the secondary treatment is followed and this involves the handling of pre-treated cuttings (from the primary treatment facility) in cuttings dryer and thermal desorption unit.

These two methods of secondary treatment are employed to reduce drilling fluid retention on cuttings (ROC). Base oil recovery and extraction of environmental friendly drill cuttings are performed by the thermal desorption unit (TDU). The process separates incoming material (contaminated drill cuttings) and produces products like organic oil, water and pre-dried material. For instance, the employed thermal desorption unit feed system is shown in Figure 2 while its schematic diagram is illustrated in Figure 3.



Figure 2: Thermal desorption unit feed system

The incoming contaminated waste is fed to the feed hopper of the TDU. Subsequently, adjustable and controlled feeding is obtained by means of screw conveyers and gas sluices leading to the central processing unit as illustrated in Figure 3. The processor is a specially designed rotary heat exchanger which is heated by a closed loop circulation of thermal fluid

(boiler) heat. Thus, gaseous hydrocarbons and steam leaves the processor by means of a lower over pressure into the controlled condensation stage where liquefying is achieved. The liquid phase is collected in a separation tank; and consequently, condensed oil/organic and water are separated and pumped away respectively. Consequently, the percentage and composition analyses of the recovered oil with respect to the inlet tonnage of cuttings were carried out. However, section 2.1 gives the detailed descriptions of the compartments and procedures of the TDU employed for this study.

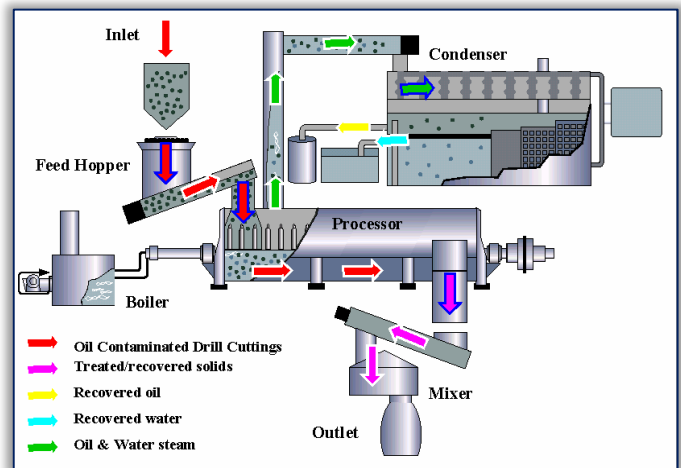


Figure 3: Schematics of the Thermal desorption unit (TDU)

### THERMAL PROCESSING PROCEDURES

The thermal processing procedures are as follow:

- The contaminated drill cuttings are fed into the feed Hopper of the TDU by using a rotary head forklift to empty drill cuttings skips into the inlet hopper of the TDU;
- Material to be processed is then fed into the TDU through a single screw conveyor system attached to the TDU unit as shown in Fig 3. The heart of the TDU is a horizontal vessel with a rotating heat exchanger located inside. The heat exchanger is comprised of a hollow shaft and vein through which hot rotating fluid (hot oil) is pumped. The design provides a large surface area for heat transfer to the Oil Base Mud Cuttings (OBMC's) being processed. Paddles located on the periphery of the veins convey the OBMCs along the length of the processor as the heat exchanger rotates. The processor is capable of processing OBMCs at the rate of 20 to 40 tonnes per hour.
- The heat transfer fluid is heated by an 800kW diesel-fired boiler located within the processing system. The flow rate and temperature of the heat transfer fluid are controlled by a closed loop system to prevent degradation of the fluid. Emissions from the boiler are vented directly to the atmosphere through a 0.25m diameter stack discharging 3m above the roof level.
- Evaporation of the hydrocarbons and water contained within the raw material takes place as the OBMCs are heated to approximately to between 80 to 2800 C and

move from the inlet end towards the outlet of the processor. Air locks are fitted at both the inlet and the outlet of the processor to prevent the escape of the released vapours. To prevent a flammable mixture forming within the processor as the vapours arise, the processor is purged of any air using nitrogen prior to processing any raw material. The hot vapours realised from the raw material are then drawn through a vapour scrubber, where the steam and most of the hydrocarbons are condensed. Gases not condensed in the vapour scrubbers are directed to the boiler for incineration. In the event of a boiler malfunction, the non-condensable gasses will be diverted to an activated carbon filter.

- The mixture of water and hydrocarbon condensate generated by the process is separated into two streams by multi-stage settling. To minimize the potential for dust emissions from material handling operations, the cleaned solids arising from the process are moistened using the water recovered by the distillation. This recovered water accounts for the only wastewater generated by the process. There are no process water discharges to either public sewer or surface water.
- The condensed hydrocarbons arising from the process are stored in settling tanks that are housed within the processing building.
- The recovered water is reused in moistening and cooling down the solids at the outlet end of the treatment unit to prevent dusting effect. Excess recovered water is evaporated or can be condensed and used for other purposes if working in an arid region.
- The processed solids are collected.
- These solids are transported to the designated construction companies or are used in land filling or land spreading of swampy areas or lands with undulating topography.
- The recovered oil is collected in the designated temporary storage tanks.

## RESULTS

The base oil from contaminated drill cuttings was recovered, the negative impact on the environment from the processing of drilling for hydro-carbons (Oil, and gas) was reduced, there was economic control of the drill cuttings (due to the high cost of base oil), the resource was conserved by reuse, pure drill cuttings that is void of contaminants and which can be sold off for land filling and engineering construction was produced.

The resultant drill cuttings oil content was brought below set standard by the government that is 0.5% compared to the acceptance standard of 1% oil in treated drill cuttings this is 50% improvement over the set standard. The result of the composition analysis of the materials after treatment is as shown in Figure 4.

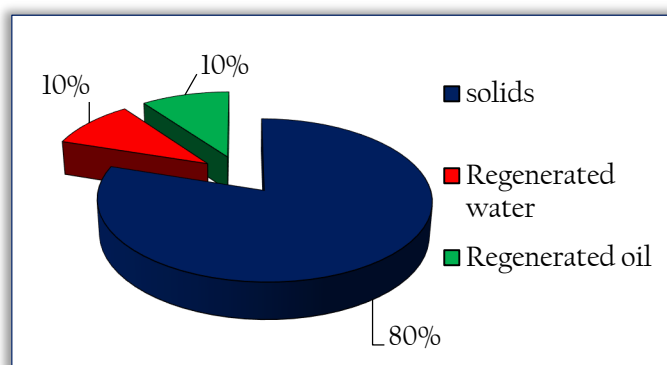


Figure 4. Composition Analysis of Materials

According to the chart provided in Figure 4, the composition assessment shows that 80% solid is obtained while oil residue in clean solids is less than 0.5% after thermal desorption treatment. Also, there is also 10% regenerated water and the recovered water in moistening and cooling down the solids at the outlet end of the treatment unit to prevent dusting effect. Excess recovered water is evaporated or can be condensed and used for other purposes if working in an arid region. Most importantly, there is 10% recovered base oil which as previously stated is of high economic value. However, Figures 5 and 6 gave the analysis of base oil before treatment and after treatment respectively.

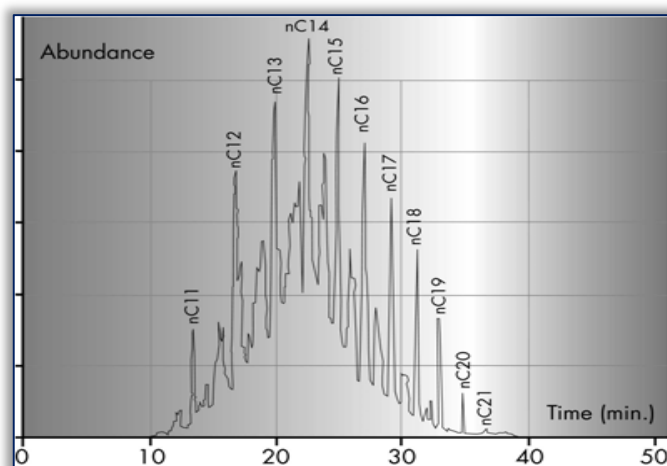


Figure 5. Analysis of base oil before treatment

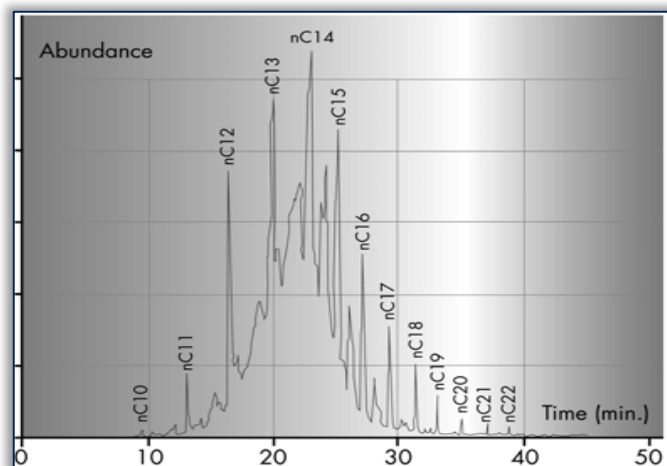


Figure 6. Analysis of recovered base oil after treatment

Similarly, Figure 5 and Figure 6 show that the structure/compositions of the recovered base oil have not been significantly altered by the thermal desorption separation process. This unchanged oil composition is one of the major advantages of the TDU processing and this occurrence is attributed to non-chemical induced treatment process. However, whenever the results are otherwise it is generally not acceptable.

Likewise, the LTDU process recovers between 10 -12 m3 of oil in every 100 tonnes of oily treated cuttings. The recovered oil is high quality oil which is suitable for reuse in the fabrication of new drilling mud. The employed TDU is capable of processing approximately 50 tons of cuttings per 24 hour period. However, if maintenance time is taken into consideration, the TDU has a capacity to process 70,000 tons of cuttings per annum. Routinely, the recovered base oils inclusions are Baroid XP-07, star AP Envirotec, EDC 99 and petrofree (Esters).

According to SPDC, the potential impact of drill cuttings can be reduced via Environmental management plan (EMP) to "as low as practically reasonable". Based on this study, one of the effective approaches for reducing environmental impacts or an effective ecological hazard control is thermal desorption of drill cuttings.

The treatment of Delta Basin drill cuttings in the thermal desorption unit (TDU) acts as an operative ecological hazard control process. Drill cuttings are obtained and transported to TDU for treatment instead of the perennial discharge to open sea. Thus, the formations of cutting piles and detrimental damage to the benthic communities of the Atlantic are utterly inhibited. Similarly, the cleaned or treated drill cuttings can be used for landfilling, as aggregate in construction, and as filler in bituminous mixtures as highlighted by Dhir et al. [31]. In addition, the recovered water from the TDU process can be retreated and use for other purposes.

### CONCLUSION

Mechanical equipment based process or thermal desorption unit (TDU) has been effectively used in the treatment of contaminated drill cuttings and the recovered oil shows no significant variance with the untreated oil. This occurrence has been attributed to the predominant mechanical treatment process or non-chemical induced reaction of constituents of cuttings at elevated temperature. Consequently, environmental protection from the dangers associated with the disposal of well cuttings can be harnessed via thermal desorption processing.

Similarly, TDU has not only helped the oil and gas industries in complying with the laws of the Federal Republic of Nigeria but it has also retrospectively saved cost of drilling by reuse of recovered base oil. Economic benefit is expected from the successive drilling processes with the recovered oil. The treated final cuttings also have economic benefits especially for engineering construction and land filling.

### References

- [1] Anna al Sandouk-Lincke, N.; Schwarzbauer, J.; Antic, V.; Antic, M.; Caase, J.; Grünelt, S.; Reßing, K.; Littke, R.; Off-line-pyrolysis–gas chromatography–mass spectrometry analyses of drilling fluids and drill cuttings – Identification of potential environmental marker substances, *Organic Geochemistry* 88 (2015) 17–28
- [2] Neff, J.M; Composition Environmental fates and Biological Effects OF water. Based Drilling Mud's and cuttings Discharged to the marine Environment. A synthesis and Annotated Biologyraphy. Prepared for Petroleum Environment Research forum (PERF) and American Petroleum Institute, MA, 2005.
- [3] Cannon, R.W.; Dale, M.; Reduction synthetic Based fluid discharges offshore by the use of vertical basket centrifuge. Exploration and production Environmental conference, 26-28 February, San Antonio, Texas, USA, SPE66535, 2001
- [4] Ormeaux, D.; Incineration of Hydrocarbon contaminated solid US pat No 4 606 283, 1986
- [5] Thermtech, A.S.; Thermo-Mechanical Cuttings clear (TCC) Commercial Specifications and Brochures, 2008.
- [6] Smith, K.; Biochemical Degradation of Hydrocarbon Contaminated Folids U.S. Pat No. 5039415, 1991.
- [7] Wait, S.T.; Oil tools (Europe) Limited and Thromas, D.SPE Amerada Hess Limited (2003). The characterization of based oil Recovered from the Low Temperature Thermal Desorption of Drill Cuttings, 2003.
- [8] Henry, L; Harries, D.; Kingston, P.; Roberts, J. M.; Historic scale and persistence of drill cuttings impacts on North Sea benthos, *Marine Environmental Research* xxx (2017) 1-10
- [9] Breur, E.; Stevenson, A. G.; Howe, J.A.; Carroll, J.; Shimmield G.B.; drill cutting accumulations in the Northern and Central North Sea: a review of environmental interactions and chemical fate, *Marine Pollution Bulletin* 48 (2004) 12-25
- [10] Breur, E., Shimmield, G.; Peppe, O.; assessment of metal concentrations found within a North Sea drill cuttings pile, *Marine pollution bulletin* 56 (2008) 1310-1322
- [11] Kogbara, R. B.; Ayotamuno J. M., Onuomah, I.; Ehio, V.; Damka, T. D.; Stabilisation/solidification and bioaugmentation treatment of petroleum drill cuttings, *Applied Geochemistry* 71 (2016) 1-8
- [12] Chen, Z.; Chen, Z.; Yin, F.; Wang, G.; Chen, H.; He, C.; Xu, Y.; Supercritical water oxidation of oil-based drill cuttings, *Journal of Hazardous Materials* 332 (2017) 205–213
- [13] Marsh, R.; A database of archived drilling records of the drill cuttings piles at the North West Hutton oil platform, *Marine Pollution Bulletin* 46 (2003) 587–593
- [14] Trannum, H.C.; Setvik, A.; Norling, K.; Nilsson, H.C.; Rapid macrofaunal colonization of water-based drill cuttings on different sediments, *Marine Pollution Bulletin* 62 (2011) 2145–2156
- [15] Trannum, H.C.; Nilsson, H.C.; Schaanning, M.T.; Øxnevad, S.; Effects of sedimentation from water-based drill cuttings and natural sediment on benthic macrofaunal community structure and ecosystem processes, *Journal*

- of Experimental Marine Biology and Ecology 383 (2010) 111–121
- [16] Pabortsava, K.; Perser, A.; Wagner, H.; Thomsen, L.; the influence of drill cuttings on physical characteristics of phytodetritus, Marine pollution bulletin, 62 (2011) 2170-2180
- [17] Pereira, M.S.; de Ávila Panisset, M.C.; Martins, A.L.; de Sá, C.H.M.; de Souza Barrozo, M.A.; Ataíde, C.H.; Microwave treatment of drilled cuttings contaminated by synthetic drilling fluid, Separation and Purification Technology 124 (2014) 68–73
- [18] Robinson, J.P.; Kingman, S.W.; Snape, C.E.; Bradshaw, S.M.; Bradley, M.S.A.; Shang, H.; Barranco, R.; Scale-up and design of a continuous microwave treatment system for the processing of oil-contaminated drill cuttings, chemical engineering research and design 88 (2010) 146–154
- [19] Robinson, J.P.; Snape, C.E.; Kingman, S.W.; Shang, H.; Thermal desorption and pyrolysis of oil contaminated drill cuttings by microwave heating, Journal Anal. Appl. Pyrolysis 81 (2008) 27–32
- [20] Júnior, I.P.; Martins, A.L.; Ataíde, C. H.; Duarte, C. R.; Microwave drying remediation of petroleum-contaminated drill cuttings, Journal of Environmental Management 196 (2017) 659-665
- [21] Kogbara, R.B.; Dumkhana, B.B.; Ayotamuno, J.M.; Okparanma, R.N.; Recycling stabilised/solidified drill cuttings for forage production in acidic soils, Chemosphere 184 (2017) 652-663
- [22] Chaillan, F.; Chaineau, C.H.; Point, V.; Saliot, A.; Oudot, J.; Factors inhibiting bioremediation of soil contaminated with weathered oils and drill cuttings, Environmental Pollution 144 (2006) 255-265
- [23] Yan, P.; Lu, M.; Guan, Y.; Zhang, W.; Zhang, Z.; Remediation of oil-based drill cuttings through a biosurfactant-based washing followed by a biodegradation treatment, Bioresource Technology 102 (2011) 10252–10259
- [24] Gabbita; stabilization and Encapsulation of contaminated Drill cutting U.S. pat 4913586, 1996
- [25] Fang, C.S.; Shuniray, W.; Enhanced Thermal Desorption process can Extend Life of Based oil and Reduced ENERGY COSTS. S & P Environmental and safely conference 5- 7 march 2007 Galveston, Texas, USA, SPE106798,
- [26] Delta Environmental logistics operation manual, February, 2010.
- [27] George, J.M.; Smith, J.D.; Method and Apparatus for washing Drilling cutting. U.S. patent 4462416, 1984
- [28] Perez – Cordova, R.; Drill Cuttings Treatment United State Patent 6978851, 2010
- [29] Pierce, D.C.G.; Wood, B.; Lessons Learned from Treating 500,000 Tonnes Oil Base Drill Cuttings in five Continents. ADC/SPE99027, 2006
- [30] Ritter, N.; Chemical Oxidation of Hydrocarbon Contaminated Solids U.S. Pat No. 544207, 1995.
- [31] Dhir, R.K.; Csetenyi, L.J.; Dyer, T.D.; Smith, G.W.; Cleaned oil-drill cuttings for use as filler in bituminous mixtures, Construction and Building Materials 24 (2010) 322–325



ISSN: 2067-3809

copyright © University POLITEHNICA Timisoara,  
Faculty of Engineering Hunedoara,  
5, Revolutiei, 331128, Hunedoara, ROMANIA  
<http://acta.fih.upt.ro>

<sup>1</sup>Viktor József VOJNICH, <sup>2</sup>Endre PÖLÖS, <sup>3</sup>András PALKOVICS, <sup>4</sup>Ferenc BAGLYAS

## EXAMINATION OF WEED VEGETATION OF A VINEYARD ON SANDY SOIL

<sup>1-4</sup> Pallas Athena University, Faculty of Horticulture and Rural Development, Kecskemét, HUNGARY

**Abstract:** Weeds are particularly competitive with grapes on sandy soil. They extract water and nutrients from the crops besides they shade plants. A weed survey was carried out in the demonstration vineyard of the Faculty of Horticulture and Rural Development of Pallas Athena University, in Kecskemét, in Hungary. The coenological survey was in 10<sup>th</sup> September 2015. The recordings were made in 5 x 2 m plots with Braun-Blanquet methods. Factors affecting of weed communities: 1. Grown in culture; 2. Climatic factors; 3. Soil type; 4. Soil cultivation; 5. Methods of weed control; 6. Allelopathy. We found four types of weed communities: 1. Puncture vine (*Tribulus terrestris*); 2. Common purslane (*Portulaca oleracea*); 3. White goosefoot (*Chenopodium album*); 4. Bindweed (*Convolvulus arvensis*).

**Keywords:** weed control, soil cover, allelopathy, vineyard, Braun-Blanquet methods

### INTRODUCTION

It is well known that the field and horticultural crop production have among the primary factors reducing crop of weed plants. The weeds in the early stages of cultivation, when people of different wild plants were placed in culture, mass appeared in the sowing of crops such as pests. Since then the ecologically better adapted to characterize weeds and cultivated plants are less adaptable ceaseless struggle between them. The soil cultivation, plant care, in general, is that modern agricultural technology to, determines how much damage caused by weeds. The loss is estimated to reach 25-30% respectively.

Factors affecting weed associations:

- Cultivated culture
- Climatic factors
- Soil type
- Soil cultivation
- Weed control methods
- Allelopathy

Weed associations characterized by:

- Influenced by human activity
- Varied in appearance, often a result of random events occurs
- High degree of adaptation, tolerance
- Low stability in
- A large proportion of invasive adventives species
- Due to anthropogenic influence is difficult to organize
- Are spreading due to the natural environment disturbance.

The aim of the experiment was to examine how the above mentioned factors affect the composition of the weed flora in the investigated territory.

### MATERIALS AND METHODS

A weed survey was carried out in the demonstration vineyard of the Faculty of Horticulture and Rural Development of Pallas Athena University, in Kecskemét, in Hungary. The area was

added to coenological comment carried out on 10 September 2015. The survey was weighed and phytosociological survey was carried out 5 x 2 meter area. The quadrates were evaluated Braun-Blanquet's method [1].

The definition of weed:

- Ujvárosi [2]: The natural vegetation does not occur only in the areas of culture, or members of the ancient vegetation, but cultivated areas conquered space.
- Lehoczky [3]: Weed is any plant which there occurs where undesirable.
- Holzner [4]: A man weeds growing plants best adapted to the activities that significantly affect agricultural cultivation.
- Bunting [5]: The weeds are pioneer species in secondary succession.
- Hunyadi [6]: Weeds are called plants or plant parts (rhizome, onion, etc.) of any stage of development which occur where it is not desired.

The emergence of the weed plant of vegetation was adaptation to the environment formed by man. Any weed plant can be considered harmful to us under the circumstances.

According of habitats:

- field, pasture;
- cutting areas;
- disturbance areas, around of human domiciles

The damages caused by pest's weeds forms:

- The habitat occupation
- The use of soil water reserves
- The use of nutrient stocks
- Parasitism
- Intermediate hosts of diseases, of pests propagation
- Increasing the cost of production
- Value of the downgrading
- Toxic weeds [2].

We found four types of weed communities:

- Puncture vine (*Tribulus terrestris*)
- Common purslane (*Portulaca oleracea*)
- White goosefoot (*Chenopodium album*)
- Bindweed (*Convolvulus arvensis*)

**Puncture vine** (*Tribulus terrestris*)

*T. terrestris* is an annual plant. The plant is slim, 60 cm height. Time of flowering was from July till late autumn. The flower colour is yellow. Spread through the tropical and subtropical areas. Nowadays is a cosmopolitan species. In Hungary of the Great Plains hacked in the loose, dry, wind blew, sandy soil was very common. Puncture vine was one of the most unpleasant weeds in Hungary.

In open fields, it is mostly found in capture cultures and stubble, but it is often found in gardens and vineyards. In cereals (if they are rare) they reach development until flowering. *Tribulus terrestris* disinfected with stubble and cereals at the end of summer. Where the soil was richer in humus, and ceases its quicksand nature, the Puncture vine is no longer alive. Life forms: T<sub>4</sub> (annual plant, germination of spring, flowering of late summer) [2, 7, 8].

**Bindweed** (*Convolvulus arvensis*)

*C. arvensis* is a perennial plant; bindweed was one of the most common arable weeds. The underground stems and roots can also go down to a depth of 2-3 meter of soil. Time of flowering was from early June till the first autumn frost. The flowers are white or pink. Throughout the world was spread and is one of the most pernicious weeds. It was originally in Europe and Asia was native to warmer regions, spread out in all directions here. In Hungary of the Great Plains Plain high levelled in the hot, dry regions of strongly bound soils, especially clay of meadow.

It is common in fields, gardens, orchards, vineyards, roads, artificial or planed grasslands. The damage is very large, because it not only takes up the place of the crop and takes away the food, but it is overshadowed by its massive foliage, it is hindered by its close attachment to development and, in particular, it is a major cause of the collapse of cereals.

It also tolerates the highest dryness, because its roots penetrate to the constantly damp ground floor several meters deep. *Convolvulus arvensis* does not like shading. Regular autumn deep plowing and crop density significantly suppresses the spread. Life forms: G<sub>3</sub> (in soil for wintering perennials) [2, 7, 8].

**White goosefoot** (*Chenopodium album*)

*C. album* is a most common annual weed. White goosefoot was not only in the open fields, but all the nutrient-rich cultures occur. The plant height was 20-150 cm. Time of flowering was from mid-June till autumn (frosts onset). The flower colour is green. It is spread all over the Earth except the polar circles.

In Hungary, it is very common in all kinds of soil, both in arable land and on plains, along roads, in gardens, in vineyards, everywhere where humus is disturbed. Frequent in all types of crops, but mainly in cereals. The soil is full of seeds, and

when humidity is ensured, it sprouts well from spring to autumn. *Chenopodium album* damage is very high, because he grows fast and does not absorb the food and the water from the sown plant, but it completely overshadows and destroys it. Gardens, vineyards can only defend against constant hoeing. Life forms: T<sub>4</sub> (annual plant, germination of spring, flowering of late summer) [2, 7, 8].

**Common purslane** (*Portulaca oleracea*)

*P. oleracea* is an annual plant, 15-30 cm height, succulent's plant. The sandy soil was of most burdensome weeds. Time of flowering was from July till frosts. The flower colour is yellow. Today almost on the Earth carried into temperate zone and warm zone, cosmopolitan species. It is spread in Hungary in sandy and loamy soils, but especially in the loose sand area.

In some places it is still heavily saline soils. In the middle of summer, it is found in large quantities in all cereals and stubble, in gardens, in vineyards, on cracked sandy soils, on abandoned fields, along roads, but especially in sandy garden and vineyards. Its seeds are large in the soil, they are full of reality.

After each hoeing, a new seed begins to germinate. It is precisely this property that we use to control it, because in this way we can spill it out of the soil in almost unlimited quantities, and gradually deepen the cultivation, and we can clean the top layer of the soil. It is extremely sensitive to freezing and in the late May frosts and in the autumn, the first dwarf completely destroys it. The heat of summer was incredible to grown rapidly. Life forms: T<sub>4</sub> (annual plant, germination of spring, flowering of late summer) [2, 7, 8].

**RESULTS**

- The area we were able to isolate four weed territories:
- Puncture vine (*Tribulus terrestris*) (Table 1 and Figure 1);
- Bindweed (*Convolvulus arvensis*) (Table 2 and Figure 2);
- White goosefoot (*Chenopodium album*) (Table 3 and Figure 3);
- Common purslane (*Portulaca oleracea*) (Table 4 and Figure 4).

Table 1. Puncture vine (*Tribulus terrestris*) area

Plant species	Casing (%)	A-D value
<i>Tribulus terrestris</i>	50	3-4
<i>Portulaca oleracea</i>	10	2
<i>Digitaria sanguinalis</i>	10	2
<i>Setaria viridis</i>	5	1-2
<i>Amaranthus retroflexus</i>	5	1-2
<i>Melandrium album</i>	0.5	+

Table 2. Bindweed (*Convolvulus arvensis*) area

Plant species	Casing (%)	A-D value
<i>Convolvulus arvensis</i>	60	4
<i>Portulaca oleracea</i>	10	2
<i>Eragrostis poaeoides</i>	5	1
<i>Setaria viridis</i>	3	+1
<i>Amaranthus retroflexus</i>	5	1



Figure 1. Puncture vine (*Tribulus terrestris*) area

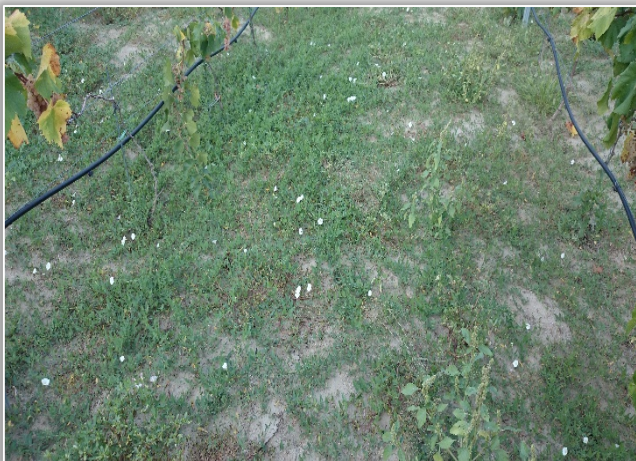


Figure 2. Bindweed (*Convolvulus arvensis*) area



Figure 3. White goosefoot (*Chenopodium album*) area

Table 3. White goosefoot (*Chenopodium album*) area

Plant species	Casing (%)	A-D value
<i>Chenopodium album</i>	30	2-3
<i>Portulaca oleracea</i>	10	1-2
<i>Chenopodium aristatum</i>	5	1
<i>Amaranthus retroflexus</i>	5	1
<i>Eragrostis poaeoides</i>	5	1
<i>Agropyron repens</i>	3	+ -1
<i>Ailanthus altissima</i>	0.5	+



Figure 4. Common purslane (*Portulaca oleracea*) area

Table 4. Common purslane (*Portulaca oleracea*) area

Plant species	Casing (%)	A-D value
<i>Portulaca oleracea</i>	70	4-5
<i>Eragrostis poaeoides</i>	10	2
<i>Chenopodium aristatum</i>	5	1-2

All four examined areas can be found in common purslane (*Portulaca oleracea*). Three places were found in *Amaranthus retroflexus* and *Eragrostis poaeoides*. Two study areas there are *Setaria viridis* and *Chenopodium aristatum*.

#### CONCLUSIONS

- On the sandy soil has a low humus content of extreme dryness tolerant weeds typically: *Tribulus terrestris* and *Portulaca oleracea*.
- On the sandy soil warm up quickly accumulating weeds: *Chenopodium aristatum*, *Chenopodium album*, *Amaranthus retroflexus* and *Convolvulus arvensis*.
- Mechanical weed control (hoeing) forced back as a result of the perennial plant species.
- Weed species has been area with allelopathy: *Chenopodium album*, *Portulaca oleracea* and *Tribulus terrestris*.

#### Acknowledgements

This research is supported by EFOP-3.6.1-16-2016-00006 "The development and enhancement of the research potential at Pallas Athena University" project. The Project is supported by the Hungarian Government and co-financed by the European Social Fund.

## References

- [1] J. Braun-Blanquet, Pflanzensoziologie, Grundzüge der Vegetationskunde. (3. Auflage). Springer Verlag, Wien (1964)
- [2] M. Ujvárosi, Weeds. Agriculture Publisher, Budapest (1973)
- [3] É. Lehoczky, The competition of weeds and cultivated plants for nutrients. Academic Publisher, Budapest (1994)
- [4] W. Holzner, M. Numata, Biology and ecology of weeds. Springer Netherlands, Dordrecht (1978)
- [5] A. H. Bunting, Some reflection on the ecology of weeds. Blackwell, Oxford (1960)
- [6] K. Hunyadi, Chemical weed control, Part I. University note, Keszthely (1974)
- [7] K. Hunyadi, I. Béres, G. Kazinczi, Weed species, weed biology, weed control. Agriculture Publisher, Budapest (2011)
- [8] A. Kádár, Chemical weed control and crop control. Agriculture Publisher, Budapest (2016)



ISSN: 2067-3809

copyright © University POLITEHNICA Timisoara,  
Faculty of Engineering Hunedoara,  
5, Revolutiei, 331128, Hunedoara, ROMANIA  
<http://acta.fih.upt.ro>



<sup>1</sup>Zoran PANDILOV, <sup>2</sup>Betim SHABANI, <sup>3</sup>Dejan SHISHKOVSKI, <sup>1</sup>Gligorche VRTANOSKI

# REVERSE ENGINEERING – AN EFFECTIVE TOOL FOR DESIGN AND DEVELOPMENT OF MECHANICAL PARTS

<sup>1</sup>Institute of Production Engineering and Management, Faculty of Mechanical Engineering, SS. Cyril and Methodius University in Skopje, Skopje, MACEDONIA

<sup>2</sup>Tools Factory “PLUS” A.E, Ferizaj, KOSOVO

<sup>3</sup> Metal-solutions, Skopje, MACEDONIA

**Abstract:** The Reverse Engineering has already found an extensive application in industry and other different fields. Reverse engineering (RE) is a process of taking the existing physical model and reproducing its surface geometry in three-dimensional (3D) data file on a computer-aided design (CAD) system. This paper will analyze the real situation in one industrial plant and provide comparative analysis of the application of current measuring methods and possibility of incorporating digital measurement. The Reverse Engineering (RE) is based on a method of reducing the time of dimensioning and modeling of mechanical parts which can be complex by geometry or dimensionally very accurate. In this paper we can give some practical examples of parts that are really produced in one manufacturing factory. Recommendation for digitalization will be of crucial importance for every company in its measurement and quality control activities.

**Keywords:** Reverse Engineering (RE), Manufacturing, CAD, Measurement, Digitalization

## INTRODUCTION

Global competition in the world industry today is very high. So the companies are trying continually to be competitive on global market by looking for new ways to reduce production times and develop new products to meet all the consumers requirements. Mostly, the investments of the manufacturing companies are concentrated on Reverse Engineering (RE), CAD / CAM, Rapid Prototyping (RP) and a large number of new technologies that offer greater production, business benefits and greater profit.

Reverse Engineering (RE) is now considered as one of the new technologies that provides bigger business benefits using shortening the product development cycle.

Reverse Engineering has been associated with the copying of an original product design for competitive purposes. In the manufacturing world today, however, the concept of reverse engineering is being legally applied for producing new products or variations of old products. The term reverse comes from the concept of bi-directional data exchange between the digital and physical world [12].

Its application is already proven in many areas of engineering and everyday life. There are many reasons why it should be used.

Some of the reasons for using Reverse Engineering are given below:

- The original manufacturer no longer exists, but a customer needs the product.
- The original product design documentation has been lost or never existed.
- Creating data for renewing or manufacturing a part for which there is no CAD data, or for which the data have become unusable or lost.

- Inspection Quality Control—Comparing a fabricated part to its CAD description or to a standard item.
- Some bad features of a product need to be eliminated.
- Strengthening the good features of a product based on long-term usage.
- Exploring new ways to improve product performance and features.
- Architectural and construction documentation and measurement.
- Fitting clothing or footwear to individuals and determining the anthropometry of a population.
- Generating data to create dental or surgical prosthetics, artificial engineered body parts, or for surgical planning.
- Creating 3-D data from a model or sculpture for animation in games and movies.
- Creating 3-D data from an individual, model or sculpture to create, scale, or reproduce art work.

The above list is not exhaustive and there are many more reasons for using Reverse Engineering, than documented above [1].

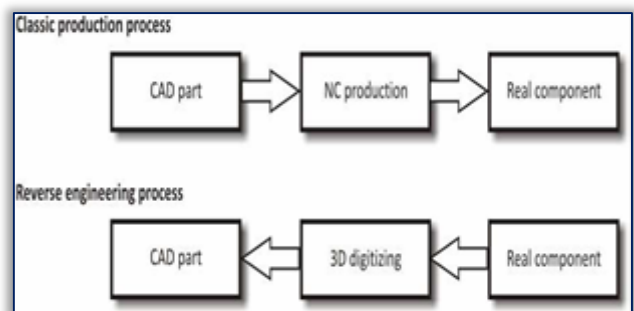


Figure 1. Comparison of Reverse Engineering and classic production processes [2]

Classic machining process begins from CAD model and ends by component production. Reverse Engineering process is opposite. At the beginning is real component and it ends with digital model. This is shown on Figure 1 [2].

## DEVELOPMENT AND APPLICATION OF REVERSE ENGINEERING

Reverse Engineering covers a variety of approaches to reproduce a physical object with the aid of drawings, documentation, or computer model data. In the broadest sense, Reverse Engineering is manual work or use of computer and some kind of software to reproduce something.

Reverse Engineering is one of the methods used by companies in order to accelerate their product design process and this method is desired for access to the new technologies with minimum cost, risk and time [11]. This method in the developing countries that are not so advanced in terms of product and technology design knowledge, compared to the developed countries, is a logical response to increase designing capability and accelerate the design and manufacturing process.

Reverse Engineering is no longer used just only for bringing again the old technology back to life. It is also for using existing or old technology as a launch pad directly into the future [3].

Reverse Engineering techniques are being used in a wide range of applications and it is not restricted only to the industry. The type of Reverse Engineering that will be discussed in this paper is a technique where the physical dimensions of a part are being captured in order to be produced a detailed drawing of the part. In the Computer Aided Manufacturing (CAM) world, this is referred as part to CAD conversion, where the geometry of the physical objects is captured as digital 3-D CAD Data [4].

The generic process of Reverse Engineering is a three-phase process shown in Figure 2. The three phases are: scanning, point processing, and development for the particular application specific geometric model [1].

— **Scanning Phase:** This phase is connected with the scanning strategy. Its include: selecting the correct scanning technique, preparing the part to be scanned, and performing the actual scanning to capture information that describes all geometric features of the part such as steps, slots, pockets, and holes.

— **Point Processing Phase:** This phase involves importing the point cloud data, reducing the noise in the data collected, and reducing the number of points. A wide range of commercial software are available for point processing. The output of the point processing phase is a clean, merged, point cloud data set in the most convenient format.

— **Application-Geometric Model Development Phase:** The generation of CAD models from point data is probably the most complex activity within Reverse Engineering. Sophisticated surface fitting algorithms are required in

order to be generated surfaces that accurately represent the three-dimensional information described within the point cloud data sets.

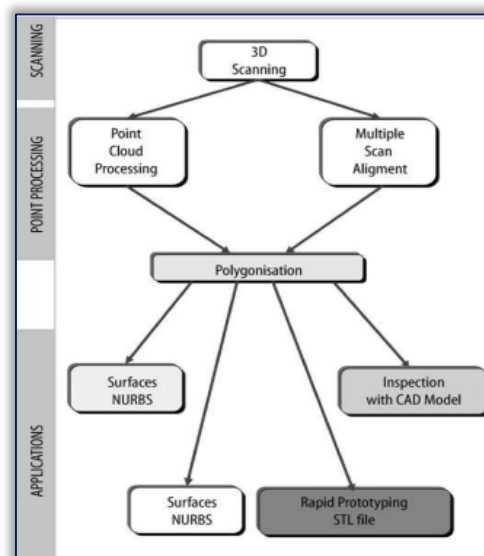


Figure 2. Reverse Engineering – the generic process [1]

Reverse Engineering strategy must consider the following:

- Reason for Reverse Engineering of a part
- Number of parts to be scanned—single or multiple
- Part size—large or small
- Part complexity—simple or complex
- Part material—hard or soft
- Part finish—shiny or blurry
- Part geometry—cylindrical or prismatic and internal or external
- Accuracy required—linear or volumetric

Computer-Aided Reverse Engineering (CARE) relies on the use of computer-aided tools for obtaining the part geometry, identifying its material, improving the design, tooling fabrication, manufacturing planning and physical realisation. The structure is shown in Figure 3.

A solid model of the part is the backbone for Computer-Aided Reverse Engineering. The model data can be exported from or imported into CAD/CAE/CAM system using standard formats such as IGES, STL, VDA and STEP. The three most important sets of data in Reverse Engineering activities are related to the CAD model generation, material identification, and manufacturing [5].

Reverse Engineering (RE) is generally defined as a process of analyzing an object or existing system using hardware and software, to identify its components, their interrelationships and to investigate how it works in order to redesign it or produce a copy without access to the design from which it was originally produced.

Reverse Engineering hardware is used for Reverse Engineering data acquisition, which for 3-D modeling, is the collection of geometric data that represent a physical object. There are three main technologies for Reverse Engineering data acquisition: contact (Figure 4.), noncontact and destructive. Outputs of the Reverse Engineering data

acquisition process are 2-D cross-sectional images and point clouds that define the geometry of an object.

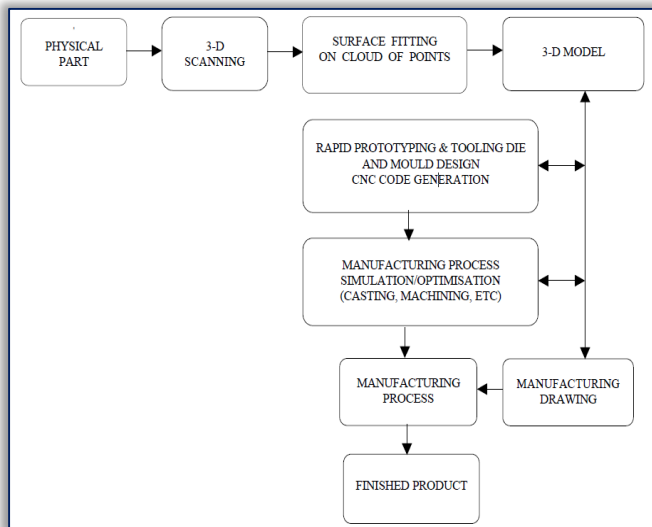


Figure 3. Computer-Aided Reverse Engineering framework [5]

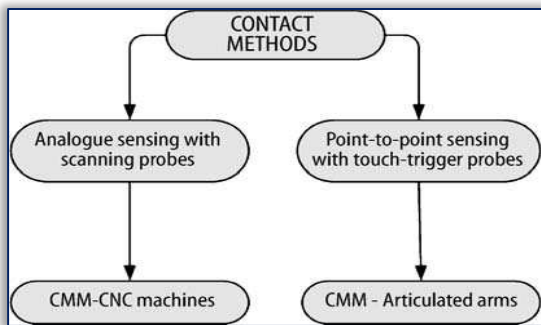


Figure 4. Reverse Engineering hardware classification [1]

Reverse Engineering software is used to transform the Reverse Engineering data produced by Reverse Engineering hardware into 3-D geometric models. The final outputs of the Reverse Engineering data processing chain can be one of two types of 3-D data: (i) polygons or (ii) NURBS (no uniform rational B-splines). Polygon models, which are normally in the STL, VRML, or DXF format, are commonly used for rapid prototyping, laser milling, 3-D graphics, simulation, and animations. NURBS surfaces or solids, are frequently used in Computer-Aided Design, Manufacturing, and Engineering (CAD-CAM-CAE) applications [1].

Except the advantages obtained by the use of Reverse Engineering, during the implementation, we encountered some barriers that are necessary to be overcome for its wider acceptance. As can be seen from Figure 5, this study proposes a three-phased factor analysis approach in order to determine the critical factors that effects the adoption of Reverse Engineering technologies.

— **Factor determination** phase is a hypothetical research model and it uses a multidimensional model to represent the organizational, environmental, and project dimensional factors. Using of such dimensional model allows clustering the factors, and also facilitates a logical data collection and analysis study.

— **Data collection phase** offers a qualitative approach using interviews with experts in the field of Reverse Engineering. The data collection was carried out by Reverse Engineering Expert and a qualified Coordinate Measuring Machine (CMM) operator. Both of them analyzed the collected data. Face-to-face interviews, approximately 50 minutes long, were conducted. The number of interviewees was determined during data collection. The interviewing was stopped in the moment, when no new information was obtained from interviewees and saturation was reached.

— **Data analysis phase** is closely aligned with the empirical phase. After data are collected, the data are prepared for analysis. The quantitative data are typically entered into a statistical program and qualitative data are often transcribed in order to facilitate data analysis.

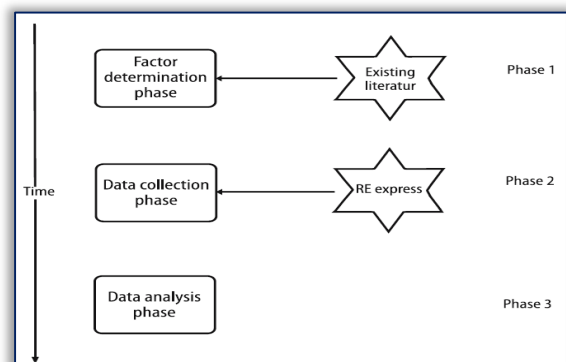


Figure 5. Factor analysis approach [1]

As we know with Reverse Engineering, for an existing mechanical part we make the technical drawings in order to make a production of it. Because the original part already physically exists, some people believe that Reverse Engineering and duplicating are the same.

But this is not true, because duplicating process is based on expected short time benefits in order to make profit through manufacturing of products which will provide less of the properties and functional specifications compared with the original products. Duplicating differs from Reverse Engineering in sense that products made with duplicating will result in products on low level technology. In case of complicated products, duplicating will not result in adoption of technology of manufacturing. Instead of that, Reverse Engineering will result in preparing production technology, similar or better, than previous used for manufacturing the original part. Manufacturing of products with Reverse Engineering approach is based on a long term benefits and innovations. Application of updated standards, manufacturing of optimized products and working on products development and improvement is the best scheme in adopting Reverse Engineering methods [3].

#### TECHNIQUES AND TOOLS FOR CASE STUDY

Main techniques used by Reverse Engineering for our case study are calipers used for measurement, Autodesk Inventor software used for CAD modelling and CNC Milling machine that it used for realising the physical part. The current

situation in the factory offers the above mentioned possibilities. The production is mainly individual with different quality requirements. So the application of Reverse Engineering is not continuous, but it depends on every specific case.

### A. Calipers

Using the calipers as device of measurement is considering as (Reverse Engineering) manual process for taking the dimensions from different mechanical parts. Then, from these measurements, we could manually define a 3D computer model using CAD primitives. There are different constructions of calipers, but in principle there are not very big differences between them. All of them have a purpose of reducing the measuring error and increasing the accuracy of the reading. The Figure 6 shows standard vernier caliper.

The parts of the caliper include:

1. **Outside large jaws:** used to measure external diameter or width of an object
2. **Inside small jaws:** used to measure internal diameter of an object
3. **Depth probe/rod:** used to measure depths of an object or a hole
4. **Main scale:** scale marked every mm
5. **Main scale:** scale marked in inches and fractions
6. **Vernier scale** gives interpolated measurements to 0.1 mm or better
7. **Vernier scale** gives interpolated measurements in fractions of an inch
8. **Retainer:** used to block movable part to allow the easy transferring of a measurement

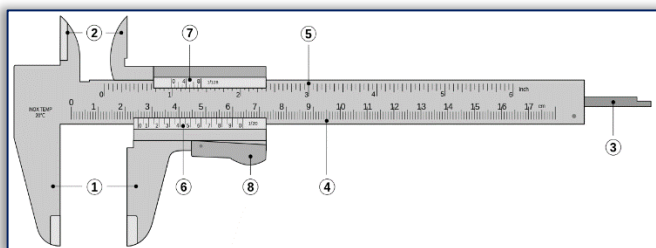


Figure 6 . Vernier caliper [6]

### B. CNC Milling Machine

CNC is the abbreviation of Computer Numerical Control. The working principle of these highly flexible machines is based on converting the CAD (Computer Aided Design) of the part with CAM (Computer Aided Manufacturing) software in cutting tool trajectory (in coordinates). These Computer Numerical Control Machines made revolution in manufacturing, enabling production of different complex parts, with different accuracy and different materials. CNC milling machines are the most widely used type of CNC machines. Typically, they are grouped by the number of axes simultaneously operating. Axes are labeled with various letters [7].

The machine shown in Figure 7 was taken from the Factory where the mechanical parts presented in this paper, as case study, were produced.



Figure 7. CNC Milling machine [8]

### PRACTICAL ANALYSIS

Damage of machine parts is a serious problem in production. It affects production efficiency and causes financial losses due to machine(s) malfunction. Most threatened are components like transmission parts, tools or electronics. Our examples show cases of a damaged: tool part (precision) and mechanical part (complex geometry).

#### A. Tool part (precision)

Figure 8 shows tool part which has some damage or cracks along the channels and holes.

For this part, which has to be produced again, first must be estimated the costs and required time for manufacturing. The precision and the type of tool material are the two main components necessary for the measurement and reconstruction procedure.



Figure 8. Tool (original version) [8]

Based on the damages that exist on the tool, we have recommended that it should be produced a completely new part. In this case it is possible to apply Reverse Engineering to eliminate possible machine damage due to the tool damage. The tool part was measured with calipers and we made a CAD model of the part (tool) with Autodesk Inventor.



Figure 9. Measurement of tool part [8]

After we have made the measurements of the existing work piece (Figure 9) and created a 3D model through the software

(Figure 10), the next step was the machining the part on the respective machine (Figure 11),  
The tool part was drawn in 1:1 ratio, so its conversion in required different forms was very easy.  
The software used in this case (Autodesk INVENTOR 2017) is very professional and provides many opportunities for designing and correction of parts.

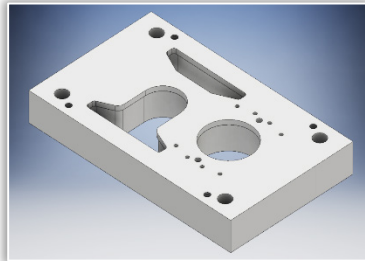


Figure 10. CAD model of tool part

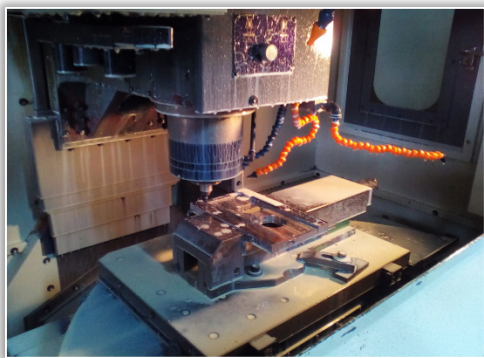


Figure 11. Production of tool part with CNC Milling machine [8]

### B. Mechanical part (complex geometry)

The mechanical part shown in Figure 12 is used like housing for holding shafts with bearings and it makes an assembly with bolts with another part. This broken mechanical part should have been manufactured again with previous estimation of costs and necessary time for production. The complex geometry of this mechanical part was very difficult to be measured and to be created a 3D geometrical model. The requirement was to compare the original part produced with casting, with the part made of construction steel manufactured by milling. We made some optimization in geometric shape of the mechanical part in order to obtain easier manufacturing, but the functionality remained still unchanged, the same like in the original part.



Figure 12. Mechanical part (original version) [8]

Based on the damages that are presented in the Figure 12, we recommended that mechanical part should be produced as

a new one. In this case it is also possible to apply Reverse Engineering in order to eliminate the part damage. The part was measured with calipers and we made a CAD model of the mechanical part with Autodesk Inventor (Figure 13).

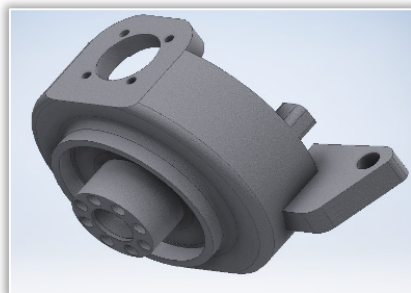
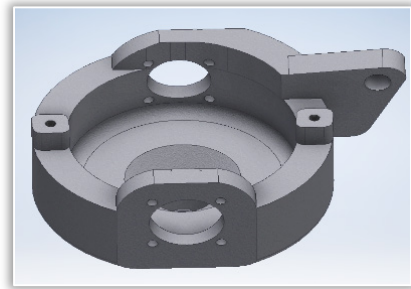


Figure 13. CAD model of the mechanical part

After we have made the measurement of the existing work piece and creating the 3D model through the software (Figure 13), the next step was the manufacturing on the milling machine (figure 14).



Figure 14. New mechanical part produced with milling and welding

### RECOMMENDATIONS FOR IMPROVEMENT

Analyzing the current situation in the Factory which was given as a practical example, it could be mentioned that the measurement of the machine parts with calipers affects on continuous loss of time during the measurement process and reduces the reliability for accurate measurements.

Error criteria set by the parts ordered for rejection of mechanical parts was 0.1 mm. Parts with errors above 0.1 mm were considered as a scrap.

The above given examples, show us that the application of Coordinate Measuring Machine (CMM) technology would be much better, because the accuracy will be higher and the ability to make corrections will be much faster.

Coordinate Measuring Machine (CMM) consists of a probe supported on three mutually perpendicular (x, y, and z) axes (Figure 15).

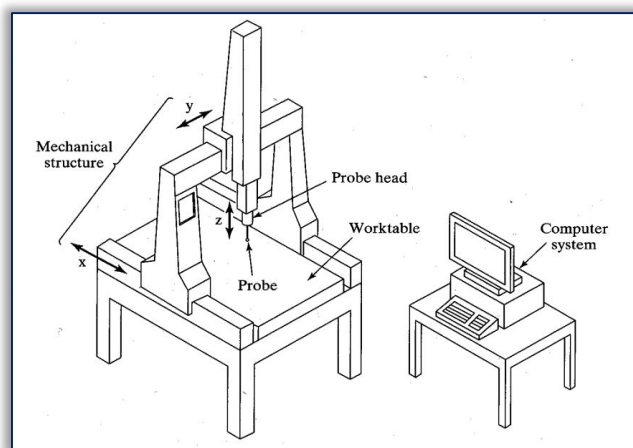


Figure 15. Conceptual view of a Coordinate Measuring Machine (CMM) [1]

Coordinate Measuring Machine (CMM) generates 3-D coordinate points, as the probe moves across the surface of the part. Operators may run Coordinate Measuring Machine (CMM) in a manual mode where they move the probe around an object and collect coordinate measurements, or they may program the probe to move automatically around the part [1].

The Coordinate Measuring Machines (CMM) can be divided into mainly two major types: with contact-type measurement system and with non-contact measurement system [9].

Reverse Engineering using 3D digitizing is a potential methodology to make virtual prototype models for analysis and 3D visualization of the products [10].

Applying Reverse Engineering will be essential for the technical and economic development of the analyzed Factory in general.

#### CONCLUSION

In this paper, the mechanical parts that have been selected for analysis were: tool part (precision) and mechanical part (complex geometry).

The form used for measurement the mechanical parts was through the calipers, which is currently the only opportunity in the Factory used as an example. Drawing of the parts and creating their CAD models was on computer using Autodesk Inventor software.

Taking into the account the analysis that were made, we can conclude that digital scanning is indispensable and irreplaceable for application to minimize errors and reduce the time of measurement

#### References

- [1] Raja V., Fernandes J. K.: Reverse Engineering, Springer series in Advanced Manufacturing, 2008
- [2] Dúbravčík M., Kender Š.: Application of reverse engineering techniques in mechanics system services, Elsevier, MMaMS, Procedia Engineering, Vol. 48 pp. 96-104, 2012
- [3] Dehagh R. M., Goodarzi M.: Reverse Engineering: A Way of Technology Transfer in Developing Countries like Iran, International Journal of e-Education, e-Business, e-Management and e-Learning, Vol. 1, No. 5, pp. 347-353, December 2011

- [4] Barai D. G., Shete S. S., Raut R. L.: Design and development of a component by Reverse Engineering, IJRET: International Journal of Research in Engineering and Technology, eISSN: 2319-1163, pISSN: 2321-7308, Volume 04, Issue 5, pp. 539-546, May 2015
- [5] Pal K. D., Ravi B., Bhargava S. L., Chandrasekhar U.: Computer-aided Reverse Engineering for Rapid Replacement of Parts, Defence Science Journal, DESSIDOC, DRDO, New Delhi, Vol. 56, No. 2, April 2006, pp. 225-238, 2006,
- [6] <http://ecatalog.mitutoyo.com/Vernier-Calipers-Series-530-Standard-Model-C1401.aspx>: Mitutoyo Vernier Calipers Series 530 - Standard Model, 2017
- [7] <http://www.thomasnet.com/about/cnc-milling-51276103.html>: Thomasnet, More about CNC Milling, 2017
- [8] Tools Factory "PLUS" A.E., 2017
- [9] Huang S. T., Lin Y. S.: The Role of Reverse Engineering and Rapid Prototyping for the Development of Objects made of Soft Material, <http://ir.lib.cyut.edu.tw:8080/bitstream/310901800/8984/1/42.pdf>
- [10] Kumar A., Jain P.K., Pathak P. M.: Machine element reconstruction using integrated reverse engineering and rapid prototyping approach, Proceedings of the 5th International & 26th All India Manufacturing Technology, Design and Research Conference (AIMTDR 2014) December 12th–14th, 2014, IIT Guwahati, Assam, India, pp.123-1 – 123-5, 2014
- [11] Khalili, H.A., Maleki A., Ayatollahi, S.: Using combination of Reverse Engineering and Value Engineering for improvement in designs, construction projects and manufacturing industries. Proceedings of 41st International Conference on Computers and Industrial Engineering, pp.166-171, 2011
- [12] Kumar A, Jain P. K, Pathak P. M.: Reverse Engineering in product manufacturing - An overview, DAAAM international scientific book 2013, pp. 665-678, Chapter 39, 2013



ISSN: 2067-3809

copyright © University POLITEHNICA Timisoara,  
Faculty of Engineering Hunedoara,  
5, Revolutiei, 331128, Hunedoara, ROMANIA  
<http://acta.fih.upt.ro>

<sup>1</sup>Radko Petrov MIHAJLOW, <sup>2</sup>Lazar Georgiev PANAIOTOV,  
<sup>3</sup>Svilen Hristov STOIANOV, <sup>4</sup>Desislava Palcheva MIHAJLOVA

## SIMULATION MODELING AND PROCESSING THE DATA RECEIVED IN MEASURING WASTE BIOMASS

<sup>1-4</sup>: Technical University of Varna, Dobrudzha College of Technology, Dobrich, BULGARIA

**Abstract:** The object of current investigation is a device designed to measure the biomass waste mounted directly on a harvester. An original measuring gadget based on a four linked planar mechanism is proposed and examined by use of a prototype equipped with sensors. Experiments conducted under real conditions demonstrate the operability of the device. Information on the amount and parameters of biomass waste is digitally processed, visualized and stored in computer memory. This is realized by use of a proper software platform implying an original processing algorithm. The results of experiments are reported and discussed below. Notes on further studies in this direction are made.

**Keywords:** biomass, measurement, planar mechanism, averaging

### INTRODUCTION

Current study focuses on the collection of optimal and precise information about the biomass wasted at the time of harvesting. Still on field, together with the data issued from the contemporary harvesting machinery it is important to know the amount of biomass waste (BMW). The last is considered a valuable product, secondary resource, which can be used in the agricultural sector, particularly as a food or green manure in stock-raising and crops. It can also be implemented in the production of heat and energy [3].

This investigation envisions data processing and real time measurement of BMW produced immediately after the harvester. An original technique for monitoring and measurement the amount of BMW is proposed. It takes into consideration the fact that the biomass waste obtained at the time of cereals harvesting actually represents a layer of cornstalks forming a dynamic flow with fixed width and variable height. Respectively, the common principle for the level determination over certain surface [1, 2, 5] is applied.

The kinematics of the mechanical device used as a primary transformer, sensor for the BMW flow height is observed by means of a simulation approach.

Main task of the current study is to demonstrate an effective technique for collection and processing sensor data in real time in order to obtain the amount of BMW.

### EXPERIMENTAL

The investigated simulation model, created using the SolidWorks software [7], is shown in Figure 1. It is based on the kinematic scheme of a four linked planar mechanism, namely slotted-link mechanism. The specific movement of the assembly is characterized by an equation derived after kinematic analysis. The equation represents the relation between the input and output parameters in the form of a transfer function, [4]:

$$\cos \alpha_1 = 0,877 \cos \alpha_2 - 0,14 \quad (1)$$

where the angles  $\alpha_1$ ,  $\alpha_2$  are specified according to Figure 1 and the constants are empirically determined from the prototype created in [4].

The sensor operates on the following principle: the BMW flow is the one that moves the part called "Silencer" herein - this is considered the inlet of the device. The next parts named "Roll" and "Arm" is responsible for the angular turning of the slider of the potentiometric "Sensor" - the last is considered to be the outlet of the mechanism. Any change of the angle  $\alpha_2$  is registered by a sensor, mounted on top of the device, which turns it into a voltage signal. Afterwards, the measured signal is recorded and processed to obtain the final characteristics. For the purpose a specialized program is applied. In its interface the signal can be visualized in analog and digital form. Thus, a real time measurement of the necessary parameters is performed. The numerical transformations of the recorded signal are executed in seconds.

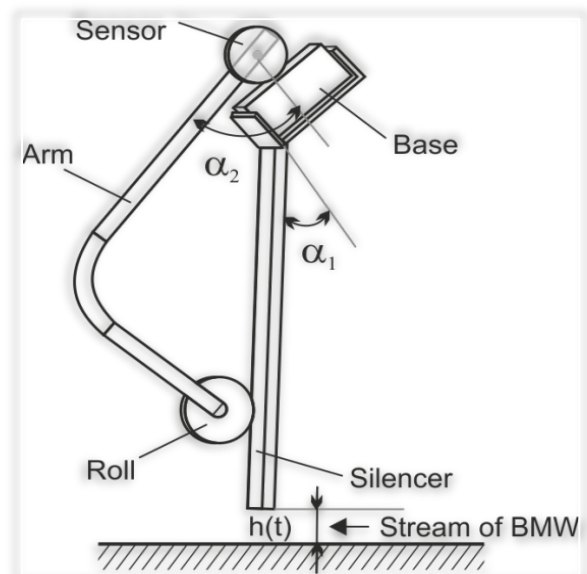


Figure 1. Simulation model of the device used as a BMW level sensor

An original program is created for the particular investigation based on the software platform LabVIEW [6]. The relevant algorithm is shown in Figure 2.

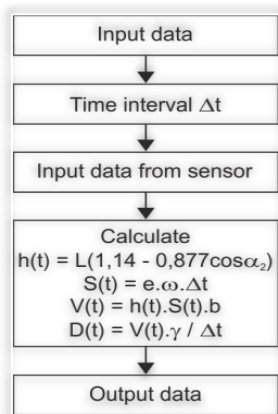


Figure 2. Algorithm

The following constants are initially set as input data for the particular measurement of the amount of BMW:

- $\Delta t$  – period of measurement in which the sensor signal is measured (it is set to correspond the period value in the transforming program);
- $b$  – width of the BMW flow (measured on the harvester, [8]);
- $\omega$  – angular velocity and eccentricity  $e$  of the straw-trailer crankshaft (measured on the harvester for once);
- $L$  – length of the part used as a „Silencer“ for the moving waste biomass (Figure 1);
- $\gamma$  – density – relative weight of the particular BMW.

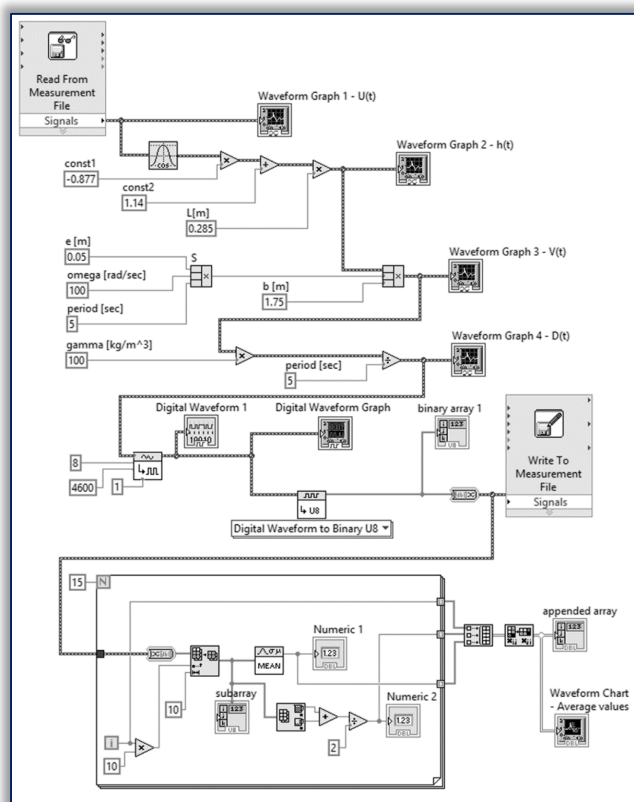


Figure 3. Block diagram of the application program in the LabVIEW environment

Figure 3 shows the block diagram of the main application program. At the beginning there is a proper virtual instrument (VI) for reading the information obtained from the sensor.

The final measurement data file (Figure 4) is saved in the required form for processing in LabVIEW. The results from data transformation are visualized in a Front Panel. The Waveform Graph 1 represents the initial analog signal (Figure 5a). As mentioned, data are manipulated by entering specific constants and the necessary arithmetic operations by means of specific VIs. Subsequently several time depending functions are calculated: the current values of  $h(t)$  function (Figure 5b), which is the variable BMW height reflecting the change of the angle  $\alpha_2$ ; the values of the distance  $S(t)$  function (Figure 2) within the period  $\Delta t$ ; the volume  $V(t)$  (Figure 5c), as well as the calculated amount  $D(t)$  of BMW (Figure 5d).

### RESULTS AND DISCUSSION

The experimental data obtained from the sensor showing the change of the angle  $\alpha_2$  are displayed in Figure 4.

No	Time	DC/AC	Value	Unit
1	15:32:24	DC	12389,00	V
2	15:32:29	DC	11658,00	V
3	15:32:34	DC	13119,00	V
4	15:32:45	DC	15311,00	V
5	15:32:49	DC	22586,00	V
6	15:32:55	DC	45566,00	V
7	15:32:59	DC	22920,00	V
8	15:33:04	DC	17441,00	V
9	15:33:09	DC	12328,00	V
10	15:33:14	DC	42644,00	V

Figure 4. Experimental data in Excel form

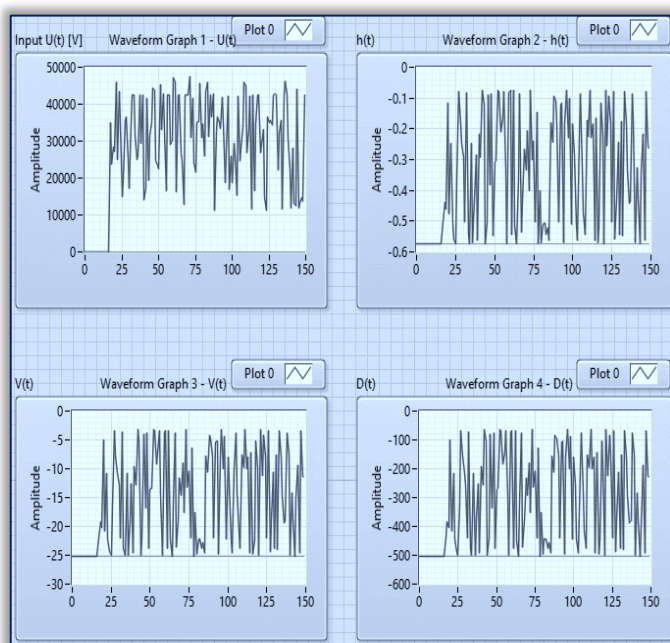


Figure 5. Waveform Graphs in the application environment of LabVIEW: a) analog signal from the potentiometric sensor; b) analog signal corresponding to the variable height  $h(t)$  of the BMW stream; c) BMW volume  $V(t)$ ; d) amount  $D(t)$  of BMW



It should be noted that the values of the  $D(t)$  function are additionally processed in order to be more appropriate for the final assessment. In a sub-program (the last section in Figure 3) a loop function is used to divide all data in arrays of 10 consequent samples. The array values are then averaged for each array subset. This operation is executed in a number of iterations. The final result is represented in Figure 6.

Two approaches have been applied to obtain the average amount  $D(t)$ . The first one implies a VI for mean value (Numeric 1 in Figure 3) and the second one follows the equation below:

$$D_{av} = \frac{\sum_{i=1}^{10} D_{min} + \sum_{i=1}^{10} D_{max}}{2} \quad (2)$$

As seen in Figure 6 the final curve of the averaged  $D(t)$  function grounded on (2) has less fluctuations.

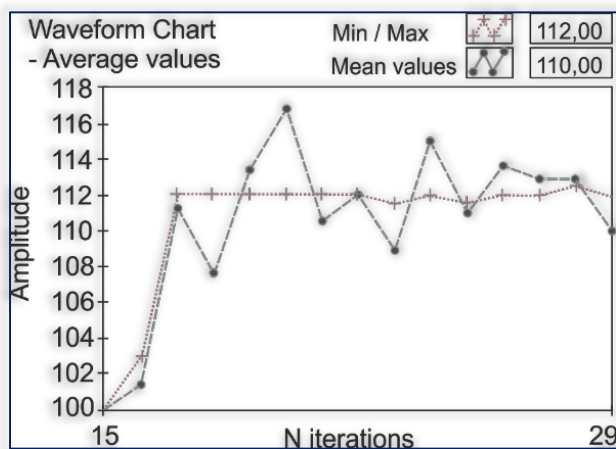


Figure 6. Average values for the amount of BMW

The average amount of 112 kg/m<sup>3</sup> straw fits well the corresponding values obtained from relevant BMW investigations [9, 10].

## CONCLUSIONS

A simulation model was constructed in the SolidWorks interface (Figure 1) which supplied additional information about the kinematics of the sensor device.

The final values for the volume and amount of biomass waste resulted immediately from an original application program in LabVIEW (shown in Figure 6). They correspond in maximum extent to the initial experimental data and relevant assessments of straw parameters.

Furthermore, a study on the relationship between both parameters, amount and surface of BMW, is to be performed. It will provide precise information about the amount of biomass waste at the end of the harvesting period.

## Acknowledgement

The authors wish to acknowledge Bulgarian Ministry of Education and Science and Technical University of Varna for the financial support under the Project NP24/2016.

## References

[1.] Asenov: Measuring flow of fluids (in Bulgarian), Sofia, Bulgaria, Technical University of Sofia, 2007.

- [2.] Kremlevskij, P.: Flow meters and devices for measuring quantities (in Russian), Leningrad, Mashinostroene, 1975.
- [3.] Krisnawati, A. and Muchlish, A. M.: Variability of Biomass and Harvest Index from Several Soybean Genotypes as Renewable Energy Source, [www.sciencedirect.com](http://www.sciencedirect.com), The 3rd Indo-EBTKE ConEx 2014, Indonesia, Energy Procedia65, pp. 14-21, 2015.
- [4.] Panaiotov, L.: Device for measuring the parameters of waste biomass obtained from the harvest of cereals (in Bulgarian under print), Ruse, Bulgaria, Technical papers of the Ruse University, 2016.
- [5.] Reyns, P., Missotten, B., Ramon, H. and De Baerdemaeker, J.: A Review of Combine Sensors for Precision Farming, Precision Agriculture (manufactured in the Netherlands), vol. 3, pp. 169 – 182, 2002.
- [6.] Shiralkar, M.: LabVIEW Graphical Programming Course, Collection Editor: National Instruments, on-line: <http://cnx.org/content/col10241/1.4/>, Rice University.
- [7.] SolidWorks – general course (in Bulgarian), Sofia, Bulgaria, TechnoLogika Ltd., 2004.
- [8.] <http://www.agrister.com/combiners/claas-medion-340>
- [9.] [http://nd-international.com/onewebmedia/Strawbale\\_Dom-zajiveene.pdf](http://nd-international.com/onewebmedia/Strawbale_Dom-zajiveene.pdf)
- [10.] <http://ires.bg/straw.php>



ISSN: 2067-3809

copyright © University POLITEHNICA Timisoara,  
Faculty of Engineering Hunedoara,  
5, Revolutiei, 331128, Hunedoara, ROMANIA  
<http://acta.fih.upt.ro>

# Fascicule 2

## [ April - June ]

### t o m e

# [2018] XI

**ACTA**Technica**CORVINIENSIS**  
BULLETIN OF ENGINEERING



**ISSN: 2067-3809**

copyright © University POLITEHNICA Timisoara,  
Faculty of Engineering Hunedoara,  
5, Revolutiei, 331128, Hunedoara, ROMANIA  
<http://acta.fih.upt.ro>

<sup>1</sup>Monday Itopa MOMOH, <sup>2</sup>Mohammed Sani ADAMS

# CORROSION BEHAVIOR OF GALVANNEALED STEEL SUBSTRATE IN SALINE ENVIRONMENT

<sup>1,2</sup> Department of Metallurgical & Materials Engineering, Kogi State Polytechnic, NIGERIA

**Abstract:** In this research, low carbon steel and Al-1200 series was used in the development of galvanized steel; hot dip technique was adopted for the immersion at varied time ranging between 0 and 60 seconds. Muffle furnace was used for the annealing operation which precedes the corrosion experiment where weight loss technique was adopted. From the result, it was observed that the sample hot-dipped and held for 30 seconds gives better adhesive property between Al-Zn and Fe substrate thus indicating that it is feasible to develop galvanized steel using low carbon steel. Aluminium (1200 series) and zinc was generally found to improve the corrosion resistance of the steel, thus galvanized steel has better corrosion resistance in simulated sea water to represent the saline environment.

**Keywords:** Annealing, In-line annealing, Galvannealing, retention time

## INTRODUCTION

Corrosion is a natural phenomenon, which converts refined metal to their more stable oxide. It is the gradual destruction of materials (usually metals) by chemical reaction with their environment. To avert this phenomenon, different routes or techniques have been adopted to improve on the sustainability of the unstable and thermodynamically stable materials.

The developments of new and improved materials as an 'underpinning technology', which is one of the implored techniques, have been well regarded by most industrial nation (Small and Bishop, 1999). This is because it enhances innovation in all branches of engineering. One engineering material that has greatly explored a wide range of application is ferrous materials. The versatility application of ferrous materials is attributed to its amenability to alloying and heat-treatment which makes it possible to modify its properties to site specific service requirements (Momoh and Alaneme, 2015). One of such application is in the development of galvanized steel that has final use in areas where high corrosion and reasonable wear resistance is required (Abdulhameed, 2005).

Developed galvanized low carbon steel has been widely used in chemical plant in order to improve the corrosion resistance of vessels or section call units or lines that are interconnected by metal piping. Such material streams can include fluids (gas or liquid carried in piping) or sometimes solid or mixture such as slurries. Galvanized steel provides corrosion protection without affecting the integrity of the steel. It has been observed that galvanized steel exhibited excellent durability despite the harsh industrial and coastal environment or pH environment; this is due to its high resistant to corrosion (Max *et al.* 2003).

Galvanized or galvanized is the result from the combined process of galvanizing and annealing to produce specialized sheets of steel. The galvanization is made through the hot –

dipping (hot – dip galvanizing) process and immediate in-lines annealing and gives a very fine greyish matter finish. Galvanized does not flake of its galvanized coating when formed, stamped, and bent. The very fine malte finish acts like a primer, allowing paint to adhere easily, and is very rust proof; only white to dark grey marks appear if it comes in contact with water.

Galvanized sheet is carbon steel sheet coated with zinc on both sides by the continuous hot-dipped process. Immediately as the stripe exits the coating, the zinc coating is subject to an in-line heat treatment that converts the entire coating to a zinc iron alloy (Hambidge and Krebs, 2007). Conversion to the alloy results in a non-spangle finish which makes the sheet suitable for painting after fabrication (Sere *et al.*, 2015). This research is to generate a high adhesive Fe-Al-Zn ternary structure intermetallic compound on the corrosion resistance and investigate the feasibility and reliability of indigenous produced low carbon steel.

## MATERIALS AND METHOD

### — Materials and Equipments

Materials used for this project includes; low carbon steel plate of chemical composition shown in Table 1, zinc (Zn) and (Al). The equipment used for this research includes; metallurgical microscope of varied magnifications for microstructural view/examination. Muffle furnace was used for heat treatment operation (annealing) during the research. Micro hardness tester also used to determine the thickness of the coated steel. Digital weighing balance of 0.1g accuracy was used in the corrosion experiment to determine the weight lost and the corresponding rate.

### — Method

The specimen was delivered in smooth 5 mm thickness form and some preparations need to be carried with the chemical composition as shown in Table 4.1. The sample was prepared by sourcing of low carbon steel which was machined into corrosion coupons. By using hack saw to cut

it into a size of 2.8 x 1.8 x 0.5 cm. A binary Al-Zn phase was formed by the melting of 99.7 % Zn was melted in 0.3 % Al at 660°C, stirred to ensure thorough homogeneity. A hot dip approach was adopted in coating the substrate in the Al-Zn molten solution. And each sample was immersed in the melt and allowed to soak for 0, 30 and 60 seconds. This is followed by *annealing* operation in a muffle furnace maintained at 400°C and allowed to soaked again for 45 minutes. The produced GA-steel were later immersed in a simulated saline environment by dissolving 3.5g NaCl in 500ml distilled water to form the desired environment. The weight was measured at a regular interval of 3 days, before calculating the metal loss and the corrosion rate of the samples using equation (i) and (ii) as adapted from ASTM G1-G4 standard (Momoh, 2012).

$$\text{Metal Loss} = \frac{\text{Weight Loss (g)} * K}{\text{Alloy Density (gcm}^{-3}) * \text{Exposed Area (A)}} \quad (i)$$

$$\text{Corrosion Rate} = \frac{\text{Weight Loss (g)} * K}{\text{Alloy Density (gcm}^{-3}) * \text{Exposed Area (A)} * \text{Exposure Time (hr)}} \quad (ii)$$

### RESULTS AND DISCUSSION

The results of the experiment before and after corrosion are shown thus.



Figure 1: Picture of developed GA-steel (at 0 seconds retention)

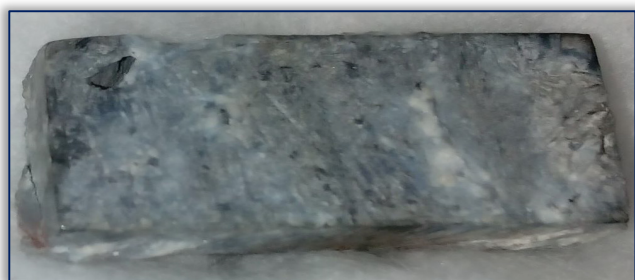


Figure 2: Picture of developed GA-steel (after 30 seconds retention)



Figure 3: Picture of developed GA-steel (at 60 seconds retention)

Table 1: Chemical composition of the steel

Element	Composition (wt.%)
C	0.0407
Si	0.1129
S	0.0004
P	0.0052
Mn	0.6122
Ni	0.1320
Al	0.0147
Fe	98.5323

Table 2: Sample designation

S/N	Sample	Soaking time (Seconds)
1	A	Control
2	B	0
3	C	30
4	D	60

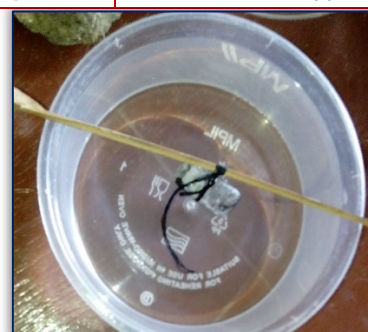


Figure 4: Picture of corrosion setup

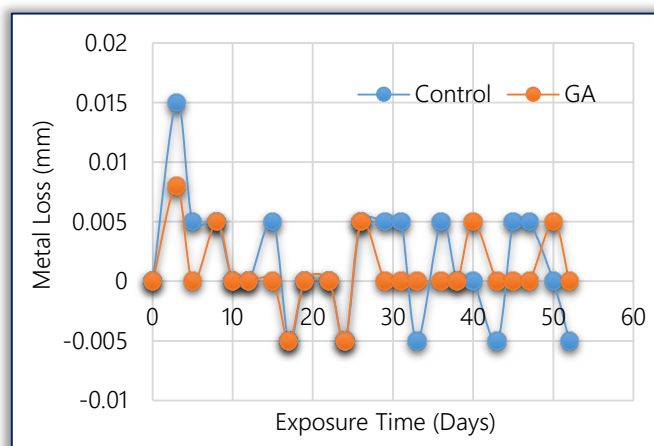


Figure 5: Variation of weight loss against Exposure time

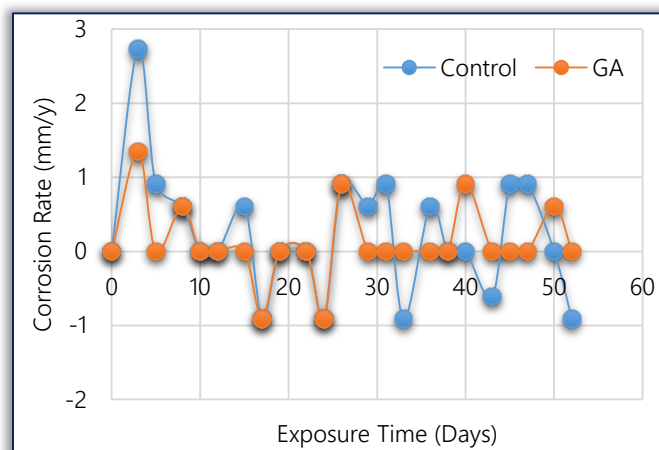


Figure 6: Corrosion rate versus Exposure time (in days)

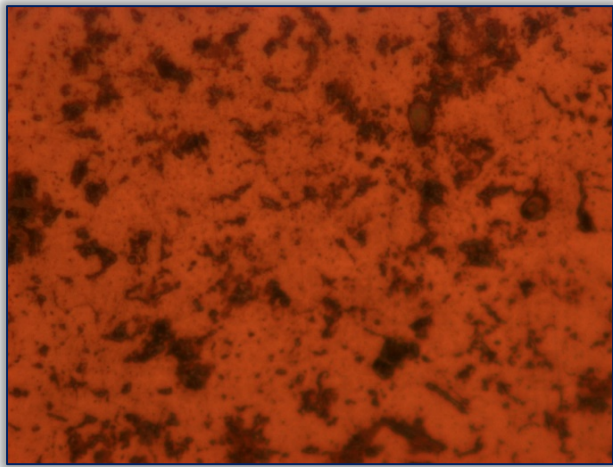


Figure7: Micrograph of the as-received steel (Sample A, X200)

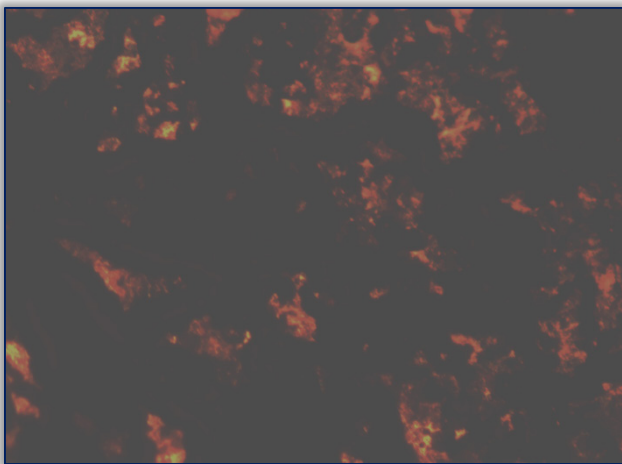


Figure 8: Micrograph of sample A after 52 days of immersion displaying predominantly corrosion products (dark phases), X200

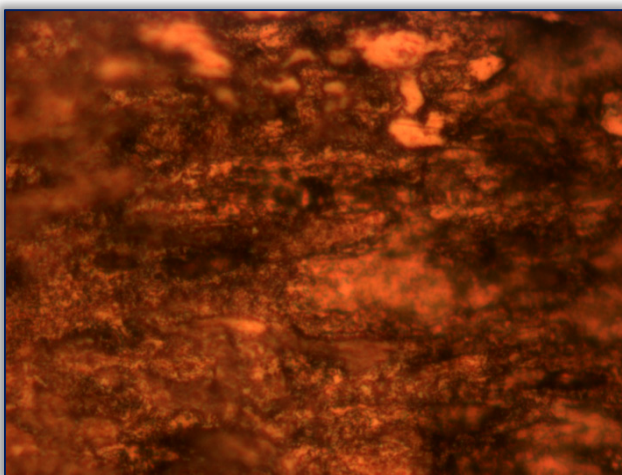


Figure 9: Micrograph of the developed GA steel after 52 days of immersion showing slight corrosion products (dark phases) on the exposed area, X200

This project has made a tremendous attempt to develop the same galvanneal steel with a different aluminum grade (1200 series). The results are as shown in Figures 1–9. From the results, it was observed that the Fe-Al-Zn ternary phase formed on the surface of sample B and D (i.e at 0 and

60 seconds retention time as shown in Figure 1 and 3) has a very poor adhesive property. Wherefore, sample C with 30 seconds retention time (Figure 2) before annealing operation was found to possess a better adhesive property as it stocked to the steel surface.

After 52 days of immersion in the prepared NaCl environment, Figure 5 shows the metal or mass loss of the sample C (which has a better adhesion). Here, it was observed that the developed GA-steel, in most of the time spent in the environment, was immune to the attack as it maintains stability. The initial loss experienced by the sample could be as a result of the of the expose area since the coating was not homogenously distributed over the sample surface. This is further explained in the corrosion rate plot in Figure 6, where the sinusoidal trend of the sample A (control sample) is clearly shown.

Figure 7–9 show the microstructures of the samples before and after immersion in the prepared simulated sea water environment.

Figure 7 shows the conventional ferrite/pearlite in the microstructure of the low carbon steel. After a total 52 days of immersion, the resulting structures were also viewed and as shown in Figures 8 and 9 for the control and the GA steel respectively, the GA-steel was observed to have been able to resist the attack of the environment; wherefore the blank shows different dark spots indicating corrosion products.

### CONCLUSIONS

In the development of galvanneal steel, low carbon steel and Al-1200 was selected alongside zinc granules, and hot-dip galvanizing method was adopted which precedes the simultaneous annealing operation prior to microstructural examination and which was done before and after corrosion experiment. And from the result, the following were observed:

- Development of GA-steel using low carbon steel is feasible with Al-1200 to improve on the adhesive property
- Al-1200 and Zn granules can form a ternary phase which improves the corrosion resistance of low carbon steel, and
- Galvanneal steel has better corrosion resistance in marine environment.

### References

- [1] Smallman R.E and Bishop R.J, (1999): Modern Physical Metallurgy and Materials Engineering. 6<sup>th</sup> Edition. Butterworth Heinemann. UK. Pp. 120 – 176.
- [2] Momoh I.M. and Alaneme K.K. (2014): Mechanical Properties and corrosion behaviour of micro-duplex medium carbon low alloy steel. International Journal of Engineering. Vol. 12, Pp 386 – 392.
- [3] Abdulhameed A. (2005): Evaluation of quality of steels produced locally. B.Eng Thesis, Department of Mechanical Engineering, University of Ilorin, Ilorin, Nigeria. pp 1 – 5.
- [4] Kharakwal J.S. & Gurjar L.K. (2006): "Zinc and Brass in Archaeological Perspective. Ancient Asia. 1". Journal of the Society of South Asian Archeology. Pp 139 – 159.

- [5] Hambidge, K. M. & Krebs, N. F. (2007): "Zinc deficiency: a special challenge". *J. Nutr.* Vol. 137 Issue 4, Pp.1101–5.
- [6] Seré P.R., Deyá C., Elsner C.I., Di Sarli A.R. (2015): Corrosion of painted galvanized steel. *Procedia Materials Science* 8. International Congress of Science and Technology of Metallurgy and Materials, SAM - CONAMET 2013. Pp 1 - 10.
- [7] Momoh, I.M. (2012), "Microstructures, Corrosion and Mechanical behavior of dual phase medium carbon low alloy steels", Unpublished Master Thesis, Federal University of Technology, Nigeria. Pp 36-40.



ISSN: 2067-3809

copyright © University POLITEHNICA Timisoara,  
Faculty of Engineering Hunedoara,  
5, Revolutiei, 331128, Hunedoara, ROMANIA  
<http://acta.fih.upt.ro>

<sup>1</sup>Milica JOVIĆ, <sup>2</sup>Mirjana LAKOVIĆ

# CARBON FOOTPRINT METHOD - A CASE STUDY FOR THERMAL POWER PLANTS IN REPUBLIC OF SERBIA

<sup>1,2</sup>University of Niš, Faculty of Mechanical Engineering, Niš, SERBIA

**Abstract:** There are many methods for the analysis of the negative impact of thermal power plants on the environment. In this paper will be presented a method Carbon footprint. Carbon footprint originated from the Ecological Footprint and independently developed. This method is one of the newer methods. By defining this method the goal is to raise the awareness of citizens about pollution. This method can be applied in other areas, not only in terms of the power plant. Carbon footprint is based on the definition of greenhouse gasses through carbon dioxide equivalent. From there the name of this method Carbon footprint. In this paper, is done research how the work of thermal power plants that use coal as fuel affect emissions. Was analyzed the operation of thermal power plants that use fossil fuels because in the Republic of Serbia the most electricity is obtained from these plants.

**Keywords:** carbon footprint, carbon dioxide, coal, thermal power plants, emission factor

## INTRODUCTION

The tendency of increasing emissions of greenhouse gasses leads to the long-term goal of establishing control of environmental impacts caused by climate change. The carbon footprint has become a widely used concept in emissions assessments [1].

The term carbon footprint is used for greenhouse gas emissions and is generally expressed as CO<sub>2</sub> equivalents (CO<sub>2</sub>e), which consists of emissions of CO<sub>2</sub>, CH<sub>4</sub> and N<sub>2</sub>O. These gasses are translated into the amount of CO<sub>2</sub> (this is called the equivalent amount of CO<sub>2</sub>). It is a measure of the total amount of carbon dioxide in the atmosphere in a given time frame which is directly or indirectly transmitted. Carbon footprint helps us to determine the amount of emissions from various sectors, which is useful for quantifying the impact of human activities on the environment and global warming. In the postindustrial era, the concentration of carbon dioxide in the atmosphere is increasing alarmingly.

It is necessary to strive to reduce CO<sub>2</sub> emissions from all sectors but with special emphasis on the reduction of CO<sub>2</sub> emissions from the power plant sector. Approximate values of CO<sub>2</sub> emissions along with few major greenhouse gasses are referred as Carbon Footprint.

Carbon Footprint is a concept which is yet in developing stage. Carbon footprint as an indicator of the environment is used. Carbon footprint quantifies the main sources of emissions and represents an effective tool for environmental protection and energy management.

In the case of thermal power plants the equation to calculate the carbon footprint is [2]:

$$\text{Carbon footprint (tons CO}_2\text{/year)} = \text{Yearly electricity consumption of the plant (MWh/year)} \times \text{Emission factor (tons CO}_2\text{/MWh)}.$$

It is necessary to strive to reduce CO<sub>2</sub> emissions from all sectors but with special emphasis on the reduction of CO<sub>2</sub> emissions from the power plant sector. Approximate values of CO<sub>2</sub> emissions along with few major greenhouse gasses are referred as Carbon Footprint. Carbon Footprint is a concept which is yet in developing stage. Carbon footprint as an indicator of the environment is used. Carbon footprint quantifies the main sources of emissions and represents an effective tool for environmental protection and energy management.

## ANALYSIS OF CARBON FOOTPRINT FROM THE THERMAL POWER PLANTS IN REPUBLIC OF SERBIA

In the Republic of Serbia, the installed power capacity for electricity production is 8 359 MW [3]. Eight power plants with 25 blocks that use lignite as a fuel and the installed capacity of 5.171 MW, two of these power plants are located in Kosovo and Metohija. Cogeneration plant with a total installed capacity of 425 MW of electricity generation, 505MW for the production of thermal energy. From 1 June 1999, the Electric Power Industry of Serbia does not manage its capacity in Kosovo and Metohija.

The energy sector in Serbia has some characteristic weaknesses that contribute to high energy consumption and high emissions of CO<sub>2</sub>. These disadvantages are low efficiency due to outdated technology in the sectors of production and consumption, high losses in electricity distribution. In order to reduce CO<sub>2</sub> emissions is necessary to implement a project that will examine what is possible to improve the thermal power plants to reduce emissions of CO<sub>2</sub> and then put into practice these tests. Any minimal reduction of this gas would bring great benefits to air quality.

Table 1 shows the production of electricity for 2014 by months.

Table 1. Produced electricity by month for the 2014 year from the power plant Nikola Tesla A and B, Kolubara, Morava and Kostolac [3]

The produced electricity in GWh for the 2014 year					
Month	Nikola Tesla A	Nikola Tesla B	Kolubara	Morava	Kostolac
January	1028	847	109	47	
February	968	750	95	48	
March	1005	859	87	53	
April	931	639	65	52	
May	368	335	17	56	
June	440	364	3	18	
July	537	418	11	65	
August	459	415	0	31	
September	510	645	0	0	
October	549	749	23	22	
November	504	757	19	62	
December	550	745	30	35	
In total	7849	7523	459	488	4132

On the basis of the Report on operations for 2014 was obtained data on the total quantity of electricity in thermal power plant Kostolac and it amounts to 4132 GWh. In addition, to calculate the amount of carbon footprint from thermal power plants, it is necessary to know the value of the emission factor. The emission factor is different for each thermal power plant.

Based on the research that has been shown in [4] values for carbon dioxide emission factor for thermal power plants Nikola Tesla A and Nikola Tesla B were used and that values are shown in Table 2.

Table 2. Carbon dioxide emission factor

Power plant	The mean value of CO <sub>2</sub> emission factor [kg CO <sub>2</sub> /kWh]
Nikola Tesla A	1,16
Nikola Tesla B	1,09

Due to lack of data on the mean value of CO<sub>2</sub> emission factor for others power plants in the Republic of Serbia, a value 1.15 [kg CO<sub>2</sub> / kWh] was used. Based on the known production of electricity and the value of CO<sub>2</sub> emission factor can be calculated the carbon footprint of power plants whose values are shown in Table 3 and Figure 1.

Table 3. Carbon footprint from thermal power plants for the 2014 year

Termoelektrana	Carbon footprint [t CO <sub>2</sub> /year]
Nikola Tesla A	9 104 840
Nikola Tesla B	8 200 070
Kolubara	527 850
Morava	561 200
Kostolac	4 751 800
Ukupno	23 145 760

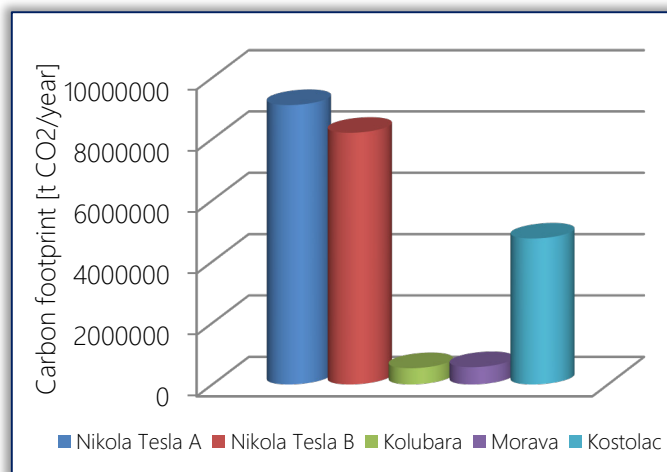


Figure 1. Carbon footprint from thermal power plants for the 2014 year

From the table above, and the Figure 1 can be concluded that the thermal power plants Nikola Tesla A and B produce the greatest amount of CO<sub>2</sub> e. The reason is that these plants are the biggest producers of electricity in the Republic of Serbia. It is necessary to improve individual systems in these thermal power plants in order to reduce the overall pollution which they produce. These thermal power plants constantly improve their systems and have environmental protection projects. Projects that are currently open in thermal power plants Nikola Tesla are [5]:

- » reconstruction of electrostatic precipitator
- » improvement of the system for transport and disposal of ash and slag
- » construction of desulphurization and reduction of NO<sub>x</sub> primary measures
- » continuous measurement of emissions of hazardous and harmful substances in the blocks
- » eliminating the negative impact of waste on land and water
- » reduction of the impact of ash on the environment

In addition to these projects carried out within the thermal power plant Nikola Tesla with the goal of reducing greenhouse gas emissions and reduce the impact on global warming from the energy sector is necessary to implement and renewable energy sources for electricity production.

## CONCLUSIONS

Fossil fuels are closely related to environmental pollution. It pollutes environmental on the direct or indirect way by using fossil fuels in the exploitation, processing, or their consumption. The threat of global warming requires more efficient technologies for the use of fossil fuels and other sources of energy that do not produce carbon dioxide. The environment can be protected using various measures and methods.

In this paper a method Carbon Footprint is presented. Carbon footprint has appeared as a strong and popular indicator of greenhouse gasses with special emphasis on carbon dioxide. This method confirms that the power plants are big polluters



and that the work of thermal power plants using fossil fuel impacts negatively on global warming.

Discussed the specific case of the Republic of Serbia because there most of the electricity is produced from fossil fuels. This study found that in the near future must be more intensive work on the modernization and improvement of electrostatic precipitators and systems for gas emissions in order to reduce the negative impact.

As shown methods Carbon footprint is directly related to the production of electricity. People are becoming more dependent on electricity, which will cause the increase in capacity for the production of electricity and with that increase, if we continue with this trend, there will be an increase in carbon dioxide emissions. It is necessary to consider the application of alternative energy sources. In order to maintain climatic conditions, it is necessary to continue to invest in energy-efficient systems that make better use of energy.

#### Note

This paper is based on the paper presented at 13th International Conference on Accomplishments in Mechanical and Industrial Engineering – DEMI 2017, organized by University of Banja Luka, Faculty of Mechanical Engineering, in Banja Luka, BOSNIA & HERZEGOVINA, 26 – 27 May 2017.

#### References

- [1] Andri et al. Environmental performance assessment of retrofitting existing coal fired power plants to co-firing with biomass: carbon footprint and emergy approach, Journal of Cleaner Production 103 (2015) 13-27
- [2] Chrysi Laspidou et al., Carbon Footprint Calculation Of Desalination Units In Greece, Fresenius Environmental Bulletin, Volume 21, No. 8b, January 2012
- [3] www.eps.rs, accessed on 2017-03-25.
- [4] Marković et al., Determination of the Specific Carbon Dioxide Emission Factor from Thermal Power Plants Nikola Tesla A and B, Full Papers Proceeding of International Conference "Power Plants 2014", 28-31.October, 2014, Zlatibor Serbia, ISBN 978-86-7877-024-1
- [5] www.tent.rs, accessed on 2017-03-26



ISSN: 2067-3809

copyright © University POLITEHNICA Timisoara,  
Faculty of Engineering Hunedoara,  
5, Revolutiei, 331128, Hunedoara, ROMANIA  
<http://acta.fih.upt.ro>

# Fascicule 2

## [ April - June ]

### t o m e

# [2018] XI

**ACTA**Technica**CORVINIENSIS**  
BULLETIN OF ENGINEERING



**ISSN: 2067-3809**

copyright © University POLITEHNICA Timisoara,  
Faculty of Engineering Hunedoara,  
5, Revolutiei, 331128, Hunedoara, ROMANIA  
<http://acta.fih.upt.ro>

<sup>1</sup>Dimitar LOLOV, <sup>2</sup>Svetlana V. LILKOVA- MARKOVA

## DYNAMIC STABILITY OF DOUBLE-WALLED CARBON NANOTUBES

<sup>1,2</sup> University of Architecture, Civil Engineering and Geodesy, Department of Technical Mechanics, Sofia, BULGARIA

**Abstract:** This paper investigates the stability of a simply supported DWCNT conveying fluid inside its innermost tube. The van der Waals interaction between the adjacent carbon layers are taken into account. The Euler elastic beam model is employed in order to study the dynamic stability behavior of the system. The aim is to analyze the influence of the density of the conveyed fluid, the length of the tube and the dimensions of its cross section on the critical flow velocity of the fluid in the pipe under consideration and to draw conclusions about the stability of the system. This problem is approached numerically using the spectral Galerkin method. Results reveal that all above mentioned parameters have a significant effect on the stability of the nanotube.

**Keywords:** dynamic stability, fluid-conveying carbon nanotubes, van der Waals interaction, critical velocity

### INTRODUCTION

Carbon nanotubes (CNTs) are formed by a crystal lattice of carbon atoms in a periodic hexagonal arrangement and have a cylindrical shell shape. Since 1991 these tubes are used in nanophysics, nanobiology and nanomechanics in nanofluidic devices, nanocontainers for gas storage and nanopipes conveying fluid. They are with perfect hollow cylindrical geometry and superior mechanical strength. The flowing fluid can be water, oil, dynamic flow of methane, ethane and ethylene molecules. These flows inside carbon nanotubes are attractive research topic in recent years.

In [6] the problem of fluid-structure interaction is considered in the case of nanoscale. However, the experiments at the nanoscale are difficult and expensive. That is why the continuum elastic models have been used to study the fluid-structure interaction. The carbon nanotubes are considered with Euler- and Timoshenko-beam models.

Yoon et al. in [9] applied the Euler beam model for investigation of a cantilevered carbon nanotube conveying fluid, with or without being embedded into an elastic medium such as polymer. The same authors in [10] investigated carbon nanotubes, this time simply supported or clamped at both ends. They obtained the critical flow velocity of the transported fluid in the case of loss of stability of the pipe. The numerical results indicate that the flowing fluid has a substantial effect on vibrational frequencies of the system. On the other hand, their results showed that surrounding elastic medium influence on the effect of internal moving fluid on the vibration of the system.

L.Wang in [5] investigated double-walled carbon nanotubes (DWCNT) with flowing fluid. Y.Yan et al. in [8] studied the instability of triple-walled carbon nanotubes (TWCNT) conveying fluid based on the Euler–Bernoulli beam model. The obtained critical flow velocities of the transported fluid are by a pitchfork bifurcation and a Hamiltonian Hopf bifurcation. The Van der Waals interactions between different carbon nanotubes are taken into account. Numerical results

show that these interactions influence on the natural frequencies and the stability of nanotubes.

E. Ghavanloo et al., [1] investigated the multi-walled carbon nanotubes (MWCNT) as an elastic Euler–Bernoulli beam in order to study the stability of the system. Y. Kuang et al. considered in [3] the influence of the geometric nonlinearity and the nonlinearity of van der Waals forces on the vibration of the double-walled carbon nanotubes conveying fluid. R. Tuzun et al., [4] investigated nanotubes with flowing fluid. The conclusion of their paper is that the dynamic behavior of the fluid depends on the physical and geometric characteristics of the pipe and the density of the fluid.

### FORMULATION OF THE PROBLEM AND METHOD OF THE SOLUTION

A double-walled carbon nanotube (DWCNT) with van der Waals interaction between the adjacent layers is considered herein. A fluid with constant velocity is flowing in the nanotube. The differential equations of the free transverse vibrations of the pipe, shown in [7], are:

$$EI_1 \frac{\partial^4 w_1}{\partial x^4} + m_f V^2 \frac{\partial^2 w_1}{\partial x^2} + 2m_f V \frac{\partial^2 w_1}{\partial x \partial t} + (m_f + m_{p1}) \frac{\partial^2 w_1}{\partial t^2} = p_1; \quad (1)$$

$$EI_2 \frac{\partial^4 w_2}{\partial x^4} + m_{p2} \frac{\partial^2 w_2}{\partial t^2} = p_2. \quad (2)$$

Here  $x$  is the axis coordinate,  $t$  is the time,  $w_1$  and  $w_2$  are respectively the transverse displacements of the innermost and the outermost layer of DWCNT.  $E$  is the modulus of the linear deformations. The names  $I_1$ ,  $I_2$  and  $m_{p1}$ ,  $m_{p2}$  are respectively the moments of inertia of the cross-section and the masses per unit length of the innermost and outermost layers of the nanotube.  $V$  is the velocity of the flowing fluid.  $p_1$  and  $p_2$  are the van der Waals forces between the two adjacent layers of the pipe. They act respectively on the innermost ( $p_1$ ) and on the outermost ( $p_2$ ) layers of the tube.

These interaction forces are expressed as follows [2]:

$$p_1 = c_{12}(w_1 - w_2); \quad (3)$$

$$p_2 = c_{21}(w_2 - w_1); \quad (4)$$

$$c_{12} = -2R_1R_2 \left( \frac{1001 \pi \varepsilon \sigma^{12}}{3 a^4} E_{12}^{13} - \frac{1120 \pi \varepsilon \sigma^6}{9 a^4} E_{12}^7 \right); \quad (5)$$

$$E_{12}^7 = (R_1 + R_2)^{-7} \int_0^{\pi/2} \frac{d\theta}{(1 - k_{12} \cos^2 \theta)^{3.5}}; \quad (6)$$

$$E_{12}^{13} = (R_1 + R_2)^{-13} \int_0^{\pi/2} \frac{d\theta}{(1 - k_{12} \cos^2 \theta)^{6.5}}; \quad (7)$$

$$k_{12} = \frac{4R_1R_2}{(R_1 + R_2)^2}. \quad (8)$$

$R_1$  and  $R_2$  are the inner radii of the two layers of the nanotube,  $a$  is the C–C bond length.  $\varepsilon$  is the depth of the potential,  $\sigma$  – a parameter that is determined by the equilibrium distance in [2].

For convenience of the solution of the differential equations (1) and (2) non-dimensional coordinates are introduced:

$$\xi = \frac{x}{L}; \quad \eta_1 = \frac{w_1}{L}; \quad \eta_2 = \frac{w_2}{L};$$

$$\tau = \sqrt{\frac{EI_1}{m_f + m_{p1}}} LV;$$

$$u = \sqrt{\frac{m_f}{EI_1}} LV; \quad \beta_1 = \frac{m_f}{m_f + m_{p1}}; \quad (9)$$

$$\beta_2 = \frac{m_{p2} l_1}{(m_f + m_{p1}) l_2};$$

$$\bar{c}_{12} = \frac{c_{12} L^4}{EI_1}; \quad \bar{c}_{21} = \frac{c_{21} L^4}{EI_2}.$$

$L$  is the length of the nanotube. Then the equations (1) and (2) rewritten in dimensionless form are:

$$\frac{\partial^4 \eta_1}{\partial \xi^4} + u^2 \frac{\partial^2 \eta_1}{\partial \xi^2} + 2\sqrt{\beta_1} u \frac{\partial^2 \eta_1}{\partial \xi \partial \tau} + \frac{\partial^2 \eta_1}{\partial \tau^2} - \bar{c}_{12}(\eta_1 - \eta_2) = 0; \quad (10)$$

$$\frac{\partial^4 \eta_2}{\partial \xi^4} + \beta_2 \frac{\partial^2 \eta_2}{\partial \tau^2} - \bar{c}_{21}(\eta_2 - \eta_1) = 0. \quad (11)$$

The spectral Galerkin method is applied to approximate the solution of the boundary value problem (10), (11). According to this method, an approximate solution is sought in the form:

$$\eta_1 = \sum_{i=1}^n q_i(\tau) \phi_i(\xi);$$

$$\eta_2 = \sum_{i=1}^n q_{i+n}(\tau) \phi_i(\xi). \quad (12)$$

In these expressions  $q_i(\tau)$  and  $q_{i+n}(\tau)$  are unknown functions.  $\phi_i(\xi)$  are basic functions satisfying the boundary

conditions of the tube. The eigenfunctions for the nanotube with stationary fluid ( $\mathbf{V} = \mathbf{0}$ ) are used as basic functions in the present paper.

Substituting (12) in equations (10) and (11) one obtains the residual functions, which do not vanish identically since  $\eta_1(\xi, \tau)$  and  $\eta_2(\xi, \tau)$  are not exact solutions of equations (10) and (11). Here, and in the sequel, dots denote derivatives with respect to  $\tau$  and primes denote derivatives with respect to  $\xi$ .

$$R_1(\xi, \tau) = \sum_{i=1}^n \left[ q_i \phi_i^{IV} + u^2 q_i \phi_i^{II} + 2\sqrt{\beta_1} u \dot{q}_i \phi_i^I \right] + \dot{q}_i \phi_i - \bar{c}_{12}(q_i - q_{i+n}) \phi_i; \quad (13)$$

$$R_2(\xi, \tau) = \sum_{i=1}^n \left[ q_{i+n} \phi_i^{IV} + \beta_2 \ddot{q}_{i+n} \phi_i \right] - \bar{c}_{21}(q_{i+n} - q_i) \phi_i. \quad (14)$$

According to the standard Galerkin procedure, the residual functions  $R_1(\xi, \tau)$  and  $R_2(\xi, \tau)$  should be orthogonal to the basic functions in the area  $\xi \in [0; 1]$ :

$$\int_0^1 R_1(\xi, \tau) \phi_s(\xi) d\xi = 0, \quad s = 1, \dots, n \quad (15)$$

$$\int_0^1 R_2(\xi, \tau) \phi_s(\xi) d\xi = 0, \quad s = 1, \dots, n. \quad (16)$$

The result of the application of (15) and (16) is a system of  $2n$  differential equations about the unknown functions  $q_i(\tau)$ . This system for the differential equations (10) and (11) is:

$$\int_0^1 \sum_{i=1}^n \phi_s \left[ q_i \phi_i^{IV} + u^2 q_i \phi_i^{II} + 2\sqrt{\beta_1} u \dot{q}_i \phi_i^I \right] d\xi = 0; \quad (17)$$

$$\int_0^1 \sum_{i=1}^n \phi_s \left[ q_{i+n} \phi_i^{IV} + \beta_2 \ddot{q}_{i+n} \phi_i \right] - \bar{c}_{21}(q_{i+n} - q_i) \phi_i d\xi = 0. \quad (18)$$

For a pipe with a static scheme of a simply supported beam the basic functions are:

$$\phi_i(\xi) = \sin(\lambda_i \xi). \quad (19)$$

The following expressions are valid:

$$\delta_{si} = \int_0^1 \phi_s \phi_i d\xi = \begin{cases} 0.5, & s = i; \\ 0, & s \neq i; \end{cases} \quad (20)$$

$$b_{si} = \int_0^1 \phi_s \phi_i^I d\xi = \begin{cases} \frac{\lambda_s \lambda_i [1 - (-1)^{s+i}]}{\lambda_s^2 - \lambda_i^2}, & s \neq i; \\ 0, & s = i; \end{cases} \quad (21)$$

$$d_{si} = \int_0^1 \phi_s \phi_i^{II} d\xi = -0.5 \lambda_i^2 \delta_{si}. \quad (22)$$

The expressions (20), (21) and (22) are substituted in (17) and (18). Then the following system of  $2n$  pcs second-order differential equations for the unknown functions  $q_i(\tau)$  is obtained:

$$\sum_{i=1}^n \left[ \delta_{si} \lambda_i^4 q_i + u^2 d_{si} q_i + 2\sqrt{\beta_1} u b_{si} \dot{q}_i \right] + \delta_{si} \dot{q}_i - \bar{c}_{12}(q_i - q_{i+n}) \delta_{si} = 0; \quad (23)$$

$$\sum_{i=1}^n \left[ \lambda_i^4 \delta_{si} q_{i+n} + \beta_2 \delta_{si} \ddot{q}_{i+n} \right] - \bar{c}_{21}(q_{i+n} - q_i) \delta_{si} = 0. \quad (24)$$

The system of differential equations (23) and (24) can be written in the following matrix form:

$$|M|\ddot{q} + |C|\dot{q} + |K|q = 0. \quad (25)$$

The characteristic equation of the system (25) is:

$$\det(X) = 0. \quad (26)$$

The members of the matrix  $X$  are obtained by the following formula:

$$X_{km} = \lambda^2 M_{km} + \lambda C_{km} + K_{km} \quad (27)$$

It is well known that the knowledge of the roots  $\lambda$  of the characteristic equation (25) is sufficient for the stability analysis. The system is stable if the real parts of the roots are negative. The characteristics of the system and the velocity of the transported fluid influence on these roots. Then the critical velocity of the flowing fluid  $V_{cr}$  can be obtained

### NUMERICAL RESULTS

A double-walled carbon nanotube (DWCNT) supported as a simple beam is considered. The thickness of the two adjacent layers of the tube and the gap between them are 0.34 nm (Figure 1).

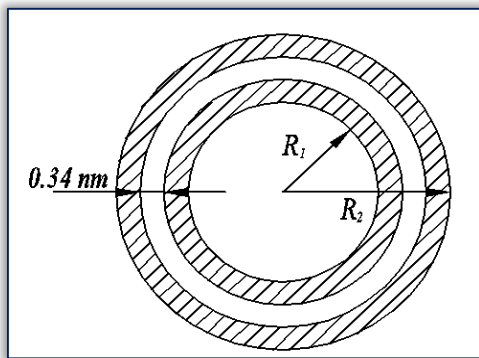


Figure 1: Cross-section of the tube

The parameters that are used to calculate van der Waals' forces according to formula (5) are:

$$\varepsilon = 2.968 \text{ meV},$$

$$a = 1.42 \text{ \AA} \text{ and } \sigma = 3,407 \text{ \AA}.$$

The characteristics of the material of the tube are: modulus of linear elasticity  $E = 1 \text{ TPA}$ , density  $2.3 \text{ g/cm}^3$ . Several types of flowing fluid are investigated with its density ranging in the interval  $0.5 - 1.5 \text{ g/cm}^3$ .

The results obtained show the relationship between the density of the fluid and its critical velocity for tubes with lengths  $L = 10 \mu\text{m}$ ,  $20 \mu\text{m}$  and  $30 \mu\text{m}$  and for two different cross-sections of the pipe (Figure 2 and Figure 3).

The first cross-section under consideration is with a radius  $R_1 = 12 \text{ nm}$  (inner radius of the first layer) and  $R_2 = 12.64 \text{ nm}$  (inner radius of the second layer). The second cross-section is with  $R_1 = 20 \text{ nm}$  and  $R_2 = 20.64 \text{ nm}$ .

The results are shown in Figure 2 and Figure 3.

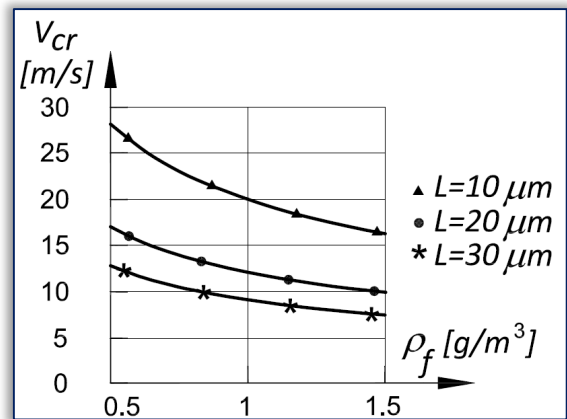


Figure 2: DWCNT with  $R_1 = 12 \text{ nm}$  and  $R_2 = 12.64 \text{ nm}$

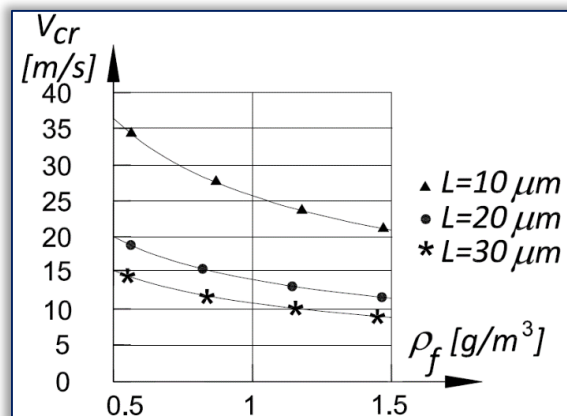


Figure 3: DWCNT with  $R_1 = 20 \text{ nm}$  and  $R_2 = 20.64 \text{ nm}$

### CONCLUSION

The results from numerical investigations show that for all considered tubes the critical velocity of the flowing fluid is reduced when the density of the fluid is increasing. The pipes with bigger length are less stable. Amongst the pipes with different cross section, more stable is the one with the largest radii  $R_1$  and  $R_2$ .

All obtained critical velocities in this paper correspond to loss of stability of the tube in divergent form.

### References

- [1] Ghavanloo E, Daneshmand F and Rafiei M 2010 Vibration and instability analysis of carbon nanotubes conveying fluid and resting on a linear viscoelastic Winkler foundation. *Physica E: Low-dimensional Systems and Nanostructures*. 42(9): 2218-2224
- [2] He X, Kitipornchai S and Liew K 2005 Buckling analysis of multi-walled carbon nanotubes: a continuum model accounting for van der Waals interaction. *Journal of Mechanics and Physics of solids*. 53: 303-326
- [3] Kuang Y and He X 2009 Analysis of nonlinear vibrations of double-walled carbon nanotubes conveying fluid. *Computational Materials Science*. 45(4): 875-880
- [4] R. Tuzun, D. Noid, B. Sumpter, R. Merkle, Dynamics of fluid flow inside carbon nanotubes. In: *Nanotechnology*, 7(3): 241-246, (1996).
- [5] L. Wang, Dynamical behaviors of double-walled carbon nanotubes conveying fluid accounting for the role of small

- length scale. In: Computational Materials Science, 45(2): 584-588, (2009).
- [6] M. Whitby, N. Quirke, Fluid flow in carbon nanotubes and nanopipes, In: Nature Nanotechnology, 2: 87-94, (2007).
- [7] Y. Yan, W. Wang, L. Zhang, Dynamical behaviors of fluid-conveying multi-walled carbon nanotubes, I: Applied Mathematical Modelling, 33: 1430-1440, (2007).
- [8] Y. Yan, X. He, L. Zhang, C. Wang, Dynamic behavior of triple-walled carbon nanotubes conveying fluid, In: Journal of Sound and Vibration, 319(3-5): 1003-1018, (2009).
- [9] J. Yoon, C. Ru, A. Mioduchowski, Flow-induced flutter instability of cantilever carbon nanotubes, In: International Journal of Solids and Structures, 43(11-12): 3337-3349, (2006).
- [10] J. Yoon, C. Ru, A. Mioduchowski, Vibration and instability of carbon nanotubes conveying fluid. In: Composites Science and Technology, 65(9): 1326-1336, (2005).



ISSN: 2067-3809

copyright © University POLITEHNICA Timisoara,  
Faculty of Engineering Hunedoara,  
5, Revolutiei, 331128, Hunedoara, ROMANIA  
<http://acta.fih.upt.ro>

<sup>1</sup>. Adewole Ayobami ADERINLEWO, <sup>2</sup> Abdul Kareem Adisa AGBOOLA,  
<sup>3</sup>. Olayemi Johnson ADEOSUN, <sup>4</sup>. Emmanuel Sunday Akin AJISEGIRI, <sup>5</sup>. Alex Folami ADISA

## INVESTIGATION OF SEPARATION OF PALM KERNEL AND SHELL ON AN INCLINED PLANE SEPARATOR

<sup>1-5</sup>Department of Agricultural Engineering, Federal University of Agriculture, Abeokuta, NIGERIA

**Abstract:** The separation of shell from kernel of two varieties of oil palm in Nigeria was investigated in a laboratory inclined plane separator. Four angles of projection of 25, 30, 35, 40 and 45° were used and three structural surfaces namely mild steel, galvanised steel and plywood were used for the separation experiment. Results show that the highest separation of 7.7 and 8.6 cm occurred on mild steel for dura and tenera at angles of projection of 35 and 40° respectively. That of galvanised steel was 8.7 and 9.7 cm at angles of 30 and 25° respectively while that of plywood was 17.0 and 13.0 cm at angles of 30 and 25° respectively. These provide useful guide in the selection of material and angle of projection for separation.

**Keywords:** Palm kernel, inclined plane separator, angle of projection, oil palm

### INTRODUCTION

Processing of palm kernels into palm kernel oil (PKO) and other byproducts involves cracking the palm kernels to obtain palm kernel nuts from where the oil is expressed. In developing countries like Nigeria, cracking is done by manual and mechanical methods. Cracking produces a mixture of broken shells and kernels. The nuts must be separated from the mixture for further processing into PKO. In small scale processing mills, the separation is done manually. However, manual separation is slow, tedious and not suitable for large scale production. Large scale processing mills adopt techniques based on density difference between the kernels and shells to effect separation. The two methods under this technique are clay-bath and hydro-cyclones. The two methods are known as wet processes since water is always involved and the kernels have to be dried at the end of the separation (Okorokwo et al, 2013). This increases both the time and cost of production. Thus their application in small scale mill is difficult (Poku, 2002).

Research efforts are now focused on developing dry separators to ameliorate the limitations of existing methods of separation. Different researchers have developed different dry separators for this purpose, a spinning disc separator (Koya and Faborode, 2006), incline table separator (Akubuo and Eje, 2002), sieve separator (Amoah et al, 2007), tray separator (Oke, 2007), angular projection separation (Onaku et al, 2013), winnowing system (Halim et al, 2009), nut and fibre separator (Ologunagba, 2010) and rotary separator (Olasunboye and Koya, 2014). However, the limitation of these separators is low separation efficiency. There is therefore the need to develop dry mechanical separators with high separating efficiency.

This work was therefore carried out to investigate the separation of palm kernel shell and nut on an inclined plane separator using different structural surfaces.

### METHODOLOGY

#### The Inclined Plane Separator

The laboratory inclined plane separator was designed and constructed at the Department of Agricultural and Bioresources Engineering, Federal University of Agriculture, Abeokuta, Nigeria. It consists of a hopper, an adjustable inclined plane and a collector. The material to be separated is poured into the hopper from where it flows into the inclined plane. The coefficient of friction of the components of the material on the inclined plane determines their motion on the inclined plane. The differences in motion cause them to fall at different spots on the collector where separation takes place. The picture and isometric view of the inclined plane separator are shown in Figure 1.

#### Separation Experiment on a Laboratory Incline Plane Separator

Dura and tenera varieties of palm kernels were obtained from the teaching and research farms of the Federal Universities of Agriculture, Abeokuta, Nigeria. The kernels were manually cleaned to remove foreign materials, dust, dirt and broken kernels. The kernels were then cracked with a palm kernel cracking machine available at the College of Engineering of the University.

The moisture content of the shell and kernel were determined by oven drying method and was found to be 4.5% and 5.0% w.b. for dura shell and kernel while for tenera it was 5.1% and 4.5% w.b. respectively.

Twenty kernels and shells of each of dura and tenera varieties were randomly selected and poured into the hopper of the separator from where they flow into the inclined plane by gravity. After sliding through the plane the shell and kernel fall into the collector. The base of the collector is filled with sand to enable the range (distance of fall of the kernel and the shell) to be measured. The separating plane of three structural surfaces namely mild steel, galvanized steel and plywood were used. They were inclined at different angles of 25, 30, 35,

40 and 45°. The difference in the distance of fall of both nut and shell (separation) was determined for each angle. The experiment was repeated five times for each angle and surface.

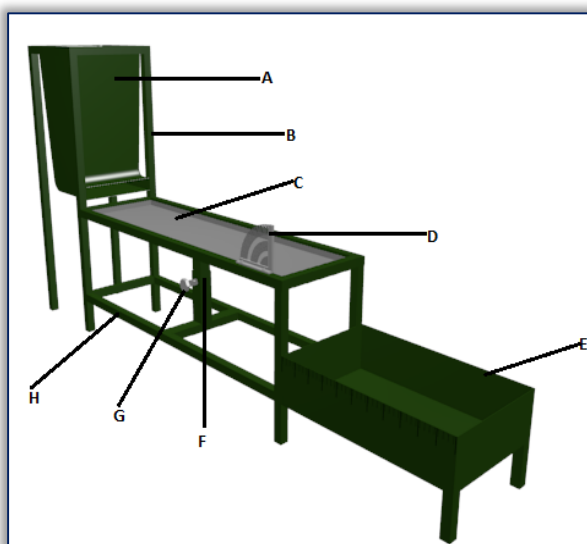


Figure 1. Picture and Isometric view of the inclined Plane Separator  
A – Hopper, B – Frame, C – Surface plane, D – Protactor,  
E – Collector, F – Adjuster, G – Screw, H – Base

## RESULTS AND DISCUSSION

The separation between the kernel and shell of the two varieties of oil palm on the three structural surfaces are shown in Tables 1 to 3.

Table 1. Average separation on Mild Steel for Dura and Tenera

Angle of Projection (°)	Dura Separation (cm)	Tenera Separation (cm)
25	6.3	6.3
30	7.4	8.6
35	7.7	7.3
40	7.3	7.7
45	5.3	6.0

Table 2. Average separation on Galvanized Steel for Dura and Tenera

Angle of Projection (°)	Dura Separation (cm)	Tenera Separation (cm)
25	6.7	9.7
30	8.7	8.3
35	7.6	7.3
40	7.3	7.6
45	5.7	6.6

Table 3. Average separation on Plywood for Dura and Tenera

Angle of Projection (°)	Dura Separation (cm)	Tenera Separation (cm)
25	10.0	13.6
30	17.0	10.7
35	11.0	10.0
40	10.4	8.8
45	9.3	7.0

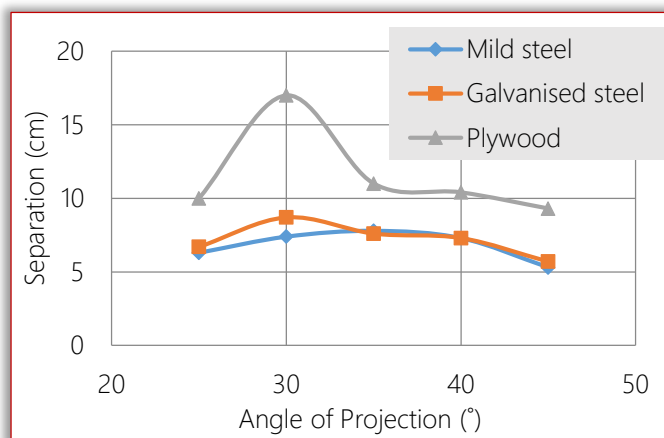


Figure 2. Variation of angle of projection with separation for Dura

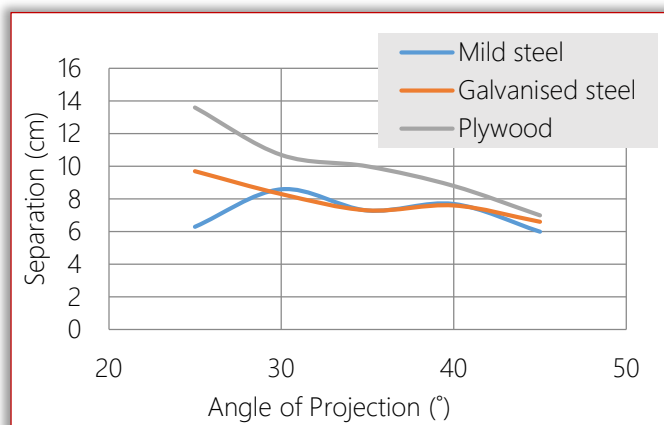


Figure 3. Variation of angle of projection with separation for Tenera

It is observed that the highest separation on mild steel for dura is 7.7 cm at angle of projection of 35° and for tenera it is 8.6 cm at angle of projection of 40°. On galvanized steel the highest separation for dura is 8.7 cm at angle of projection of 30° while it is 9.7 cm at 25° for tenera.

For plywood the highest separation obtained for dura is 17.0 cm at 30° while it is 13.0 cm for tenera at angle of projection



of 25°. The trends of separation for the two varieties on the three surfaces are shown in Figure 2 and Figure 3. It can be observed from Figures 2 and 3 that the highest separation for dura and tenera took place on plywood at angles of 30 and 25° respectively. Mild steel and galvanised steel have similar trend of separation but with galvanised steel having a slightly higher separation at 30 and 25° for both dura and tenera respectively. This is a useful guide in the choice of material and angle of projection for separation.

### CONCLUSIONS

- » The separation of palm kernel and shell of dura and tenera varieties of oil palm on an inclined plane separator was investigated.
- » On mild steel the highest separation for dura is 7.7 cm at angle of projection of 35° and for tenera it is 8.6 cm at angle of projection of 40°.
- » On galvanised steel the highest separation for dura is 8.7 cm at angle of projection of 30° while it is 9.7 cm at 25° for tenera.
- » The highest separation on plywood obtained for dura is 17.0 cm at 30° while it is 13.0 cm for tenera at angle of projection of 25°.

### References

- [1.] Akubuo, C.O. and Eje, B.E. (2002). Palm kernel and shell separator. *Biosystems Engineering* 81(2):193- 199.
- [2.] Amoah J. Y., Aggey M. and Annumu S. (2007). Cracked-mixture sieving rates and efficiencies in small-scale palm nut processing in Ghana. *Ghana Journal of Science*, 47: 69 – 81.
- [3.] Halim, R M; Bakar, N. A; Wahid, M B.; May C. Y; Ramli, Ridzuan; Ngan, Ma Ah; M, R(2009): Maximizing the recovery of dry kernel and shell via a four stage winnowing column. *MPOB Information Series (MPOB TT No. 427)*.
- [4.] Koya, O. A. and Faborode, M. O., (2006). Separation Theory for Palm Kernel and Shell Mixture on a Spinning Disc, *Journal of Biosystems Engineering*, 95(3): 405-412
- [5.] Oke P. K. (2007). Development and performance evaluation of indigenuous palm kernel dual processing machine. *Journal of Engineering and Applied Sciences*, 2(4): 701 -705
- [6.] Okoronkwo, C. A., Ngozi-Olehi, L. C., Nwufu, O. C. (2013). The adaptation of clay-bath and hydro-cyclones in palm nut cracked-mixture separation to small-scale oil palm processing industry. *International Journal of Modern Engineering Research*, 3(4):2023-2026.
- [7.] Olasunboye A. and Koya O. (2014). A Rotary Separator for the Dry Mixture of Palm Kernel and Shell. *Innovative Systems Design and Engineering*, 5(7):32-41
- [8.] Ologumagba F. O., Olutayo I. A. and Alex M. O. (2010). Development of a palm nut fibre separator. *ARPN Journal of Engineering and Applied Sciences*.5(12): 10-15
- [9.] Onaku E. C., Agulanna C. N, Edeh I. C. and Nwaphewihe H. U.(2013). Determination of Optimal angle of projection

and Separation of palm nut shell and kernel using a designed cracker/separator machine. *International Journal of Scientific and Technology Research*, 2(10):289-292

- [10.] Poku K. (2002). Palm oil processing in Africa. *FAO Agricultural Services Bulletin* 148, [www.fao.org](http://www.fao.org)



ISSN: 2067-3809

copyright © University POLITEHNICA Timisoara,  
Faculty of Engineering Hunedoara,  
5, Revolutiei, 331128, Hunedoara, ROMANIA  
<http://acta.fih.upt.ro>

# Fascicule 2

## [ April - June ]

### t o m e

# [2018] XI

**ACTA**Technica**CORVINIENSIS**  
BULLETIN OF ENGINEERING



**ISSN: 2067-3809**

copyright © University POLITEHNICA Timisoara,  
Faculty of Engineering Hunedoara,  
5, Revolutiei, 331128, Hunedoara, ROMANIA  
<http://acta.fih.upt.ro>

## MANUSCRIPT PREPARATION – GENERAL GUIDELINES

Manuscripts submitted for consideration to **ACTA TECHNICA CORVINIENSIS – Bulletin of Engineering** must conform to the following requirements that will facilitate preparation of the article for publication. These instructions are written in a form that satisfies all of the formatting requirements for the author manuscript. Please use them as a template in preparing your manuscript. Authors must take special care to follow these instructions concerning margins.

### INVITATION

We are looking forward to a fruitful collaboration and we welcome you to publish in our **ACTA TECHNICA CORVINIENSIS – Bulletin of Engineering**. You are invited to contribute review or research papers as well as opinion in the fields of science and technology including engineering. We accept contributions (full papers) in the fields of applied sciences and technology including all branches of engineering and management.

**ACTA TECHNICA CORVINIENSIS – Bulletin of Engineering** publishes invited review papers covering the full spectrum of engineering and management. The reviews, both experimental and theoretical, provide general background information as well as a critical assessment on topics in a state of flux. We are primarily interested in those contributions which bring new insights, and papers will be selected on the basis of the importance of the new knowledge they provide.

Submission of a paper implies that the work described has not been published previously (except in the form of an abstract or as part of a published lecture or academic thesis) that it is not under consideration for publication elsewhere. It is not accepted to submit materials which in any way violate copyrights of third persons or law rights. An author is fully responsible ethically and legally for breaking given conditions or misleading the Editor or the Publisher.

**ACTA TECHNICA CORVINIENSIS – Bulletin of Engineering** is an international and interdisciplinary journal which reports on scientific and technical contributions. Every year, in four online issues (fascicules 1 – 4), **ACTA TECHNICA CORVINIENSIS – Bulletin of Engineering [e-ISSN: 2067-3809]** publishes a series of reviews covering the most exciting and developing areas of engineering. Each issue contains papers reviewed by international researchers who are experts in their fields. The result is a journal that gives the scientists and engineers the opportunity to keep informed of all the current developments in their own, and related, areas of research, ensuring the new ideas across an increasingly the interdisciplinary field. Topical reviews in materials science and engineering, each including:

- ✓ surveys of work accomplished to date
- ✓ current trends in research and applications
- ✓ future prospects.

As an open-access journal **ACTA TECHNICA CORVINIENSIS – Bulletin of Engineering** will serve the whole engineering research community, offering a stimulating combination of the following:

- ✓ Research Papers – concise, high impact original research articles,
- ✓ Scientific Papers – concise, high impact original theoretical articles,
- ✓ Perspectives – commissioned commentaries highlighting the impact and wider implications of research appearing in the journal.

**ACTA TECHNICA CORVINIENSIS – Bulletin of Engineering** encourages the submission of comments on papers published particularly in our journal. The journal publishes articles focused on topics of current interest within the scope of the journal and coordinated by invited guest editors. Interested authors are invited to contact one of the Editors for further details.

### BASIC INSTRUCTIONS AND MANUSCRIPT REQUIREMENTS

The basic instructions and manuscript requirements are simple:

- » Manuscript shall be formatted for an A4 size page.
- » The all margins (top, bottom, left, and right) shall be 25 mm.
- » The text shall have both the left and right margins justified.
- » Single-spaced text, tables, and references, written with 11 or 12-point Georgia or Times Roman typeface.
- » No Line numbering on any pages and no page numbers.
- » Manuscript length must not exceed 15 pages (including text and references).
- » Number of figures and tables combined must not exceed 20.
- » Manuscripts that exceed these guidelines will be subject to reductions in length.

The original of the technical paper will be sent through e-mail as attached document (\*.doc, Windows 95 or higher). Manuscripts should be submitted to e-mail: [redactie@fih.upt.ro](mailto:redactie@fih.upt.ro), with mention “for ACTA TECHNICA CORVINIENSIS”.

### STRUCTURE

The manuscript should be organized in the following order: Title of the paper, Authors' names and affiliation, Abstract, Key Words, Introduction, Body of the paper (in sequential

headings), Discussion & Results, Conclusion or Concluding Remarks, Acknowledgements (where applicable), References, and Appendices (where applicable).

#### THE TITLE

The title is centered on the page and is CAPITALIZED AND SET IN BOLDFACE (font size 14 pt). It should adequately describe the content of the paper. An abbreviated title of less than 60 characters (including spaces) should also be suggested. Maximum length of title: 20 words.

#### AUTHOR'S NAME AND AFFILIATION

The author's name(s) follows the title and is also centered on the page (font size 11 pt). A blank line is required between the title and the author's name(s). Last names should be spelled out in full and succeeded by author's initials. The author's affiliation (in font size 11 pt) is provided below. Phone and fax numbers do not appear.

#### ABSTRACT

State the paper's purpose, methods or procedures presentation, new results, and conclusions are presented. A nonmathematical abstract, not exceeding 200 words, is required for all papers. It should be an abbreviated, accurate presentation of the contents of the paper. It should contain sufficient information to enable readers to decide whether they should obtain and read the entire paper. Do not cite references in the abstract.

#### KEY WORDS

The author should provide a list of three to five key words that clearly describe the subject matter of the paper.

#### TEXT LAYOUT

The manuscript must be typed single spacing. Use extra line spacing between equations, illustrations, figures and tables. The body of the text should be prepared using Georgia or Times New Roman. The font size used for preparation of the manuscript must be 11 or 12 points. The first paragraph following a heading should not be indented. The following paragraphs must be indented 10 mm. Note that there is no line spacing between paragraphs unless a subheading is used. Symbols for physical quantities in the text should be written in italics. Conclude the text with a summary or conclusion section. Spell out all initials, acronyms, or abbreviations (not units of measure) at first use. Put the initials or abbreviation in parentheses after the spelled-out version. The manuscript must be writing in the third person ("the author concludes...").

#### FIGURES AND TABLES

Figures (diagrams and photographs) should be numbered consecutively using Arabic numbers. They should be placed in the text soon after the point where they are referenced. Figures should be centered in a column and should have a figure caption placed underneath. Captions should be centered in the column, in the format "Figure 1" and are in upper and lower case letters.

When referring to a figure in the body of the text, the abbreviation "Figure" is used. Illustrations must be submitted in digital format, with a good resolution. Table captions

appear centered above the table in upper and lower case letters.

When referring to a table in the text, "Table" with the proper number is used. Captions should be centered in the column, in the format "Table 1" and are in upper and lower case letters. Tables are numbered consecutively and independently of any figures. All figures and tables must be incorporated into the text.

#### EQUATIONS & MATHEMATICAL EXPRESSIONS

Place equations on separate lines, centered, and numbered in parentheses at the right margin. Equation numbers should appear in parentheses and be numbered consecutively. All equation numbers must appear on the right-hand side of the equation and should be referred to within the text.

#### CONCLUSIONS

A conclusion section must be included and should indicate clearly the advantages, limitations and possible applications of the paper. Discuss about future work.

#### Acknowledgements

An acknowledgement section may be presented after the conclusion, if desired. Individuals or units other than authors who were of direct help in the work could be acknowledged by a brief statement following the text. The acknowledgment should give essential credits, but its length should be kept to a minimum; word count should be <100 words.

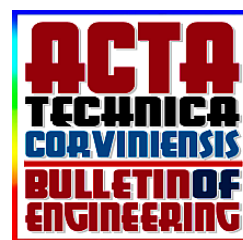
#### References

References should be listed together at the end of the paper in alphabetical order by author's surname. List of references indent 10 mm from the second line of each references. Personal communications and unpublished data are not acceptable references.

**Journal Papers:** Surname 1, Initials; Surname 2, Initials and Surname 3, Initials: Title, Journal Name, volume (number), pages, year.

**Books:** Surname 1, Initials and Surname 2, Initials: Title, Edition (if existent), Place of publication, Publisher, year.

**Proceedings Papers:** Surname 1, Initials; Surname 2, Initials and Surname 3, Initials: Paper title, Proceedings title, pages, year.



ISSN: 2067-3809

copyright © University POLITEHNICA Timisoara,  
Faculty of Engineering Hunedoara,  
5, Revolutiei, 331128, Hunedoara, ROMANIA  
<http://acta.fih.upt.ro>

**ACTA TECHNICA CORVINIENSIS – Bulletin of Engineering** is an international and interdisciplinary journal which reports on scientific and technical contributions.

The **ACTA TECHNICA CORVINIENSIS – Bulletin of Engineering** advances the understanding of both the fundamentals of engineering science and its application to the solution of challenges and problems in engineering and management, dedicated to the publication of high quality papers on all aspects of the engineering sciences and the management.

You are invited to contribute review or research papers as well as opinion in the fields of science and technology including engineering. We accept contributions (full papers) in the fields of applied sciences and technology including all branches of engineering and management. Submission of a paper implies that the work described has not been published previously (except in the form of an abstract or as part of a published lecture or academic thesis) that it is not under consideration for publication elsewhere. It is not accepted to submit materials which in any way violate copyrights of third persons or law rights. An author is fully responsible ethically and legally for breaking given conditions or misleading the Editor or the Publisher.

The Editor reserves the right to return papers that do not conform to the instructions for paper preparation and template as well as papers that do not fit the scope of the journal, prior to refereeing. The Editor reserves the right not to accept the paper for print in the case of a negative review made by reviewers and also in the case of not paying the required fees if such will be fixed and in the case time of waiting for the publication of the paper would extend the period fixed by the Editor as a result of too big number of papers waiting for print. The decision of the Editor in that matter is irrevocable and their aim is care about the high content-related level of that journal.

The mission of the **ACTA TECHNICA CORVINIENSIS – Bulletin of Engineering** is to disseminate academic knowledge across the scientific realms and to provide applied research knowledge to the appropriate stakeholders. We are keen to receive original contributions from researchers representing any Science related field. We strongly believe that the open access model will spur research across the world especially as researchers gain unrestricted access to high quality research articles. Being an Open Access Publisher, Academic Journals does not receive payment for subscription as the journals are freely accessible over the internet.

## GENERAL TOPICS

### ENGINEERING

- ✓ Mechanical Engineering
- ✓ Metallurgical Engineering
- ✓ Agricultural Engineering
- ✓ Control Engineering
- ✓ Electrical Engineering
- ✓ Civil Engineering
- ✓ Biomedical Engineering
- ✓ Transport Engineering
- ✓ Nanoengineering

### CHEMISTRY

- ✓ General Chemistry
- ✓ Analytical Chemistry
- ✓ Inorganic Chemistry
- ✓ Materials Science & Metallography
- ✓ Polymer Chemistry
- ✓ Spectroscopy
- ✓ Thermo-chemistry

### ECONOMICS

- ✓ Agricultural Economics
- ✓ Development Economics
- ✓ Environmental Economics
- ✓ Industrial Organization
- ✓ Mathematical Economics
- ✓ Monetary Economics
- ✓ Resource Economics
- ✓ Transport Economics
- ✓ General Management
- ✓ Managerial Economics
- ✓ Logistics

### INFORMATION SCIENCES

- ✓ Computer Science
- ✓ Information Science

### EARTH SCIENCES

- ✓ Geodesy
- ✓ Geology
- ✓ Hydrology
- ✓ Seismology
- ✓ Soil science

### ENVIRONMENTAL

- ✓ Environmental Chemistry
- ✓ Environmental Science & Ecology
- ✓ Environmental Soil Science
- ✓ Environmental Health

## AGRICULTURE

- ✓ Agricultural & Biological Engineering
- ✓ Food Science & Engineering
- ✓ Horticulture

## BIOTECHNOLOGY

- ✓ Biomechanics
- ✓ Biotechnology
- ✓ Biomaterials

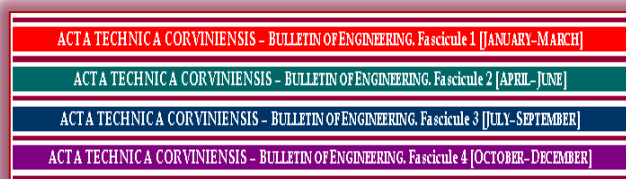
## MATHEMATICS

- ✓ Applied mathematics
- ✓ Modeling & Optimization
- ✓ Foundations & Methods

**ACTA TECHNICA CORVINIENSIS – Bulletin of Engineering** has been published since 2008, as an online, free-access, international and multidisciplinary publication of the Faculty of Engineering Hunedoara.

We are very pleased to inform that our international and interdisciplinary journal **ACTA TECHNICA CORVINIENSIS – Bulletin of Engineering** completed its ten years of publication successfully [issues of years 2008 –2017, Tome I–X]. In a very short period it has acquired global presence and scholars from all over the world have taken it with great enthusiasm.

Every year, in four online issues (fascicules 1 – 4), **ACTA TECHNICA CORVINIENSIS – Bulletin of Engineering** [e-ISSN: 2067-3809] publishes a series of reviews covering the most exciting and developing fields of science and technology. Each issue contains papers reviewed by international researchers who are experts in their fields. The result is a journal that gives the scientists and engineers the opportunity to keep informed of all the current developments in their own, and related, areas of research, ensuring the new ideas across an increasingly the interdisciplinary field.



Now, when we celebrate the tenth years anniversary of **ACTA TECHNICA CORVINIENSIS – Bulletin of Engineering**, we are extremely grateful and heartily acknowledge the kind of support and encouragement from all contributors and all collaborators!

On behalf of the Editorial Board and Scientific Committees of **ACTA TECHNICA CORVINIENSIS – Bulletin of Engineering**, we would like to thank the many people who helped make this journal successful. We thank all authors who submitted their work to **ACTA TECHNICA CORVINIENSIS – Bulletin of Engineering**.

**ACTA TECHNICA CORVINIENSIS – Bulletin of Engineering** exchange similar publications with similar institutions of our country and from abroad.



ISSN: 2067-3809

copyright © University POLITEHNICA Timisoara,  
Faculty of Engineering Hunedoara,  
5, Revolutiei, 331128, Hunedoara, ROMANIA  
<http://acta.fih.upt.ro>

## INDEXES & DATABASES

We are very pleased to inform that our international scientific journal **ACTA TECHNICA CORVINIENSIS – Bulletin of Engineering** completed its ten years of publication successfully [2008–2017, Tome I–X].

In a very short period the **ACTA TECHNICA CORVINIENSIS – Bulletin of Engineering** has acquired global presence and scholars from all over the world have taken it with great enthusiasm.

We are extremely grateful and heartily acknowledge the kind of support and encouragement from all contributors and all collaborators!

**ACTA TECHNICA CORVINIENSIS – Bulletin of Engineering** is accredited and ranked in the “B+” CATEGORY Journal by CNCIS – The National University Research Council’s Classification of Romanian Journals, position no. 940 (<http://cncsis.gov.ro/>).

**ACTA TECHNICA CORVINIENSIS – Bulletin of Engineering** is a part of the ROAD, the Directory of Open Access scholarly Resources (<http://road.issn.org/>).

**ACTA TECHNICA CORVINIENSIS – Bulletin of Engineering** is also indexed in the digital libraries of the following world’s universities and research centers:

WorldCat – the world’s largest library catalog

<https://www.worldcat.org/>

National Library of Australia

<http://trove.nla.gov.au/>

University Library of Regensburg – GIGA German Institute of Global and Area Studies

<http://opac.giga-hamburg.de/ezb/>

Simon Fraser University – Electronic Journals Library

<http://cufts2.lib.sfu.ca/>

University of Wisconsin-Madison Libraries

<http://library.wisc.edu/>

University of Toronto Libraries

<http://search.library.utoronto.ca/>

The University of Queensland

<https://www.library.uq.edu.au/>

The New York Public Library

<http://nypl.bibliocommons.com/>

State Library of New South Wales

<http://library.sl.nsw.gov.au/>

University of Alberta Libraries - University of Alberta

<http://www.library.ualberta.ca/>

The University of Hong Kong Libraries

<http://sunzi.lib.hku.hk/>

The University Library - The University of California

<http://harvest.lib.ucdavis.edu/>

**ACTA TECHNICA CORVINIENSIS – Bulletin of Engineering** is indexed, abstracted and covered in the world-known bibliographical databases and directories including:

INDEX COPERNICUS – JOURNAL MASTER LIST

<http://journals.indexcopernicus.com/>

GENAMICSJOURNALSEEK Database

<http://journalseek.net/>

DOAJ – Directory of Open Access Journals

<http://www.doaj.org/>

EVISA Database

<http://www.speciation.net/>

CHEMICAL ABSTRACTS SERVICE (CAS)

<http://www.cas.org/>

EBSCO Publishing

<http://www.ebscohost.com/>

GOOGLE SCHOLAR

<http://scholar.google.com>

SCIRUS- Elsevier

<http://www.scirus.com/>

ULRICHWeb – Global serials directory

<http://ulrichsweb.serialsolutions.com>

getCITED

<http://www.getcited.org>

BASE - Bielefeld Academic Search Engine

<http://www.base-search.net>

Electronic Journals Library

<http://rzblx1.uni-regensburg.de>

Open J-Gate

<http://www.openj-gate.com>

ProQUEST Research Library

<http://www.proquest.com>

Directory of Research Journals Indexing

<http://www.drji.org/>

Directory Indexing of International Research Journals

<http://www.citefactor.org/>



ISSN: 2067-3809

copyright © University POLITEHNICA Timisoara,

Faculty of Engineering Hunedoara,

5, Revolutiei, 331128, Hunedoara, ROMANIA

<http://acta.fih.upt.ro>



copyright © University POLITEHNICA Timisoara,  
Faculty of Engineering Hunedoara,  
5, Revolutiei, 331128, Hunedoara, ROMANIA  
<http://acta.fih.upt.ro>